UNIVERSITY OF SOUTHAMPTON

Faculty of Social and Human Sciences

Geography and Environment

Patterns of mid-Holocene climate change

– Evidence from the peat archive –

By

Gunnar Mallon

Thesis for the degree of Doctor of Philosophy

August 2012

UNIVERSITY OF SOUTHAMPTON

ABSTRACT

FACULTY OF SOCIAL AND HUMAN SCIENCES

GEOGRAPHY AND ENVIRONMENT

Doctor of Philosophy

PATTERNS OF MID-HOLOCENE CLIMATE CHANGE – EVIDENCE FROM THE PEAT ARCHIVE

By Gunnar Mallon

With growing concerns over future climate change, the need to understand past climate variability has become an important topic of research. In this thesis, a gap in knowledge of the transition to modern climatic conditions during the mid-Holocene is identified and addressed. Mid-Holocene atmospheric moisture availability has been reconstructed from five raised mires (Kortlandamossen, Tore Hill Moss, Raeburn Flow, Gällseredsmossen, and Misten Bog) located on geographical and climatological gradients across northwest Europe.

In this thesis, a new testate amoebae-based palaeohydrological transfer function for south-central Sweden and an improved indicator-weighted Hydroclimatic Index (HCI) were created in order to establish univariate measures of mid-Holocene bog surface wetness (BSW). Together with detrended correspondence analysis, the HCI and testate amoebae transfer function were applied to palaeoecological data from the five bogs, in order to reconstruct climatic variability across northwest Europe from *c*. 9000 before present (BP) until *c*. 3500 BP. A series of wet and dry excursions of the bog surfaces were identified on all five bogs. These BSW changes were compared with palaeoclimatic evidence from the wider literature on a local, regional, continental and hemispheric scale. Throughout the early- to mid-Holocene, increased BSW on Misten Bog closely coincided with episodes of reduced SST in the North Atlantic. A similar link was established between SST and BSW on Raeburn Flow and Gällseredsmossen, following the end of the Holocene Thermal Maximum (HTM).

The results from the analysis demonstrate that the HTM occurred asynchronously across northwest Europe. Reconstructions from all five bogs, except Misten Bog, showed a prolonged dry phase on the bog surface starting prior to *c*. 7000 BP. The end of the HTM occurred between *c*. 5600 BP and *c*. 4800 BP on all sites except Kortlandamossen, where regional environmental mechanisms delayed the end of the HTM. A climatic boundary at the end of the HTM was detected around 57ºN, with sites south of 57ºN experiencing the termination between *c*. 5600 BP and *c*. 5300, while it occurred between *c*. 4800 BP and *c*. 4400 BP on the sites north of this latitude. The only period when all five sites displayed similar BSW changes was between *c*. 4400 BP and *c*. 4000 BP, a period of global climatic change. A major wetting on the bogs during this time coincided with increased BSW and glacial advances across Europe as well as high lake levels in France and Switzerland.

Table of contents

List of Figures

List of Tables

List of Equations

Declaration of Authorship

I, GUNNAR MALLON, declare that the thesis entitled

PATTERNS OF MID-HOLOCENE CLIMATE CHANGE – EVIDENCE FROM THE PEAT ARCHIVE

and the work presented in the thesis are both my own, and have been generated by me as the result of my own original research. I confirm that:

- this work was done wholly or mainly while in candidature for a research degree at this University;
- where any part of this thesis has previously been submitted for a degree or any other qualification at this University or any other institution, this has been clearly stated;
- where I have consulted the published work of others, this is always clearly attributed;
- where I have quoted from the work of others, the source is always given. With the exception of such quotations, this thesis is entirely my own work;
- I have acknowledged all main sources of help;
- where the thesis is based on work done by myself jointly with others, I have made clear exactly what was done by others and what I have contributed myself;
- none of this work has been published before submission

Signed: _____

Date: _____

Acknowledgements

First and foremost, I would like to express my sincere gratitude to my Ph.D. supervisors Dr. Paul Hughes and Professor Keith Barber. Without their inspiration, patience and support this project would not have been possible.

Academic advice and guidance comes in many forms and I would like to thank Dr. Rob Scaife, Professor Mary Edwards, Dr. Pete Langdon and Professor Dan Charman for their support and advice throughout my research.

Professor Stefan Wastegård and Professor Lars Franzén helped to select appropriate peat bogs in Sweden. Professor Maurice Streel and Dr. Freddy Damblon suggested Misten Bog and helped obtain access permission. Dr. Gaël LeRoux, Professor Emmanuelle Javaux and Sam Bateman were invaluable fieldwork helpers.

Many thanks are also due to Gunhild Lorenzen, Anna C. Mallon and the rest of my family for constantly reminding me that there are more important things in life than mid-Holocene climate change. Thanks are also in place to Dr. Catherine Langdon, Dr. Matt Amesbury, IM Valeri Lilov, Dr. Rong Wang and Hayley Essex for putting up with me during all of my tantrums.

The main sponsor of this research was the School of Geography, University of Southampton. Further support came from NERC for 30 radiocarbon dates, the QRA for help with cost of fieldwork in Sweden and Dr. Gaël LeRoux for two rangefinder ^{14}C dates.

Last but by no means least: Matt Lunn, Liam Goodes, Helen Mackay and Kim Davies took time to proofread this thesis.

To everyone who made the thesis possible: THANK YOU!

"… Imagination is more important than knowledge. For knowledge is limited, whereas imagination embraces the entire world, stimulating progress, giving birth to evolution. It is, strictly speaking, a real factor in scientific research."

- (Einstein, 1931)

"The voyage of discovery lies not in seeking new horizons, but in seeing with new eyes."

- (Proust, 1913-1927)

1 Introduction and aims

1.1 Background and justification of research

With growing concerns over predicted changes to the global climate system, a large research emphasis has recently been placed on understanding past climates in order to model future climate variability (IPCC, 2007). Models and predictions show that moisture availability will have a greater impact on human life than temperature change in the coming decades (IPCC, 2007; Verschuren and Charman, 2008), with moisture availability across north-western Europe being closely linked to sea surface temperatures of the North Atlantic and the strength of the thermohaline circulation (THC) (Bianchi and McCave, 1999; Sutton and Hodson, 2005). The intensity of North Atlantic Deep Water (NADW) formation, which largely drives the THC, is primarily controlled by the delicate balance between fresh and saline waters in the Labrador Sea and Greenland Sea (Figure 1.1).

Projections of increased melt-water input into the Nordic Seas (Chen *et al.*, 2006; IPCC, 2007; Dodd *et al.*, 2009; Kuhlbrodt *et al.*, 2009; Swingedouw *et al.*, 2009) and into the Arctic Ocean from increased river run-off (Arnell, 2005) therefore make it possible that the current state of the THC will be disrupted in the near future (Bianchi and McCave, 1999; Thornalley *et al.*, 2009). Even small changes in the THC have been shown to have large knock-on effects in the ocean-atmosphere-climate system, triggering major climate events across north-western Europe (Denton and Broecker, 2008). It is therefore imperative to gain a better understanding of ocean-atmosphere-climate interactions and their impact on

terrestrial ecosystems in order to identify possible drivers of northwest European climate and understand changes in moisture availability in response to changes in the North Atlantic. Reconstructing climate variability since the last ice age, and before any noticeable human impact, provides an excellent platform for gaining valuable insights into natural climate variability and to fully understand present climatic conditions and future climate scenarios.

Figure 1.1 - Regions of North Atlantic Deep Water formation (indicated by crosses). DSOW, Denmark Straight Overflow Water; LSW, Labrador Sea Water; NEADW, Northeast Atlantic Deep Water; NADW, North Atlantic Deep Water. Adapted from (Hillaire-Marcel *et al.*, 2001)

Whilst we are starting to understand the factors influencing ocean-atmosphere interactions, terrestrial responses to these drivers still remain largely unexplored.

Ombrotrophic peat bogs provide suitable environments to study terrestrial-based responses as they are entirely 'rain-fed' and changes in bog surface wetness (BSW) are primarily driven by variability in the balance between precipitation and evapotranspiration (P-E), known as effective precipitation. Because of the unique link with the atmosphere, reconstructions of BSW have become an established measure of past climate change that allows valuable inferences to be made about past variability in atmospheric moisture (Booth and Jackson, 2003; Barber *et al.*, 2004; Chambers and Charman, 2004; Hughes and Barber, 2004; Langdon and Barber, 2005; Hughes *et al.*, 2006; Barber and Langdon, 2007; Sillasoo *et al.*, 2007; Charman *et al.*, 2009; Booth, 2010; Booth *et al.*, 2010; Mauquoy *et al.*, 2010; Amesbury *et al.*, 2011).

In a palaeoclimatic context, atmospheric moisture transport and moisture availability across northwest Europe is still poorly understood and no comprehensive dataset of changes in atmospheric moisture transport across northwestern Europe exists for the early- to mid-Holocene. The research emphasis so far has largely focused on temperature reconstructions throughout specific time periods, such as the 'Little Ice Age' (Lamb, 1982; Bradley and Jones, 1993; Matthews and Briffa, 2005; Helama *et al.*, 2009) or the entirety of the Holocene (Davis *et al.*, 2003; Seppä *et al.*, 2009). Studies looking at the entire Holocene often lack the spatial and temporal resolution needed to detect subtle changes in climate patterns on a continental scale (Hughes *et al.*, 2000a). The majority of work focussing on reconstructing moisture availability has so far been limited to the early- or late-Holocene (Charman *et al.*, 1999; Mauquoy and Barber, 1999; Langdon *et al.*, 2003; Blundell and Barber, 2005; Langdon and Barber, 2005) and very little work has been carried out on the mid-

Holocene. The mid-Holocene, however, is a period of particular interest because of the large-scale environmental reorganisation that took place (Steig, 1999). Following the end of major melt water pulses into the North Atlantic around 6800 BP (Carlson *et al.*, 2008), sea level stabilization around 6000 BP (Bard *et al.*, 1996) and the final disappearance of the Laurentian ice-sheet, oceanic and atmospheric reorganisation took place. It is believed that the polar jet-stream was split by the high-pressure system built up over the Laurentian Ice Sheet (LIS) (Mann and Hamilton, 1995) and that during the early- to mid-Holocene the two branches of the polar jet merged back into one. This period of atmospheric and oceanic re-organization, also known as the mid-Holocene transition (MHT), is clearly a period of particular research interest as it marks the transition to modern climatic conditions. The exact timing of the MHT, however, has still not been fully explored and a gap in knowledge clearly exists with respect to the terrestrial response to variability in moisture balance across northwest Europe during the MHT.

Studying the mechanisms driving lake level changes in the French Jura, Magny (2003b; 2006) concluded that the spatial distribution of Holocene moisture transport across Europe resulted from changes in the position and intensity of persistent Atlantic Westerlies. However, these studies have a relatively low spatial resolution, include mountainous regions and use mixed evidence from climate proxies that contain a seasonal bias. Given the intricate nature of present synoptic conditions across Europe, it is likely that a more complex arrangement of prevailing air masses was responsible for the spatial distribution of temperature and effective precipitation regimes across the continent. Determining changes in bog surface wetness (BSW), therefore, provides an excellent terrestrial proxy source of palaeoclimatic

information, which can be linked to changes in the North Atlantic Ocean via atmospheric moisture transport.

Based on ice-core records, the climate of our present interglacial period has long been regarded as relatively stable (Dansgaard *et al.*, 1993). This view of a complacent Holocene climate system is, however, being revised after several cycles of climate variability, ranging in length from millennial (Denton and Karlén, 1973; Bond and Lotti, 1995; Bond *et al.*, 1997; Bianchi and McCave, 1999; Chapman and Shackleton, 2000; Hughes *et al.*, 2000a; Langdon *et al.*, 2003; Wanner and Bütikofer, 2008; Thornalley *et al.*, 2009) to decadal (Delworth and Mann, 2000; Kerr, 2000; Sutton and Hodson, 2003; Sutton and Hodson, 2005; Denton and Broecker, 2008) have been detected in atmospheric, oceanic and terrestrial palaeo-records. Evidence from the North Atlantic region points to naturally occurring centennial- to millennial-scale cycles of sea surface temperature variation (Andersen *et al.*, 2004; Thornalley *et al.*, 2009) and changes in the intensity of the THC (Bianchi and McCave, 1999; Chapman and Shackleton, 2000). The variability in THC strongly affects heat and moisture transport to NW Europe and is therefore an important driver of European climate (Sutton and Hodson, 2005; Denton and Broecker, 2008). However, uncertainties still exist about the timing and frequency of this millennial-scale pacing, and periods of 2500, 1500 and 1000 years have been detected.

In addition to the 1000-year cycle, Chapman and Shackleton (2000) further identified a 550-year cycle in the strength of the THC. Centennial- to millennial-scale periodicities have also started to emerge in the terrestrial records of northern Britain (Hughes *et al.*, 2000a; Langdon *et al.*, 2003) and North America (Viau *et al.*,

2002). It has been suggested that this millennial-scale pacing has had different triggers throughout the Holocene (Wanner and Bütikofer, 2008), but the exact nature of this pacing is still subject to much debate. Evidence points to solar output driving this quasi-periodic millennial pulse during the early Holocene, interrupted by large-scale melt water fluxes (Denton and Karlén, 1973; Chapman and Shackleton, 2000; Bond *et al.*, 2001; Daley *et al.*, 2009; Dima and Lohmann, 2009; Thornalley *et al.*, 2010) and ocean-internal processes amplifying the signal following the stabilization of the North Atlantic Ocean (Debret *et al.*, 2009). Evidence from sea surface temperature reconstructions and wavelet analysis has identified a clear change in amplitude of the millennial-scale pacing at around 6000-5500 BP (Berner *et al.*, 2008; Debret *et al.*, 2009) (Figure 1.2). A similar shift in the amplitude of the climate cycle has been detected as early as 6600 BP (Schulz and Paul, 2002a).

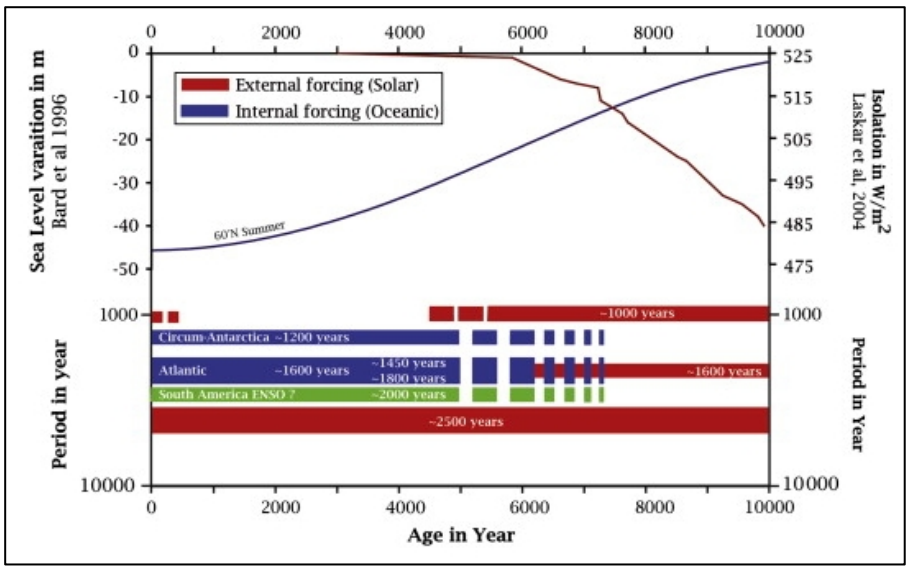

Figure 1.2 - Holocene climate cycle patterns highlighting a strong transition from external to internal forcing between 6000 - 5000 cal. yr. BP. Source: (Debret *et al.*, 2009)

In addition to solar and ocean-internal drivers, Milankovitch forcing played a key role in driving European climate during the early Holocene (Berner *et al.*, 2008) following an initial insolation maximum. During the MHT, variability in insolation reached its Holocene maximum value and climate variability peaked, as a result of orbital forcing. If accurate climate predictions are to be made, it is important to fully understand the drivers of these centennial- and millennial-scale periodicities in relation to orbital forcing impacts. Studying the mid-Holocene transition provides an excellent measure of the change from a mixed melt water and solar forced system to one driven by ocean-internal processes and solar output.

1.2 Aims and objectives

The aim of the thesis is to use the unique coupling between raised bogs and the atmosphere in order to reconstruct spatio-temporal patterns of atmospheric moisture availability in northwestern Europe during the mid-Holocene. To realize this aim, a series of ombrotrophic peat bogs on an 'oceanic' north-south transect and a second 'more continental' north-south transect were cored and analysed for plant macrofossil and testate amoebae remains in order to reconstruct changes in BSW. The following research questions will be addressed:

Q1: Do changes in bog surface wetness across NW Europe correspond to known events of increased ice rafting in the North Atlantic Ocean (Bond *et al.*, 1997)?

Q2: Did patterns of atmospheric moisture availability differ between northern and southern sites along the study transects during the mid-Holocene?

Q3: How did climatic conditions across northwest Europe compare before, during and after the mid-Holocene transition?

Q4: Did the Holocene Thermal Maximum (HTM) occur synchronously across NW Europe?

Reconstructions of moisture availability patterns across northwest Europe during the mid-Holocene transition will be very useful for the palaeo-modelling community, as no such high-resolution datasets exist at present.

1.3 Thesis structure

The thesis is organised into seven chapters and will follow a standard scientific structure. The present chapter serves as general background to the project and to summarise and outline the aims of this thesis.

Chapter 2 presents a synthesis of relevant published research focusing largely on evidence of climate change across northwest European since the start of the Holocene. A special focus is placed on environmental changes throughout the early- to mid-Holocene that have affected atmospheric and oceanic circulation and shaped northwest European climate.

Chapter 3 provides detailed information on each of the study sites including modern climatic conditions and the strategies used to determine coring locations. The methods used to collect surface samples and deep peat cores are explained alongside a detailed methodological description of the techniques employed to identify plant macrofossils and testate amoebae. The chapter concludes by discussing the methods used to create robust age depth models for each of the sites using a ^{14}C radiocarbon dating framework.

Chapter 4 reviews different statistical approaches used to interpret palaeoecological data in order to make inferences about changes in palaeohydrological regimes. A new plant macrofossil-based hydroclimatic index is presented. Furthermore, a new testate amoebae-based palaeohydrological transfer function for south-central Sweden is constructed and discussed.

Chapter 5 presents results from the analyses described in Chapters 3 and 4 including results from radiocarbon based age-depth modelling and plant macrofossil and testate amoebae analyses. The statistical techniques presented in Chapter 4 are applied to all palaeoecological data. Key features and abnormalities in past BSW as well as their relation to radiocarbon calibration curves are highlighted.

Chapter 6 discusses and interprets the results presented in Chapter 5, looking at patterns of atmospheric moisture availability alongside palaeoecological evidence in relation to climate cycles with a particular focus on centennial- to millennial-scale climate cycles. The chapter will also present a closer look at Bond cycles and evidence of a millennial and 500 year climate cycle, which has been detected in the peat archive. The timing and manifestation of the mid-Holocene transition across

northwest Europe is discussed with a special focus on temporal and spatial synchronicities of climate change and the influence of the North Atlantic Ocean in driving the transition to modern climatic conditions. Synchronicities between sites and possible climatic boundaries across the study transects are outlined and discussed alongside possible explanations for these patterns.

Chapter 7 summarises the conclusions drawn from the research and presents a synthesis of the findings. Further research avenues that stem from the findings presented and discussed in the previous chapters are outlined. A list of new research project alongside ideas to improve the data of this research is presented.

1.4 Definitions and terminology

To avoid ambiguities associated with historically ill-defined terminology, the terms peat bog, raised bog and bog will be used synonymously to refer to acidic ombrotrophic (rain-fed) mires throughout the thesis. The term mid-Holocene refers to the time period between 8 kyr BP and 3.5 kyr BP. Definitions of important terminology, used frequently throughout the thesis are given in the relevant sections of Chapter 2 where these are first discussed. All dates are expressed as calibrated calendar years before present (cal. yr. BP), with the present defined as A.D. 1950, with calibration methodology discussed in Chapter 3. Nomenclature follows (Stace, 1991) for vascular plants, (Smith, 2004) for bryophytes, and (Charman *et al.*, 2000) for testate amoebae from the palaeo records and Booth (pers. comm., 2010) for the testate amoebae transfer function presented in Chapter 4.

2 Literature review

2.1 Introduction

This chapter will review the existing literature in order to highlight gaps in the current knowledge of mid-Holocene climate change across northwest Europe and to support the importance of the thesis' research questions. A summary of what is known about mid-Holocene environmental change in northwest Europe and the broader North Atlantic region will follow a brief history of palaeoecological research on peat bogs. A particular focus will be placed on the influence of the North Atlantic Ocean on moisture transport to Europe. Consequently, centennial- to millennial-scale climate cycles relating to European climate will be reviewed and summarised. The review will include a summary of their driving mechanisms in relation to Holocene moisture transport and their impact on bog surface wetness across European peat bogs. Finally, this chapter will review evidence of European mid-Holocene climate change, focussing on the peat archive, glacial movements and lake level fluctuations.

2.2 Peat bogs as source of palaeoclimatic information

In recent decades, the use of peat bogs to reconstruct palaeoclimatic change has become increasingly popular, with an expanding body of research on new proxy sources of palaeoclimatic information, such as the use of stable isotopes (Moschen *et al.*, 2009; Brader *et al.*, 2010; Daley *et al.*, 2010; Kaislahti Tillman *et al.*, 2010; Daley *et al.*, 2011; Moschen *et al.*, 2011). In the early days of peat-based palaeo-environmental reconstruction, information was largely limited to the comparison of

changes in peat stratigraphy based on the degree of peat humification (Blytt, 1876; Weber, 1900; Weber, 1908). The differences between light and dark coloured peat were interpreted as wet, cold and fast-accumulating (light) periods or dry, warm and slow-accumulating (dark) ones (Weber, 1900). Using this simple peat type classification system, the epoch since the last glaciation was divided into five broad periods (preboreal, boreal, atlantic, subboreal, subatlantic), known as the Blytt-Sernander climatic periods (Sernander, 1894). The main problem with the Blytt-Sernander scheme, however, was that the exact timing of these chronozones was not well defined, with the exception of the subboreal-subatlantic transition, which was characterised by a very sharp shift from dark and humified to fresh *Sphagnum* peat, known as the "*Grenzhorizont*" (Weber, 1900; Weber, 1926). This contact between strongly humified and fresh *Sphagnum* peat is generally accepted to reflect climatic changes to cooler conditions (Godwin, 1975; Overbeck, 1975). With advances in modern dating techniques, such as radiocarbon dating, the use of the Blytt-Sernander scheme in literature has declined sharply and it is rarely used to describe the timing of palaeoclimatic change. However, the presence of the "*Grenzhorizont*" is still occasionally used as evidence of relatively sudden climatic change (e.g. Van Geel *et al.*, 1996; Seppä, 2002).

Since the initial use of peat in palaeoclimatic reconstructions (e.g. von Post, 1916), peat-based palaeoclimatology has undergone a host of methodological advances (Chambers *et al.*, 2012). Almost a century after the pioneering work by Blytt, Barber (1981) demonstrated the influence of climate on the relative abundance of bog plant species. At the time the generally accepted belief was that peat bogs underwent a cyclic shift between pool and hummocks phases, called 'cyclic regeneration theory'

(Osvald, 1923). The implication of the concept was that bog surface conditions were primarily driven by bog internal processes, rather than by climate. However, examinations of exposures on eight Irish bogs showed synchronous changes in bog surface, casting doubts on the 'cyclic regeneration theory' (Walker and Walker, 1961). Aaby's (1976) reconstructions of synchronous changes in peat humification on five Danish bogs put the theory even further in question. It was finally disproven by Barber's work on Bolton Fell Moss (Barber, 1981). By analysing an array of exposed sections, Barber concluded that peat formation did not undergo a cyclic pattern but was instead primarily driven by climatic factors. Barber's work furthermore suggested that internal bog hydrology plays a less important role in controlling surface conditions than climate. This discovery demonstrated a clear link between climate and bog surface wetness, laying the foundation for a wealth of palaeoecological research using peat bogs as source of palaeoenvironmental and palaeoclimatic proxy information.

Following Barber's work, there was a subsequent shift in research towards the use of peat stratigraphy for the reconstruction of climate curves rather than the identification of fixed points of climatic conditions (e.g. Hendon *et al.*, 2001; Gunnarson *et al.*, 2003; Blundell and Barber, 2005; Blundell *et al.*, 2008; Borgmark and Wastegård, 2008; Mauquoy *et al.*, 2010). Peat-based palaeoclimatic research has since developed into a more exact discipline (Chambers *et al.*, 2012) that provides reconstructions of past climatic conditions from the biological (e.g. Digerfeldt, 1988; Barber *et al.*, 1994; Barber *et al.*, 1998; Hughes *et al.*, 2000a; Langdon *et al.*, 2003; Blundell and Barber, 2005; Langdon and Barber, 2005; Hughes *et al.*, 2006; Charman *et al.*, 2007; Hughes *et al.*, 2007; Mauquoy *et al.*, 2008; Amesbury *et al.*,

2011) as well as chemical (e.g. De Vleeschouwer *et al.*, 2007; De Vleeschouwer *et al.*, 2009; Moschen *et al.*, 2009; Andersson and Schoning, 2010; Brader *et al.*, 2010; Daley *et al.*, 2010; Kaislahti Tillman *et al.*, 2010; Moschen *et al.*, 2011) (Figure 2.1) and physical (e.g. Blackford and Chambers, 1993; Chambers and Charman, 2004; Chambers *et al.*, 2010; Loisel and Garneau, 2010; van Bellen *et al.*, 2011; Hughes *et al.*, 2012) properties of peat. The history of peat based palaeoclimatic research is reviewed in greater detail by Barber (1981; 1994).

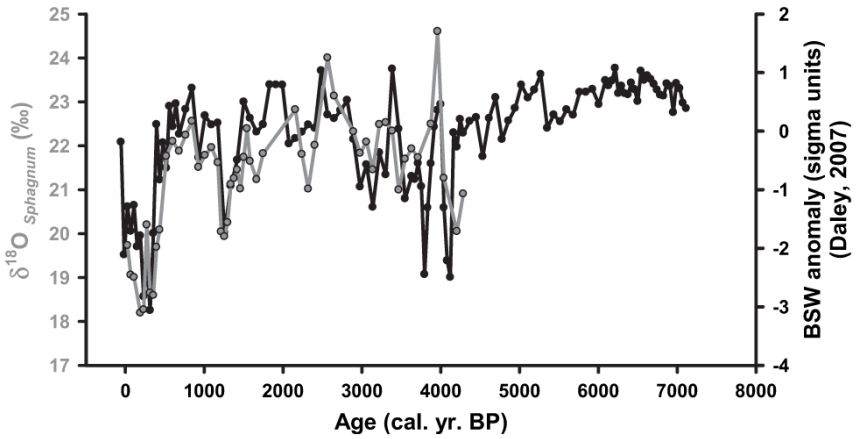

Figure 2.1 - Comparison of BSW reconstruction and $\delta^{18}O_{Sphagnum}$ values from Walton Moss (WLM22). The two records are shown to correspond in both general pattern and detail (Source: Daley *et al.*, 2010).

However, the exact climatic parameters that control BSW are still debated. Knowing which climatic parameters are driving ecological changes on the bog is desirable in order to compare reconstructions of BSW with other sources of palaeoclimatic information, such as glacial mass balance fluctuations. It is still debated whether

temperature or precipitation control BSW on a short- or long-term timescale. Barber *et al.* (2000) and Barber and Langdon (2007) argue that BSW responds to changes in temperature rather than in precipitation patterns over the decadal and centennial timescale. However, looking at a 50 year record of measured water table fluctuations from Estonia and comparing them to reconstructed BSW changes, Charman *et al.* (2004) argue that summer temperatures only play a greater role over longer timescales and that precipitation shows a higher correspondence to BSW. However, by comparing BSW reconstructions from Walton Moss with chironomid-inferred temperatures from a nearby lake, Talkin Tarn, Barber and Langdon (2007) argue that overall summer temperatures play a dominant role but that over very short timescales, years and decades, the precipitation signal may be the more dominant driver of BSW. Charman (2007) pointed out that temperature plays a more important role in controlling BSW than precipitation in more continental settings and that it played a particularly important role during the early- to mid-Holocene. In order to determine the responses of individual proxy-climate indicators from bogs, Amesbury *et al.* (2012b) compared high-resolution climate reconstructions from Fågelmossen, Sweden, to meteorological data. Their results showed that both plant macrofossils and testate amoebae changes correlated significantly to precipitation, whereas plant macrofossils also exhibited a strong association with temperature. It is now accepted that the length and severity of the summer water deficit are the primary controls on BSW, which in turn is driven primarily by precipitation and reinforced by temperature (Charman *et al.*, 2009).

BSW can be reconstructed using a number of palaeoclimatic proxy sources as described below. The two proxy methods employed throughout this thesis are the use of plant macrofossil and testate amoebae analyses.

2.2.1 Plant macrofossil analysis

Plant macrofossils refer to the parts of plants, taken from the peat matrix, that are visible with the naked eye (Birks and Birks, 2004). They are largely made up of branches, roots and leaves of bryophytes, Ericaceae, monocotyledons and dicotyledons as well as seeds and any other plant debris. Bog plants all have optimal environmental ranges in which they grow best (Rydin and Jeglum, 2006; Brooker *et al.*, 2008; Lamentowicz *et al.*, 2010) and it is within these ranges that species have a competitive edge and tend to out-compete others in their struggle for resources. When environmental conditions change to less favourable ones, often as a result of climatic changes, some species lose their competitive edge and soon get replaced. This competitive nature between plants growing on ombrotrophic peat bogs is illustrated by Bu *et al.* (2011) and Granath *et al.*'s (2012) studies of the impact of nitrogen enrichment on *Sphagnum* species growing on different types of peatlands. Acidic raised bogs provide a habitat where only highly specialised species can survive, because of the low pH and poor nutrient availability. They are mainly home to well adapted hydrophytic species such as Sphagnaceae and other bryophytes, Ericaceae species, such as *Erica tetralix*, *Calluna vulgaris*, *Andromeda polifolia*, *Empetrum nigrum* and *Vaccinium* spp. and a number of monocotyledon, such as *Eriophorum vaginatum*, *E. angustifolium*, *Rhynchospora alba*, *Trichophorum cespitosum*, a small number of *Carex* species and *Scheuzeria palustris*. Depending on the surface microform and moisture availability, the main peat plant species

assemblage tends to be made up of these plants (Figure 2.2). Other species such as birch trees, *Molinia caerulea*, *Rubus* spp. and *Narthecium ossifragum* can also be found on raised bogs, but often point to disturbance or drying out of the site.

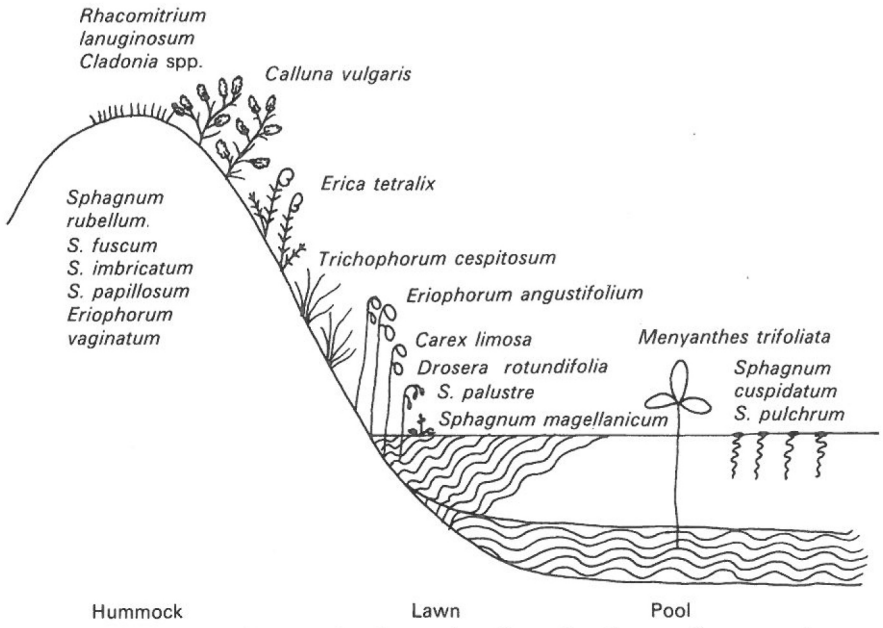

Figure 2.2 - Generalised vegetation zonation on a hummock-pool gradient on a British raised bog (Source: Birks and Birks, 2004).

The use of plant macrofossils in palaeoclimatic reconstructions is well established (e.g. Barber, 1981; Barber, 1994; Van Geel *et al.*, 1996; Barber *et al.*, 1998; Hughes *et al.*, 2000a; Barber *et al.*, 2003; Langdon *et al.*, 2003; Hughes *et al.*, 2006; Swindles *et al.*, 2007; Mauquoy *et al.*, 2008; Mauquoy *et al.*, 2010; Amesbury *et al.*, 2011; Daley and Barber, 2012; Swindles *et al.*, 2012a; Swindles *et al.*, 2012b) and forms an integral part of any peat-based palaeoclimatic study (Birks and Seppä,

2010). Plant macrofossils provide an excellent source of past BSW information as they are largely deposited *in situ* and are rarely transported any distance. Any plant components that are transported, such as seeds, are largely excluded from BSW reconstructions. The ecological niches and hydrological preferences of north-west European bog plant species are discussed and reviewed in detail in Hughes (1997), Mauquoy (1997), and McMullen (2000) and it is beyond the scope of this thesis to expand further on the discussion.

The relationship between plant community assemblage and BSW is not linear and it is worth noting that the shift in plant communities, in response to climate change, generally occur in a step-wise way (Magyari *et al.*, 2001). The tolerance of plants to environmental changes, such as water table fluctuations, is much greater than for testate amoebae, which tend to respond quickly to small-scale fluctuations in the water table (Lamentowicz *et al.*, 2010). Some bog species, such as *Eriophorum vaginatum*, thrive in fluctuating water table conditions (Wein, 1973), whereas other species, such as *Sphagnum fuscum,* tolerate a wide range of moisture regimes and can be found along most of the moisture gradient from lawn to hummock (Grosvernier *et al.*, 1997). Plant macrofossil-based BSW reconstructions perform best when there is a mixture of *Sphagnum* species present. As plants do not respond in a linear fashion to changes in water table, plant macrofossils are unsuitable for making inferences about subtle or short-lived changes to the water table. They do, however, provide an excellent means to reconstruct long-term trends from the peat record on a decadal to centennial timescale as major shifts in BSW trigger plant community changes.

A further problem associated with the use of plant macrofossils in palaeoclimatic reconstructions is their response to non-climatic factors. Throughout most of the mid to late Holocene, *Sphagnum austinii* (formerly known as *S. imbricatum*) was abundant on most raised bogs and played an important role as a peat-building species. However, in recent decades, it has become very rare on British bogs, growing on only a handful of sites. In their work on raised bogs in Wales, Hughes *et al.* (2007; 2008) pointed to the possible influence of nitrogen and metal loading as cause of large-scale disappearance of *S. austinii*. In parallel, McClymont *et al.* (2008) investigated the decline of *S. austinii* from Butterburn Flow, Cumbria, and concluded that changes in nutrient input resulting from human disturbance alongside changes in water tables were responsible for its decline. In the context of palaeoclimatic reconstruction this can pose a problem since it is unclear whether the disappearance of the species is a result of changes in climate or other allogenic factors, especially when *S. austinii* is replaced by a more eurytopic species such as *S. magellanicum* or *S. papillosum*. However, in the context of this thesis, the time period in question is outside of any considerable human impacts on the sites. As the sites are ombrotrophic, all nitrogen and metal loading must come from atmospheric deposition and these pollutants are largely a result of industrial manufacturing and large-scale farming (Hughes *et al.*, 2008). Both of these factors were absent during the early- to mid-Holocene and sizeable changes in nutrient status on the bogs, as a result of human activity, can be ruled out. Nutrient inputs from leaching of tephra deposits can also be ruled out as only small amounts of crypto-tephra were deposited across northwest Europe during the mid-Holocene. Changes in *Sphagnum* community compositions can therefore be explained by changes in climatic

conditions. These changes are primarily the result of climate and in part the result of interspecies competition (Mauquoy and Barber, 1999; Langdon and Barber, 2005).

Where plant species that can tolerate water table fluctuations or those with a wide range of habitats thrive (e.g. *Sphagnum fuscum*), small changes in BSW will go undetected and will not show up in hydroclimatic reconstruction. Several bog plant species are therefore climatically insensitive, as they do not react to small-scale changes in BSW (Hughes and Barber, 2004). With their work on Tore Hill Moss, Scotland, Blundell & Barber (2005) showed that given the wide hydrological tolerance range of *S.* section *Acutifolia* and *S. austinii*, their use in palaeoclimatic reconstructions needs to be considered very carefully. *Sphagnum* moss, however, remains an important indicator of BSW changes. Many bog plants will respond 'sluggishly' to reduction in moisture availability and plant communities can take some time to change over, contrary to testate amoebae, which respond very quickly to changes in hydrological regime. Shifts to wetter conditions, on the other hand, are generally registered very quickly in the plant macrofossil and testate amoebae reconstructions.

A further problem often associated with plant macrofossils is their different resilience to decay. *Cladonia* spp., for example, is very rarely found in the fossil record since it breaks down very quickly under prolonged acidic wet conditions. Roots of *Eriophorum vaginatum*, on the other hand, will preserve very well over time (Hughes and Barber, 2004). This can lead to preferential preservation and overrepresentation of different species and plant components (Kuder and Kruge, 1998), which can cause problems in their interpretation. As growing conditions for all species found in the assemblage needed to be right, preferential preservation does

not pose a problem for palaeoclimatic reconstructions. The absence of species from the profile will therefore not skew the results, as small-scale changes in BSW tend to go undetected in the plant macrofossil record. Plant macrofossils therefore provide a very good record of long-term changes in bog surface hydrology (Barber, 1994; Barber and Langdon, 2007; Daley and Barber, 2012) and are an essential component of any peat-based palaeoecological study (Birks and Seppä, 2010).

2.2.2 Testate amoebae analysis

Testate amoebae (Protozoa: Rhizopoda) are microscopic organisms that measure between 15 and 250 μm and live in the water films on bryophytes and vascular plants (Charman *et al.*, 2000). They are very sensitive to changes in moisture availability and consequently water table depth. Amoebae form shells either from secretion, plates, surrounding material, such as diatoms or quartz particles, or a combination of the three. When amoebae die, the species-characteristic shells largely preserve in the peat matrix. Counts of these shells in a peat sample can be used to determine past community assemblages, which in turn can be used to make inferences about past BSW. Steinecke (1927) and Harnisch (1927) were the first to use testate amoebae in peat deposits. They related selected testate amoebae species to different mire types. Initial work in the UK focussed on the relationship between testate amoebae communities and sediment pH (Heal, 1961) and on dividing the assemblages into fen, bog pool and wet/dry hummock systems (Heal, 1963). Heal investigated the vertical and seasonal distribution of testates in Northern England, contrasting the results with the work carried out in Europe by Harnisch (1927) and concluded that their ecological behaviour was comparable between the European and British studies and that larger species tend to occupy wetter habitats (Heal, 1963).

This hypothesis was supported by Bobrov's (1999) detailed work that concluded that larger taxa within a related group tend to live in wetter conditions as a result of thicker leaf water films. Ever since the work by Tolonen *et al.* (1985) and Tolonen (1986), which linked testate amoebae assemblages to modern hydrological conditions, testate amoebae have been recognised as useful indicators of palaeohydrological change on ombrotrophic peat bogs. The work by Tolonen (1994), Woodland (1998), Mitchell (1999) and Bobrov (1999) showed that the mean annual water table was the most important environmental variable determining the abundance of testate amoebae species in peat. A detailed history of the use of testate amoebae in ecological and palaeohydrological studies is given in Charman *et al.* (2000) and Amesbury (2007).

Testate amoebae have a high rate of reproduction, with between 10 and 27 generations of amoebae per year (Charman, 2001), and high biodiversity, with around 15 species per 4 cm^3 of peat (Woodland *et al.*, 1998). Their community assemblage can therefore change very quickly in response to changes in surface hydrology. This quick response makes them an ideal source of palaeohydrological information. Blundell and Barber (2005) argue that testate amoebae are an excellent indicator of BSW change when plants do not react to changes as quickly. Plants and testate amoebae will often react similarly to increased BSW but plants generally take a longer time to change over when a pool dries out. This can lead to some inertia in plant macrofossil-based reconstructions. Furthermore, because of their short lifespan and generally higher biodiversity than plants, short-lived changes in BSW that would not trigger plant community changes, will be reflected in changes in testate amoebae assemblages.

The use of testate amoebae poses certain problems that need to be carefully considered when interpreting fossil testate data. Bobrov (1999) suggested that there may be a species signal of the host plant in the testate amoebae species assemblage linked to factors such as the size and of the leaves habit of the plant that they grow on. This would mean that a change in plant communities could trigger a change in amoebae assemblage, which would result in a co-variance between the resulting BSW curves. However, since the change in plant communities are climatically driven, the species signal will in part be as well. Close attention therefore needs to be paid to this feature when interpreting testate amoebae-based reconstructions.

A further problem with testate amoebae-based palaeoclimatic reconstructions is that some species do not preserve very well with time and different species decompose at different rates (Mitchell *et al.*, 2008). Looking at testate amoebae preservation in forest soils, Lousier and Parkinson (1981) discovered that testate amoebae which were made up of cemented particles and those made up of chitinous material were less likely to decompose than those that were made up of pre-formed siliceous plates held together by secretion. This fact might explain why *Euglypha* spp. are largely absent from deep peat profiles. Different *Euglypha* spp. species thrive in a host of hydrological conditions (Section 4.3) and their presence in reconstructions would add valuable palaeohydrological information. Selective species decomposition can, therefore, be a problem when looking at fossil assemblages (Charman, 2001). This problem was investigated further with laboratory experiments and extended field observations by Swindles and Roe (2007) and Mitchell *et al.* (2008). Mitchell *et al.* (2008) found that the experiments carried out by Swindles and Roe over-exaggerated the possible acidity of ombrotrophic peat bogs by 3 pH units and were therefore not

very representative of real conditions. Mitchell *et al.* (2008) demonstrated that conditions in ombrotrophic peat are suitable for testate amoebae preservation and that preservation issues do not influence palaeoclimatic interpretations from ombrotrophic peat.

2.2.2.1 Testate amoebae-based transfer functions

The use of transfer functions in reconstructing BSW curves and to quantify water table fluctuations from testate amoebae data is widely used around the globe. Transfer functions quantify biostratigraphic information into a single hydrological index, which can then be compared between sites (Charman *et al.*, 1999). Testate amoebae-based palaeohydrological transfer functions have been created for the UK (Woodland *et al.*, 1998), Europe (Charman *et al.*, 2007), New Zealand (Charman, 1997; Wilmshurst *et al.*, 2003), Newfoundland (Charman and Warner, 1997), parts of the USA (Booth, 2002; Booth, 2008), Turkey (Payne *et al.*, 2008), Ireland (Swindles *et al.*, 2009), Alaska (Payne *et al.*, 2006) and Poland (Lamentowicz *et al.*, 2008). Wilmshurst (2003), however, questioned the use of testate amoebae-based transfer functions, highlighting in particular the absence of some modern analogues for species that are very abundant in the peat stratigraphy. It has been noted by Woodland (1998) that *Difflugia pulex*, a species that can largely dominate sections of fossil peat was absent from her transfer function because not enough modern occurrence had been counted. This shortcoming of transfer functions was addressed by Charman (2007), who ensured that sufficient modern analogues of all species found commonly in the fossil record were counted. To successfully apply transfer functions to fossil datasets it is important that indicator species and species that are relatively abundant in the fossil record are represented in the training set. Given the

frequent abundance of *D. pulex* in fossil data and its absence from the training set, the UK testate amoebae transfer function (Woodland *et al.*, 1998) is rarely used. Most reconstructions in Europe, in the absence of a local function, use Charman *et al.*'s (2007) European training set. A review of problems associated with using a transfer function from a different geographical region or one that spans a very large geographical area is presented in Chapter 4, where a transfer function for south-central Sweden is presented. With advances in understanding of modern testate amoebae ecology and improvement to transfer function models, testate amoebae have now become an integral part of peat-based palaeohydrological reconstructions.

To ensure that testate amoebae-based palaeohydrological reconstructions from a single peat core are representative of hydrological changes on the entire bog, Hendon *et al.* (2001) carried out work on duplicate cores from Coom Rigg Moss and Butterburn Flow. Their work showed that testate amoebae records from a single peat core are representative of a whole bog and can be compared with records from other bogs (Figure 2.3). Climatic influences on testate amoebae assemblages were shown to be more significant than autogenic bog processes, which have a relatively minor control. Charman *et al.* (2007) suggested problems of general peatland functioning (e.g. differences between cores) are more problematic than details of functioning. Since water table reconstructions are an absolute measure, simply looking at a single point on the bog can be problematic because of the hummocky nature of the bog. It is more important to look at the changes and the rate of change in the signal, so that inferences can be made about the entire site.

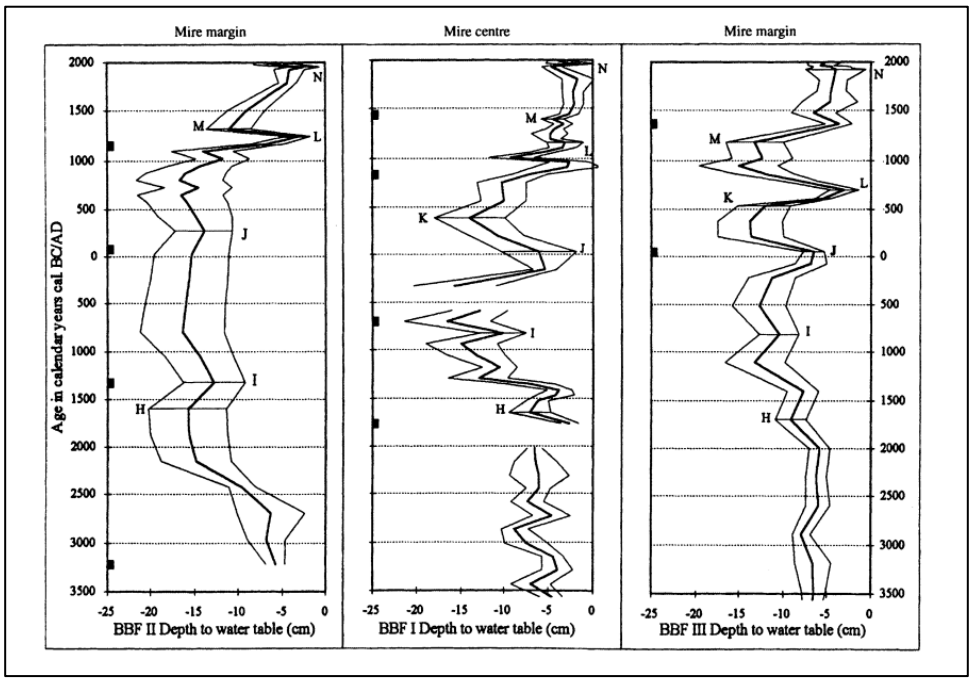

Figure 2.3 - Water table curves for Butterbum Flow from 3500 cal. BC to present, showing mean reconstructed water table values with RMSE of predictions based on 1000 bootstrap cycles. (Source: Hendon *et al.*, 2001)

2.2.3 Other proxy sources of palaeoclimatic information

Pollen analysis of peat deposits is a well-established proxy source of palaeoenvironmental change (von Post, 1916; Godwin, 1940; Iversen, 1941; Jessen, 1949; Seppä and Birks, 2001; Birks and Birks, 2004; Langdon *et al.*, 2004; Birks and Seppä, 2010; Bartlein *et al.*, 2011). Its use in BSW reconstruction, however, is limited (e.g. Tipping, 1995a; Tipping, 1995b; Tipping, 1995c). Pollen modelling and comparisons with modern analogues have made palynology a suitable source of broad palaeo-temperature information (e.g. Huntley, 1991; Prentice *et al.*, 1996; Peyron *et al.*, 1998; Seppä and Birks, 2001; Huntley *et al.*, 2002). The studies of Davis *et al.* (2003), Antonsson and Seppä (2007) and Seppä *et al.* (2009) serve as a

very good indicator for broad temperature shifts for the entire study area. However, using pollen as an indicator of climatic change is an involved process and requires large counts and stacking of records (Birks and Seppä, 2004) and it is therefore beyond the scope of this thesis.

Changes in BSW can also be reconstructed using colorimetric peat humification (Aaby, 1976; Blackford and Chambers, 1991; Blackford and Chambers, 1993; Borgmark, 2005; Borgmark and Wastegård, 2008; Hughes *et al.*, 2012), which determines changes in the extent of decay of plant material and the related by-products of this breakdown, such as humic acids. It is believed that more aerated peat breaks down to a larger extent than waterlogged peat (Weber, 1900; Blackford and Chambers, 1993; Chambers *et al.*, 1997; Chambers and Blackford, 2001; Chambers *et al.*, 2012). However, it is still unclear which forcing mechanism (e.g. summer temperature, winter precipitation) underlies the humification signal and there is still disagreement in the literature about the driving factors. It has been suggested that the degree of peat humification is largely a function of local climatic variables (Blackford and Chambers, 1991; Blackford and Chambers, 1993; Chambers *et al.*, 1997; Chambers and Blackford, 2001; Chiverrell, 2001; Borgmark, 2005; Andersson and Schoning, 2010; Chambers *et al.*, 2012; Swindles *et al.*, 2012b) and a plant species signal (Overbeck, 1947; Yeloff and Mauquoy, 2006; Hughes *et al.*, 2012). In hyper-oceanic settings, where moisture supply is relatively constant, temperature will play a larger role in driving peat humification, whereas in continental settings a mixture of both will have a big impact. Given the uncertainties regarding peat humification and the link to autogenic processes, the method was not applied to the data presented in this thesis.

Geochemical analysis of peat can be used to determine the timing of the separation of the growing surface from ground water sources (Franzén, 2006; Franzén and Cropp, 2007), information about anthropogenic inputs (Renson *et al.*, 2008) and dust deposition (De Vleeschouwer *et al.*, 2007; De Vleeschouwer *et al.*, 2009). Furthermore, it can give clues about possible influences of nutrients and metals on plant species communities (Hughes *et al.*, 2007). In recent years, work has been carried out to reconstruct climate changes from variations in peat geochemistry (De Vleeschouwer *et al.*, 2007; De Vleeschouwer *et al.*, 2012). However, it remains difficult to directly link geochemical changes in the peat to changes in climate; as a result no geochemical analyses were carried out on the cores.

The isotopic composition of *Sphagnum* leaves also holds a wealth of palaeoenvironmental information (Moschen *et al.*, 2009; Brader *et al.*, 2010; Daley *et al.*, 2010; Daley *et al.*, 2011; Moschen *et al.*, 2011). *Sphagnum* moss does not fractionate water molecules and reflects the isotopic composition of rainwater (Daley *et al.*, 2009) which can be linked to climatic conditions. Daley *et al.* (2009) showed that the analysis of stable isotopes ^{18}O and ^{2}H can be used to determine the moisture source of inputs into the system. However, the method for isolating and preparing *Sphagnum* leaves for analysis is very time consuming and costly. Given the time constraints on this project, stable isotope analyses were not carried out in order to allow for plant macrofossil and testate amoebae analyses to be performed on multiple sites.

2.3 The European climate system

The two main climatic parameters that control effective precipitation, and hence BSW on northwest European bogs, are atmospheric moisture availability and temperature (Barber and Langdon, 2007; Charman, 2007; Charman *et al.*, 2009). An understanding of the influences on the European climate system is therefore essential for understanding palaeoclimates. The climatology of northwest Europe, however, is very complex and is influenced by the interplay of several large scale air masses, frontal depressions and anticyclones, as well as oceanic heat transport, distance from the North Atlantic, topographic influences, orbital parameters and solar output.

European climate is controlled by the meeting of several large opposing air masses: wet and cold polar maritime (mP) and arctic maritime (mA); warm and moist tropical maritime (mT); hot and dry tropical continental (cT); cold in winter and hot in summer and dry polar continental (cP). The interplay of these air masses influences temperatures and moisture availability across northwest Europe at any given time. This relationship can change on a weekly basis and their exact interaction cannot be reconstructed from the peat archive. However, prevailing air mass influences over longer timescales can be determined and form the basis for BSW reconstructions.

Given the proximity to the North Atlantic, most sites in 'oceanic' northwest Europe will be predominantly influenced by maritime mP, mA and mT air masses (O'Hare *et al.*, 2005). The most important interaction between two air masses in this sector is between the mP and mT air masses, which meet over the North Atlantic (Barry and

Chorley, 2010). The boundary where these two systems collide is called the Polar Front along which mid-latitude frontal depressions are formed that bring moisture to the European continent. The latitudinal position of the Polar Front shifts during the year and, correspondingly, the position of the North Atlantic frontal depressions that make landfall across northwest Europe. It is the position of the Polar Front and associated depressions that is the dominant precipitation-controlling feature for northwest Europe (O'Hare *et al.*, 2005).

2.3.1 Atmospheric circulations

As a result of the Coriolis effect strong Atlantic Westerlies, which bring moisture from the North Atlantic, make landfall in northwest Europe. They are a major source of moisture transport to northwest Europe and their position and strength varies greatly through the seasons (Barry and Chorley, 2010). Magny *et al.* (2003b; 2006) demonstrated that sea ice-driven changes in the position of the westerlies can lead to a tripartite division of moisture availability across Europe that shows up in the palaeo-record. During extreme climatic anomalies, such as the '8.2k' event, the northern boundary of this mid-European wet zone was located around 50ºN (Magny *et al.*, 2003b) (Figure 2.4). Magny *et al.* argue that during less severe sea surface temperature (SST) anomalies, the northern climate divide is centred on 58ºN. The placement of this boundary, however, is based on very few data points, with none north of 55ºN in the British Isles. This thesis aims to address this shortcoming by reconstructing BSW changes from four bogs located between 55ºN and 59ºN (Research Question Q2).

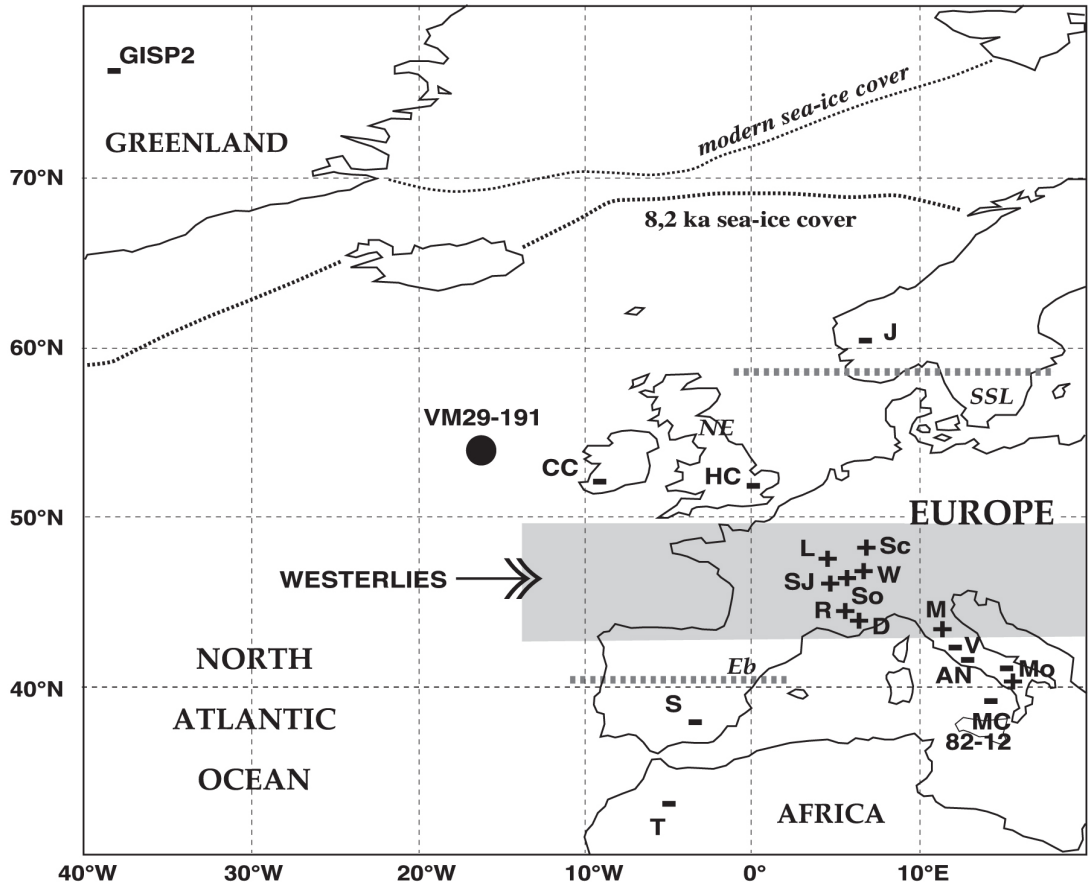

Figure 2.4 – Extent of the mid-European wet zone. The grey box indicates northern and southern limits of the wet zone during the '8.2k' event, the thick dotted lines indicate the latitudes of the climatic divide during less pronounced SST anomalies. (Source: Magny *et al.*, 2003b). [AN = lakes Albano and Nemi; CC = Crag Cave; D = Durance valley; HC = Holywell Coombe; J = Jostedalsbreen; L = Le Locle; M = Lago di Mezzano; Mo = Lago Grande di Monticchio; R = middle Rhone valley; S = lake Siles; Sc = Schleinsee; SJ = Saint-Jorioz; SO = Soppensee; T = lake Tigalmamine; V = Lago di Vico; W = Wallisellen]

Two jet streams are responsible for accelerating prevailing westerly winds and driving storm tracks across Europe. The sub-tropical jet, which sits predominantly over northern Africa and southern Europe, is created by the poleward momentum associated with the Hadley circulation. During the summer months, it can sit as far north as mid-latitude Europe. In addition to the sub-tropical jet stream, there exists an eddy-driven jet stream, which sits further north around 60ºN. It is created by

transient eddies, which are pervasive in the troposphere and lead to vorticity and heat transport, accelerating westerly storms tracking across the North Atlantic (Hoskins *et al.*, 1983). Atmospheric circulation patterns and the jet streams are largely driven by the pressure gradient between the Icelandic Low and Azores High (O'Hare *et al.*, 2005). Both these pressure systems exist throughout the year, although their location and intensity changes considerably through the seasons. As temperature largely affects the strength of the gradient, the strength of the Westerlies decreases by over half during the summer months compared with the winter. The eddy-driven jet and the Polar Front largely control the intensity and position of the weather fronts hitting Europe. They are responsible for the largest variability in weather owing to their seasonal north-south shift (Thompson *et al.*, 2002a; Vallis and Gerber, 2008). This shift can result from small changes in sea-level pressure gradients. Similar to the weakening of the Iceland-Azores pressure gradient during the summer months, the weakening of the equator-pole temperature gradient results in a northward shift of both jets.

Storm tracks are also important and a common feature of European climate. Storm tracks originate in eastern North America and track across the North Atlantic, picking up moisture. These cyclonic systems are part of an important heat transport system that transfers warm air from the tropics to northwest Europe. In the summer months, the storm tracks are weaker, again as a result of the weakened equator-pole temperature gradient, and they tend to sit further north. However, in the eastern Atlantic the position of the storm tracks only shifts marginally, when compared with the western Atlantic, and generally sit between 50ºN and 65ºN during the summer months (Seppä and Birks, 2001). Storm tracks sit over Scotland in the summer and

over southern England in the winter. When compared with the winter, depressions in the summer are often less intense and the reduced air mass contrast produce weaker fronts. Summer rainfall is often associated with more localised convection cells as well as storm tracks.

2.3.2 Oceanic influence on European climate

Northwestern Europe lies downstream from large oceanic currents that transport heat from tropical latitudes to northern latitudes. One of the most important factors influencing European climate is the meridonal overturning circulation (MOC), which transports warm water from the tropics to northern latitudes, creating mild conditions along the eastern North Atlantic seaboard. Winter temperatures in northwest Europe are approximately 11ºC warmer than would be expected for the latitude (Barry and Chorley, 2010). This thermohaline circulation-driven heat transport was investigated by Allen *et al.* (2007), who showed that warm waters are transported as far north as northern Finnmark via the Norwegian Current during periods when the THC is strong. When polar and Arctic air masses around Iceland come into contact with warm THC-driven seawater, air temperatures can rise by as much as 9ºC. Heat is exchanged between adjacent air masses, warming them up and therefore allowing them to carry more moisture. The THC has weakened during periods throughout the Holocene (Bianchi and McCave, 1999; Broecker, 2000), following large-scale fresh water inputs into the North Atlantic (Barber *et al.*, 1999), which had cooling effects on northwest Europe. A major THC slowing event occurred around 5.3 kyr BP, resulting in lower annual temperatures across Europe (Haas *et al.*, 1998; Heikkila and Seppä, 2003; Magny and Haas, 2004).

2.4 Environmental change during the early- to mid-Holocene

The Holocene can generally be divided into three main periods (Marchal *et al.*, 2002; Wanner *et al.*, 2008) that relate to different climatic conditions. The first of these periods, the early Holocene is characterised by reorganisation of the climate system after the last glaciation and high solar insolation caused by a peak in precession from 11600 BP to 9000 BP. The following phase, known as the Hypsithermal or Holocene Thermal Maximum, encompasses the mid-Holocene and includes the warm Atlantic Blytt-Sernander chronozone. This period is sometimes also referred to as the Holocene Climatic Optimum and lasted from 9000 BP to *c*. 5400 BP. Wanner *et al.* (2008) attempted to put age constraints on HTM; however, the timing of the period is highly dependent on geographical location (Kaufman *et al.*, 2004). The final period of the Holocene is from around 5400 BP to present (Marchal *et al.*, 2002), characterised by near-modern climatic conditions in northwest Europe. Studying the transition between the latter two periods is the main subject of this thesis as only very few reconstructions of BSW cover this transition in high resolution. The late-Holocene, from 5400 BP to present, is also referred to as the Neoglacial period as it is characterised by sizable glacial advances in the Alps (Deline and Orombelli, 2005) and across Scandinavia (Nesje and Dahl, 1993; Matthews *et al.*, 2005).

A major environmental climate-driving parameter on a global to local scale is the earth's position in relation to the sun and the amount of solar radiation that is consequently received. Originating from the Earth's wobble around its own axis (precession) coupled with the wobble in the Earth's tilt (obliquity) in relation to its rotational axis and the circularity of the Earth's orbit (eccentricity), the amount of

solar radiation received by any point in the Northern Hemisphere follows a cyclic shift (Milankovitch, 1941; Imbrie *et al.*, 1993; Davis and Brewer, 2009). These predictable changes in the amount of radiation received together with the changing trajectory of the Earth around the sun have been modelled by Berger (1978). Berger showed that the amount of solar energy reaching the Earth follows simple equations and can therefore be reconstructed for the past and predicted for the future. These calculations, however, do not take into account short-term variation in solar activity. Berger's calculations showed that following an early-Holocene maximum, a steady decline in insolation ensued with maximum variability during the mid-Holocene (Figure 2.5 – Label A) across northwest Europe (Berger and Loutre, 1991; Debret *et al.*, 2009).

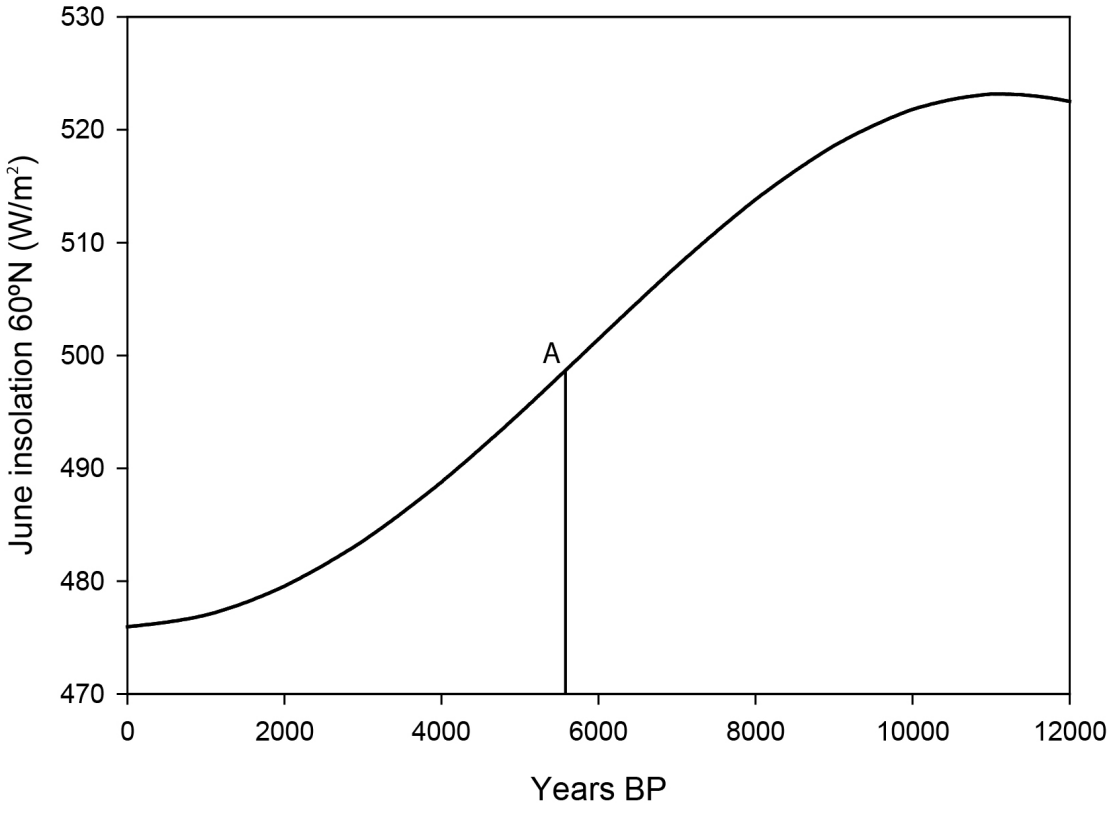

Figure 2.5 - 60ºN insolation for mid-month June. Point 'A' indicates time of maximum insolation variability – after Berger and Loutre (1991)

The early-Holocene was a period that saw the largest environmental changes since the last deglaciation with the final waning of the large Devensian ice sheets which covered large parts of North America and Scandinavia (Dyke and Prest, 1987; Kleman *et al.*, 1997), associated rises in sea level from meltwater (Fairbanks, 1989; Lambeck, 1990; Rinterknecht *et al.*, 2006), atmospheric reorganisation as a result of the disappearing high pressure systems over the ice sheets (Seppä and Birks, 2001) and the reorganisation of ocean currents (Fairbanks, 1989; Broecker, 2003). The Fennoscandian ice sheet had largely melted away by 9000 BP (Hyvärinen, 1973), making way for kettle holes and depressions that were left behind to be filled in, and for peat formation to initiate. The continuous melting and final collapse of the Laurentide ice sheet culminated in the catastrophic release of blocked up melt-water from Lake Agassiz into the North Atlantic Ocean approximately 8450 – 8200 years ago (Alley *et al.*, 1997; Barber *et al.*, 1999; Nesje and Dahl, 2001). The consequent influx of freshwater into an area of North Atlantic Deep Water formation (Figure 1.1) had a significant effect on the strength of the North Atlantic Overturning Circulation and the associated global oceanic circulation patterns (Renssen *et al.*, 2001; Renssen *et al.*, 2002; Wiersma and Renssen, 2006; Daley *et al.*, 2011). The slowing of the THC brought about very cold conditions in northwest Europe that saw the advance of Scandinavian glaciers around 8200 BP during the so-called 'Finse Event' (Matthews *et al.*, 2005; Nesje *et al.*, 2006; Nesje, 2009), highlighting the influence of the thermohaline circulation on northwest European temperatures (Fairbanks, 1989; Barber *et al.*, 1999; Broecker, 2000; Palastanga *et al.*, 2011). Once rapid sea level rise had ceased, at around 7000 BP (Section 2.4.1), the impact of further sea level change on inland northwest European bogs was minimal as oceanic climate conditions and large moisture source areas had been established.

2.4.1 Eustatic sea level rise

The waning of the continental ice over Scandinavia and North America had a profound effect on the North Atlantic and on global sea levels. Using evidence from corals in Barbados, Fairbanks (1989) estimated an increase in eustatic sea level of about 120 m since the last glacial maximum (LGM). Using a series of reconstructions from around the world a rise of approximately 120 m has been confirmed (Lambeck, 1990; Peltier, 2002; Peltier and Fairbanks, 2006). After a series of melt water pulses (Fairbanks, 1989), the speed of global sea level rise slowed considerably since between 7000 BP and 6500 BP (Fairbanks, 1989; Lambeck, 1990; Fleming *et al.*, 1998; Keigwin *et al.*, 2006; Behre, 2007; Bird *et al.*, 2007; Smith *et al.*, 2011) in line with the disappearance of the North American ice sheets (Lambeck, 1990). However, not all of the inputs came from the melting of the large Northern Hemisphere ice sheets. Antarctic melt and melt from the Barents and Kara ice sheets are likely to have contributed notably (Lambeck, 1990; Shennan *et al.*, 2002). Since the end of the major sea level rise in the mid-Holocene, global sea levels have been rising at a much slower rate, amounting to a total rise of between 3 m (Fleming *et al.*, 1998; Shennan *et al.*, 2000; Bird *et al.*, 2010) and 10 m (Lambeck, 1990; Behre, 2007).

In addition to changes in ocean circulations and associated atmospheric patterns, eustatic sea level rise during the early- to mid-Holocene had a large impact on northwest European climate. Rising sea levels resulted in closer proximity to the ocean of previously more continental sites (Waller and Long, 2003). The flooding of the North Sea at around 9200 BP to near modern conditions by 8000 BP (Behre, 2007) led to sites in the Belgian Ardennes and central Scandinavia being influenced

by maritime climate conditions. Furthermore, with rising sea levels across the European continental shelf the surface area of the North Atlantic increased, providing more area for storm tracks and frontal depressions to gather moisture to transport to continental Europe (Smith *et al.*, 2011).

2.4.2 Holocene thermal maximum

The Holocene Thermal Maximum was a period in the mid-Holocene of higher than present temperatures in northwest Europe. This maximum in temperature has been recorded in many sites across the northern hemisphere (e.g. Seppä and Birks, 2001; Davis *et al.*, 2003; Kaufman *et al.*, 2004; Moros *et al.*, 2004; Seppä *et al.*, 2005; Caseldine *et al.*, 2006; Kaplan and Wolfe, 2006; Antonsson and Seppa, 2007; Axford *et al.*, 2007; Knudsen *et al.*, 2008; Litt *et al.*, 2009; Renssen *et al.*, 2009; Pyne-O'Donnell, 2011; Salonen *et al.*, 2011; Edvardsson *et al.*, 2012) and its timing and drivers are subject to much debate. It is generally accepted that the early Holocene insolation maximum was largely responsible for increased temperatures (Kaufman *et al.*, 2004; Seppä *et al.*, 2005; Axford *et al.*, 2007; Renssen *et al.*, 2009). However, the HTM did not occur synchronously across the northern hemisphere and its time-transgressive nature has been documented in previous research (e.g. Kaufman *et al.*, 2004; Kaplan and Wolfe, 2006; Salonen *et al.*, 2011). In their summary paper looking at evidence of the HTM in the western Arctic, Kaufman *et al.* (2004) showed that there was a clear east-west lag in the onset and termination of the HTM, which was largely a result of the lingering Laurentide ice sheet. The remains of the LIS were shown to have affected SST and atmospheric temperatures, delaying the HTM in eastern Canada until the mid-Holocene. The influence of the continental ice on the HTM showed that although orbital forcing played a major role

in driving Holocene temperature, other environmental factors also strongly influence regional temperature (Seppä and Birks, 2001; Davis *et al.*, 2003; Kaufman *et al.*, 2004; Moros *et al.*, 2004; Seppä *et al.*, 2005; Salonen *et al.*, 2011). Using pollen-based temperature and precipitation reconstructions from northwest Finland, Seppä and Birks (2001) highlighted the influence of regional environmental mechanisms on the timing of the HTM. They showed that the North Atlantic ocean-atmospheric circulation played a key role in shaping Holocene climate in northern Europe and that long-term insolation patterns were subordinate. As a result of the predominantly westerly airflow being replaced by more meridonal flow patterns after the '8.2 k' event and the development of predominantly anti-cyclonic summer conditions, precipitation was shown to have dropped significantly during the HTM. Pollen reconstructions from a lake in northern Finland, a region sensitive to changes in the strength of the thermohaline circulation, place the temperature maximum between 7950 BP and 6750 BP (Seppä and Birks, 2001). Temperatures were 1.7 ºC warmer during this period than at present. However, in accordance with Kaufman *et al.*'s model of a time-transgressive HTM, the HTM did not manifest synchronously and to the same extent across northwest Europe.

Using evidence from 500 pollen-based temperature reconstructions, Davis *et al.* (2003) created summer and winter temperature curves as well as mean annual temperature curves. Their findings showed that the HTM was most pronounced in the northern European sectors and that a mid-Holocene cooling took place in southern Europe. Northwest and central-west Europe had a clear temperature maximum around 6000 BP when temperatures were 1.5 ºC warmer than present (Figure 2.6). In southern Scandinavia, the temperature difference was even greater

with conditions approximately 2.5ºC-3ºC warmer than present (Antonsson and Seppa, 2007). Davis *et al.* further showed that the HTM was predominantly a summer signal and that there was a major spatial and seasonal difference in Holocene temperatures.

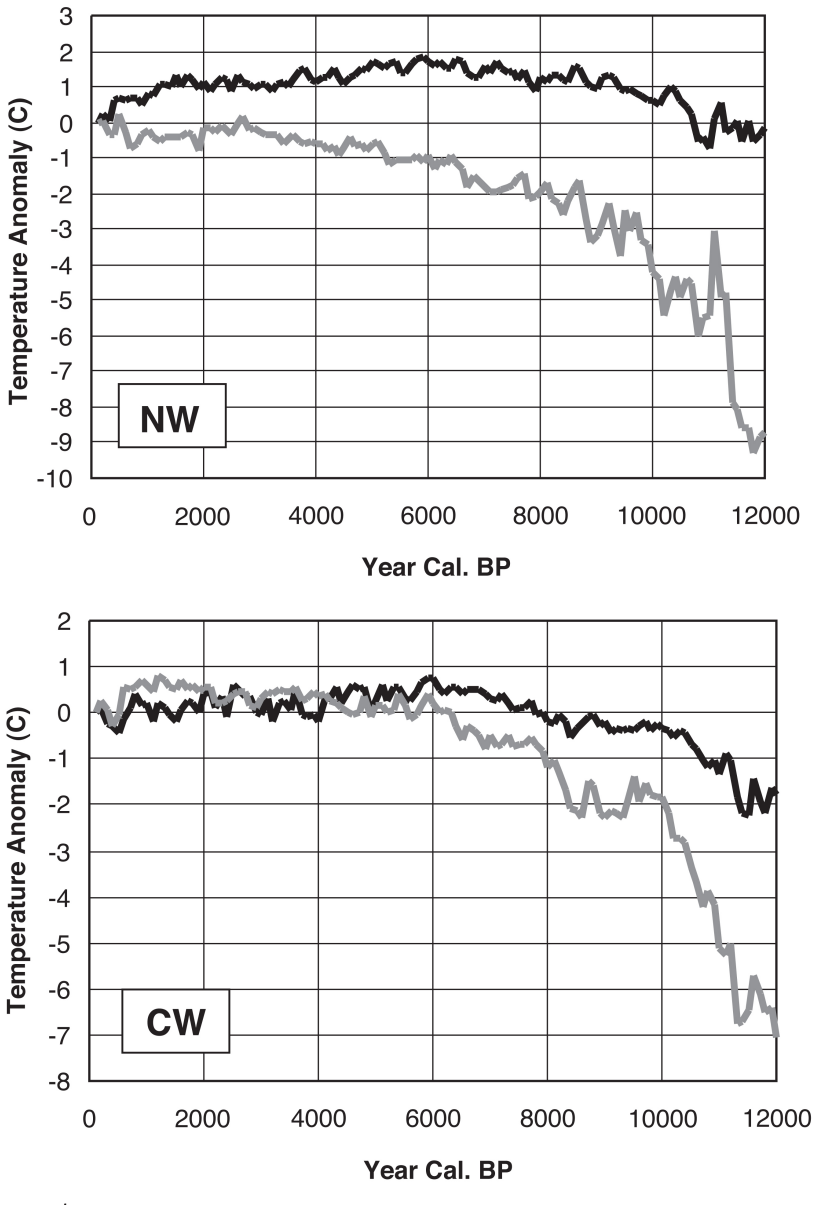

Figure 2.6 - Pollen-based temperature reconstructions for northwest and centralwest European sectors by Davis *et al.* (2003). Dark line shows summer temperatures and light line shows winter temperatures.

The majority of temperature reconstructions across Europe and the eastern North Atlantic place the onset of the HTM between 8000 BP and 7000 BP and the end between 6700 and 6000 BP. Seppä *et al.* (2005), however, showed that a longer HTM existed across south-central Sweden with temperatures up to 2.5 ºC warmer than present from 8000 BP until 4300 BP. This stands in contrast to Edvardsson *et al.*'s (2012) findings of a HTM in south-central Sweden that lasted from 7200 BP to 5750 BP, based on pine trees found in peat bogs. Seppä *et al.* also showed that atmospheric blocking of anti-cyclonic circulation during the summer months was responsible for the mid-Holocene temperature maximum. The period was characterised by warm and dry conditions, which came to an abrupt end around 4300 BP, when cool and wet conditions set in. By stacking 36 Holocene pollen-based July mean temperature records and comparing them to independent chironomid-inferred temperature reconstructions, Seppä *et al.* (2009), revised their timing of the HTM and noted that it dated to 8000-4800 BP in northern Europe. Seppä *et al.* furthermore showed that the HTM was not a period of uninterrupted warm conditions and that cold anomalies existed at 7000 BP, 5300 BP and between 3800-3000 BP. Brown *et al.* (Brown *et al.*, 2012) supported these findings and showed that the HTM existed in southern Sweden between 8000-4500 BP (> 2.0 ºC) with maximum warmth from 6700 BP to 5400 BP (> 2.5 ºC).

The exact cause the HTM still remains to be fully explored. However, the current consensus is that overlying an orbital forced insolation maximum (Kaufman *et al.*, 2004; Moros *et al.*, 2004; Wanner *et al.*, 2008; Renssen *et al.*, 2009), North Atlantic SST and thermohaline circulation intensity (Moros *et al.*, 2004; Caseldine *et al.*, 2006) coupled with atmospheric circulation (Seppä and Birks, 2001) and anti-

cyclonic blocking (Seppä *et al.*, 2005) were responsible for creating a thermal maximum across northwest Europe between 8000 BP and 4500 BP. It is likely that the melting of the LIS and the consequent '8.2 k' event delayed the onset of the HTM across Europe by slowing down the thermohaline circulation and reducing North Atlantic SST (Knudsen *et al.*, 2008; Renssen *et al.*, 2009; Salonen *et al.*, 2011).

As shown by Davis *et al.* (2003) and Moros (2004), the HTM was linked to summer temperatures across Europe. Together with the increased seasonality resulting from higher insolation, the summer water deficit is likely to have been higher during the HTM. Higher temperatures and reduced precipitation (Seppä and Birks, 2001) will have reduced BSW on northwest European bogs (e.g. Hughes *et al.*, 2000a; Barber *et al.*, 2003; Langdon *et al.*, 2003). However, as discussed above, the HTM did not occur synchronously across Europe and the data from the thesis will allow for a more detailed picture of the spatial (Research Question Q3) and temporal (Research Question Q4) extent of the HTM.

2.5 Climate cycles

The most prominent and best-documented climatic cycles are those relating to the Earth's changing position relative to the sun. Three main cycles, namely the precession, obliquity and eccentricity cycles were originally calculated in magnitude and linked to changes in the Earth's climate by the Serbian mathematician Milutin Milankovitch (Milankovitch, 1941). These cycles with a periodicity of 400k, 110k, 41k and ~26k-23k years reflect changes in the amount of solar radiation received by

locations on the planet. The longest of these cycles is believed to be primarily responsible for driving glacial cycles during the past 2.6m years (Hays *et al.*, 1976; Imbrie and Imbrie, 1980; Imbrie *et al.*, 1993; Jouzel *et al.*, 2007). The shorter 41k and ~23-26k cycles have been shown to have a stronger effect on global climate (Davis and Brewer, 2011). The cycle with the most pronounced variability over the studied time period reflects the precession in the Earth's axis of rotation and has a periodicity of ~23-26k years. It manifests itself as a latitudinal change in insolation and is believed to be responsible for driving European climate during the early part of the Holocene (COHMAP, 1988; Guiot *et al.*, 1993; Wanner *et al.*, 2008; Shuman and Plank, 2011).

2.5.1 Millennial-scale climate cycles

Superimposed on the orbital Milankovitch cycles are faster-paced climate cycles of millennial-scale frequency. O'Brien *et al.* (1995), amongst others, questioned whether these centennial- to millennial-scale climate variations during the Holocene were cyclic or not. Using measurements of soluble impurities in Greenland ice, O'Brien *et al.* (1995) demonstrated that Holocene atmospheric circulation above the ice cap was punctuated by a series of millennial-scale shifts. This supported Denton and Karlen's (1973) suggestions, based on glacial advances and retreats, that Holocene climate followed regular millennial scale cyclicity, and Fairbridge and Hilliare-Marcel's (1977) findings of predominant climate modes on a millennial timescale. Based on the findings by Denton and Karlen (1973) and O'Brien (1995), Bond *et al.* (1997) investigated petrologic tracers of drift ice in the North Atlantic for evidence of millennial-scale cyclicity (Figure 2.7). Sampled at 50- to 100-year resolution the results suggested that a quasi-periodic 1500-year cycle was present

throughout the Holocene (Bond *et al.*, 1997; Bond *et al.*, 2001). Episodes of increased ice rafting at 1400, 2800, 4200, 5900, 8100, 9400, 10300 and 11000 BP became known as 'Bond Events'.

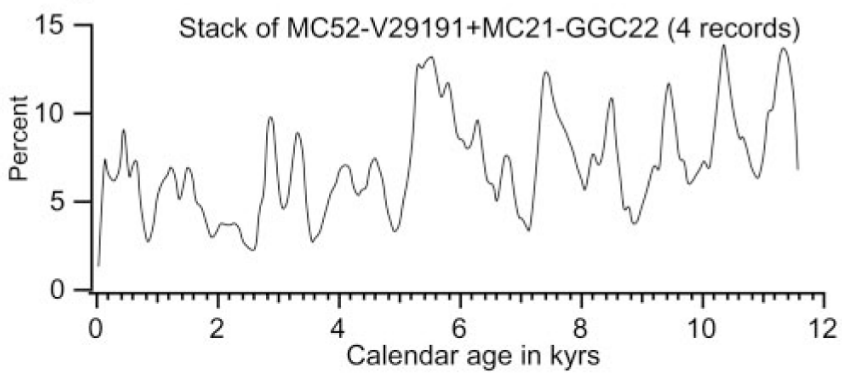

Figure 2.7 - Stacked record of Holocene drift ice in the North Atlantic presented as percentage variations in petrologic tracers (Source: Bond *et al.*, 2001)

Using datasets with robust, high-resolution chronologies, these millennial-scale climate cycles have since been identified in the terrestrial (e.g. Barber *et al.*, 1994; Hughes *et al.*, 2000a; Viau *et al.*, 2002; Langdon *et al.*, 2003; Yu *et al.*, 2003; Turney *et al.*, 2005), lacustrine (e.g. Hu *et al.*, 2003; Baker *et al.*, 2005; Russell and Johnson, 2005; Yu *et al.*, 2006; Allen *et al.*, 2007), glacial (e.g. Denton and Karlén, 1973; Fairbridge and Hillairemarcel, 1977; O'Brien *et al.*, 1995; Stuiver *et al.*, 1995) and marine (e.g. Bond and Lotti, 1995; Bond *et al.*, 1997; Bianchi and McCave, 1999; Chapman and Shackleton, 2000; Giraudeau *et al.*, 2000; Bond *et al.*, 2001; Berger and von Rad, 2002) palaeo-records. With the exception of the Pacific area, Australia and Antarctica, proxy evidence of millennial-scale climate cycles is

interpreted to be associated with 'Bond Cycles'. The quasi-1500 year pacing has also been documented in Holocene climate studies in the Tropics (deMenocal *et al.*, 2000; Thompson *et al.*, 2003). Evidence for 'Bond Cycles', however, is still overwhelmingly from the North Atlantic region (Wanner *et al.*, 2008). Analysis of these and other records has prompted a continuing, and still not fully resolved, debate over the driving mechanisms behind this millennial-scale pacing.

Since the pioneering work by Bond *et al.* (1997), many different forcing factors for the millennial-scale pacing have been proposed, such as solar variability (Chapman and Shackleton, 2000; Bond *et al.*, 2001; Renssen *et al.*, 2002; Fleitmann *et al.*, 2003; Hu *et al.*, 2003; Niggemann *et al.*, 2003; Yu *et al.*, 2003; Braun *et al.*, 2005; Gupta *et al.*, 2005; Lamy *et al.*, 2006; Viau *et al.*, 2006; Allen *et al.*, 2007), ocean internal dynamics (Bianchi and McCave, 1999; Broecker, 2000; Paul and Schulz, 2002; Renssen *et al.*, 2002; Turney *et al.*, 2005; Schulz *et al.*, 2007), ice-sheet dynamics (van Kreveld *et al.*, 2000), tidal forcing (Berger and von Rad, 2002) and atmospheric processes linked to the North Atlantic Oscillation (NAO) (Giraudeau *et al.*, 2000). Orbital forcing of the pacing can be ruled out given its long periodicity.

In order to fully understand the driving mechanisms behind the millennial-scale climate cycle, the nature of the cyclicity needed to be explored further. Schulz and Paul (2002a; 2002b), Moros *et al.* (2006) and Debret *et al.* (2007; 2009) questioned the uniformity of the temporal structure and spatial representation of the Bond events. Consequently, the previously held belief of a single pervasive 1500-year Holocene climate cycle as an extension of the Dansgaard-Oeschger events (Bond *et al.*, 1997; Ditlevsen *et al.*, 2007) was scrutinised. Using sophisticated wavelet analysis, Debret *et al.* (2007) demonstrated that not one, but three millennial-scale

cyclicities are present in the Holocene climate history, of 1000-, 1500- and 2500-year duration respectively. This supported previous studies that had independently described these cycles (Stuiver and Braziunas, 1993; Bianchi and McCave, 1999; Chapman and Shackleton, 2000; Hughes *et al.*, 2000a). Comparing the original data used by Bond *et al.* (2001) to reconstructions of atmospheric ^{14}C and ^{10}Be production, which is considered a proxy source of solar variability data, Debret *et al.* (2009) concluded that solar forcing was the driving mechanism behind the 1000- and 2500-year cycles. The wavelet analysis further demonstrated that a shift in dominant climate cycle occurred during the Holocene. During the mid- to late-Holocene, when the influence of meltwater pulses on North Atlantic Ocean circulations had ceased, the 1500-year climate cycle, which is believed to be ocean-internally forced (Bianchi and McCave, 1999; Debret *et al.*, 2007; Debret *et al.*, 2009), became dominant. This phase shift in the climate system was further investigated by Wirtz *et al.* (2010), who integrated 124 proxy time-series of different types into a moving-window Lomb-Scargle analysis, to determine if the shift in system was regionally bound. The results of their analysis, however, showed that a major reorganisation in variability of the climate system and a shift in periodicity of the prevailing millennial-scale climate cycles was a global event. A further review of evidence of millennial-scale climate change is given in Wirtz *et al.* (2010) and Wanner and Bütikofer (2008). However, neither study included evidence from BSW reconstructions to determine the extent of millennial-scale climate cycles. This thesis will address this shortcoming by comparing palaeoclimatic reconstructions from the peat archive with records of millennial-scale episodes of increased North Atlantic drift ice (Bond *et al.*, 1997; Bond *et al.*, 2001) (Research Question Q1). These comparisons will be

used to determine if millennial-scale climate cycles that have been recorded in other palaeoclimate proxy sources are recorded in the peat archive.

2.5.2 Sub-millennial scale climate cycles

Superimposed on the large-scale millennial climate cycles, a host of periodicities with shorter frequencies on multi-centennial time scales have also been detected (Stuiver *et al.*, 1995; Chapman and Shackleton, 2000; Hughes *et al.*, 2000a; McDermott *et al.*, 2001; Benson *et al.*, 2002; Langdon *et al.*, 2003; Sarnthein *et al.*, 2003; Blundell and Barber, 2005; Turney *et al.*, 2005; Springer *et al.*, 2008; Swindles *et al.*, 2012b). Looking at peat deposits from Walton Moss in Cumbria and comparing them with the adjacent Bolton Fell Moss and other sites, Hughes *et al.* (2000a) identified periodicities of *c.* 1100 years and *c.* 600 years between wet-shifts in the peat stratigraphy. Their work was based on fewer than eight bulk radiocarbon dates per core with additional chronological support from pollen-based cross-correlation to Bolton Fell Moss, Cumbria. Given the linear age-depth relationship of the core, Hughes *et al.* estimated an accumulation rate of 10 years / cm of peat for Walton Moss in order to establish the centennial-scale cyclicity. Further dating of the core by Barber and Langdon (2007) and Daley *et al.* (2010) confirmed the accumulation rate estimates by Hughes *et al.*, supporting the evidence for a *c.* 600 year climate cycle at Walton Moss.

In contrast to Hughes *et al.*'s (2000a) work, Blundell and Barber's (2005) time-series analysis of BSW reconstructions from Tore Hill Moss, Scotland suffered from a short timespan over which the analysis was carried out. Similar to Hughes *et al.*, Blundell and Barber found a cycle of 560 years in the testate amoebae-inferred wet-

shifts from the peat record. However, a record only spanning back the past 2800 years was subject to time series analysis, allowing for a maximum of five full oscillations of the cycle. Furthermore, peat cutting on Tore Hill Moss will have had an impact on the upper part of the site, reducing the possible amount of cycles even further to four.

Sub-millennial scale climate cycles are not a purely terrestrial feature and have also been detected in North Atlantic Ocean cores. Chapman and Shackleton (2000) reconstructed variability in North Atlantic Deep Water (NADW) circulation pattern, using the same core as Bianci and McCave (1999). In addition to the millennial periodicity that Bianci and McCave detected, Chapman and Shackleton identified a 550-year cyclicity in NADW circulation, which appeared to be coherent with fluctuation in atmospheric conditions over Greenland and short-term variations in atmospheric ^{14}C values. This supports the findings by Stuiver *et al.* (1995), who postulated that the 530-year cycle might have solar origins. However, similar to the shortcomings of Hughes *et al.* (2000a), the dating constraints on the core used by Chapman and Shackleton were not tight enough. A total of 16 AMS radiocarbon dates were used to create a chronological framework on a ~14000 year long sequence. With equal spacing and without considering the error margins attached to the radiocarbon assays, the density of dated points along the core is lower than the length of the frequency of the 550-year periodicity.

Similarly, the work by Hu *et al.* (2003), which looked at biological and geochemical analysis in an Alaskan lake, based the chronology of a 10,000 year long sequence on 9 AMS dates and one tephra layer. Hu *et al.* detected periodicities of 135, 170, 195, 435, 590 and 950 years in their palaeoclimatic reconstructions. Given the limited

chronological control, periodicities of less than 500 years should be rejected. Detection of a 590-year cycle is also questionable, but corroborates previous findings of a 550-600 year climate cycle. The dating control on reconstructions within this thesis is robust enough to detect millennial-scale cycles of BSW change. However, the length of the records is insufficient for millennial-scale time series analysis. Instead, BSW anomalies will be compared to well-dated centennial- and millennial-scale Holocene climate cycles (Research Question Q1).

By analysing drought periods in a stalagmite record from West Virginia, Springer *et al.* (2008) hypothesised that the '500-year' climate cycle might be interpreted as a harmonic of the millennial-scale Bond events. Further high-resolution time-series work, however, is still needed to confirm these findings and to determine from which of the three millennial-scale cycles the harmonic originates. Millennial-scale climate variability throughout the Holocene is now considered to be a combination of the 1500-year ocean-internal driven cycle, early Holocene meltwater pulses, the solar driven 1000- and 2500-year cycles and harmonics thereof. The centennial-scale climate cycle is largely believed to be solar forced, based on correlation of atmospheric ^{14}C and ^{10}Be production to changes in NADW and wet-shifts in BSW. Regardless of whether these centennial- to millennial-scale climate events are solar forced (Mauquoy and Barber, 2002; Mauquoy *et al.*, 2008) or ocean-internal driven (Broecker, 2003), they should be contained in the palaeo-peat record, as both drivers influence atmospheric moisture transport (Yu *et al.*, 2009).

2.6 Records of mid-Holocene climate change

2.6.1 Records of bog surface wetness

As discussed above, reconstructions of European BSW changes are largely limited to the mid- to late-Holocene and only a few records exist that go back to the early- to mid-Holocene (Hughes *et al.*, 2000a; Langdon *et al.*, 2003). However, there are a few notable exceptions and several long records of BSW reconstructions do exist from the British Isles and Scandinavia. This thesis aims to supplement these, to build a more complete picture of Holocene climate change across northwest Europe.

Barber *et al.* (2003) analysed a long record from Bolton Fell Moss, an ombrotrophic peat bog in Cumbria, in order to establish a climatic history for the Holocene. However, the peat stratigraphy consisted largely of *Eriophorum vaginatum* for the period from 9800 BP to 6100 BP, indicating dry surface conditions. However, small pockets of *Sphagnum* section *Acutifolia* at 8600 BP, 7800 BP, 7500 BP and 6200 BP indicated intermittent wetting of the site. The first major wetting and open pool phase was not recorded until 4400 BP. Barber *et al.* (2003) extended their earlier work on Bolton Fell Moss by comparing that record to Irish records from Abbeyknockmoy Bog and Mongan Bog in order to establish teleconnection between sites that were nearly 500 km apart (Figure 2.8). Despite being ombrotrophic since 8000 BP, Abbeyknockmoy Bog did not yield much palaeoclimatic information prior to 4500 BP as it was also dominated by *E. vaginatum* and was very dry. However, a clear shift in climatic regime was detected that brought the early-Holocene dry phase to an abrupt end, similar to Bolton Fell Moss. This abrupt climatic shift to wetter

surface conditions is likely to mark the end of the HTM as indicated by Seppä (2005). Mongan Bog was monocotyledon-dominated and dry leading up to 3300 BP.

Also in Cumbria, Hughes *et al.* (2000a) investigated the fen-bog transition and consequent palaeoclimatic changes on Walton Moss, which is situated approximately 2 km from Bolton Fell Moss. Like Bolton Fell Moss, the record from Walton Moss dates to the early-Holocene. However, the site became climatically sensitive around 7800 BP when the dominant *E. vaginatum* was largely replaced by *Sphagnum* spp. Hughes *et al.* noted that wet shifts found in the peat record at 7800 BP, 5300 BP, 4410-3990 BP, 3500 BP and 3170-2860 BP generally agreed very well with evidence of ice-rafted debris in the North Atlantic (Bond and Lotti, 1995; Bond *et al.*, 1997; Bianchi and McCave, 1999). The 5300 BP and 4400 BP wet shifts have also been observed in numerous other peat-based palaeoclimatic reconstructions (e.g. Aaby, 1976; Tipping, 1995a; Gunnarson *et al.*, 2003; Langdon *et al.*, 2003; Hughes *et al.*, 2006; Borgmark and Wastegård, 2008; Edvardsson *et al.*, 2012).

A further notable early- to mid-Holocene record of BSW variability was created by Langdon *et al.* (2003) who carried out a multi-proxy analysis of Temple Hill Moss near Edinburgh (Figure 2.9). The ombrotrophic phase at Temple Hill Moss started at around 7500 BP and a number of wet and dry shifts have been observed in the peat stratigraphy. In addition to the wet shifts at 5300 BP, 4400 BP and 3500 BP found by Hughes *et al.* (2000a) and Barber *et al.* (1994; 2003), further wet excursions existed at 6650 BP, 5850 BP and 3850 BP. Like the Cumbrian sites, Temple Hill Moss was initially dry, with very dry phases at 6850 BP, 6350 BP, 4850 BP and 3700 BP. Comparing the earlier BSW reconstructions with six further Scottish sites, Langdon and Barber (2005) identified wet shifts in Scotland at 4450 BP, 4200 BP,

3600 BP and 3300 BP. The 4200 BP wet anomaly at Longbridge Muir was shown to be the most pronounced shift with a high water table.

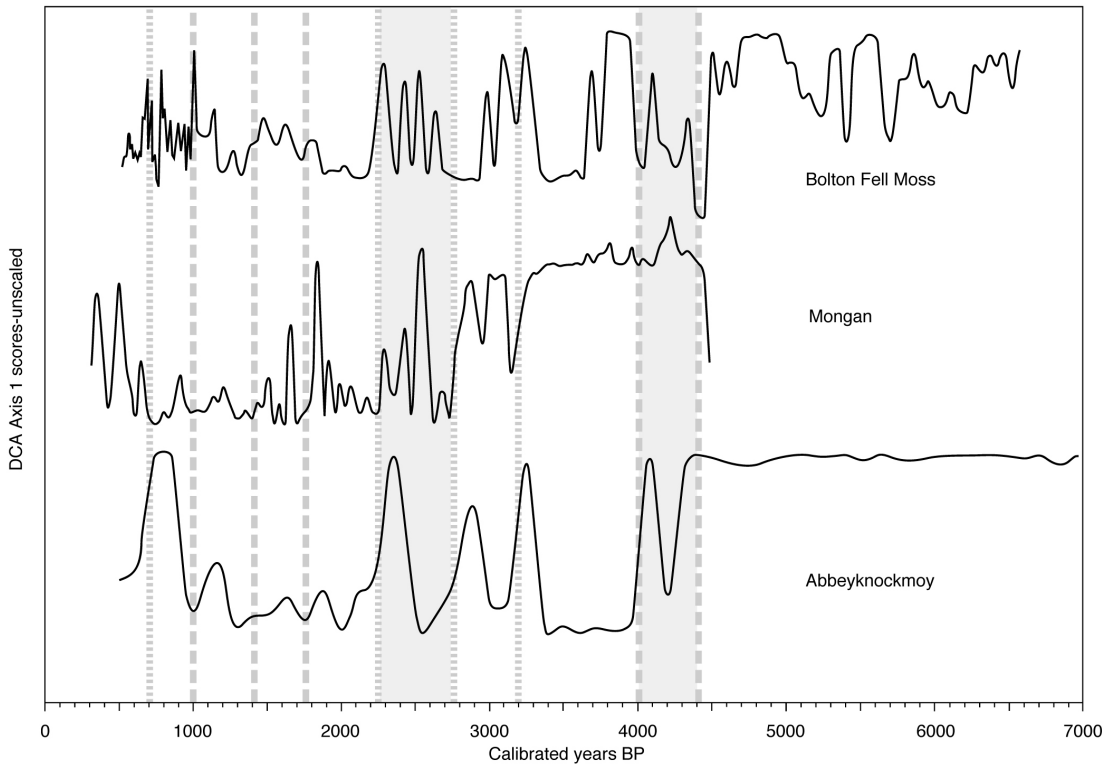

Figure 2.8 - BSW reconstruction for two Irish and a Cumbrian bog highlighting episodes of synchronous BSW change. The shaded area emphasises two major phases of synchronous change *c*. 4400-4000 BP and *c*. 2750-2250 BP (Source: Barber *et al.*, 2003).

Most other reconstructions of early- to mid-Holocene BSW fluctuations come from Scandinavia. In line with tradition (Blytt, 1876; Sernander, 1908), reconstructions of BSW change from the early Holocene onwards are largely based on peat humification in Sweden. Looking at peat humification changes in a sequence from

Draved Mose, Aaby (1976) showed that distinct wet shifts occurred in the past. Mid-Holocene changes to lighter, less humified peat at Draved Mose occurred at 5400 BP, 5050 BP, 4850 BP, 4600 BP, 4300 and 4000 BP. Looking further back in time, Gunnarson *et al.* (2003) analysed the colorimetric peat humification of Stömyren Bog and compared the results to tree ring data in order to identify and compare humidity changes in Fennoscandia. However, Gunnarson *et al.* used 2 cm thick slices for analysis, which average climatic conditions over an approximately 20-year period. Therefore, an additional inherent 20-year error has to be taken into account in the dating of climatic anomalies. The analysis showed that the climate was relatively stable from 7500 BP to 4500 BP, which is largely in line with finding from Seppä *et al.* (2005), and less stable thereafter. Two distinct wet phases during this stable period around 5600-5400 BP and 5200-4900 BP, as well as a clear dry phase between 6900 BP and 6800 BP, were identified. A strong wetting phase from 4200 BP to 4100 BP interrupted much drier conditions that lasted from 4400 BP to 3800 BP. The last mid-Holocene wet shift identified by Gunnarson *et al.* occurred at 3700 BP.

Following on from the work by Gunnarson *et al.* (2003), Borgmark (2005) and Borgmark and Wastegård (2008) continued to look at peat humification in Swedish bogs in order to identify climatic anomalies and to investigate local and regional responses to climate change during the entire Holocene. Continuing work on Stömyren Bog, Borgmark and Wastegård (2008) also investigated the nearby Kortlandamossen and Fågelmossen. Clear wet shifts at 7500 BP, 5500 BP, 4200 BP, 3700-3500 BP and 2900 BP were evident from the peat stratigraphy, supporting the earlier work. Borgmark and Wastegård noted that the most pronounced and abrupt

wet shift occurred at 4200 BP; this pronounced wet anomaly has been recorded in many records that reconstruct mid- to late- Holocene climate (e.g. Barber *et al.*, 1994; Hughes *et al.*, 2000a; Mauquoy and Barber, 2002; Barber *et al.*, 2003; Gunnarson *et al.*, 2003; Langdon and Barber, 2004; Borgmark, 2005; Langdon and Barber, 2005; Borgmark and Wastegård, 2008; Mauquoy *et al.*, 2008).

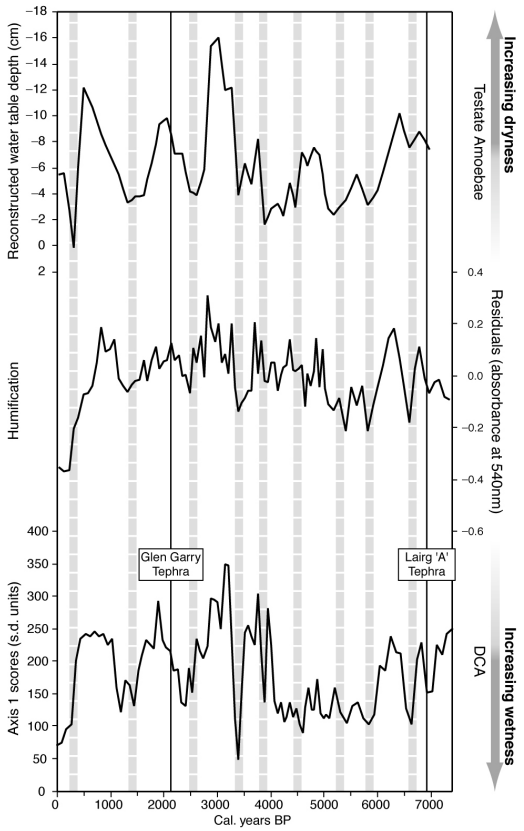

Figure 2.9 - Multi-proxy reconstructions of BSW from Temple Hill Moss. Vertical shaded bars highlight period of wetter/cooler conditions (Source: Langdon *et al.*, 2003).

With the aim of comparing palaeoclimatic reconstructions from Butterburn Flow and Lille Vildemossen with solar variability, Mauquoy *et al.* (2008) identified a wet shift in the bog surface at around 4100 BP on both sites. Langdon and Barber (2004) identified the '4.2 k' wet anomaly in several sites across Scotland during and shortly after the Hekla 4 tephra isochron. In their consequent work, Langdon and Barber (2005) identified a wet anomaly at around 4150 BP at Mallachie Moss in the Scottish Cairngorms. Wetting at Raeburn Flow (Mauquoy and Barber, 2002) occurred slightly before the other Scottish sites, at 4350 BP. This may have been the result of a combination of error margins within the dating framework and a faster response to the climatic anomaly. Although the peat humification-based BSW reconstructions for Scandinavia and Denmark largely agree with one another, a note of caution is necessary. As discussed in Section 2.2.3, there are strong limitations to using colorimetric peat humification as the sole palaeoclimatic proxy source (Hughes *et al.*, 2012) as other underlying factors can be driving the peat humification signal.

Further synchronous wetting events have been identified, such as those around 3300 BP (Barber *et al.*, 1994; Mauquoy and Barber, 2002; Barber *et al.*, 2003; Langdon *et al.*, 2003; Langdon and Barber, 2005; Swindles *et al.*, 2007) and 2800 BP (Denton and Karlén, 1973; Charman and Hendon, 2000; Langdon and Barber, 2001; Barber *et al.*, 2003; Gunnarson *et al.*, 2003; Borgmark, 2005; Charman *et al.*, 2006; Swindles *et al.*, 2007; Mauquoy *et al.*, 2008; Amesbury *et al.*, 2011), but this timeframe is not within the remit of this thesis.

2.6.2 Holocene glacial movements in Scandinavia and the Alps

Reconstructions of glacial mass balance changes during the early- and mid-Holocene can provide valuable records of temperature and precipitation variability. However, varying climatic factors can be responsible for triggering glacial advances and retreats (Nesje *et al.*, 2008; Wanner *et al.*, 2008). The mass balance of Scandinavian glaciers has been shown to be directly linked to summer temperatures and winter precipitation (Nesje and Dahl, 2003; Bjune *et al.*, 2005; Nesje *et al.*, 2006; Nesje *et al.*, 2008), whereas their Alpine counterparts are predominantly controlled by summer temperature (Oerlemans, 2001; Joerin *et al.*, 2006; Grosjean *et al.*, 2007; Joerin *et al.*, 2008). As shown by Barber and Langdon (2007) and Charman *et al.* (2009), long-term changes in the length and severity of the summer water deficit, and therefore BSW, are largely driven by summer temperature changes. Records of glacial movements can therefore be compared to long-term trends in BSW changes. Increases in BSW are expected during periods of glacial advances, with drying of the bog surface predicted during periods of glacial retreat.

Karlén (1976; 1988) investigated a series of glaciers in northern Sweden in order to establish mass balance changes throughout the Holocene using a multi-proxy approach. He concluded that glaciers existed throughout the Holocene and that a number of glacial advances occurred at 7400-7200 BP, 6300-6100 BP, 5900-5800 BP, 5600-5300 BP, 5100-4800 BP, 4600-4200 BP and 3400-3200 BP, amongst others. This view however has been challenged by Snowball and Sandgren (1996), and more recently by Rosqvist (2004), who found no evidence of any glacial movements and concluded that all glaciers in northern Sweden were likely to have disappeared during the HTM. It is possible that the glacial movements detected by

Karlén were those of small glaciers, which might have existed through the Holocene (Ivy-Ochs *et al.*, 2009)

The view that most Scandinavian glaciers melted completely or remained in a contracted state during the mid-Holocene is generally accepted (Nesje and Dahl, 1993; Matthews *et al.*, 2000; Lie *et al.*, 2004; Bakke *et al.*, 2005; Matthews *et al.*, 2005; Nesje, 2009). However, melting and consequent readvance of glaciers is not synchronous across Scandinavia. Figure 2.10 shows a summary of glacial movements from 16 Scandinavian glaciers during the Holocene. It is important to note that at some point during the mid-Holocene each glacier melted away. Most glaciers advanced during (or just following) the Finse event (Matthews *et al.*, 2000; Matthews *et al.*, 2005; Nesje *et al.*, 2008), a period of strong glacial advances linked to the '8.2k' event.

Based on their earlier work, Bakke *et al.* (2010) queried the total absence of glaciers in northern Norway during the HTM and suggest that glaciers at Okstindan may have survived and even shown glacial advances around 7400-7000 BP, 4050 BP and 2750 BP, questioning the results and methodology of Nesje and Dahl (1993). Bakke *et al.* (2010) demonstrated that the glacier at Okstindan was most retreated between 7000 BP and 5000 BP with a series of three short-lived advances. These advances were only 50 years in duration, and therefore probably too short-lived to show up in the peat record. However, a major advance lasting 230 years occurred at 4500 BP. Matthews *et al.* (2000) suggested that although the large glaciers are likely to have been inactive during the majority of the HTM, smaller glaciers may have existed that were more sensitive to smaller climatic fluctuations.

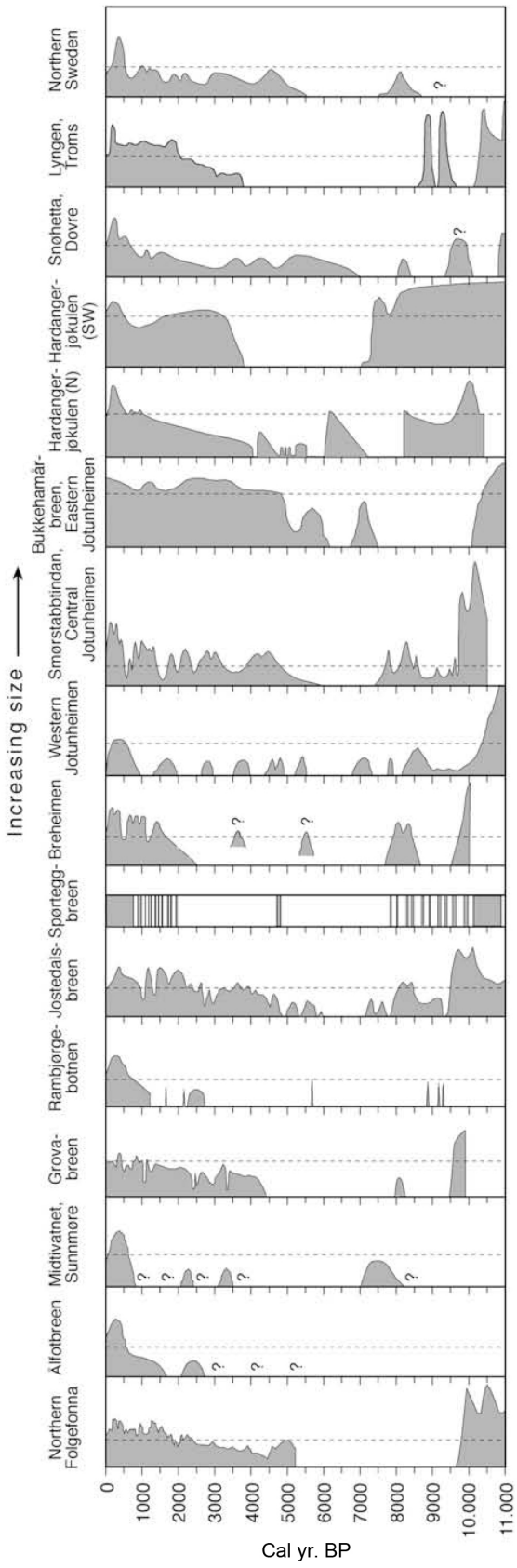

Figure 2.10 - Summary of glacial advances and retreats of Fennoscandian glaciers

Source: Nesje (2009).

The period of re-emergence of glaciers, known as the Neoglacial, was not synchronous (Figure 2.10) but is largely accepted to have occurred between 6000 BP and 5000 BP (Nesje and Dahl, 1993; Lie *et al.*, 2004; Matthews and Briffa, 2005; Matthews, 2007; Nesje *et al.*, 2008; Wanner *et al.*, 2008; Nesje, 2009; Bakke *et al.*, 2010). Following the re-establishment of Scandinavian glaciers, a series of glacial advances has been detected in numerous reconstructions. Matthews *et al.* (2005) showed that the Neoglacial started at 5730 BP with maximum glacial advances around 4420 BP and 2800 BP. Large-scale glacial advances around 4400 BP have also been identified in other records (Matthews, 2007; Nesje, 2009; Bakke *et al.*, 2010). Nesje (2009) confirmed glacial advances around 4400 BP, and showed that small glacial advances may have occurred at 5600 BP and 3300 BP.

In contrast to the evidence from Fennoscandia, most glaciers in the European Alps were in retreat or absent for a longer period given a more continental climate and less moisture availability. Ivy-Ochs *et al.* (2009) suggested that climatic conditions in the Alps between 10500 BP and 3300 BP were not conducive to significant glacial expansion, except during very short intervals, and Jörin *et al.* (2006) showed that Alpine glaciers were in recession until 3600 BP. Smaller glaciers, however, are more sensitive to smaller changes in climate than larger glaciers, which have a relatively long lead time to advances (Oerlemans, 2001). Jörin *et al.* (2008) suggested that smaller glaciers of < 5 km^2 surface area might have shown slight advances around 6630 BP, 5800 BP and 5650 BP. This theory was supported by Ivy-Ochs *et al.* (2009), who showed short-lived advances by small glaciers at 8800 BP, 8400 BP, 6300 BP and 5000 BP. However, no ice was present in the Alps from 5300 BP to 5100 BP. Based on archaeological finds, Grosjean *et al.* (2007) showed that

permanent ice has been present in the Alps since 4900 BP in the form of small high-altitude glaciers. Their evidence further highlighted a cooling phase around 4200 BP, in line with glacial advances in Scandinavia and wetting of the peat record in the British Isles.

2.6.3 Lake level reconstructions

Lake levels have been shown to be sensitive to climatic changes (Digerfeldt, 1988; Harrison *et al.*, 1993) and are therefore suitable for palaeoclimatic reconstructions. Magny (2004) suggested that lake level changes register variations in precipitation and evaporation that may go undetected in glacial mass balance and plant macrofossil reconstructions. However, caution has to be taken when interpreting lake level changes; many factors other than climate can influence lake hydrology (Dearing, 1997), including catchment events and lake internal processes, such as sediment focussing and current strength variation (Jones *et al.*, 2011).

Analysing sediment properties and pollen evidence, Jones *et al.* (2011) investigated lake level changes in Hawes Water, a small marl lake in northern England. They concluded that lake levels were generally low from 9960-6000 BP at which point a major rise in lake level took place, in contrast to predominantly lower lake levels in the Swiss Jura (Haas *et al.*, 1998; Magny *et al.*, 2003b; Magny and Haas, 2004). It is possible, however, that this rise was not directly climatically driven but a response to sea level rises and a marine highstand around 6000 BP (Jones *et al.*, 2011).

Compared with the mid-Holocene glacial history for the European Alps, lake levels show much more variation during the HTM. Looking at multi-proxy reconstructions,

Haas *et al.* (1998) showed that Holocene climate was less stable than initially believed and that a series of cold (humid) events could be identified from lake level data. These events occurred around 8400-7760 BP, 7500-7260 BP, 6150-5620 BP, 5300-5000 BP, 3800-3420 BP and 2750-2350 BP. It is interesting to note that no cold/humid event was detected around the timing of the '4.2 k' event. In his review of 26 lakes in the Jura region, based on 15 years of work, Magny (2004) expanded on the idea of an unstable Holocene and revised the dates provided by Haas *et al.* (1998). With the aim to construct a Holocene mid-European lake level framework for the Jura region, Magny identified 15 phases of high lake levels. Seven of these phases occurred during the period of interest for this thesis, that is between 8350-8050 BP, 7550-7250 BP, 6350-5900 BP, 5650-5200 BP, 4850-4800 BP, 4150-3900 BP and 3500-3100 BP. A low level stand around 5000 BP supports findings by Digerfeldt (1988) from southern Sweden, who found lake level minima around 5000 BP and 2000 BP. By comparing with data from the GISP ice core, Magny (2004) concluded that solar forcing was largely responsible for driving lake level fluctuations. He later revised this hypothesis (Magny *et al.*, 2011), showing that orbital forcing played a more dominant role than solar variation in driving major lake level change in the Jura.

A summary of the above reviewed records of palaeoclimatic information is provided in Figure 2.11. Regionally representative records have been chosen to highlight synchronous early- to mid-Holocene climate change across northwest Europe.

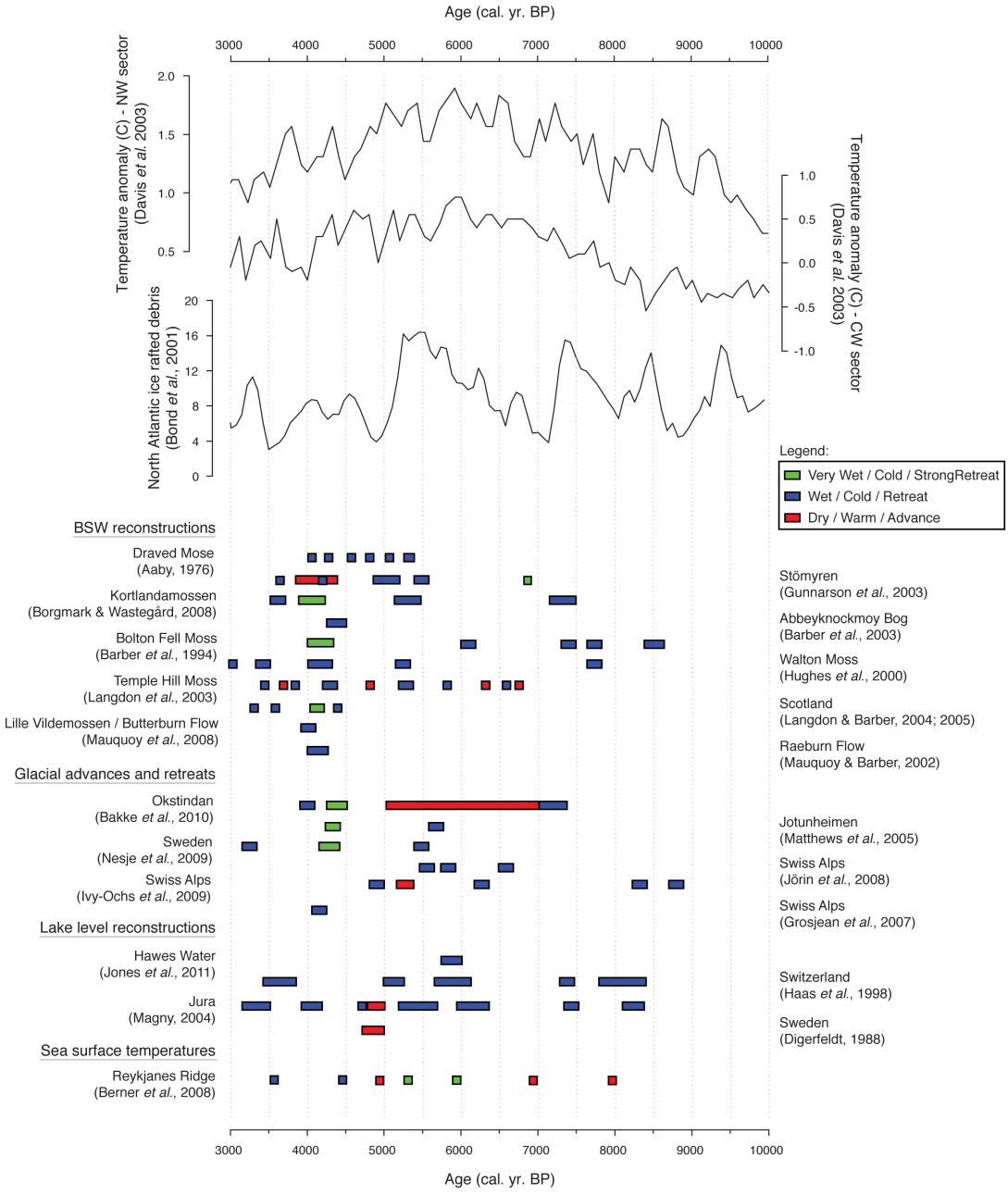

Figure 2.11 - Summary diagram of palaeoclimatic data of atmospheric temperatures, North Atlantic drift ice, BSW, glacial advances and retreat and lake levels.

2.7 Conclusion

Evidence from the peat record, glacial mass balance reconstruction, lake level and pollen-based temperature data show that a warm and time-transgressive Holocene Thermal Maximum existed that was punctuated by a series of cold and wet events. Most evidence from the palaeo-record points to an abrupt event between *c*. 4500 BP and 4000 BP that marked the shift to colder and wetter climatic conditions.

A series of gaps in knowledge have been identified in this chapter that will be addressed throughout this thesis:

- Since the time period studied within this thesis is too short for robust millennial-scale time-series analysis, comparisons to episodes of increased North Atlantic ice rafting will be made to establish whether these are detectable in the peat record (Research Question Q1).
- Only very few palaeoclimatic reconstructions were used in Magny *et al.*'s (2003b) work on a European tripartite climatic division. Magny *et al.* hypothesised the existence of a mid-European wet zone during episodes of increased North Atlantic ice rafting. Evidence from BSW reconstructions will be used to determine if such a zone existed and, if so, what the latitude of its northern boundary was (Research Question Q2).
- Detailed reconstructions of BSW during the early- to mid-Holocene are sparse and largely lack the temporal resolution needed show the nature of the transition to modern climatic conditions. This thesis aims to address this gap

in knowledge by determining the nature (Research Question Q3) and timing (Research Question Q4) of the mid-Holocene transition.

It is important to note that the mid-Holocene does not provide an analogue to modern climatic conditions because of a host of different boundary conditions, such as the disappearance of the large late-Pleistocene ice sheets, atmospheric and oceanic reorganisation and increased summer insolation. Studying the mid-Holocene, however, provides a good basis for understanding environmental and climatic changes that occurred during the transition to modern conditions.

3 Methodology

3.1 Study sites

3.1.1 Site selection criteria

Ombrotrophic peat bogs only develop in a narrow climatic envelope where the required balance between summer and winter moisture availability and temperature exists. Using the vast peatlands of Fennoscandia, Parviainen and Luoto (2007) developed a model to determine the necessary temperature and precipitation ranges for different types of peatlands to form (Figure 3.1). Although this model is very simplistic and based on data from Fennoscandia, it does provide a good basis for determining where ideal conditions for ombrotrophic peat formation exist. However, since Parviainen and Luoto (2007) only used modern data from Fennoscandia to establish their climate space, the map does not cover all past occurrences of raised bogs (e.g. Yeloff and Mauquoy, 2006).

Parviainen and Luoto (2007) concluded that the required ranges for raised bog development lie between 500 mm and 2250 mm of mean annual precipitation and 1.8°C and 7.8°C mean annual temperature. Figure 3.2 shows these climate parameters, highlighted in green, in a mean annual temperature and precipitation climate space for northwestern Europe (25°W - 30°E, 45°N - 80°N). When mapped onto longitudinal and latitudinal space the optimal present day geographic regions for ombrotrophic peat bog development become apparent (Figure 3.3). Given changes in past precipitation and temperature patterns, this region will have changed

throughout the Holocene. However, mapping present climatic conditions provided an indication where deep raised bogs were likely to exist. Fifteen peat bogs falling within the green area were selected and examined for their suitability for the research project (Table 3.1).

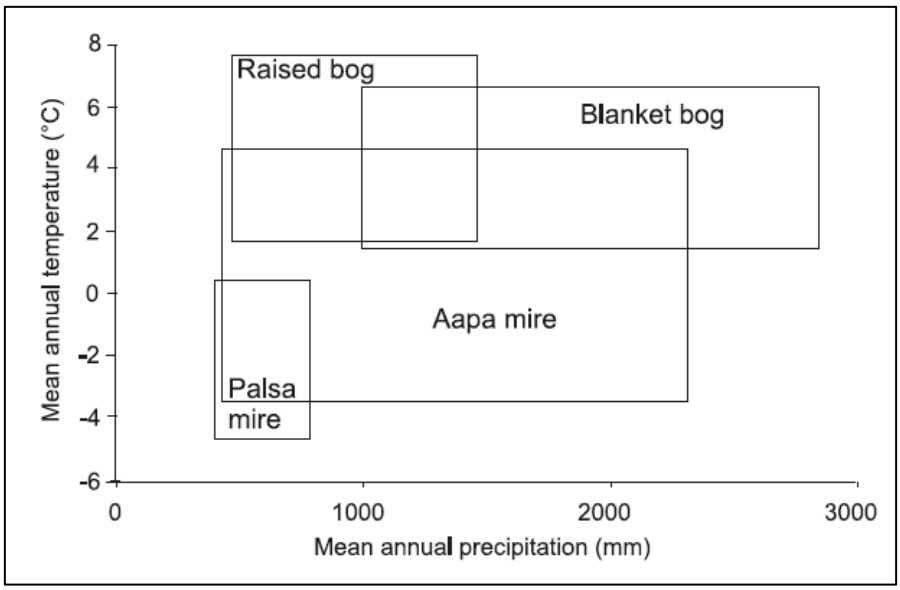

Figure 3.1 - Climate space for different bog types (Adapted from: Parviainen and Luoto, 2007)

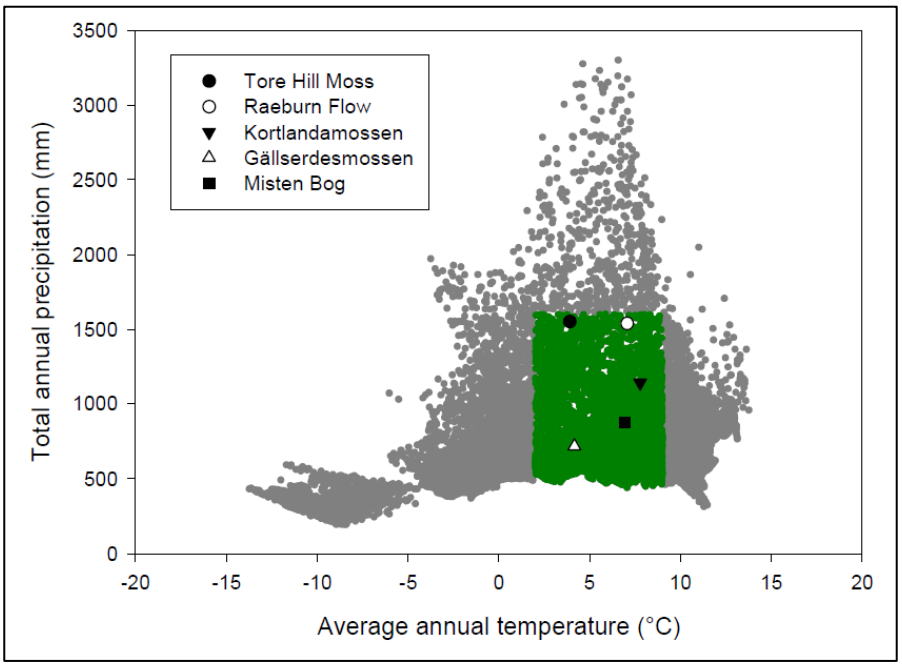

Figure 3.2 - Temperature versus precipitation climate space. Green area marks conditions conducive to raised bog growth.

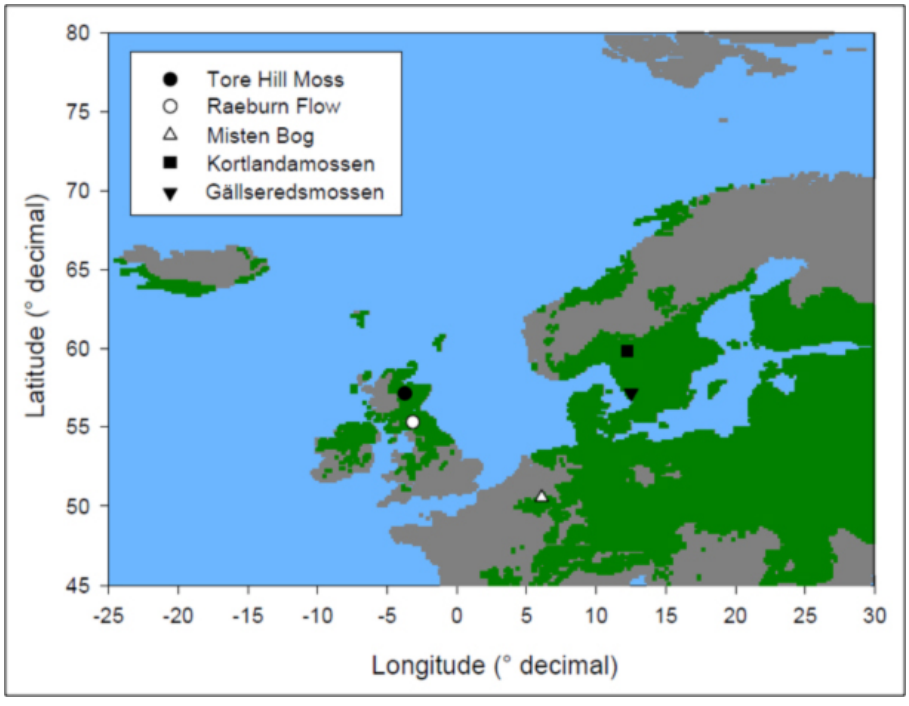

Figure 3.3 - Climate space mapped onto European map highlighting locations suitable for raised bog growth (green).

It has been suggested that the Atlantic Westerlies separate dry and moist air masses between 50°N and 60°N (Magny *et al.*, 2003b; Magny *et al.*, 2006). To capture persistent states in the climate system, only sites within this latitudinal range were investigated. Unfortunately, a large number of sites had to be excluded as a result of past industrial peat exploitation. In addition to the geographical considerations, a series of selection criteria were used to determine the suitability of potential sites for this study. To be accepted, sites needed to have *a)* been subject to as little disturbance as possible, *b)* become ombrotrophic at least 8,000 years ago and *c)* accumulated at least 0.7 cm of new peat per decade in order for a 1 cm slice of peat to represent the smallest temporal slice possible. Finer resolution sampling runs the risk that the same plant could be sampled multiple times, especially for monocotyledons (Amesbury *et al.*, 2011).

Table 3.1 - List of investigated sites and their suitability for the project:

Site	Location		Description	Suitability
Tore Hill Moss	57°14'N	3°40'W	All criteria satisfied	Accepted
Raeburn Flow	55°20'N	3°06'W	All criteria satisfied	Accepted
Kortlandamossen	59°51'N	12°17'E	All criteria satisfied	Accepted
Gällseredsmossen	56°10'N	12°35'E	All criteria satisfied	Accepted
Misten Bog	50°33'N	6°09'E	All criteria satisfied	Accepted
Longbridge Muir	55°00'N	3°29'W	Evidence of tidal over-washing of site	Rejected
Langlands Moss	55°44'N	4°10'W	Site too shallow	Rejected
Killorn Moss	56°08'N	4°13'W	Site too shallow	Rejected
Tulloch Moss	57°13'N	3°43'W	Site too shallow	Rejected
Bell's Flow	56°08'N	4°10'W	Site too shallow	Rejected
Shirgarton Moss	55°04'N	3°0'3W	Too close to Raeburn Flow	Rejected
Clefay Bog	50°30'N	6°06'E	Site not ombrotrophic until 6000 BP	Rejected
Kerfontaine Bog	47°41'N	2°31'E	Site accumulation too slow	Rejected
Storemossen	57°17'N	13°56'E	Site too shallow	Rejected
Dosenmoor	54°07'N	10°01'E	Site not ombrotrophic until 6000 BP	Rejected

Since the ages of these sites were not known and neither parameter *b* nor *c* could be determined, a standard estimated guideline of 1,200 years per metre of peat accumulation was used to determine the ages of the sites. Using the depth and estimated age of the sites, an annual peat accumulation rate was calculated to satisfy condition *c*. If any of these three criteria were not fulfilled, potential sites were rejected. From all investigated sites, five suitable bogs were selected and consequently cored and analysed using the methodologies outlined below. Figure 3.4 shows the location of the selected sites in relation to each other (Photos: Figures 3.6-3.10)

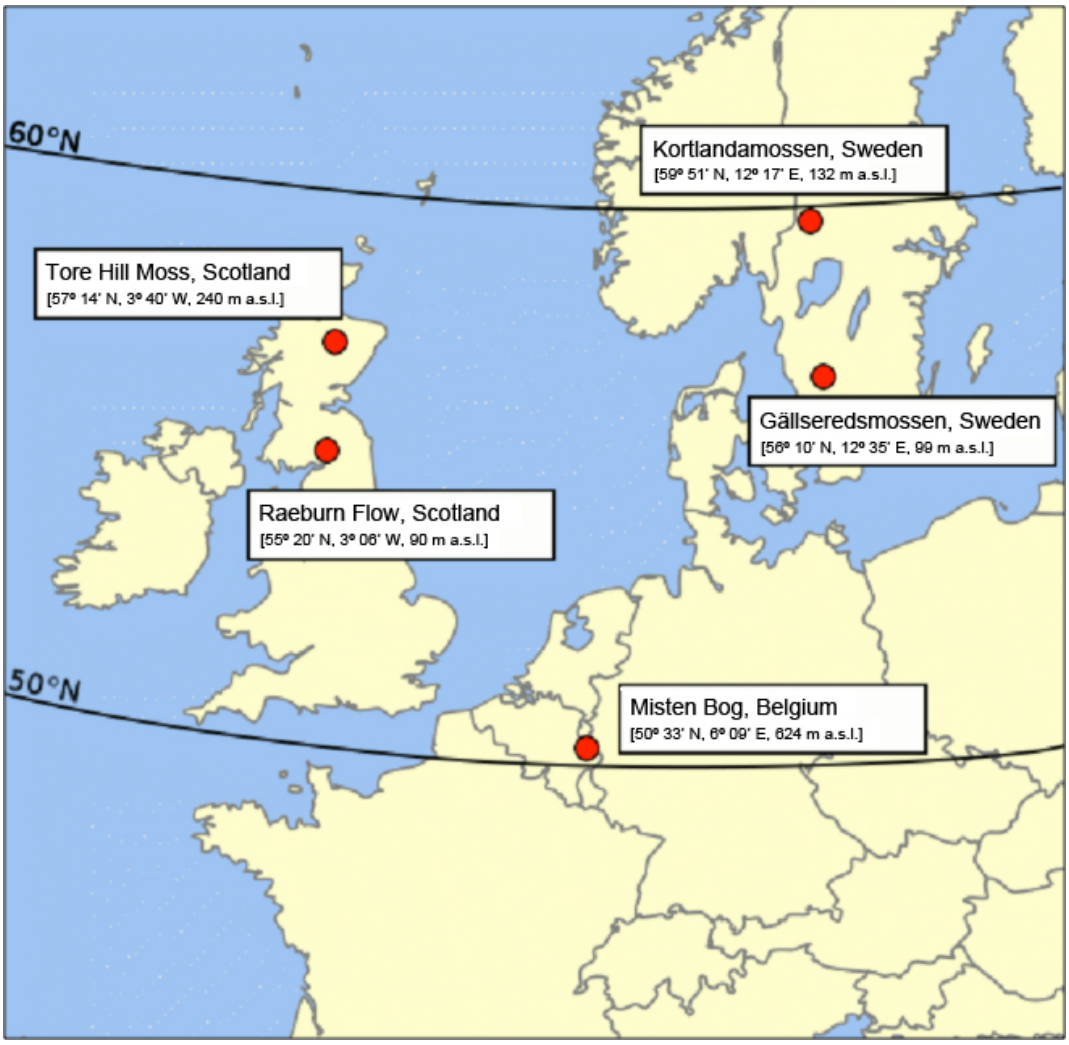

Figure 3.4 - Map of study sites across NW Europe.

In order to study the impact of the North Atlantic and associated Atlantic Westerlies on European climate, an oceanic-continental gradient was introduced by selecting two oceanic sites in Scotland and two near-continental sites in Sweden. A Belgian site on the border between oceanic and continental climate influences was selected to act as a link to the palaeohydrological reconstructions carried out in eastern France (Magny, 1993; Magny *et al.*, 2003b) and northern Switzerland (Haas *et al.*, 1998).

3.1.2 Climatic parameters

As described above, peat bogs only exist in specific climatic envelopes. Mean daily temperatures, mean monthly precipitation and monthly moisture balance, averaged over the past 101 years are shown in Figure 3.5 for all sites. All climate data have been obtained from the CRU-TS 2.0 and CRU-CL 2.0 climate data sets (New *et al.*, 2002), which average observed data from surrounding weather stations and interpolate where no such data are available. The two Swedish sites (Kortlandamossen and Gällseredsmossen) have greater temperature ranges between the coldest and warmest months than the other three research sites, which highlight the influence of continental climate systems. By contrast, temperature ranges for the two oceanic sites are clearly lower. As expected, the annual temperature range for Misten Bog lies between the two extremes. Furthermore, it is noteworthy that Raeburn Flow and Tore Hill Moss receive most of their precipitation during the winter months (Figure 3.5). The two Scandinavian sites, on the other hand, receive most inputs during the summer months and Misten Bog only receives slightly more precipitation between November and January than throughout the rest of the year. Furthermore the two Scottish sites receive far more precipitation than any of the

other sites and are therefore located towards the top extremity of the climatic envelope for ombrotrophic bog development (Figure 3.2).

To ensure a site's suitability for this study, the monthly moisture budget (MMB) was calculated to show that a positive balance exists to enable ombrotrophic peat growth. Given the fact that almost all moisture exchange occurs with the atmosphere, with the exception of limited marginal seepage and internal retention, the MMB is equal to the difference between precipitation (P) and evapotranspiration (ET_0) (Equation 3.1). Evapotranspiration was calculated using a modified version (Equation 3.2) of the extensively used Penman equation (Penman, 1948; Kellner, 2001; Valiantzas, 2006) for evapotranspiration losses from bare grass.

$$MMB = P - ET_0$$

Equation 3.1 - Monthly moisture budget

$$ET_0 \approx 0.051(1-\alpha)Rs\sqrt{T+9.5} - 2.4\left(\frac{Rs}{Ra}\right)^2 + 0.048(T+20)\left(1-\frac{RH}{100}\right)(0.5+0.536u) + 0.00012Z$$

Equation 3.2 – Penman equitation for evapotranspiration modified by Valiantzas (2006)

Where Rs is solar radiation in $MJm^{-2}d^{-1}$, Ra is the amount of extra-terrestrial radiation in $MJm^{-2}d^{-1}$, RH is the relative humidity expressed as a percentage, T is the

mean monthly temperature in °C, α is the surface albedo, u is the average monthly wind speed in ms^{-1}, and Z is the altitude above sea level in metres. Because of limited data availability for the exact albedo of each site, the albedo of grass (α=0.25) was used for all calculations, as suggested by Valiantzas (2006). Data for relative humidity, sunshine hours and wind speed was only available for the period 1961-1990 and monthly mean values were used for the calculations of MMB.

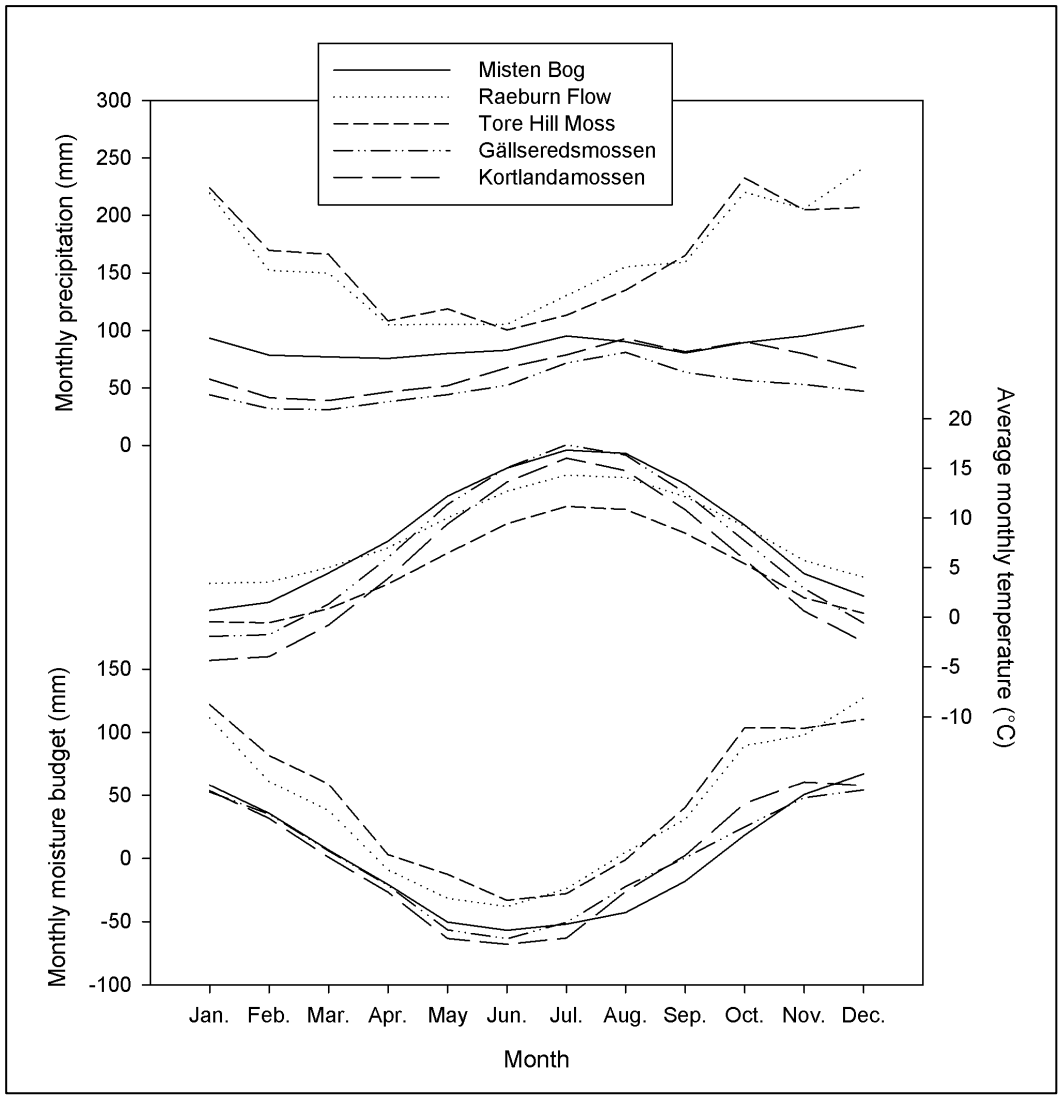

Figure 3.5 - Monthly precipitation, average monthly temperature and monthly moisture budget for all study sites taken from CRU-TS 2.0 and CRU-CL 2.0 datasets.

Figure 3.6 - View of Kortlandamossen from bog-island. (Source: G. Mallon)

Figure 3.7 - F. de Vleeschouwer (left) and G. le Roux (right) taking a Wardenaar core from Misten Bog. (Source: G. Mallon)

Figure 3.8 - Raeburn Flow with distant upland hills. (Source: G. Mallon)

Figure 3.9 - View of Tore Hill Moss with Cairngorms in the background. (Source: G. Mallon)

Figure 3.10 - View of Gällseredsmossen showing encroaching pine trees on site. (Source: G. Mallon)

3.1.3 Misten Bog, Belgium

Misten Bog, also known as Royal Fen, is located in the Belgian Ardennes [50°33'47"N; 6°09'58"E; altitude: 620 m a.s.l.] situated between the towns of Monschau (Germany) and Eupen (Belgium). Both towns were important trade centres during the Roman occupation and evidence of a Roman trade-route running through the Hautes Fagnes has been discovered (Renson *et al.*, 2008). The site is part of the large 'Hautes Fagnes' national park and is surrounded by peatlands, lithal and palsa features, and managed pine woodlands and falls into the highest protection category (Zone D). It was cored with special permission from the Belgian

government in February 2008 as part of a coring expedition undertaken in conjunction with the Royal Belgian Institute of Sciences, the University of Liege and the University of Heidelberg.

The site is located on top of the 'Stavelot Massive' and formed over hard quartzite, outcrops of sandstone and weathered Cambrian phyllite slate (Wendt, 1996). Around 8500 years BP an existing birch-alder forest paludified to start the peat accumulation processes and approximately 7.5 m of peat has since accumulated. There is visible evidence of superficial peat cutting for fuel during the late 19th and early 20th centuries on the northern edge of Misten Bog. However, given the distance to the coring location of 500 m (Figure 3.11) and the shallow nature of the cutting, disturbance to the main part of the bog is limited, making it suitable for palaeoclimatic investigation.

A series of studies have been carried out exploring the history of Misten Bog. However, the majority of these have focused on geochemical and geospatial analyses, such as the detection of metal concentrations and a detailed ground penetrating radar survey (Wastiaux and Schumacker, 2003; De Vleeschouwer *et al.*, 2007). The most notable palaeoecological study carried out on the site dates back to the mid-20th century (Persch, 1950) and recent advances in palaeoecological and chronological methods highlight the need to re-investigate the site. A major shortcoming of the initial study is that Persch did not core the deepest part of the site and his analyses were therefore limited to the late-Holocene. The conclusion that the site is dominated by *Sphagnum austinii* only holds true for the last 4,000 years of bog development on the site and the entire early- to mid-Holocene history remains largely unexplored. Currently, Misten Bog is dominated by *Molinia caerulea* grass

and *Vaccinium* spp. interspersed with a healthy acid bog community of *Sphagnum* spp., *Erica tetralix*, *Calluna vulgaris*, *Aulacomnium palustre*, *Trichophorum cespitosum*, *Narthecium ossifragum* and a few *Betula* trees.

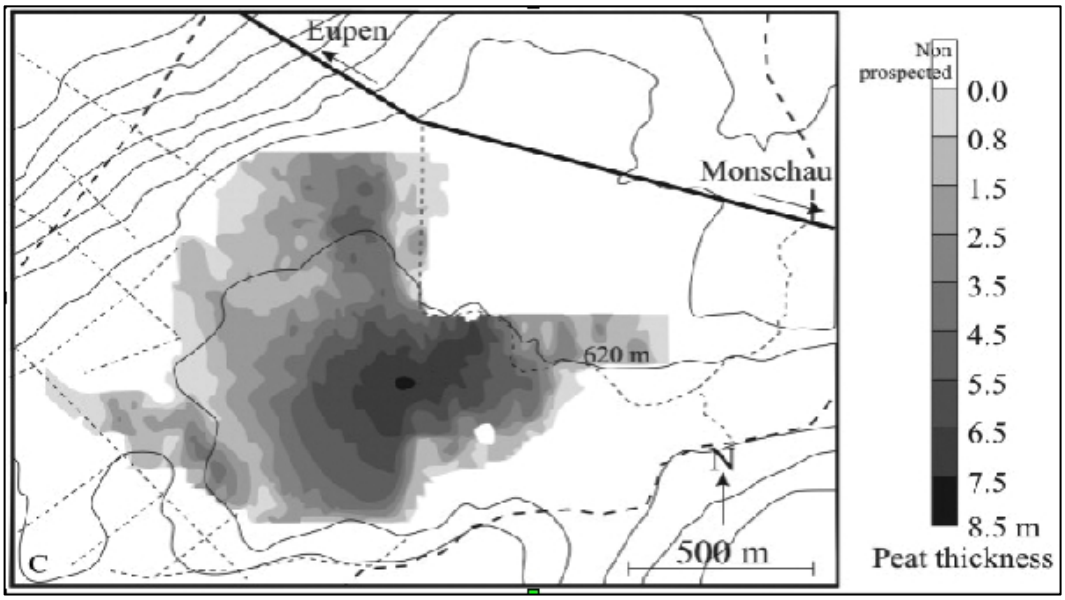

Figure 3.11 - Depth profile of Misten Bog obtained through ground penetrating radar showing the deepest part of the bog in black - adapted from De Vleeschouwer *et al.* (2007)

Misten Bog falls into the highest level of Belgium's Nature Protection Zone and because of imposed access permission restrictions, no stratigraphic survey could be carried out on the site to determine the ideal coring location. Instead results from a ground penetrating radar study of Misten Bog (Wastiaux and Schumacker, 2003), were used to determine its deepest part. The coring location was reached using a pre-programmed GPS unit and is indicated by a yellow pin in Figure 3.12. At the deepest part of the bog a main research core (MIS-08-07) of 720 cm length was extracted

next to a *Polytrichum* spp., *Aulacomnium palustre* and *Erica tetralix* dominated hummock on a *Sphagnum magellanicum* and *Eriophorum vaginatum* dominated part of the bog. The standard method for extracting a Russian core, as outlined in Section 3.2.1, was employed to extract the main research core. In addition to core MIS-08-07 a second 5 cm diameter auxiliary core (MIS-08-08) of 759 cm length was extracted five metres to the east of the main coring location.

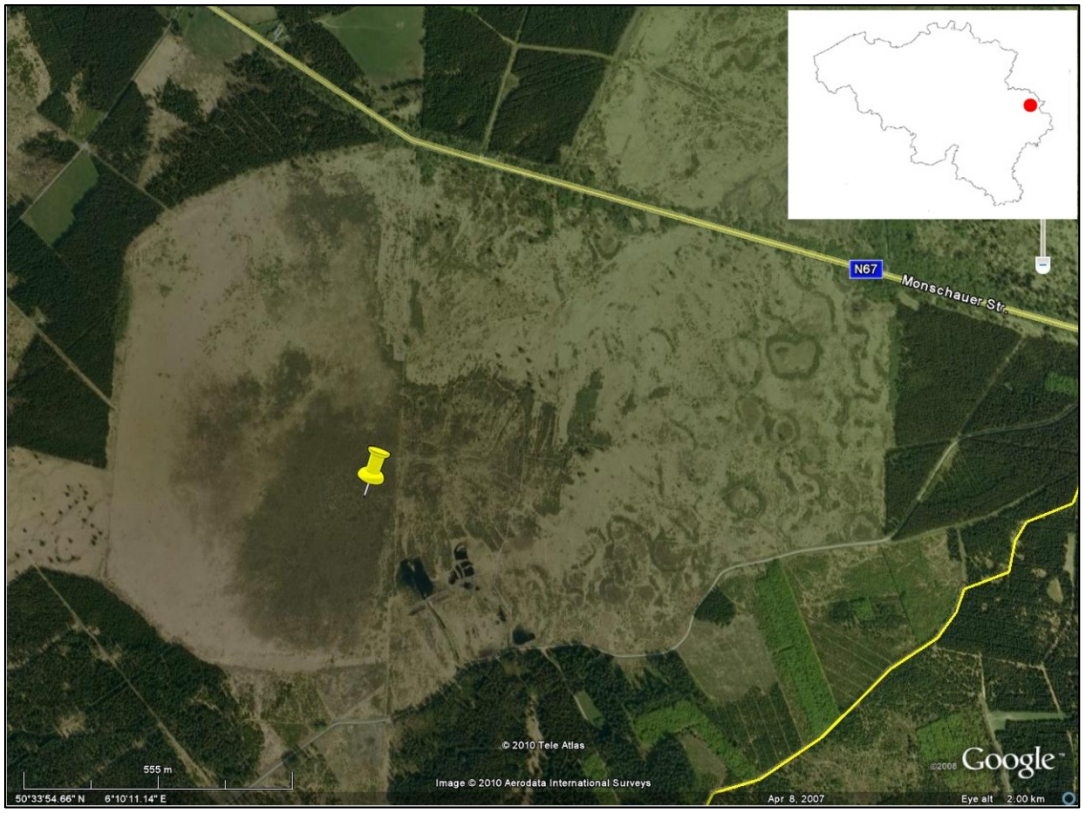

Figure 3.12 - Aerial photograph of Misten Bog. Coring location is indicated by yellow pin. (Source: Google Earth)

3.1.3.1 Climatic envelope

Precipitation levels for Misten Bog are highest between November and January, though they remain relatively steady throughout the year, with slight maxima towards the middle and the end of the year. Average annual rainfall for Misten Bog is 1042 mm and the mean annual temperature is 8.7°C, with an average difference between the hottest and coldest months of 16.1°C (Figure 3.13). Of all the sites, Misten Bog has the highest average annual temperature and a clear separation in positive and negative moisture balance can be observed throughout the year. For six months of the year (October to March) the site has a positive moisture balance. During this time the bog takes up more moisture than is lost through evapotranspiration. From April to September, however, this is reversed and the site loses more moisture than is replenished, using up moisture reserves. Nevertheless it should be noted that in September this net moisture deficit is only marginal.

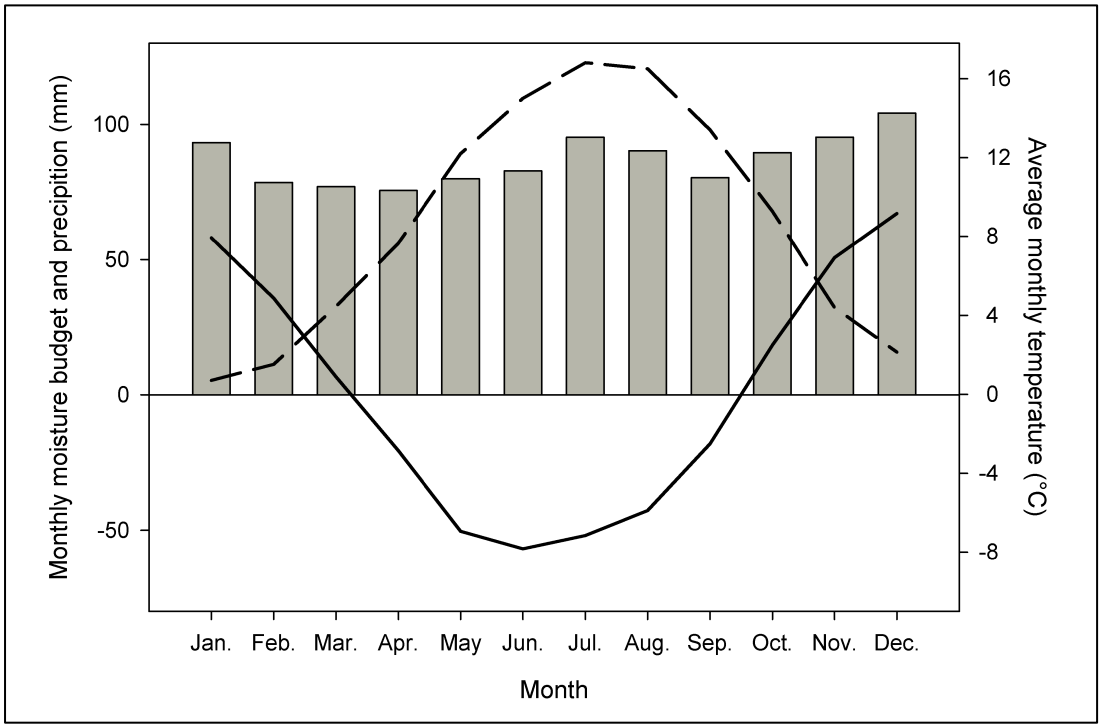

Figure 3.13 - Climate parameters for Misten Bog. Solid bars show monthly precipitation, the dashed line shows average monthly temperature and the solid line shows the monthly moisture budget.

3.1.4 Gällseredsmossen, Sweden

Gällseredsmossen [56°10'30"N; 12°35'51"E; altitude: 99 m a.s.l.] is a typical concentric ombrotrophic peat bog (Figure 3.14) in the Swedish county of Halland, 40 km from the coast at Varberg and approximately 100 km southeast of Gothenburg. Peat formation occurred as a result of a hydrosere succession in a hollow depression in the bedrock, left by the last glaciation. This is supported by an early *Phragmites australis* phase, which was followed rapidly by the invasion of bog species as discussed further in Section 5.7.1. The underlying geological strata are largely acidic to intermediate mesoproterozoic and palaeoproterozoic granite and

granodiorite bedrock. A healthy acidic *Sphagnum* spp., *Trichophorum cespitosum* and *Eriophorum vaginatum* community dominates the site, with the main *Sphagnum* species being *Sphagnum pulchrum*, *Sphagnum cuspidatum*, *Sphagnum magellanicum* and *Sphagnum fuscum*. Other species growing on Gällseredsmossen include *Rhynchospora alba*, *Vaccinium oxycoccus*, *Rubus chamaemorus*, *Erica tetralix*, *Calluna vulgaris* and various *Carex* species. The site is also home to many pine trees (*Pinus sylvestris*) and is surrounded by a managed pine forest and an alder carr to the north.

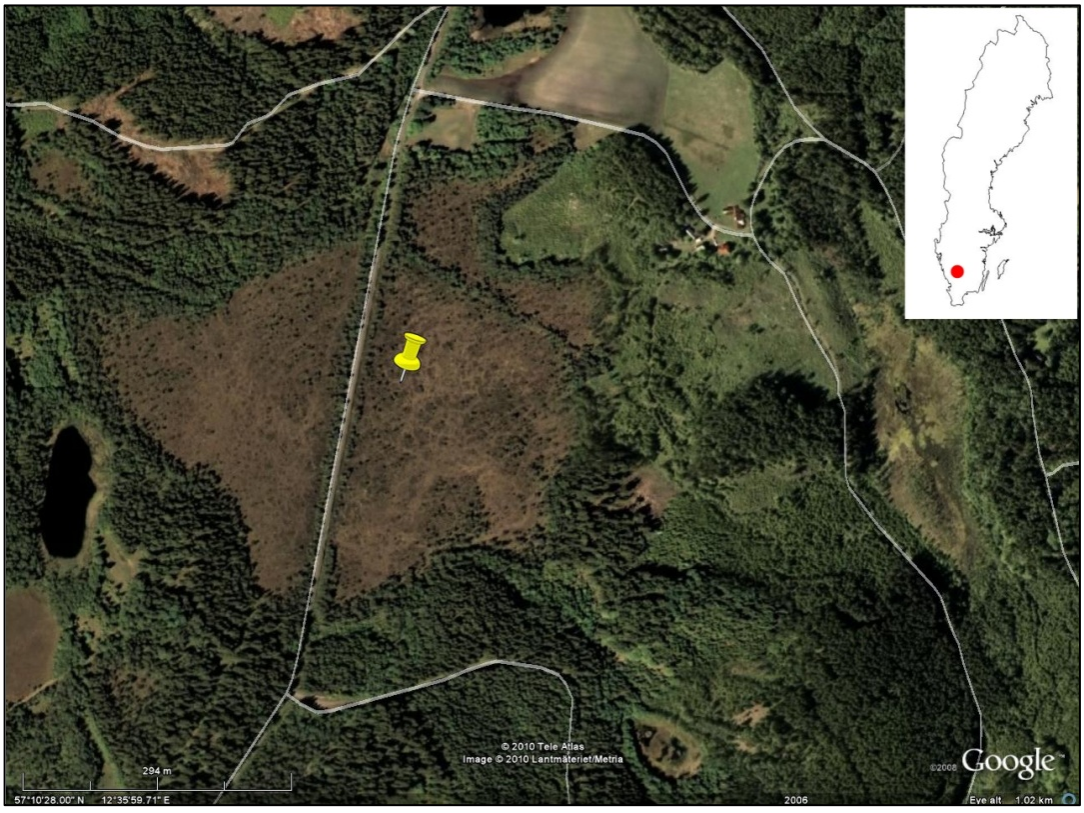

Figure 3.14 - Aerial photograph of Gällseredsmossen. The yellow pin indicates coring location. (Source: Google Earth)

As a result of the abundance of peat bogs found in Sweden, the site has not been cut. Nevertheless, the site has been disturbed and a road has been built across it. Construction of the road, however, followed traditional methods and it was built on top of hay bales instead of supporting pillars driven into the bedrock (pers. comm. Lars Franzèn – University of Gothenburg). In addition, an old disused telegraph mast can be found in the northern part of the bog. As a result of the road's traditional construction, bog hydrology of the lower strata is intact and the site is suitable for palaeoclimatic study.

The site has mainly been studied biogeochemically by Franzèn (2006; 2007) using analysis of rare-earth element versus ash concentrations to show a clear separation from groundwater at approximately 8200 BP (500 cm), which coincides with ecological changes indicative of the fen/bog transition. Prof. Franzèn, who also uses this site to teach bog ecology and bog geochemistry, helped with the stratigraphy and coring of the site in August 2009. From previous research, Prof. Franzèn was able to quickly locate the deepest part of the bog, where a stratigraphic section was described (Figure 3.14). The two stratigraphic sections confirmed the deepest part of the bog and highlighted the large stratigraphic variability. To limit the disturbance to the site, in line with site access permissions, no further stratigraphic cores were extracted. The coring location was chosen between the two stratigraphic cores, 50 cm from a small *Ericaceae* dominated hummock, to capture maximum peat history as well as maximum changes in peat composition. A 550 cm long 11 cm diameter Russian core (GAL-09-01) was extracted.

3.1.4.1 Climatic envelope

The precipitation and temperature profiles for Gällseredsmossen follow a predictable and more continental schema than those of Raeburn Flow, Tore Hill Moss and Misten Bog (Figure 3.5 and Figure 3.15). Temperatures during the winter months rarely exceed freezing and of all the sites Gällseredsmossen has on average the warmest summers (>16°C), with a mean annual temperature of around 7.2°C. Alongside Kortlandamossen, Gällseredsmossen has the largest temperature difference between mean cold and mean warm months of 20°C. Of the five study sites, Gällseredsmossen receives by far the least precipitation, totalling 614 mm per year, which it mostly receives during the summer months. It is highly likely that this is a result of a high-pressure system forming over Scandinavia during the winter months. Despite the relatively low amount of precipitation, a positive moisture balance exists for the period between September and March, and a net moisture deficit exists from April to August. Although the period of net loss is shorter than the one of moisture gain, it is more acute with an average net loss of 100 mm during the month of June. This is a result of high temperatures and long periods of direct sunshine coupled with relatively low precipitation levels. The annual MMB, however, remains positive.

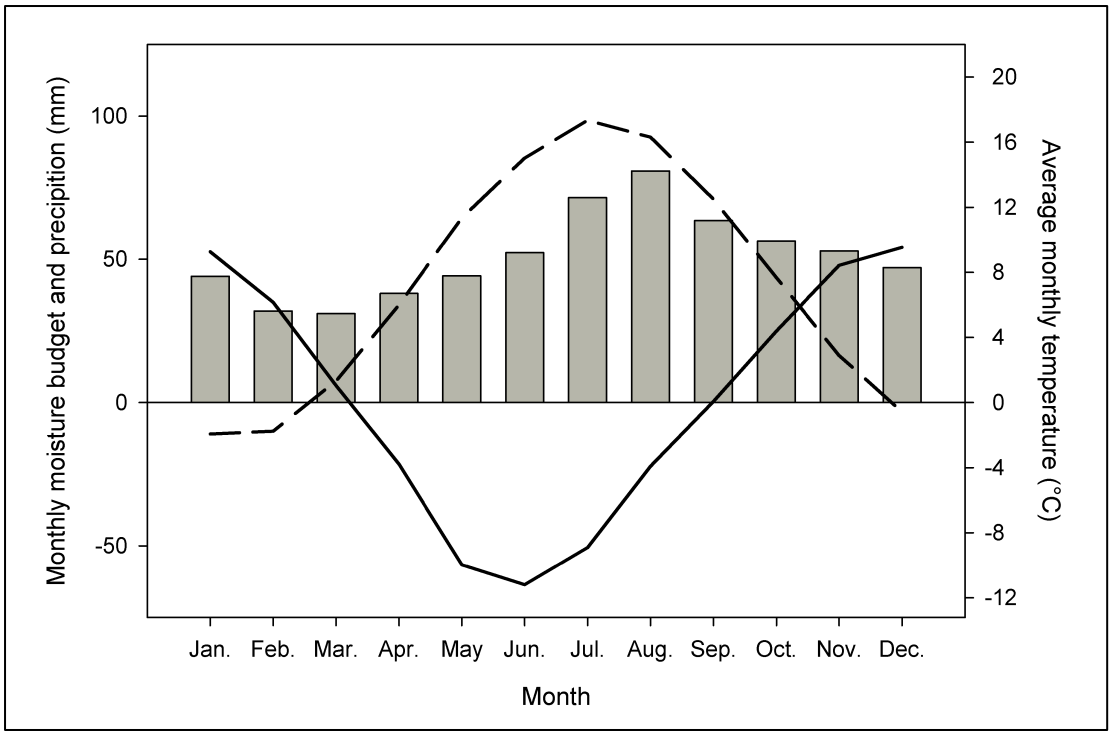

Figure 3.15 - Climate parameters for Gällseredsmossen. Solid bars show monthly precipitation, the dashed line shows average monthly temperature and the solid line shows the monthly moisture budget.

3.1.5 Kortlandamossen, Sweden

Kortlandamossen is a concentric raised peat bog (Figure 3.16) in the Swedish county of Värmland [59°50'54"N; 12°17'12"E; altitude: 132 m a.s.l] located 5 km south of the Norwegian border at Charlottenberg and approximately 50 km northeast of the raised bog Fågelmossen, which has been extensively studied by Amesbury *et al.* (2007; Amesbury *et al.*, 2012b; Amesbury *et al.*, 2012a) and Borgmark *et al.* (2006). Kortlandamossen is nearly 1 km long and 500 m wide and formed through

paludification of an underlying pine forest (Borgmark, 2005). The underlying bedrock is meso- to neo-proterozoic gneiss and amphibolite. On the western edge of the site a brittle to ductile deformation zone separates the metamorphosed rock from acidic to intermediate rhyolite and andesite. The site's peat deposits are bordered by postglacial sands to the south silts to the east and west and thin or discontinued soil cover over bedrock to the north.

Kortlandamossen is home to a typical Scandinavian acidic bog plant community dominated by *Sphagnum fuscum* and *Eriophorum* spp. In addition to the large array of *Sphagnum* species, including *Sphagnum* section *Cuspidata*, *Sphagnum* section *Sphagnum* and *Sphagnum* section *Acutifolia*, it is home to *Rhynchospora alba*, *Erica tetralix*, *Calluna vulgaris*, *Andromeda polifolia*, *Vaccinium oxycoccus* and *Rubus chamaemorus*. The site is surrounded by a natural pine (*Pinus sylvestris*) and spruce (*Picea abies*) forest. Some pine trees have settled on bog islands, which are present across the site. Growing amongst the surrounding natural forest is a diverse community of non-*Sphagnum* bryophytes and wild blueberries (*Vaccinium myrtillus*). The hydrology of the site has not been disturbed by human influence and the only disturbance of the site is a small hunting cabin, used for elk hunting, in the middle of the bog.

Figure 3.16 - Aerial photograph of Kortlandamossen. The yellow pin indicates coring location. (Source: Google Earth)

Coring of Kortlandamossen took place in August 2009. Using existing stratigraphic information from Borgmark (2005) and Lundqvist (1957) the deepest part of the bog with maximum stratigraphic variability was pre-determined and a 'thin' core (5 cm diameter) was extracted to confirm peat depth and stratigraphic variability. The stratigraphy of the thin core matched that of the deepest part of the bog (Figure 3.17) and coring was carried out on a wet *Sphagnum fuscum* lawn approximately 150 cm away from a bog island using a 'fat' (11 cm diameter) corer. A full sequence of 654 cm length (KOR-09-01) was extracted, although no contact could be made with the mineral substrate. A yellow pin on Figure 3.16 indicates the coring location.

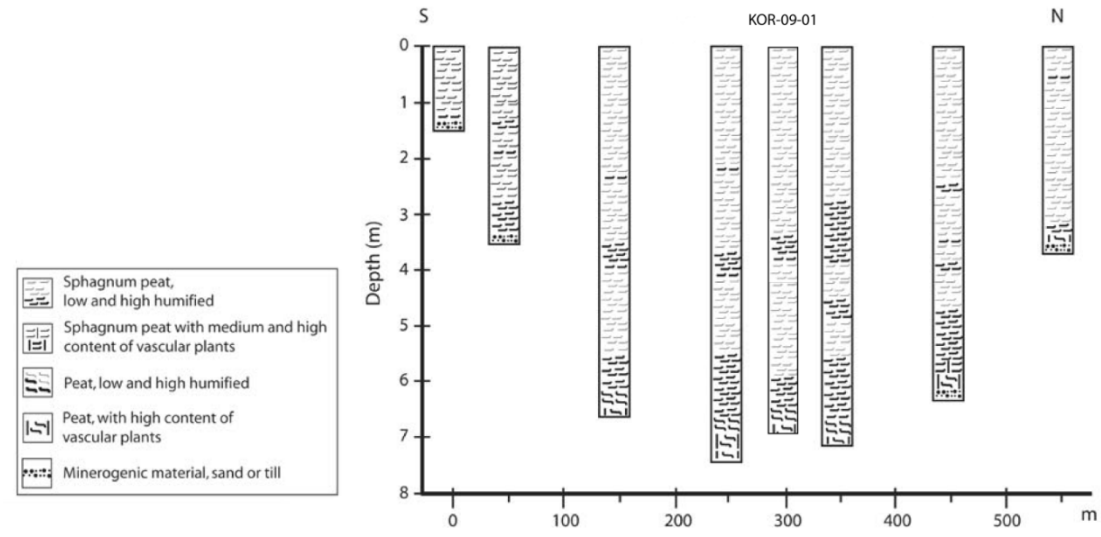

Figure 3.17 - Stratigraphy of Kortlandamossen with core KOR-09-01 at 300 m from edge. Adapted from Borgmark and Wastegård (2008).

The site has been subject to several previous studies, starting with Lundqvist's stratigraphic description (Lundqvist, 1957; Lundqvist, 1958) and Persson's geological mapping (Persson, 1966) of the site. Both studies, which based their chronology on pollen-stratigraphy, archaeological finds and the then newly developed radiocarbon dating method, overestimated the site's age but nevertheless produced very good stratigraphies. Most recent studies have been largely of a geochemical nature. Wastegård (Wastegård, 2005; Borgmark and Wastegård, 2008; Wastegård *et al.*, 2008) and Boygle (1998; 2004) extensively studied the site for tephra deposits, finding the Askja-1875, Hekla 3, Hekla Kebister and Hekla 4 layers. Borgmark (Borgmark, 2005) carried out a high resolution peat humification study in conjunction with a tephra analysis, highlighting several abrupt changes in humification levels attributed to past climate change. However, the suitability of peat

humification as a stand-alone proxy of climatic information remains questionable (Hughes *et al.*, 2012).

3.1.5.1 Climatic envelope

Similar to Gällseredsmossen, Kortlandamossen receives most of its precipitation during the summer and autumn months with maximum values between August and October (Figure 3.18). The average annual precipitation for the region is 792 mm, which is slightly higher than at Gällseredsmossen. The driest months are February and March, during which the site received half as much precipitation as during the high precipitation months. Compared to all of the studied sites, Kortlandamossen has the coldest mean monthly temperatures during the winter months (-6.3°C), during which the site freezes. It displays the greatest temperature range between warm and cold months, of 20.3°C.

As a result of the more continental temperature and precipitation patterns, a positive moisture balance exists between September and March followed by a net moisture deficit from April to August. Similar to Gällseredsmossen, the shorter period of net moisture loss is compensated by the amplitude of loss. It has to be noted that during April net losses from the bog are marginal and the annual MMB remains positive.

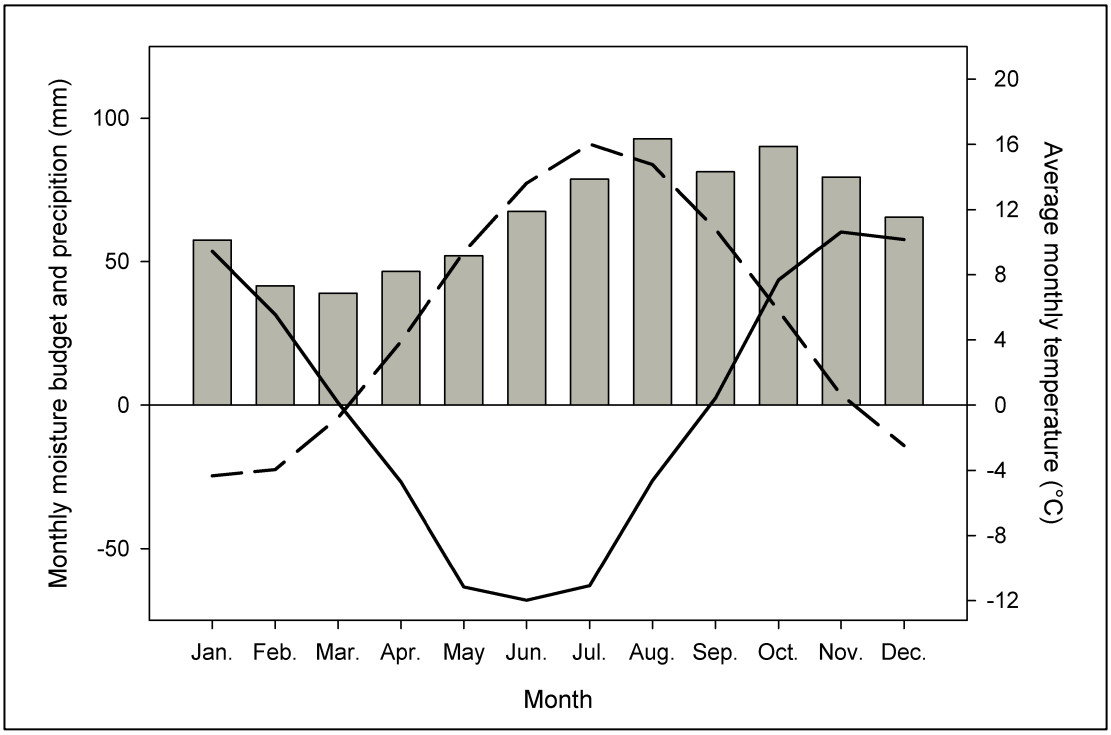

Figure 3.18 - Climate parameters for Kortlandamossen. Solid bars show monthly precipitation, the dashed line shows average monthly temperature and the solid line shows the monthly moisture budget.

3.1.6 Tore Hill Moss, Scotland

Tore Hill Moss [57°14'28"N; 3°40'01"W; altitude: 240 m a.s.l.] is the smallest of the bogs in this study, covering an area of approximately 600 m by 300 m (Figure 3.19). It is located in Abernethy Forest in the Cairngorm region of Scotland and formed as a result of a hydrosere succession in a hollow depression left by the most recent glaciation in the underlying Precambrian metamorphic rock. As shown in Section 5.5.1, an initial fen community was quickly replaced by bog species. The site is surrounded by a managed *Pinus sylvestris* forest with an extensive community of non-*Sphagnum* bryophytes. Strands of Scots pine and birch saplings encroach on the

site, especially on the southern edge, some of which have been dated to an age of over 150 years (Blundell and Barber, 2005). The study by Blundell and Barber (2005), which is the only palaeoecological study of the site, focussed on using the top 300 cm of peat to reconstruct bog surface wetness changes during the past 2,800 years and compliments the results from this research. Tore Hill Moss is not in pristine condition as peat cutting has occurred during the last 200 years. This, however, is limited to the northeastern edge of the bog. Blundell and Barber (2005) successfully reconstructed the late Holocene moisture record from Tore Hill Moss, which suggests that the bog hydrology of the lower strata has not been affected by the cutting and that an early- to mid-Holocene palaeoclimatic record can be obtained.

The current vegetation on the site is largely comprised of *Calluna vulgaris*, *Erica tetralix*, *Eriophorum vaginatum* and *Sphagnum* species, mainly *Sphagnum* section *Acutifolia* and *Sphagnum* section *Sphagnum*, in the wetter parts of the bog. The surface is reasonably hummocky although there are small patches of open *Sphagnum* rich areas. The site is, furthermore, of particular ecological interest because it is home to the rare *Sphagnum austinii* and *Sphagnum balticum*. Both species have largely become extinct across Britain and is only found on a few remaining bogs (Mauquoy and Barber, 1999; Hughes *et al.*, 2007; Hughes *et al.*, 2008; McClymont *et al.*, 2008).

Figure 3.19 - Aerial photograph of Tore Hill Moss. The yellow pin indicates coring location. (Source: Google Earth)

A three-tier strategy was employed to determine the best coring location, which ensured maximum peat depth and stratigraphic variability. The thickness of the peat deposits was established on several cross sections of the site using the coring poles to determine the site's basal topography. Once the deepest part of the bog had been identified, a detailed stratigraphic survey was undertaken (Figure 3.20) to locate a deep section with maximum stratigraphic variability. A 930 cm long research core (TOR-08-01) was extracted, showing a clear fen/bog transition at 765 cm. This transition was later supported by detailed plant macrofossil analyses. The coring location is shown in Figure 3.19.

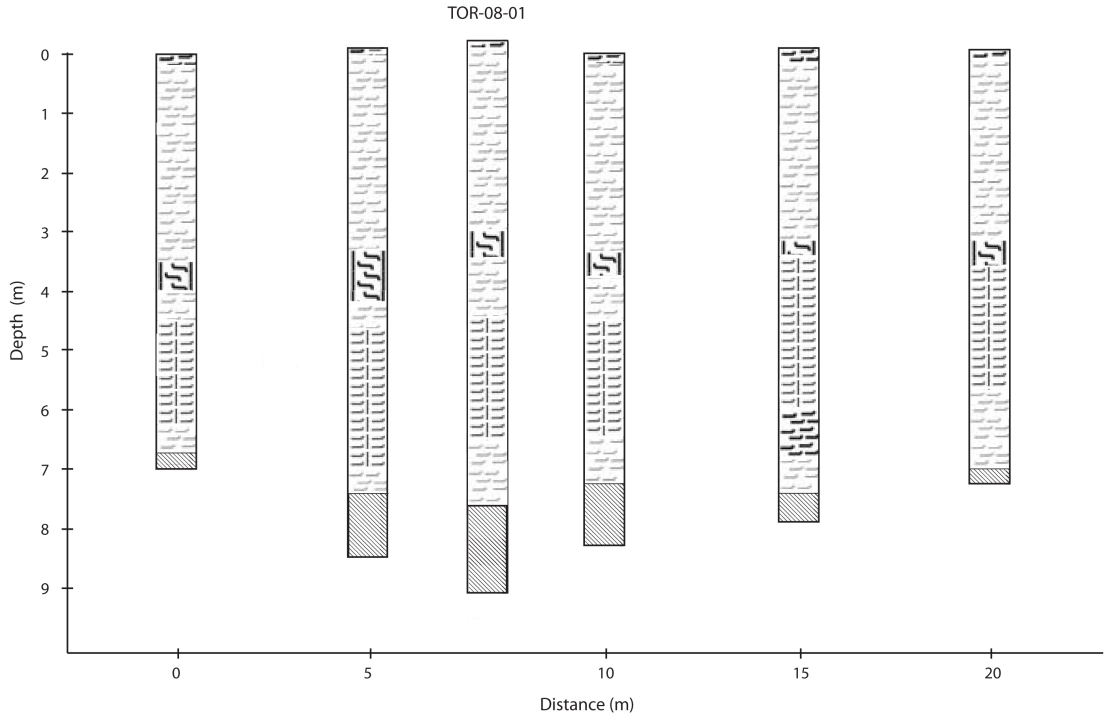

Figure 3.20 - Stratigraphy of Tore Hill Moss indicating position of TOR-08-01. Key to stratigraphy is the same as in Figure 3.17.

3.1.6.1 Climatic envelope

In contrast to the Scandinavian sites, Tore Hill Moss receives very high amounts of precipitation, averaging 1360 mm per year, with most of this precipitation occurring during the autumn and winter months (Figure 3.21). Precipitation inputs during the summer months are relatively low compared with the winter months. Temperatures at Tore Hill Moss on average do not exceed 11.1°C during the summer months, and drop to just below freezing during the winter. The annual temperature range between summer and winter months is 11.7°C and very characteristic of an oceanic location. As shown in Figure 3.21, a positive moisture balance exists during between September and March, with large gains from October to January. Gains in

September, however, are marginal. Net moisture losses between April and August are fairly constant with maximum losses occurring between June and July. The hydrological regime at Tore Hill Moss is ideal for peat accumulation and is at the upper moisture boundary for raised bog formation (Figure 3.3).

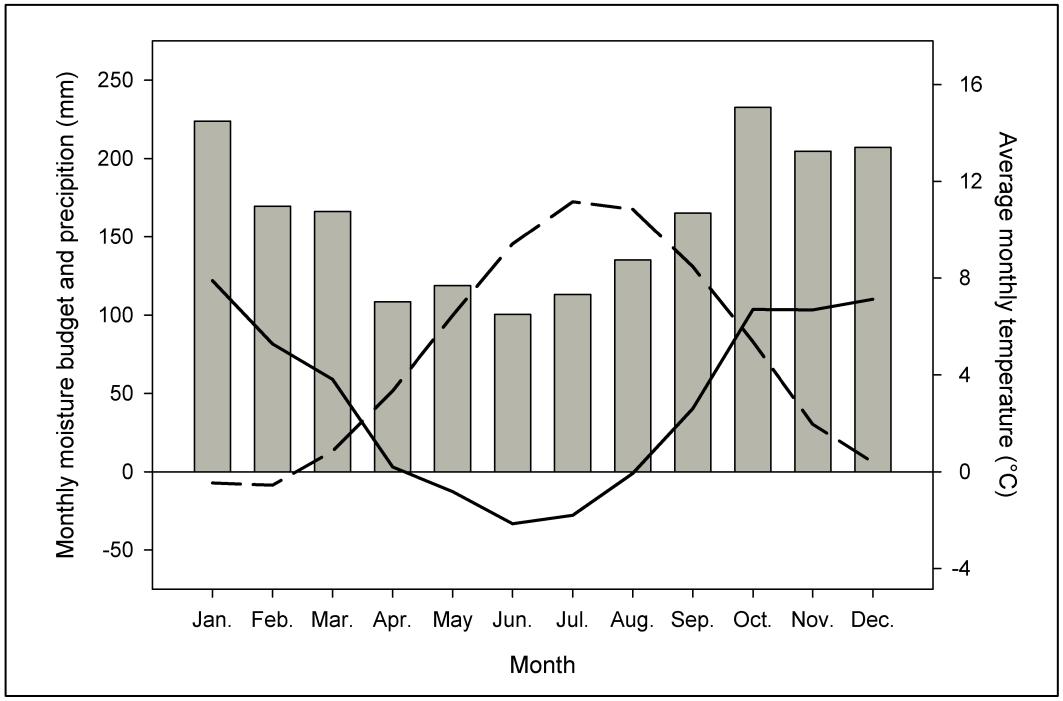

Figure 3.21 - Climate parameters for Tore Hill Moss. Solid bars show monthly precipitation, the dashed line shows average monthly temperature and the solid line shows the monthly moisture budget.

3.1.7 Raeburn Flow, Scotland

Raeburn Flow [55°02'06"N; 3°06'10"W; altitude: 70 m a.s.l] is a 64 ha ombrotrophic peat bog (Figure 3.22) in Dumfries and Galloway near Kirkpatrick-Fleming, 5 km northwest of Gretna in the Scottish Borders. Despite its proximity to the sea, no marine deposits are present in the peat profile, unlike at nearby Longbridge Muir. It

is a dedicated ‘Site of Special Scientific Interest’ (SSSI) located 20 km west-northwest from the well-studied Bolton Fell Moss and Walton Moss (Barber, 1981; Dumayne-Peaty and Barber, 1998; Hughes *et al.*, 2000a; Mauquoy and Barber, 2002; Barber *et al.*, 2003) and 4 km east of Burnfoothill Moss (Tipping, 1995a; Tipping, 1995b; Tipping, 1995c). Raeburn Flow formed over underlying Ordovician sedimentary rock as an initial fen ecosystem in a depression left by the last glaciation. The upper section of the site has been studied extensively in the past by Mauquoy and Barber (2002) and is subject to on-going monitoring and studies by Scottish Natural Heritage (S.N.H., 2009).

As part of the on-going surface management, a lot of the encroaching pine (*Pinus sylvestris*) and birch (*Betula pubescence*) scrub was removed. At present the site is dominated by *Calluna vulgaris*, *Erica tetralix* and *Eriophorum vaginatum* and it supports locally rare species such as *Andromeda polifolia*, *Narthecium ossifragum*, *Empetrum nigrum*, *Hypnum cupressiforme* and *Vaccinium oxycoccus.* Managed birch woodland is found in the middle of the bog. The site's peripheral zones are home to birch and willow scrub and open areas of *Molinia caerulea*. The surrounding area is dominated by agricultural land, sparsely forested areas and managed pine woodlands.

The site has been subject to peat cutting and drainage on the fringe throughout the past century (S.N.H., 2009). This resulted in the site’s surface drying out, but as the focus of this thesis is on the lower section of the stratigraphy, the site remains suitable for this research project. The right to cut peat is still retained to date by the owner of the site, Springkell Estate, but is not practised. Despite the disturbance to the site, it retains a large area of relatively undisturbed actively growing peatland.

Figure 3.22 - Aerial photograph of Raeburn Flow. The yellow circle indicates coring location. (Adapted from GetMapping.com)

Similar to Tore Hill Moss, the bottom topography and the deepest part of the site were determined by a series of cross-transects. At the deepest part, a more detailed stratigraphic description was created and used to determine the location with greatest stratigraphic variability (Figure 3.23). Once the optimum coring location had been identified, a 550 cm long 11 cm diameter core (RBF-08-01) was extracted from a *Sphagnum* sec. *Acutifolia* dominated low hummock / lawn area of the bog (Figure 3.22). All fieldwork on Raeburn Flow was carried out in August 2008.

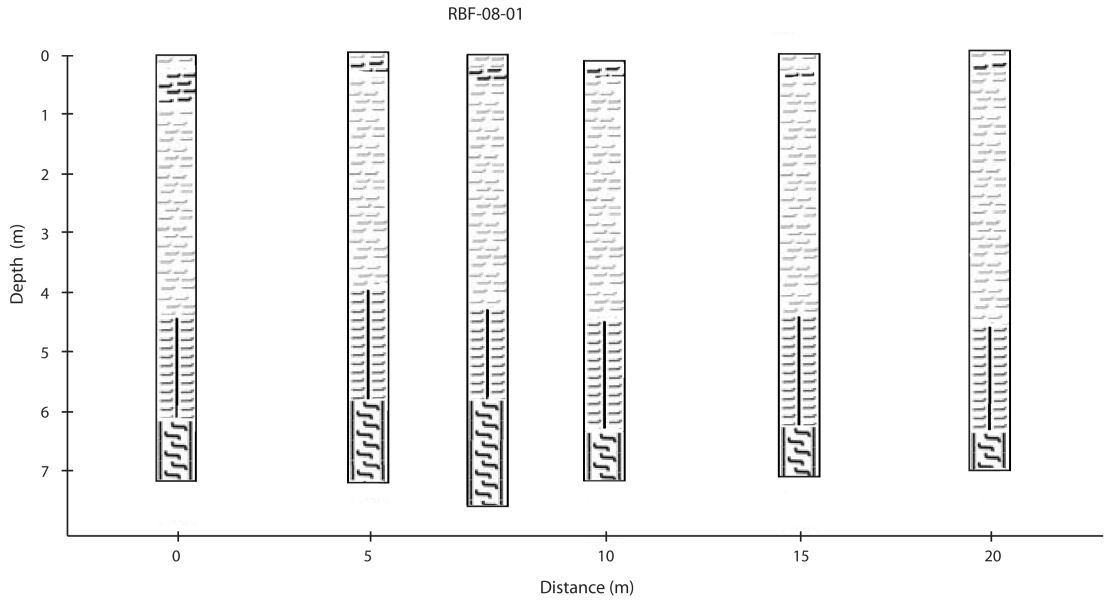

Figure 3.23 - Stratigraphy for Raeburn Flow. Coring location is at 7.5 m. Key to stratigraphy is given in **Figure 3.17**.

3.1.7.1 Climatic envelope

Precipitation patterns at Raeburn Flow closely mirror those at Tore Hill Moss, with values averaging 1300 mm per year. Most of the precipitation at Raeburn Flow falls between October and January, with relatively little precipitation during spring. The range in temperature between the hottest and coldest months is only 11°C, which highlights oceanic climate influencing Raeburn Flow. The site is the only one for which winter temperatures on average do not drop below freezing, hovering around 3°C. Summer months are relatively mild with average July-August temperatures at around 14°C. The moisture budget of the site follows that of Tore Hill Moss fairly closely, with high levels of net moisture gain between October and January,

marginal gains in September and net moisture losses from April to July (Figure 3.24).

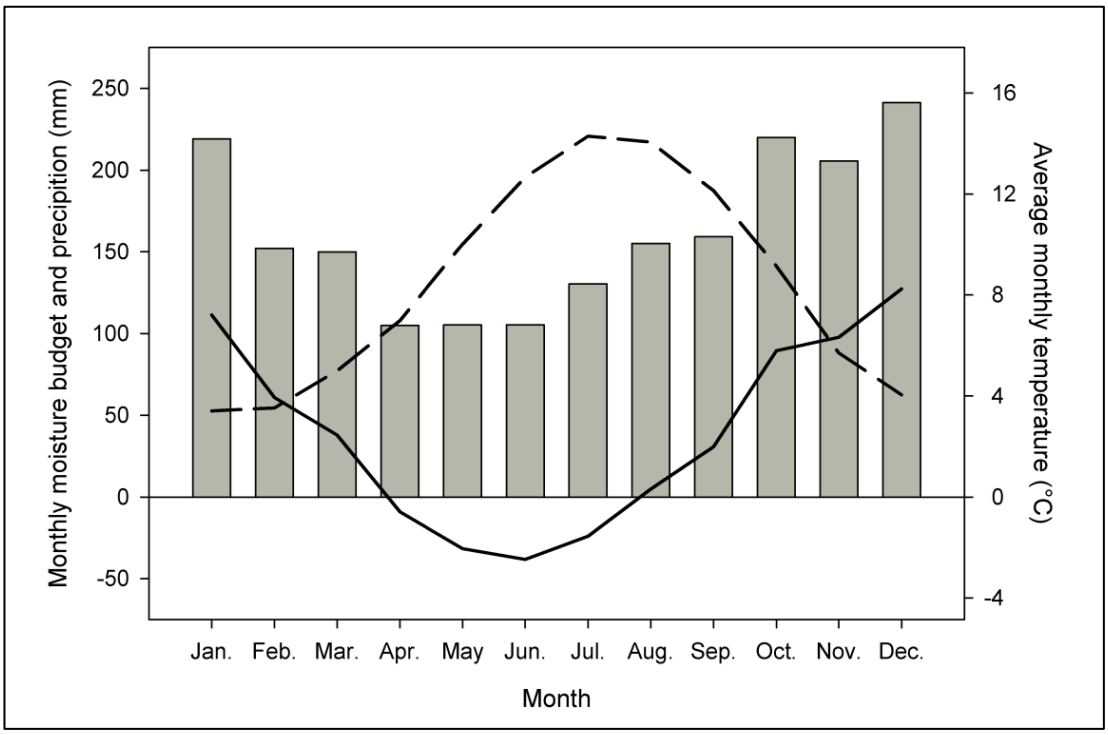

Figure 3.24 - Climate parameters for Raeburn Flow. Solid bars show monthly precipitation, the dashed line shows average monthly temperature and the solid line shows the monthly moisture budget.

3.2 Fieldwork methods

3.2.1 Core extraction

The extraction of the research cores followed a similar method at each of the sites. Because of the springy nature of the actively growing part of the bog, the acrotelm, a 50 cm x 10 cm x 10 cm monolith tin was extracted from the surface of each site, with the exception of Misten Bog, where a 1 m x 25 cm x 25 cm titanium Wardenaar corer was used. Following the sampling of the top sections, the remainder of the cores were extracted using a 'fat' 30 cm x 11 cm diameter Russian style peat corer (Barber, 1984), with the exception of Tore Hill Moss. Because of the stiff nature of the peat at Tore Hill Moss, the 11 cm diameter Russian corer could not be used to extract the core and two 5 cm diameter 'thin' Russian sections, taken 50 cm apart, were combined to form the research core. The cores were extracted from two adjacent boreholes with a 10 cm overlap between segments to overcome topographic complications and both boreholes were chosen on the same type of surface habitat. Immediately following their extraction, photographs were taken of all core segments (e.g. Figure 3.25) before being wrapped in airtight carbon-stable plastic bags. Core segments were transferred to a dark temperature-monitored coldstore as soon as possible to limit any further biological activity. All stratigraphic information was described using the Tröels-Smith classification system (Tröels-Smith, 1955).

Figure 3.25 - Core section from Misten Bog (450-480 cm) photographed immediately after extraction.

3.2.2 Surface sampling

In order to create a testate amoebae based transfer function for water table depth, ten south-central Swedish bogs were sampled, giving a total of 150 sampling locations. Four intact ombrotrophic bogs in the region of Halland, including Gällseredsmossen, and six in the region of Värmland, including Kortlandamossen, were sampled. Measurements of electrical conductivity (EC) and pH were taken from each site to ensure that all bogs were acidic and oligotrophic and therefore comparable. Once the suitability of a bog had been established, three different hummock, lawn, carpet, pool and hollow habitats were sampled giving a total of 15 samples per bog. At each sampling point, the surface vegetation in a 1 m x 1 m quadrat was described and

measurements of water table depth were taken. The water table depth was determined by digging down into the peat until water pooling occurred. After 5 – 10 minutes, to allow for the water table to equilibrate, the depth of the water table was measured relative to the peat surface. For very deep water table measurements, the vertical accuracy was lower than for more shallow water tables as in some cases the water table had not fully equilibrated after 10 minutes. Approximate measurements were taken at these locations. For near surface water tables, equilibration occurred very quickly and measurements accurately reflect water table depth at the time. As no longer term monitoring was possible, no estimates of vertical water table precision were possible. Consequently, two adjacent 5 cm x 10 cm surface samples (samples 'A' and 'B') of fresh peat were collected and sealed separately in airtight bags. Fresh peat was defined as peat where *Sphagnum* stems were vertical and not yet horizontal. GPS coordinates of each sampling location were noted and a small red flag was inserted and left at each location to aid with locating the site the following year.

In the laboratory, sample 'A' was used to determine moisture content. Fresh samples were weighed in dry ceramic crucibles of known weight, dried overnight at 105°C and reweighed. Sample 'B' was used to identify the testate amoebae species assemblage for each sampling location. The same methodology as outlined in Section 3.3.2 was used to prepare testate amoebae samples for identification. Contrary to the palaeo reconstruction, a count of 300 testate amoebae was used and samples were not 'spiked' with an exotic marker. Both the fieldwork and laboratory analysis were carried out in consultation with Charman (pers. comm.) to ensure

compatibility with the existing European testate amoebae transfer function (Charman *et al.*, 2007), which has no sampling points in Sweden.

3.3 Laboratory analysis

3.3.1 Plant macrofossils

Analysis of plant macrofossil remains followed the standard laboratory methodology set out by (Barber, 1994). A sub-sample of 4 cm^3 was washed through a 125 µm mesh sieve using 5 L of tap water to minimize systematic bias. The remaining fraction was suspended in tap water and stored in labelled Sterilin tubes. Samples were analysed in clear plastic trays under a dissecting microscope at 10 x magnification. In order to describe peat components, the Quadrat and Leaf Count (QLC) method described by Barber (Barber, 1994; Hughes *et al.*, 2012) was employed. Major peat components were noted as percentage cover within a random 1 cm x 1 cm quadrat using reference material held at the Palaeoecology Laboratory at the University of Southampton (PLUS), drawings from (Smith, 2004), and the Dutch seed atlas (Cappers *et al.*, 2006). Rare components, such as seeds, were noted as total counts. All materials which could not be identified because they were too decayed were included in an 'Unidentified Organic Matter' (UOM) category. This quadrat count procedure was repeated 15 times and the species' mean percentage abundance was calculated to give the major peat component count. All bryophytes and monocotyledon leaves were mounted on microscope slides, analysed under a high power microscope at 200x and 400x magnification and compared to the literature and existing reference material. A detailed description of the major peat

components and their ecological niches is provided in great detail by Hughes (1997), Mauquoy (1997) and McMullen (2000). All *Sphagnum* components were combined into a 'Total *Sphagnum* spp.' category. In addition to the quadrat counts, 100 *Sphagnum* leaves were picked at random per sample and identified to species level or in the case of *Sphagnum* section *Acutifolia* to section level using (Smith, 2004) at 200x and 400x magnification. The resulting *Sphagnum* leaf count data are expressed as a percentage of total peat, reflecting overall changes in *Sphagnum* abundance.

3.3.2 Testate amoebae

Testate amoebae preparation followed the recommended methodology set out by (Charman *et al.*, 2000). A sub-sample of 2 cm^3 was 'spiked' with a known quantity of *Lycopodium* spores, boiled in distilled water for 10 minutes over a hotplate and periodically stirred with a glass rod. Stirring disaggregated peat components and improved the separation of testate amoebae from peat fragments. Once boiled, the sample was sieved through a 300 µm mesh sieve to remove the coarse fraction. The filtrate was collected and sieved through a 15 µm mesh sieve to remove the fine fraction. The resultant size fraction between 300 µm and 15 µm was stored in distilled water in a stoppered glass vial.

Slides were scanned using high-powered microscopy at 100 x magnification to identify testate amoebae. Most species could be identified at this resolution, however to detect characteristic features of species such as *Difflugia pulex*, 400 x magnification was used. All species were identified using the taxonomic descriptions and key from Charman *et al.* (2000). A minimum of 150 testate amoebae or 1,000 *Lycopodium* spores were counted per sample, depending on which total was reached

first. It became evident that preservation issues of the testates affected the counts for the lower layers. Specific species, such as *Euglypha* spp., tend to break apart and dissolve quicker than others, such as *Difflugia pulex* and *Amphitrema flavum*, which results in more robust species being overrepresented. These preservation issues were taken into account in the discussion of the data. A detailed discussion of the individual testate amoebae species and their ecological preferences is provided in Section 4.3 in the context of the testate amoebae transfer function.

3.4 Chronological control

Since the project relies heavily on accurate dating a robust chronology framework based on ^{14}C dating was required. A major source of errors in ^{14}C analysis, however, is the contamination of samples by less depleted 'younger' organic material. To minimize possible sample contamination from dust and other organic matter, all preparation of radiocarbon samples was carried out at times when the laboratory was quiet. Before sub-sampling the cores for material, all surfaces in the laboratory were cleaned and covered in aluminium foil. All forceps, plastic trays, dispensing bottles, Petri dishes, sieves, scalpels and scissors were cleaned thoroughly using distilled water between samples. Samples were extracted from the core using a pair of washed scissors and a cleaned scalpel and washed through a 125 μm sieve with approximately 500 ml of distilled water. The exact amount of distilled water used to wash the samples was not important as it solely served to remove UOM.

Under a cleaned dissecting microscope, *Sphagnum* stems were 'picked' from the samples and transferred to a Petri dish, filled with distilled water. Where insufficient

Sphagnum stems were available, other above ground material, such as brown moss stems or remains of *Calluna vulgaris* were sampled. A list of samples and material used is provided in Section 5.2. The presence of fungal and root material can considerably affect the accuracy of age-depth determinations by introducing 'younger' carbon to the sample. The sub-sampled material was therefore cleaned of all root and fungal matter by splitting open and checking the *Sphagnum* stems and consequently transferred to a second Petri dish for a further wash with distilled water. After the final wash, samples were weighed to ensure enough carbon was present for analysis. A minimum weight of 300 mg of wet material was used per sample.

At the radiocarbon laboratories, samples were digested in 2M HCl (80C, 8 hours), washed free from mineral acid with deionised water then dried and homogenised. The total carbon in a known weight of the pre-treated sample was recovered as CO_2 by heating with CuO in a sealed quartz tube. The gas was converted to graphite by Fe/Zn reduction. All ^{14}C counting was carried out using accelerated mass spectrometry (AMS) in three different laboratories: Poznan University, NERC East Kilbride facility and Beta Analytic. The results of the chronological analysis are discussed in more detail in Section 5.2.

4 Quantifying bog surface wetness

4.1 Introduction

In order to make inferences about past changes in BSW, biostratigraphic data needs to be converted into a univariate index. Most peat-based palaeoecological studies so far have been based on peat humification, plant macrofossils analysis and testate amoebae analysis in order to reconstruct bog surface conditions. In numerous studies, individual BSW reconstructions are calculated for each proxy and then combined into a single index. For biological proxies, such as plant macrofossils and testate amoebae analysis, this multivariate processing generally involves the use of a weighted averaging system in the form of detrended correspondence analysis (DCA) or the calculation of a hydroclimatic index (HCI). Testate amoebae, however, tend to have a normal distribution around their mean preference for distance to the water table and therefore lend themselves to more advanced statistical modelling based on regression and calibration using modern training sets. Where modern training sets exist, the use of a transfer function is therefore recommended for testate amoebae (e.g. Hendon *et al.*, 2001; Charman *et al.*, 2007).

Once single values of BSW have been calculated for individual proxies, they are generally standardised and averaged into a final single index. The main problem with this approach is that climate signals contained in the individual proxy sources often do not respond to the same driving mechanisms. The climatic signal contained in plant macrofossils remains corresponds to conditions during the growing season, whereas testate amoebae activity can continue throughout the winter months in

snow-insulated peat or in areas where the temperature remains above freezing point. This, however, does not pose a problem as a 1 cm slice of peat averages palaeohydrological conditions across an approximate 10-year time-slice. Averaging of reconstructions becomes more problematic when ecological proxies are combined with biochemical processes, such as colorimetric peat humification. By determining the amount of light transmitted through a sample, colorimetric peat humification is a proxy measure of the amount of humic and humin acids in a peat sample, which are released as a result of the cellular breakdown of plant material. It has been established that plant species making up the peat matrix strongly influence the degree of peat humification and the level of discolouration of the humification extract (Overbeck, 1947; Yeloff and Mauquoy, 2006; Hughes *et al.*, 2012). However, the climate parameters and autogenic processes driving the peat humification signal are yet to be fully explored. Combining two proxy sources that reconstruct hydrological conditions on the bog surface with one that does not clearly respond to the same driving factors is therefore questionable and can lead to erroneous results. Peat humification was therefore not used in BSW reconstructions throughout this thesis.

4.2 Plant macrofossils as indicator of BSW

Whittaker (1967) was one of the first people to statistically describe biological communities in terms of an external environmental factor. In order to measure the extent to which plant species composition on sand dunes could be explained in terms of soil moisture, Whittaker developed and applied gradient analysis, a system based on correspondence analysis (CA). Gradient analysis, however, only explains

straightforward linear parameter-community relationships and fails when more complex or latent environmental gradients influence the ordination space. Addressing this shortcoming of gradient analysis, Hill (1973) advanced the method further by combining gradient analysis with successive approximation leading to an ordination technique similar to principle component analysis, known as reciprocal averaging. Reciprocal averaging works by constantly recalibrating species-scores along the ordination axis, greatly pushing forward the use of statistics to explain complex environment gradients in terms of floristic composition. Reciprocal averaging, however, does have the inherent problem that the ends of the correlation axis can be compressed relative to the axis' middle; furthermore the second correlation axis tends to have a systematic relationship to the first axis (Hill and Gauch, 1980; Jongman *et al.*, 1995, pp. 105). By detrending the data in segmented polynomials, Hill & Gauch (1980) addressed these inherent problems and developed Detrended Correspondence Analysis (DCA). By overcoming the problems intrinsic to CA, DCA could consequently be used to extract any complex and unknown environmental gradients from palaeoecological data (Hill and Gauch, 1980; Birks, 1995; Jongman *et al.*, 1995; Kovach, 1995). The main use of DCA in palaeoecology has since become to condense multivariate species assemblages into monovariate values relative to an underlying environmental gradient. As this method operates 'blindly' on the data, the analyst has to identify and interpret any environmental gradients that are being picked out. Because of its objective approach, DCA has been used extensively to create indices of plant macrofossil-inferred palaeohydrological change (Hughes *et al.*, 2000a; Langdon *et al.*, 2003; Barber *et al.*, 2004; Blundell and Barber, 2005). Despite its use in identifying strong environmental gradients and thresholds, such as the fen-bog transition (e.g. Hughes *et al.*, 2000b), DCA can run

into problems when constructing BSW indices from fully developed ombrotrophic peat bogs (Daley and Barber, 2012) with limited species gradients. One of the main problems with DCA is that rare species with low abundances need to be excluded from the analysis, as they can skew the distribution of plants in the environmental eigenspace created by DCA. This artificially shortens the environmental gradient that is being described. A short species gradient is undesirable as it can produce inaccurate results that do not always represent BSW as a principle component when in fact this variable does account for a key part of the variability in the dataset (Daley and Barber, 2012). When two species that largely dominate the profile are mutually exclusive, DCA will always pick out a bi-species absence-presence gradient on its principle ordination axis. This can occur when the plant communities on the bog switch between *Sphagnum* and monocotyledon dominated phases which exclude the presence of one another or when two competing *Sphagnum* species, such as *S*. section *Acutifolia* and *S*. section *Sphagnum* dominate the profile at different stages in the stratigraphy. To address this problem two separate DCAs, one for each domination phase, can be performed and combined into a single curve. Alternatively, dominant species can be excluded from the analysis altogether. Both approaches are far from ideal and negate the objectivity of DCA, making the analysis subjective and irreproducible.

Furthermore, DCA does not take into account whether species are indicative of specific BSW conditions, or whether they are catholic in nature. This subtle but valuable ecological information gets lost in the statistical processing which produces an oversimplified view of the ecosystem. The use of DCA as a means of reconstructing BSW on ombrotrophic bogs can therefore be problematic and at times

a relatively poor indicator, when compared with other methods (Daley and Barber, 2012).

To ensure that plant macrofossil data can be combined into a single index of palaeohydrological change in a reproducible manner, a Hydroclimatic Index (HCI) (Dupont and Benninkmeijer, 1984; Dupont, 1986) can be constructed. Similar to DCA, the HCI is based on weighted averaging and uses species-scores to calculate sample-scores for each peat level. Initially the HCI was devised to classify Ericaceae and *Sphagnum* species (Dupont, 1986), but recent developments (Mauquoy, 1997; Barber *et al.*, 2003; Mauquoy *et al.*, 2008) have seen the inclusion of brown mosses and further monocotyledon species. As with gradient analysis, species-scores are attributed to the individual plant species, representing their position on the BSW gradient. Species with low species-scores are those that thrive in very wet habitats, whereas those with high species-scores are those that occupy dry habitats. Individual species-scores are attributed using knowledge about modern bog surface wetness preferences of bog plant species.

The main difference between DCA and the HCI is that empirical knowledge about the plant species' BSW preferences is used to construct species-scores for the HCI, whereas DCA 'blindly' calculates species-scores from a single peat core relative to an unknown environmental variable, which needs to be interpreted using empirical knowledge. Species-scores for individual peat components and plant species that make up peat profiles have changed with advances in understanding of bog plant preferences (Mauquoy, 1997; McMullen, 2000; Daley and Barber, 2012). The most significant advantage of the HCI over DCA, however, is that the resulting values always represent BSW, as species-scores have been chosen to reflect this.

Furthermore, DCA species-scores only reflect measurements from a single core and not from a wider range of sites. Using knowledge of species preferences from a wide range of sites and plant communities adds a valuable dimension to the final BSW index.

Attempts to construct a HCI for plant macrofossil data have been elementary so far and further refinement of the individual species-scores is still needed. One of the key aspects of previous attempts to construct a HCI was the inclusion of the maximum amount of peat components in each sample-score to maximise accuracy of results. This has, however, lead to the uncritical inclusion of plant elements that distort the resulting HCI. A significant problem with previous HCI implementations is the inclusion of root material. Even in very recent publications, such as Daley and Barber (2012), *Eriophorum vaginatum* and *Eriophorum angustifolium* roots have been used as part of the HCI. These roots, however, do not represent conditions at the bog surface as *Eriophorum* spp. roots can penetrate deep into the catotelm of a bog. By including *Eriophorum* spp. root material, components of plants that are not currently growing in the coring location are being used to calculate the HCI. A similar problem arises with the inclusion of Ericaceae rootlets and monocotyledon root material. Monocotyledon plant material furthermore poses yet another problem. As shown in Table 4.1, different monocotyledon species, such as *Rhynchospora alba* and *Trichophorum cespitosum*, can have greatly varying species-scores; 3 and 6 respectively. In previous HCI reconstructions, all unidentifiable monocotyledon plant material was lumped into a single category with a species-score of 7 (Mauquoy, 1997; Daley and Barber, 2012). By attributing a single HCI species-score to a group of species with a wide range of hydrological preferences, BSW conditions

are not accurately reconstructed. The problems associated with combining different species into a single value emphasise the need to fully separate components in the original macrofossil analysis when possible. All above ground monocotyledon material that could not be identified to species level was therefore excluded from the HCI.

Material that is too broken down to be correctly identified (unidentified organic material – UOM) poses yet another challenge to reconstructing BSW using a HCI. Traditionally, UOM has been considered a sign of very dry bog surface conditions and received a species score of 8 (Mauquoy, 1997). Part of this material can, however, be algal mud, which is indicative of very wet surface conditions, as discussed by Daley and Barber (2012). Unless careful observations in the field are recorded with regards to the colour and texture of the peat at all depths, algal mud cannot easily be distinguished from UOM at a later stage under a dissecting microscope. Where possible, both peat components should be separated with individual species-scores. However, field observations of colour and texture were not taken with high enough resolution in this study and therefore UOM and algal mud are not included in the HCI.

Care also has to be taken with material that can easily be wind-blown to the coring location, such as *Betula* wood or coniferous needles. These plant fragments do not necessarily represent surface wetness conditions at the coring location and therefore cannot be accurately linked to BSW at the level in question. For this reason, all material that has a relatively high chance of being wind-blown is excluded from the HCI. Taking into account the given problems with HCI, a new weighting classification for bog plants to reconstruct BSW using HCI is presented in Table 4.1.

Table 4.1 - Plant species and corresponding species score for HCI reconstructions.

Taxon	Species-score
Aulacomnium palustre	6
Andromeda polifolia, stem and leaf	6
Brown moss undiff.	6
Calluna vulgaris, stem, leaf and seed box	8
Empetrum nigrum, stem and leaf	6
Erica tetralix, stem and leaf	8
Ericaceae wood, undiff.	8
Eriophorum angustifolium: leaves, stem and node	2
Eriophorum vaginatum: stem, leaf, node and spindles	6
Hypnum jutlandicum	6
Narcesium ossifragum	4
Phragmites australis	1
Polytrichum alpestre type	7
Rhynchospora alba: leaf, node and propagules	3
Sphagnum austinii	5
Sphagnum balticum	2
Sphagnum cuspidatum	1
Sphagnum fuscum	3
Sphagnum magellanicum	3
Sphagnum papillosum	4
Sphagnum pulchrum	2
Sphagnum section *Cuspidata*	1
Sphagnum section *Acutifolia*	6
Sphagnum tenellum	2
Trichophorum cespitosum, leaf and node	6
Vaccinium oxycoccus, stem and leaf	4

Using species-scores, a HCI was calculated by dividing the sum of species abundances multiplied by their species-score by the sum of species abundances (Equation 4.1). This ensured that samples where species without a HCI species-

score, such as root material, make up part of the peat matrix do not artificially skew the resulting HCI.

$$HCL = \frac{\sum_{i=0}^{n} x_i y_i}{\sum_{i=0}^{n} x_i}$$

Equation 4.1 - Formula for calculating the traditional HCL, where n is the number of indexed species in the level, x is the species' abundance and y is the corresponding species score.

Using species-scores, a HCI was calculated by dividing the sum of species abundances multiplied by their species-score by the sum of species abundances (Equation 4.1). This ensured that samples, where species without an HCI species score, such as root material, make up part of the peat matrix do not artificially skew the resulting HCI.

As outlined above, sensitive ecological information, such as a species' very narrow hydrological tolerance, is lost in both the DCA and HCI. This problem can be addressed by adding a new dimension to the HCI reconstruction, which takes into account how indicative each species is of BSW conditions. The new dimension is called an indicator score, resulting in an indicator-weighted HCI (IHCI).

Table 4.2 shows the IHCI scores for the same set of species that were used in the old HCI system (Table 4.1). It is worth noting that the species-scores for the individual bog taxa remain unchanged. To ensure that the resulting BSW index is not artificially skewed and that the relationship between samples is maintained, all species abundances are multiplied by their respective indicator score before summing up (Equation 4.2).

$$IHCI = \frac{\sum_{i=0}^{n} x_i y_i z_i}{\sum_{i=0}^{n} x_i z_i}$$

Equation 4.2 - Formula for calculating the new IHCI, where **z** is the indicator score of the species as outlined in Equation 4.1.

Table 4.2 - Bog plant taxa with corresponding species and indicator scores for IHCI reconstructions.

Taxon	Species-score	Indicator-score
Aulacomnium palustre	6	1
Andromeda polifolia, stem and leaf	6	1
Brown moss undiff.	6	1
Calluna vulgaris, stem, leaf and seed box	8	1
Empetrum nigrum, stem and leaf	6	1
Erica tetralix, stem and leaf	8	1
Ericaceae wood, undiff.	8	1
Eriophorum angustifolium, leaves, stem and node	2	1
Eriophorum vaginatum, stem, leaf, node and spindles	6	1
Hypnum jutlandicum	6	1
Narcesium ossifragum	4	1
Phragmites australis	1	2
Polytrichum alpestre type	7	1
Rhynchospora alba, leaf, node and propagules	3	2
Sphagnum austinii	5	1
Sphagnum balticum	2	1
Sphagnum cuspidatum	1	2
Sphagnum fuscum	3	1
Sphagnum magellanicum	3	1
Sphagnum papillosum	4	1
Sphagnum pulchrum	2	1
Sphagnum section *Cuspidata*	1	1
Sphagnum section *Acutifolia*	6	1
Sphagnum tenellum	2	1
Trichophorum cespitosum, leaf and node	6	2
Vaccinium oxycoccus, stem and leaf	4	1

4.3 Testate amoebae-based palaeohydrological reconstructions

As with plant macrofossils, a HCI can be used to reconstruct BSW from fossil testate amoebae data based on an empirical knowledge of modern testate species (Mauquoy, 1997). However, this is only necessary in very rare cases as more advanced statistics exist that allow robust handling of testate amoebae data. For geographical regions where no modern training sets exist, DCA proves a more reliable method of quantifying multivariate fossil data into a univariate measure of BSW than a HCI. Ordination of testate amoebae data often results in long ordination axes (> 4 standard deviation units), which lends itself very well to DCA. In addition, testate amoebae species tend to have a unimodal response to changes in hydrology, which matches the assumed unimodal response of DCA. Given this unimodal response to an environmental variable and their abundance in modern samples, testate amoebae are ideally suited for transfer functions modelling. The modelling of modern abundances' responses to hydrological change (regression) and the use of modelled responses to infer palaeohydrological change (calibration) has been growing in popularity ever since ter Braak and van Dam's (1989) and Birks *et al.*'s (1990) ground-breaking works on changes in diatom assemblages in responses to changes in pH. Ter Braak and van Dam (1989) initially introduced the maximum likelihood and weighted averaging (WA) models to establish a relationship between taxa and an environmental gradient. Birks *et al.* (1990) rigorously tested ter Braak and van Dam's work supporting the idea that although a maximum likelihood approach would yield better results than weighted averaging, the latter was robust enough and produced lower root mean squares of errors (RMSE). RMSE statistics are used to

gauge an estimate of the predictive power of a regression model (Wallach and Goffinet, 1989).

In order to improve the predictive power of WA, ter Braak and Juggins (1993) combined WA and partial least squares regression (WA-PLS), which successively selects linear components to maximize predictive power. Ter Braak and Juggins went on to show that WA was less vulnerable to dimensionality and that it dealt better with outliers than other previous regression models. Building on this work, Birks (1998) gave a thorough review of mathematical tools in palaeoecological regressions and concluded that WA-PLS is the best modelling method for data with little noise, whereas a simple two-way WA with inversed deshrinking works best on noisy data with a long ordination axis.

Another model that is often used in the regression and calibration of fossil data using model training-sets is a technique called weighted modern analogue technique (WMAT). Contrary to WA, WMAT does not assume an underlying species-environment response model. By re-examining a foraminiferal sea surface temperature training set for the North Atlantic, Telford and Birks (2005) concluded that the WMAT model had internalized non-temperature spatial structures to improve its performance and that WMAT performance statistics tend to overestimate the predictive power of the models. To quantify the real predictive power of WMAT models, autocorrelation tests are required to verify that test statistics are not overoptimistic (Telford and Birks, 2005; Telford and Birks, 2009; Telford and Birks, 2011). Models that assume a unimodal species-environment response tend to perform better and give more robust results than those that do not assume any species-environment response (Telford and Birks, 2005).

As no testate amoebae-based palaeohydrological transfer function exists for Sweden and the European transfer function (Charman *et al.*, 2007) does not include any Swedish sites, a series of south-central Swedish peat bogs were sampled in order to construct a modern calibration training set for the region. From a total of 10 bogs, 30 moisture gradients ranging from a pool to a high hummock were sampled (Figure 4.1, **Error! Reference source not found.**). Each moisture gradient consisted of 5 sampling locations, giving a total of 150 sampling locations, in order to maximize the gradient length and to make samples statistically representative. Water table depths ranged from 0 cm to 70 cm (see Appendix A). Problems regarding the accuracy of deep water tables are discussed in Section 3.2.2. To avoid problems of spatial autocorrelation associated with clustering of locations (Telford and Birks, 2005), all gradients were chosen from unconnected pool/hummock systems. A detailed description of the surface sampling and consequent laboratory analysis is given in Sections 3.2 and 3.3.

Table 4.3 - Sites sampled for the testate amoebae transfer function:

Location	Latitude	Longitude	Altitude (m a.s.l)	Max. WTD (cm)	Moisture range (%)
Gällseredsmossen	56°10'30"N	12°35'51"E	105	70	97.25 – 89.25
S1	56°06'50"N	12°46'52"E	151	45	95.96 – 91.58
S2	56°10'21"N	12°42'45"E	112	30	96.73 – 88.81
S3	56°10'29"N	12°38'03"E	121	35	96.41 – 93.64
Kortlandamossen	59°50'54"N	12°17'12"E	138	50	97.53 – 88.43
N1	59°51'45"N	12°19'29"E	138	40	96.57 – 90.04
N2	59°51'15"N	12°18'11"E	132	25	98.01 – 86.46
N3	59°52'31"N	12°17'29"E	134	40	96.33 – 92.70
N4	59°52'22"N	12°18'19"E	126	40	96.21 – 92.05
N5	59°55'26"N	12°16'22"E	136	30	96.95 – 91.30

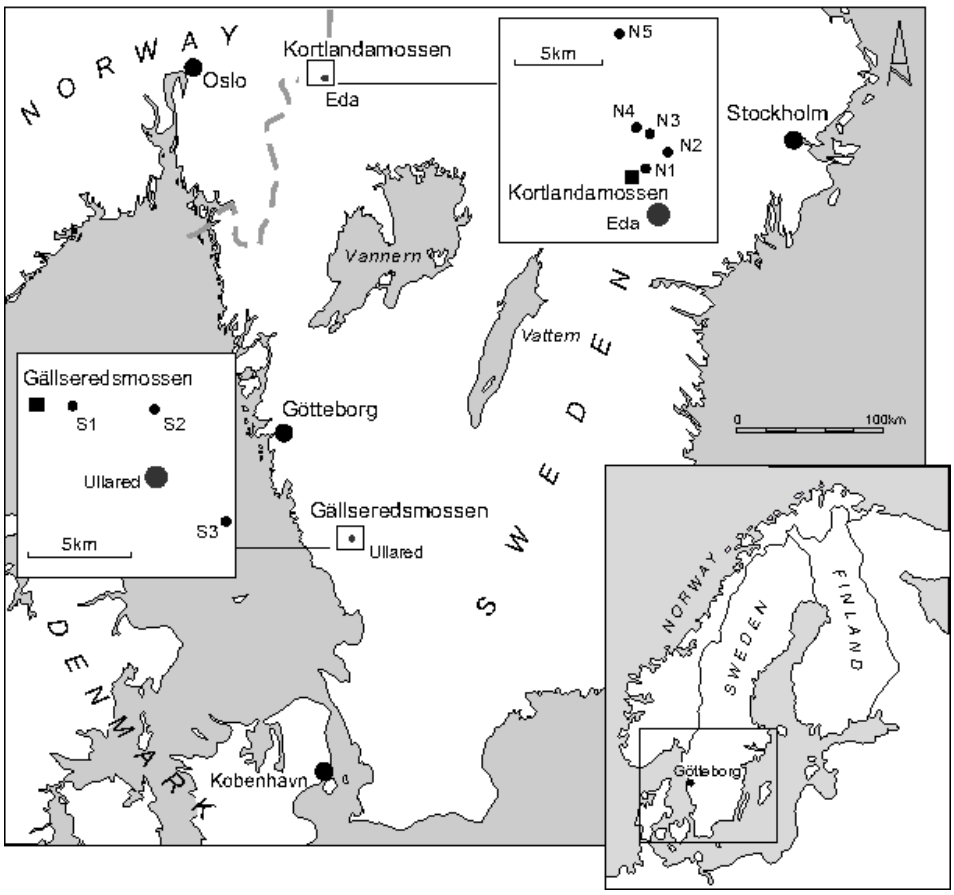

Figure 4.1 - Sampling sites included in transfer function (Drawn by Sue Rouillard).

From each of the 150 sampling locations, 150 ± 5% testates were counted (Counts – see Appendix A). In total 48 different modern testate amoebae species were identified across all samples with an average count per species of 50 individuals. Tolonen *et al.* (1994) highlighted that the influence of nutrient status on testate amoebae communities is less dominant than hydrological controls in ombrotrophic peat bogs. The pH and conductivity measurements confirmed that all sampling locations were oligotrophic, with pH ranging between 3.13 and 4.26 and conductivity between 42.45 µS/cm and 120.68 µS/cm. Testate amoebae assemblages are therefore unlikely to be affected by the nutrient status of the bog. No detailed measurements of macronutrients were taken from the locations. Moisture content of all sampling locations ranged from very wet to relatively dry, with the wettest peat

containing 98.01% moisture and the driest containing 86.46%. As expected, moisture content and depth to water table were negatively correlated (F=-0.311; p=0.04).

To ensure the cosmopolitan distribution of most testate amoebae taxa, a DCA was performed on all modern testate amoebae data and the resulting ordination space was mapped (Figure 4.2). The data show no clustering of sites with samples from all 10 bogs overlapping with one another in ordination space, suggesting cosmopolitan distribution of most taxa.

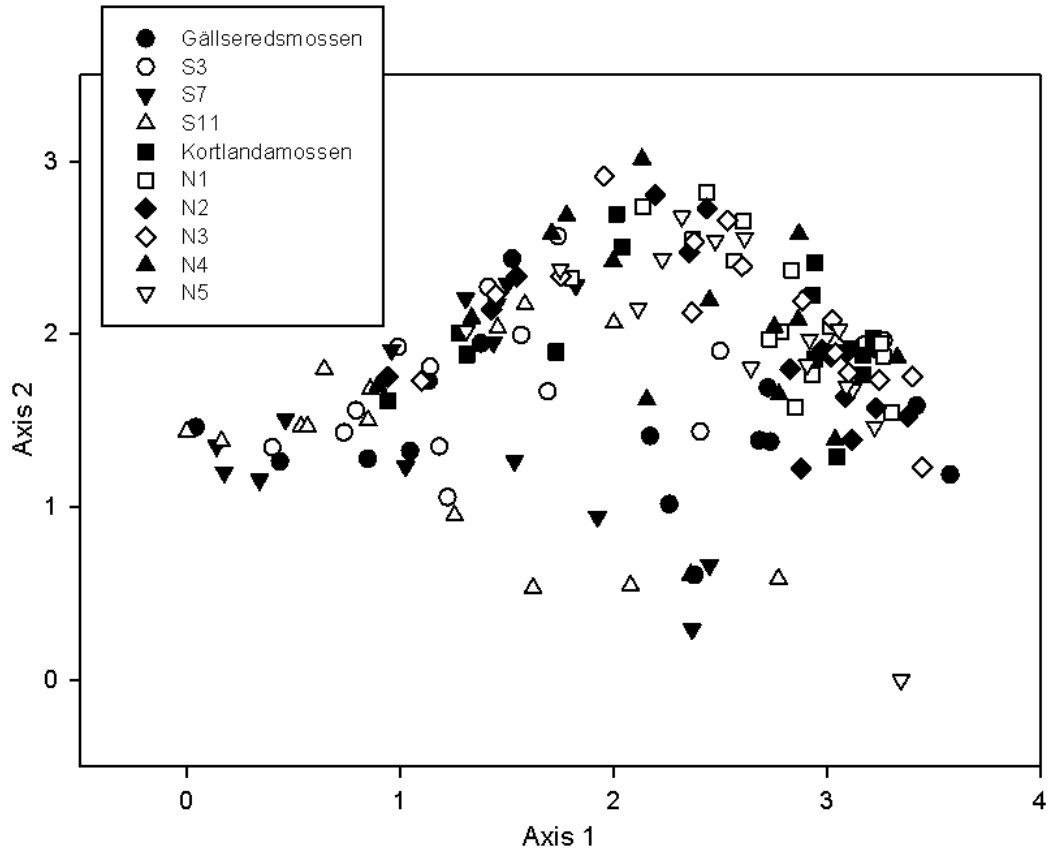

Figure 4.2 - Sample ordination based on all testate amoebae data showing the cosmopolitan nature of testate taxa.

Species ordination (Figure 4.3) largely reflects the hydrological gradient from wet (high values) to dry (low values) habitats. *Difflugia pulex*, a species for which BSW preferences are still unclear, plots centrally on DCA Axis 1, suggesting that it thrives in intermediate conditions. It has previously been suggested it mostly thrives in intermediate dry conditions (Charman *et al.*, 2007). This difference in hydrological optima highlights that more information is needed for *D. pulex* and that important species can differ considerably in their preferences for BSW conditions between Sweden and the rest of Europe. It also further emphasizes the need for a Swedish testate amoebae-based training set.

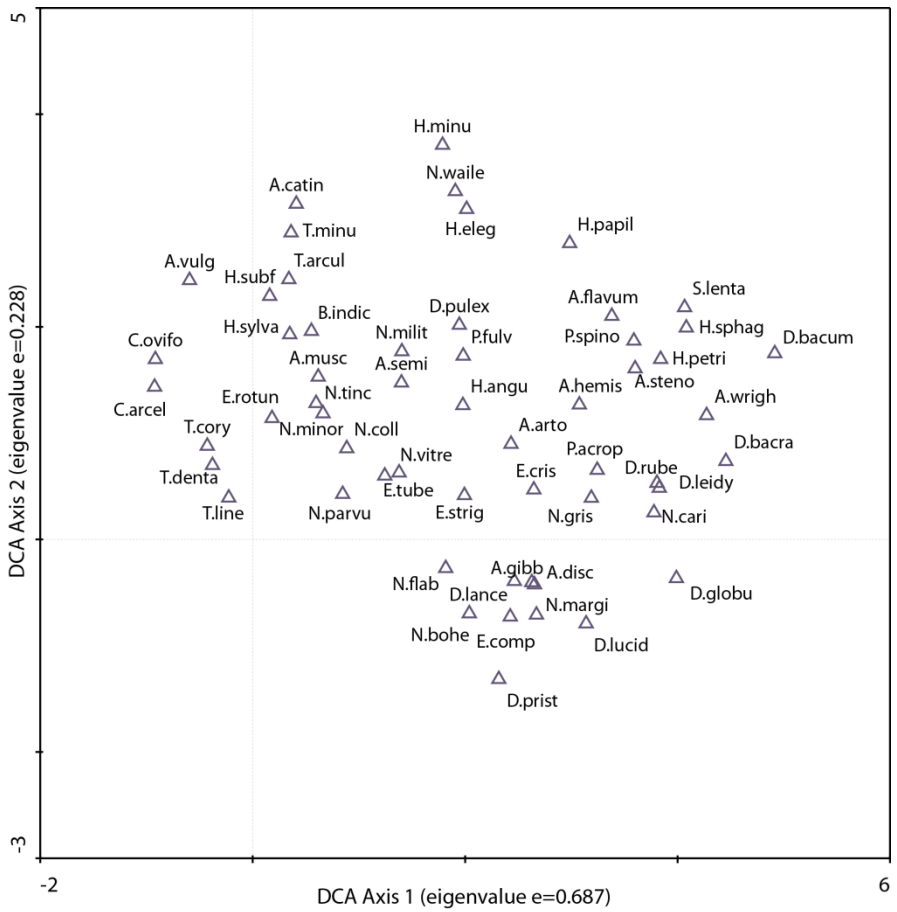

Figure 4.3 – Species ordination based on DCA of all testate amoebae data (DCA Axis 1 versus DCA Axis 2).

Although it is often abundant in the fossil record, *D. pulex* could not be included in early transfer functions (Woodland *et al.*, 1998), as not enough modern analogues were found in the surface samples. Charman *et al.* (2007) addressed this issue by including more sampling locations in their training set, ensuring that sufficient *D. pulex* specimens were counted to be included in the European transfer function. However, they went on to point out that more work is needed to establish the species' hydrological preferences. *D. pulex* was found in large numbers in the Swedish surface samples and like Charman *et al.*'s work, it showed preferences for intermediate dry hydrological conditions with an water table depth optimum of 14 cm. As with *D. pulex*, observations of *Hyalosphenia subflava* were sparse in previous training sets. *H. subflava* is a dry indicator species that is exclusively found in hummock microforms. Further observations from Swedish surface samples confirmed its position on the hydrological gradient.

In order to determine the environmental variable that has the greatest influence on a species assemblage a constrained ordination analysis using canonical correspondence analysis (CCA) was carried out on the modern data (Figure 4.4). It suggests that hydrology is the most important factor influencing species composition as depth to water table and moisture content line up closest with Axis 1. A Monte Carlo permutation test shows that DCA Axis 1 is the significant ordination axis ($p < 0.001$) and a further test on depth to water table revealed that it is significant at $p < 0.001$.

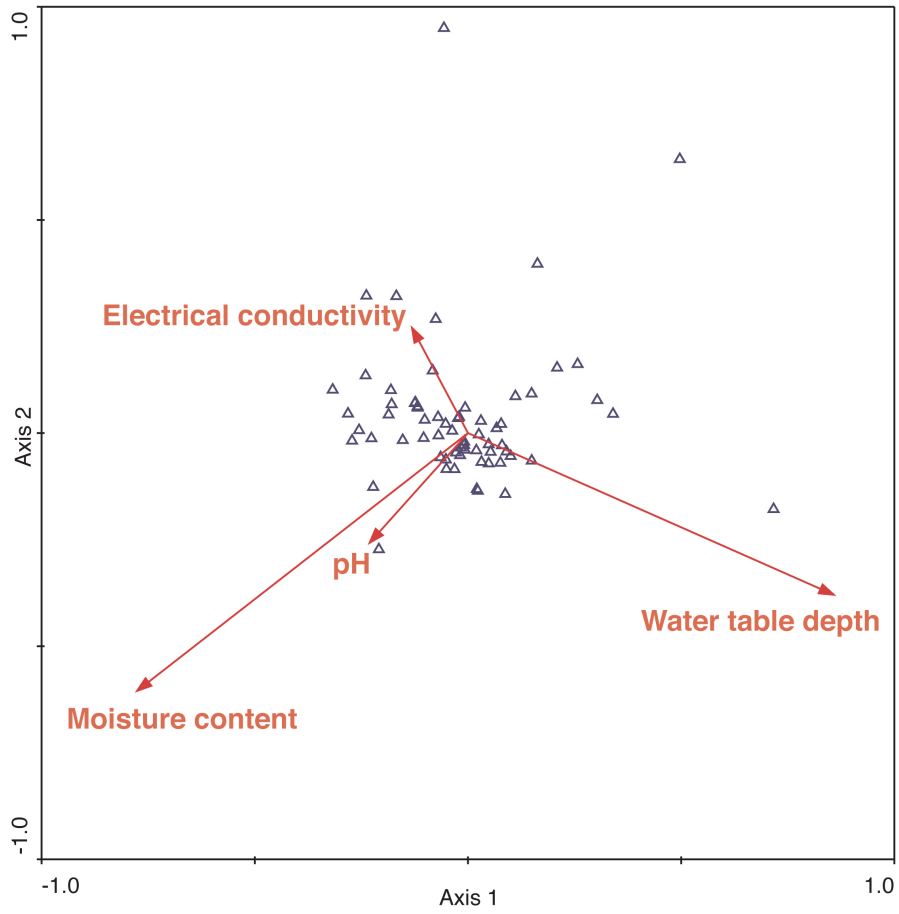

Figure 4.4 - Constrained ordination space from CCA of all testate amoebae data showing a species-environment biplot.

Both moisture content and depth-to-water table are shown to affect testate amoebae assemblages. However, as pointed out by Charman *et al.* (2007), moisture content is a less reliable parameter in correlating fossil testate amoebae data as it fluctuates on a daily basis. Furthermore, moisture will evaporate between the point of sampling and the moment of analysis. Therefore, only a transfer function for depth to water table was constructed in order to calibrate fossil data within this study.

Testate amoebae species distributions relative to the depth to water table show a strong relationship between taxa and the hydrological gradient (Figure 4.6). Taxa at the wet end of the gradient are shown to exist in a narrower tolerance range than those at the drier end. A clear division in gradient distribution between wet and dry taxa becomes apparent. Taxa at the wet end of the gradient are rarely found in dry conditions, whereas taxa that are most abundant in dry conditions can, to an extent, survive wet conditions.

Using a full testate amoebae dataset, most of the models used to construct the transfer function performed relatively well, with the weighted averaging tolerances down-weighted with inverse deshrinking model outperforming the other ones (RSEMP = 8.49cm; $r^2 = 0.71$) (Table 4.4). It is interesting to note that although the WMAT model tends to overestimate its predictive power (Telford and Birks, 2005), it was not the best performing model.

Table 4.4 - Summary of the performance of different models used for the construction of a palaeohydrological transfer function. Only the best components of the partial least square approaches are shown.

Model	r^2	Average bias	Maximum bias	RMSEP
WAPLS Component 2	0.73	0.00	31.37	9.01
WMAT	0.67	-0.26	39.57	8.50
PLS Component 3	0.69	0.00	27.59	9.00
WA-Tol (inverse deshrinking)	**0.71**	**0.00**	**32.26**	**8.49**
WA (inverse deshrinking)	0.63	0.00	31.03	9.50

Figure 4.5 shows observed water table measurements plotted against predicted values. It is worth noting that the performance of the model was particularly poor for samples with depths to water tables greater than 50 cm. When measuring the water table depth for very deep samples, levels may not have re-equilibrated fully after digging and water table depths may therefore have been overestimated in some of the field measurements. Samples with a very deep water table were consequently treated as outliers and samples with residual values greater than 20% of the full water table depth gradient (> 14 cm) were excluded from the model. Rare species that did not occur in more than three samples and did not make up a total percentage count of 5% were also excluded, as the optimum and tolerance results for these species may be statistically insignificant and misleading.

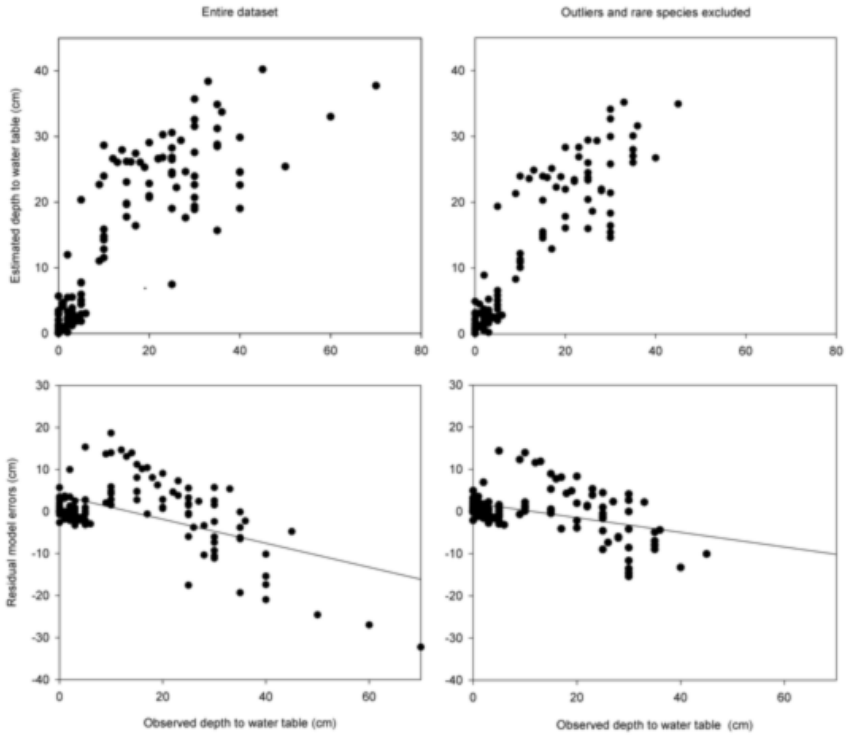

Figure 4.5 - Observed depths to water table plotted against predicted values for the entire dataset (left) and for the screened dataset (right).

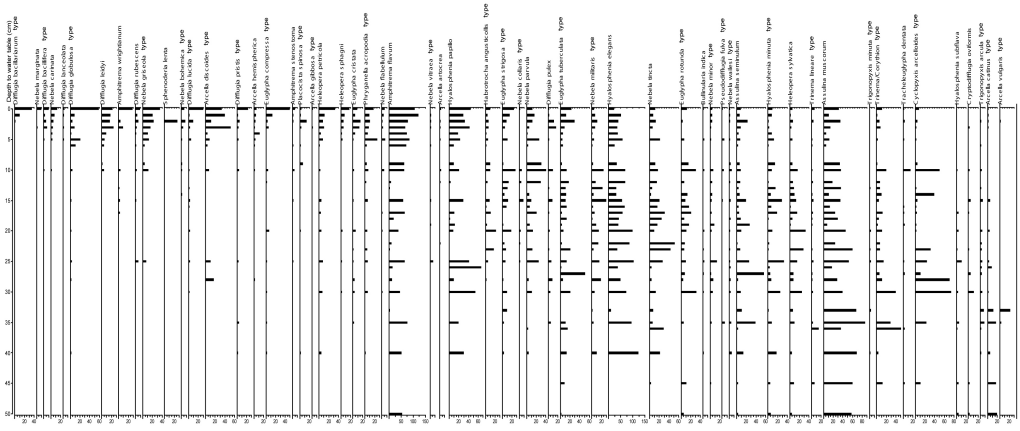

Figure 4.6 - istribution of taxa (percentage abundance) plotted against depth to water table. Zero values are not show.

After excluding outlier samples (n=11) and rare species (n=7) the predictive power of all models improved greatly (Table 4.5). Although the WMAT model became the best performing model after screening for outliers, given its sensitivity to outlying samples (Telford and Birks, 2005) and possible autocorrelation problems, it was not used to construct the transfer function. WA-Tol (inverse deshrinking) was therefore considered the best performing model (RMESP = 5.67 cm; $r^2 = 0.83$) and was used to construct the modern training set. All models were subject to 'leave-one-out' jack-knifed cross-validation and their performance was assessed by their respective root mean square error of prediction (RSMEP). In addition to the regional Swedish model, individual localised transfer functions for the Halland and Värmland were also constructed (Tables 4.6 and 4.7). However, the criteria imposed on rare species meant that 13 species were excluded from the Halland model whereas 11 were excluded form the Värmland model, compared to the 7 rare species excluded from the Swedish training set. Although the Värmland model has a higher predictive power (WA-Tol, inverse deshrinking), the exclusion of more testate amoebae species than in the Swedish training set makes it less likely to accurately reconstruct past water table depths. The RMSEP of the Halland model (WA-PLS, component 2) was considerably higher than that of the Swedish model, making it less suitable for reconstructing past water table depths. Consequently, the Swedish training set was used to reconstruct depth to water table for Gällseredsmossen and Kortlandamossen.

Table 4.5 - Summary of performance between different models for depth to water table reconstructions of Swedish model with outlier samples and rare species removed. Original values before the data was screened are shown in brackets.

Model	r^2	Average bias	Maximum bias	RMSEP
WA-PLS Component 3	0.80 (0.73)	0.01 (0.00)	12.02 (31.37)	6.58 (9.01)
WMAT	0.84 (0.67)	0.05 (-0.26)	16.74 (39.57)	5.13 (8.50)
PLS Component 3	0.79 (0.69)	0.00 (0.00)	14.21 (27.59)	6.24 (9.00)
WA-Tol(inverse deshrinking)	**0.83 (0.71)**	**0.00 (0.00)**	**13.27 (32.26)**	**5.67 (8.49)**
WA (inverse deshrinking)	0.78 (0.63)	0.00 (0.00)	13.35 (31.03)	6.12 (9.50)

Table 4.6 - Summary of performance statistics for Värmland model after exclusion of outliers and rare species. Original values are shown in brackets.

Model	r^2	Average bias	Maximum bias	RMSEP
WA-PLS Component 3	0.87 (0.84)	0.00 (0.00)	7.42 (10.35)	6.28 (7.42)
WMAT	0.81 (0.73)	0.16 (-0.04)	14.21 (23.17)	5.87 (7.26)
PLS Component 3	0.81 (0.75)	0.00 (0.00)	10.84 (23.15)	6.52 (7.43)
WA-Tol(inverse deshrinking)	**0.87 (0.79)**	**0.00 (0.00)**	**10.62 (20.14)**	**5.13 (6.96)**
WA (inverse deshrinking)	0.80 (0.72)	0.00 (0.00)	19.47 (12.00)	7.87 (6.23)

Table 4.7 - Summary of performance statistics for Halland model after exclusion of outliers and rare species. Original values are shown in brackets.

Model	r^2	Average bias	Maximum bias	RMSEP
WA-PLS Component 2	**0.86 (0.75)**	**-0.01 (0.00)**	**5.82 (25.20)**	**7.62 (11.67)**
WMAT	0.70 (0.57)	0.45 (-0.51)	22.73 (40.41)	6.97 (10.60)
PLS Component 3	0.76 (0.73)	0.00 (0.00)	17.05 (19.29)	8.71 (11.48)
WA-Tol(inverse deshrinking)	0.83 (0.74)	0.00 (0.00)	16.79 (30.68)	9.92 (13.26)
WA (inverse deshrinking)	0.75 (0.64)	0.00 (0.00)	15.08 (34.06)	7.49 (11.30)

Optimum depths-to-water table values for most testate amoebae species followed a typical pattern with taxa such as *Difflugia bacillariarum* type, *Amphitrema wrightianum*, *Difflugia leidyi* and *Nebela marginata* plotting at the wet end of the gradient and *Arcella arcula* type, *Hyalosphenia subflava*, *Cyclopyxis arcelloides* type and *Trigonopyxis arcula* type at the dry end (Figure 4.5). However, the hydrological preferences of some taxa found in the Swedish surface samples did not correspond to those presented in the European transfer function (Charman *et al.*, 2007). This suggests that although ecological niches occupied by most testate amoebae species are not bound by geographical location, regional differences do exist for selected taxa. With regional difference in hydrological preferences of several testate species, use of the continental training set is fraught with error and a regional model for Sweden is needed. Testate amoebae species on both ends of the gradient differ between the two training sets. Species such as *Nebela marginata* and *Difflugia pristis* type inhabit much wetter habitats in Sweden compared with the European transfer function, whereas *Euglypha cristata*, which ranked wettest in the European training set, has an optimum depth to water table preference of 5 cm. Two species that are often abundant in the fossil record, *Nebela minor* type and *Cyclopyxis arcelloides* type (Figure 4.6), both inhabit drier habitats than previously published. This difference in ecological niches may be the product of a more continental climate, with stronger seasonal water table fluctuations and general wetter conditions on the bogs surface.

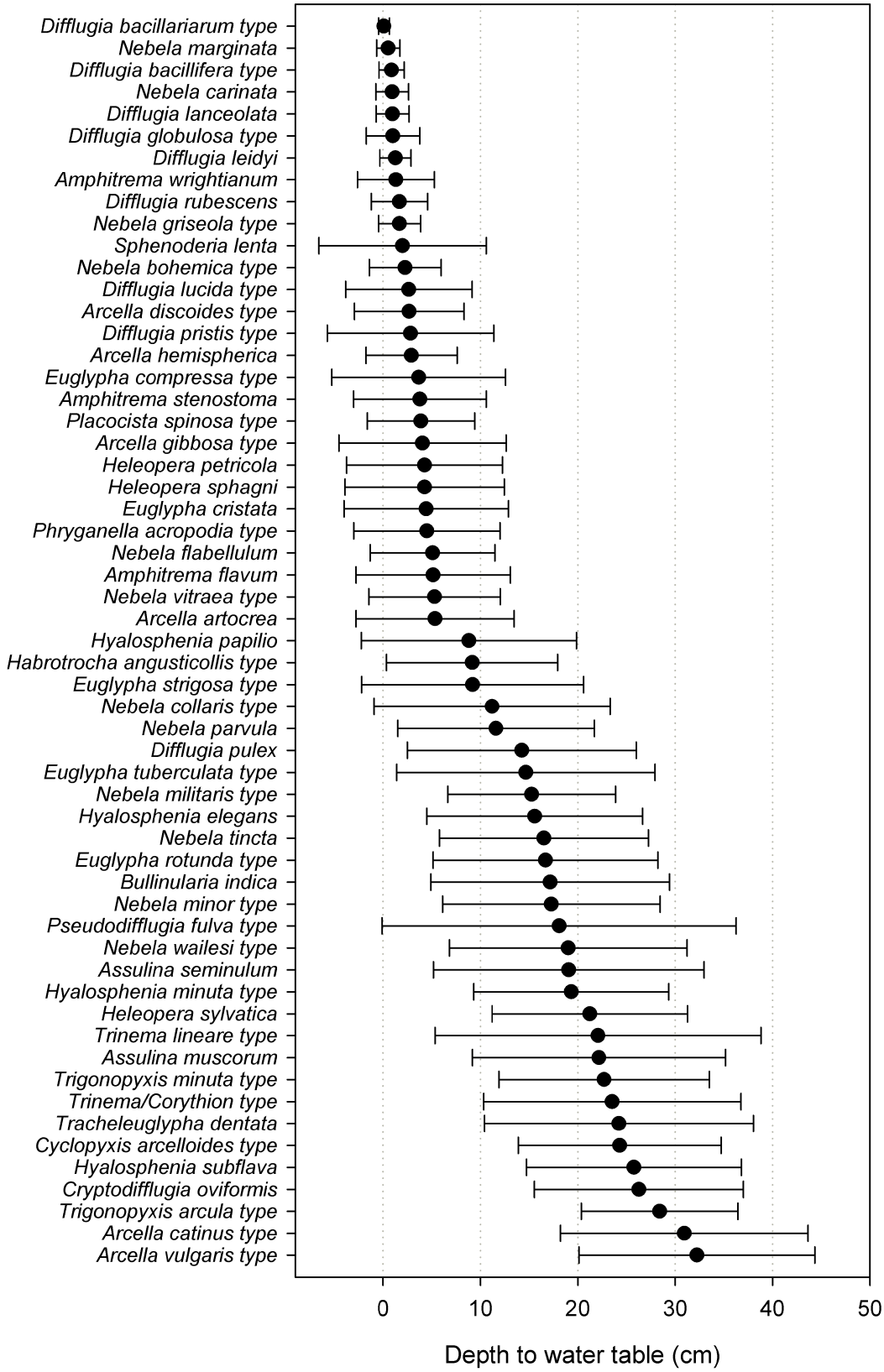

Figure 4.5 - Optima and tolerances of testate amoebae taxa from a screened dataset based on weighted averaging (inverse deshrinking) for depth to water table (n=139).

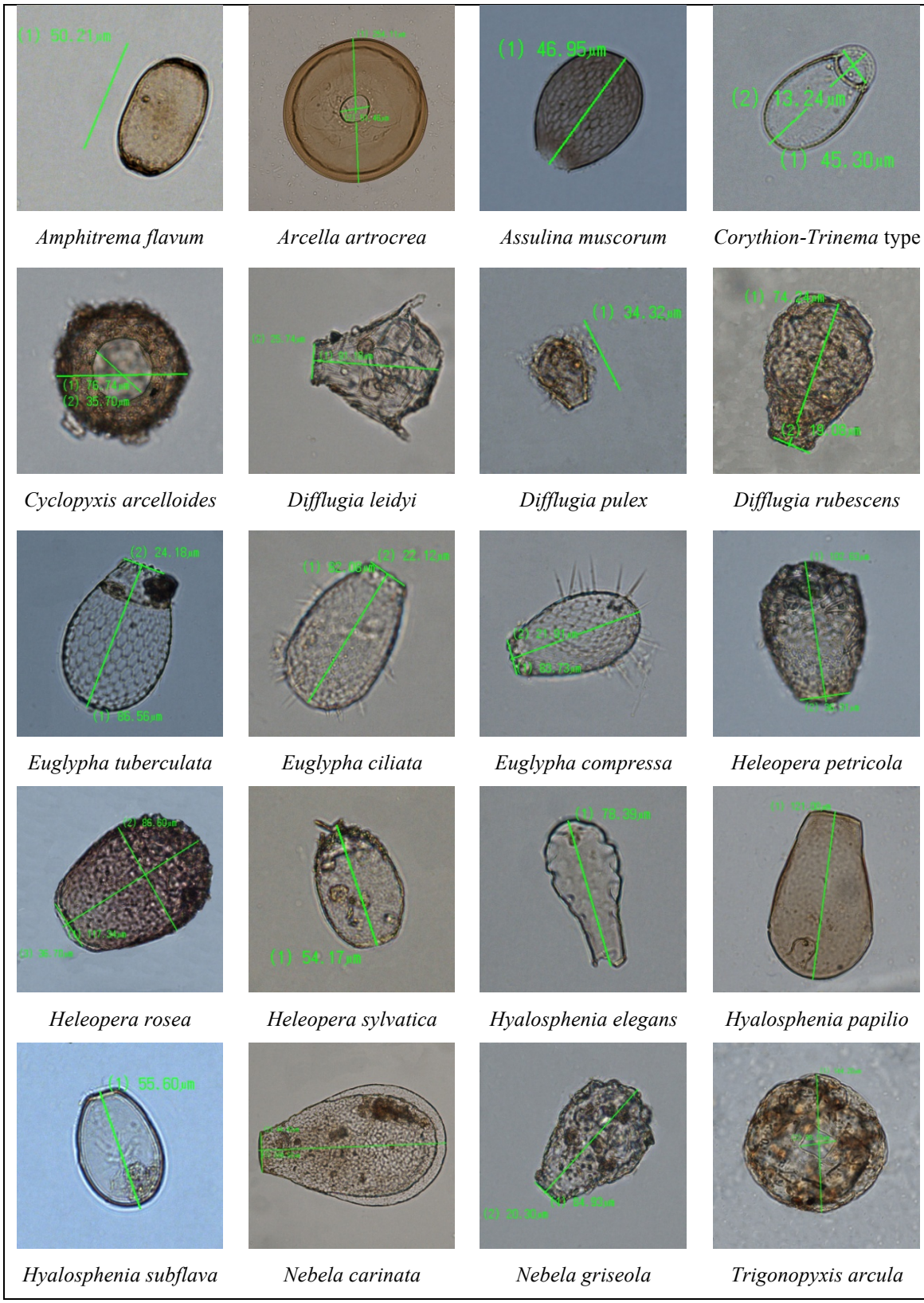

Figure 4.6 - Photographs of typical ombrotrophic bog testate amoebae species with size bars (All photos by G. Mallon).

Table 4.8 - List of taxa from training set that have not been included in the European transfer function (Charman *et al.*, 2007).

Wet	Intermediate	Dry
Arcella artrocrea	*Hylaosphenia minuta* type	*Arcella vulgaris* type
Arcella gibbosa type	*Nebela collaris* type	*Cryptodifflugia oviformis*
Arcella hemispherica	*Nebela parvula*	*Tracheleuglypha dentate*
Difflugia lanceolata	*Nebela tincta*	*Trinema lineare* type
Difflugia leidyi		
Difflugia globulosa type		
Difflugia rubescens		
Nebela bohemica type		
Placocista spinosa type		
Phryganella acropodia type		

Figure 4.7 shows a comparison between reconstructed depths to water table for Gällseredsmossen and Kortlandamossen using the Swedish, European (Charman *et al.*, 2007), UK (Woodland *et al.*, 1998) and North American (Booth, 2008) transfer functions. The European and UK models consistently reconstruct higher water tables than the Swedish model, whilst the North American training set matches the reconstructions of the Swedish function much closer. Sampling locations used in constructing the European and UK models came from regions with oceanic climate, whilst those used in the Swedish and North American functions were from regions of more continental climate. It is therefore probably that the difference in water table reconstruction between the Swedish model and the European and UK transfer functions is the result of increased continentiality of Sweden compared to the UK. The European and UK transfer functions were therefore not used throughout this thesis to reconstruct water table depths. The North American training set was deemed to be geographically too remote from the Swedish sites and was, therefore,

also not used throughout this thesis. Consequently, testate amoebae-based depth to water table reconstructions from Gällseredsmossen and Kortlandamossen were carried out using the Swedish transfer function.

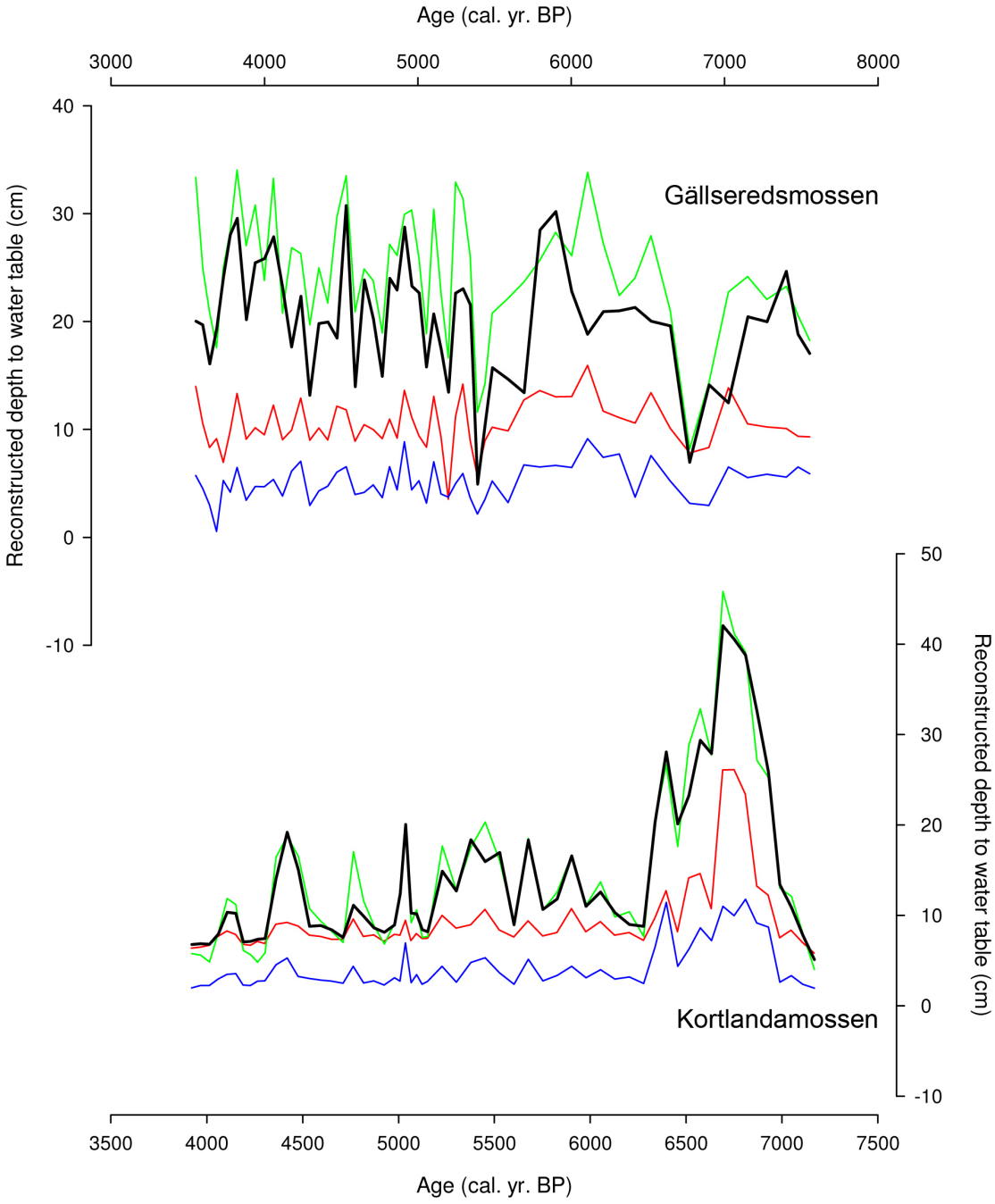

Figure 4.7 - Comparisons of reconstructed depths to water table for Gällseredsmossen and Kortlandamossen. Swedish training set = black line; North

American training set = green line; European training set = red line and UK training set = blue line.

4.4 Combined BSW indices

As discussed in Section 4.2, the IHCI, DCA and the use of a testate amoebae-based hydrological training set are each suitable methods for reconstructing bog surface wetness. In order to combine these into a single index of BSW, individual univariate curves have to be standardised and normalised to a value between -1 and 1 in order to make BSW curves of different scales comparable with one another. Subtracting the population mean and dividing the data by its standard deviation (Equation 4.3) standardises it.

$$X_s = \frac{x - \mu}{\sigma}$$

Equation 4.3 - Standardisation of dataset, where $\boldsymbol{\mu}$ is the mean and $\boldsymbol{\sigma}$ the standard deviation of the data.

In order to normalise the resulting values between -1 and 1, the formula in Equation 4.4 is applied to the data.

$$X_n = \frac{2(X_s - A)}{(B - A)} - 1$$

Equation 4.4 – Dataset normalisation between -1 and 1, where A is the minimum and B the maximum value of the data.

When BSW reconstructions for fossil plant macrofossil and testate amoebae data have been standardised and normalised, a univariate index of BSW is constructed by averaging the two reconstructed curves.

4.5 Conclusion

The above sections highlight the need for an improved version of the HCI that re-evaluates peat components included in the index and their respective species-scores. The inclusion of valuable information about the catholic or indicative nature of species in relation to BSW conditions, which had previously been ignored, is necessary for this improvement. A new IHCI was therefore constructed and will be used throughout this thesis to reconstruct BSW conditions from plant macrofossil data. However, further improvements to the length of the species gradient and the relative spacing of species are needed, as are more accurate measurements of the new indicator score as outlined in Section 4.2.

Differences between the hydrological preferences of some of the key testate amoebae species emphasised the problems associated with applying transfer functions from one geographical region to fossil records from another one. To address this issue, a new testate amoebae training set was constructed for south-central Sweden, which will be used to calibrate testate amoebae data from Gällseredsmossen and Kortlandamossen. No equivalent transfer function exists for Belgium and testate amoebae fossil data from Misten Bog will be subject to DCA in order to reconstruct BSW. Work is currently being carried out to construct a Belgian training set.

5 Results

5.1 Introduction

This chapter presents the results from analyses carried out on the five peat bogs described in Section 3.1 using the methodology outlined in Chapter 3. A detailed chronology is presented for each site using radiocarbon dating. Using the chronological framework established in Section 5.2, all data were processed following the analytical techniques detailed in Chapter 4, by means of detrended correspondence analysis, indicator-weighted Hydroclimatic indices and transfer function work.

5.2 Chronology

In order to chronologically correlate the sites and to put the findings in relation to published records, a robust chronology for each peat core was essential. A good dating framework with relatively small uncertainties attached to the dates was vital in order to identify possible climatic events extracted from the peat stratigraphy. In the absence of more exact dating proxies, ^{14}C radiocarbon analysis provided a good means to determine the age of organic material within acceptable error margins.

An initial set of 'rangefinder dates' was sought from the Natural Environment Research Council (NERC) in order to determine the depth of the 3500-year-old stratigraphy. However, the application was not supported by NERC and the requested dates were not obtained. In conjunction with the collaborative work with

the University of Liège, Belgium, two basal assays from Misten Bog were analysed (GdA-1339, GdA-1340). Following the initial 'rangefinder' application, a full application for support of 30 radiocarbon assays was made to the NERC radiocarbon steering committee, which received full support (allocation number 1455.1009) and all assays were awarded (Table 5.1 – starting with SUERC).

All 30 samples were sent to the NERC radiocarbon facility in East Kilbride for analysis. Samples SUERC-28501 and SUERC-28494 did not yield enough carbon for a reliable ^{13}C:^{14}C ratio determination and were consequently resampled and resubmitted. The basal samples from core MIS-08-07 (GdA-1339) and MIS-08-08 (GdA-1340) were sent to the radiocarbon facility at the Silesian University of Technology in Gliwice, Poland. Additionally, two samples from the auxiliary core MIS-08-08 (Beta-269676 and Beta-269677) were sent to Beta Analytic for ^{14}C analysis.

Table 5.1 - Results of radiocarbon assays showing source material, ^{14}C age and IntCal09 calibrated age of samples. Assays marked (#) were re-submitted.

Core	Depth (cm)	Lab identifier	Source material	^{14}C Age (± 1 sigma)	Calibrated Age (cal yr. BP)
TOR-08-01	356	SUERC-28461	Bryophyte stem	3505 ± 38	3688 - 3885
	444	SUERC-28462	*Sphagnum* stem	4177 ± 35	4584 - 4837
	532	SUERC-28463	Bryophyte stem	5428 ± 37	6129 - 6300
	604	SUERC-28464	Bryophyte stem	6241 ± 37	7018 - 7259
	668 (#)	SUERC-28465	Bryophyte stem	8918 ± 42	9910 - 10193
	764	SUERC-28466	*Sphagnum* stem	8443 ± 41	9407 - 9533
RBF-08-01	352	SUERC-28476	*Sphagnum* stem	3207 ± 35	3361 - 3552
	380	SUERC-28477	Bryophyte stem	3444 ± 38	3615 - 3832
	496 (#)	SUERC-28478	Bryophyte stem	4856 ± 38	5481 - 5658
	544	SUERC-28501	*Sphagnum* stem	4578 ± 36	5055 - 5448
	580	SUERC-28481	Bryophyte stem	5006 ± 38	5651 - 5893
	656	SUERC-28482	*Calluna vulgaris*	5572 ± 39	6292 - 6436
MIS-08-07	432	SUERC-28483	Bryophyte stem	3846 ± 38	4152 - 4410
	472	SUERC-28485	*Sphagnum* stem	3999 ± 38	4360 - 4777
	520	SUERC-28486	*Sphagnum* stem	4473 ± 35	4975 - 5290
	604	SUERC-28487	*Sphagnum* stem	5338 ± 37	5998 - 6267
	652	SUERC-28488	*Sphagnum* stem	5785 ± 39	6485 - 6674
	680	SUERC-28491	*Sphagnum* stem	5949 ± 39	6675 - 6883
	720	GdA-1339	*Calluna vulgaris*	6400 ± 35	7269 - 7419
MIS-08-08	721	Beta-269676	*Sphagnum* stem	6860 ± 50	7592 - 7819
	733	Beta-269677	*Sphagnum* stem	6760 ± 50	7582 - 7784
	758	GdA-1340	*Betula* wood	7710 ± 40	8417 - 8583
KOR-09-01	366	SUERC-28467	*Sphagnum* stem	3782 ± 38	3993 - 4290
	382 (#)	SUERC-28471	*Sphagnum* stem	4413 ± 38	4865 - 5273
	410	SUERC-28472	*Sphagnum* stem	4170 ± 38	4579 - 4835
	430	SUERC-28473	*Sphagnum* stem	4413 ± 38	4865 - 5273
	454	SUERC-28474	*Sphagnum* stem	4464 ± 38	4967 - 5294
	514	SUERC-28475	*Sphagnum* stem	5482 ± 39	6205 - 6395
	554	SUERC-28498	*Sphagnum* stem	6028 ± 39	6753 - 6979
GAL-09-01	346	SUERC-28492	Bryophyte stem	3543 ± 35	3706 - 3956
	410 (#)	SUERC-28493	*Sphagnum* stem	6268 ± 36	7028 - 7272
	470	SUERC-28494	*Sphagnum* stem	4745 ± 35	5328 - 5586
	510	SUERC-28495	*Sphagnum* stem	5724 ± 39	6414 - 6635
	538	SUERC-28496	*Sphagnum* stem	6500 ± 40	7319 - 7485

All results from the radiocarbon laboratories were reported as ^{14}C ages. As the amount of ^{14}C produced in the atmosphere is not constant over time, there is a discrepancy between ^{14}C and calendar age. Consequently the ^{14}C ages had to be calibrated in order to obtain the age of the samples in calendar years. Depending on the age and the source of the material, several different calibration curves are available taking into account the impacts of various reservoir effects. As all samples were of terrestrial origin and returned ^{14}C ages within the last 11,000 years, the IntCal09 calibration curve was used to convert all ^{14}C ages to calendar years (Heaton *et al.*, 2009; Reimer *et al.*, 2009). Calibrations were performed using the OxCal software (Bronk Ramsey, 2009), which allows the user to correct ^{14}C ages for differences in atmospheric $\delta^{14}C$ productivity and put them in a stratigraphic context using Bayesian algorithms.

By plotting the radiocarbon assays in stratigraphic sequential order, reversals and outliers became apparent (Figure 5.1 and Figure 5.2). At the depth that the outliers occurred, all sites were truly ombrotrophic and no 'old' carbon could have been washed in to be used by the plants growing on the surface. Given the sedimentary nature of peat bogs, reversals in the peat stratigraphy are rare and only expected as a result of human activity, bog bursts (Caseldine and Gearey, 2005), rootlet penetration or post coring contamination. As the time period in question was before any major human intervention in the landscape and since the palaeoecological analysis did not show any evidence of bog bursting, reversals within the sequence were not expected. In order to eliminate possible contamination from rootlets, all material was carefully cleaned prior to analysis as described in Section 3.4. To reduce the possibility of post-coring contamination sample material was taken from

the centre of the core, which was not exposed prior to sampling. Figure 5.1 and Figure 5.2 show that one reversed date can be identified for all bogs, except for Misten Bog. The dates obtained from assays SUERC-28471, SUERC-28465, SUERC-28478 and SUERC-24593 were deemed 'too old', putting their reliability in question. The respective ages suggest that the organic material contained in the stratigraphy level is older than the material stratigraphically below. This is highly unlikely in an ombrotrophic peat sequence and the consistent overestimation of these ages pointed to a systematic operator or machine error. The introduction of 'old carbon' was highly unlikely and the impact of contamination would be less pronounced than the effect of contamination from ‘younger’ material. Introduction of modern carbon would have a far greater impact on the age determination as it would introduce less depleted carbon into the sample, making it appear a lot younger (Charman and Garnett, 2005). Artificial ageing during the sampling process was also ruled out as no ^{14}C depleted materials were present that could have contaminated the samples. The cause of underestimating the ^{13}C:^{14}C ratio is still unclear, but the most likely explanation was an error in the processing stage of the analysis as all samples were treated in the same was and very carefully picked to avoid any form of contamination.

After discussing the results with the NERC Radiocarbon facility, the four samples in question were re-sampled and resubmitted for re-analysis. The results of the re-analysis fit the existing age-depth models much better and the levels no longer represented outliers, ruling out the possibility of a reversal in the peat stratigraphy and making a systematic analysis error more likely. The results from the repeated

analysis are presented in Table 5.2. All dates were calibrated using the OxCal software and IntCal09 calibration curve as discussed above.

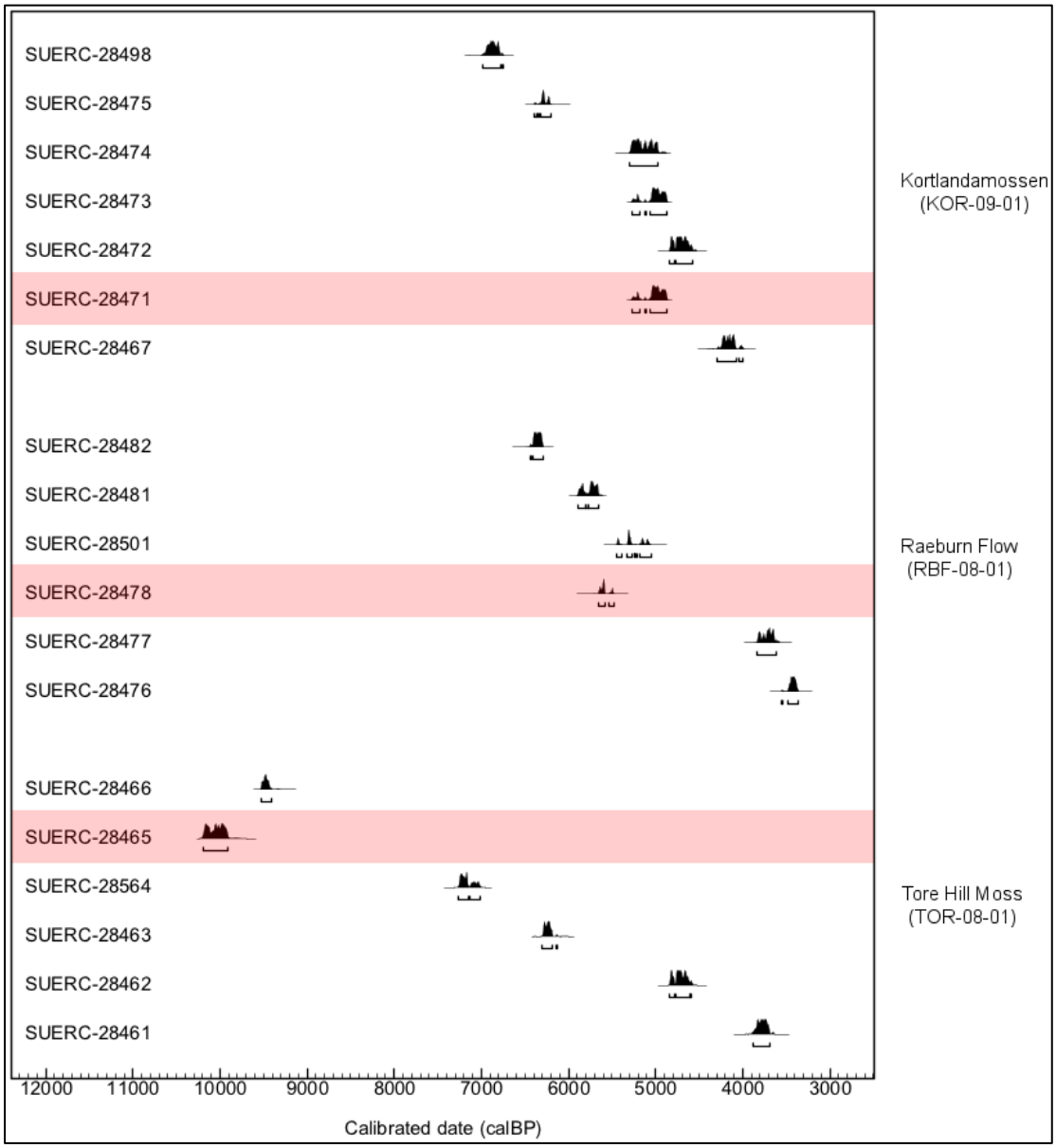

Figure 5.1- Calibrated age probability distributions for Kortlandamossen, Raeburn Flow and Tore Hill Moss (output adapted from Oxcal). Red bands highlight the outlier samples that were resubmitted to NERC.

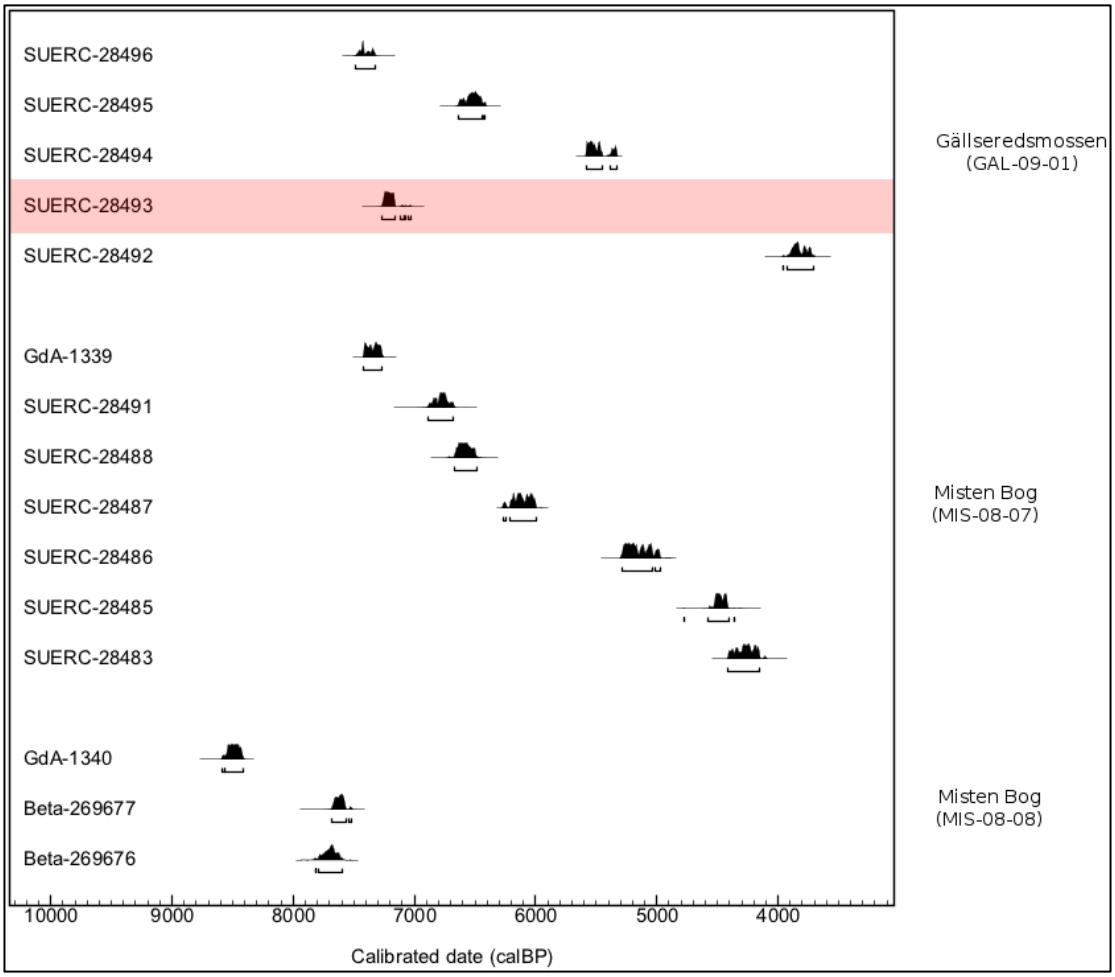

Figure 5.2 - Calibrated age probability distributions for Gällseredsmossen and Misten Bog (output adapted from Oxcal). The red band highlights the outlier sample that was resubmitted to NERC.

Table 5.2 - Results of repeat radiocarbon assays showing source material, ^{14}C age and IntCal09 calibrated age of samples.

Core	Depth (cm)	Identifier	Material	^{14}C Age (± 1 sigma)	Calibrated Age (cal a BP)
TOR-08-01	668	SUERC-30581	*Sphagnum* stem	7679 ± 40	8401 - 8546
RBF-08-01	496	SUERC-30585	*Sphagnum* stem	4183 ± 38	4583 - 4840
GAL-09-01	410	SUERC-30586	*Sphagnum* stem	4230 ± 38	4629 - 4861
KOR-09-01	382	SUERC-30584	*Sphagnum* stem	3861 ± 38	4155 - 4414

5.2.1 Age-depth models

All age-depth modelling was carried out with the 'classical' age modelling software CLAM (Blaauw, 2010), which calibrates ^{14}C ages using the IntCal09 calibration curve and selects an age from the calibrated age probability distribution proportionally to its calibrated probability. An interpolated fit was then calculated using all available age points, which produced a simple age-depth model. This process was repeated 1,000 times and subsequently provided an age probability range for each data point. The mean value of all sampled calibrated ages was then used to obtain a 'best-fit' value for each sample. Although Bayesian modelling frameworks are more advanced and better suited to high resolution age-depth modelling, a simple interpolated approach was sufficient for the age resolution of the analysed cores (Blaauw, 2010).

Plotting peat depth against calibrated years BP (Figure 5.3 to Figure 5.7), all of the five bogs are shown to be accumulating in an approximately linear fashion, with minor localised slowing and accelerating phases, such as the period around 5000 years BP at Kortlandamossen. The main exception to the linear trend is Gällseredsmossen, which accelerated in accumulation at around 5500 years BP. All outlier samples that were resubmitted were excluded from the diagrams and the resubmitted samples have been used instead.

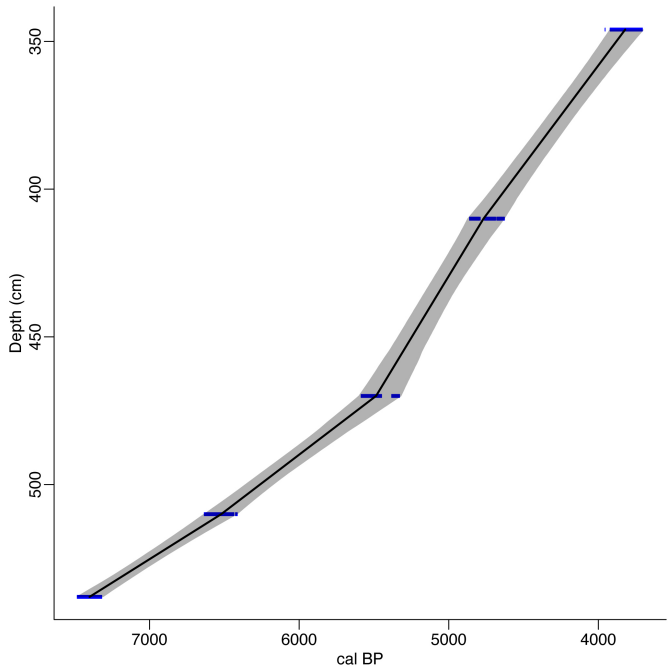

Figure 5.3 – Age-depth model for Gällseredsmossen

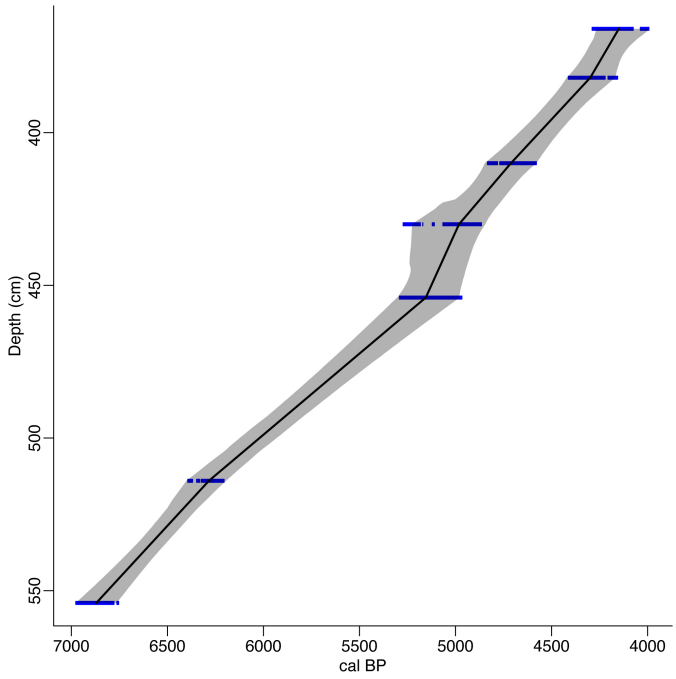

Figure 5.4 – Age-depth model for Kortlandamossen

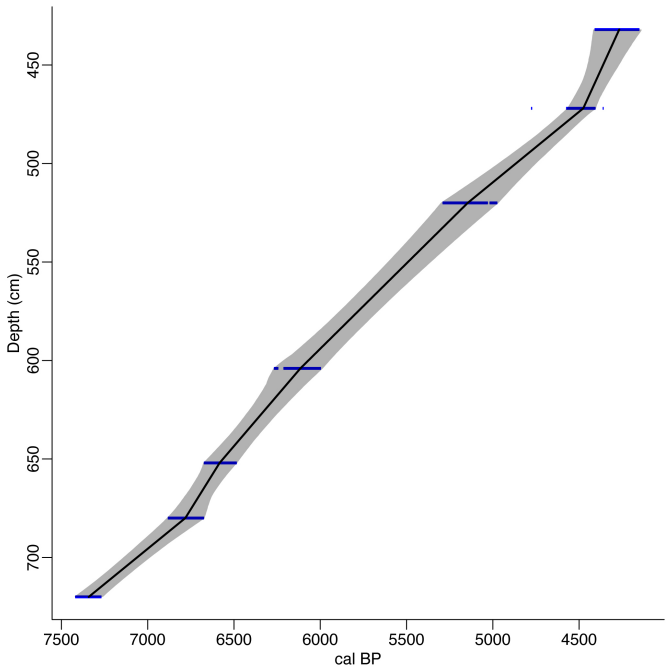

Figure 5.5 – Age-depth model for Misten Bog

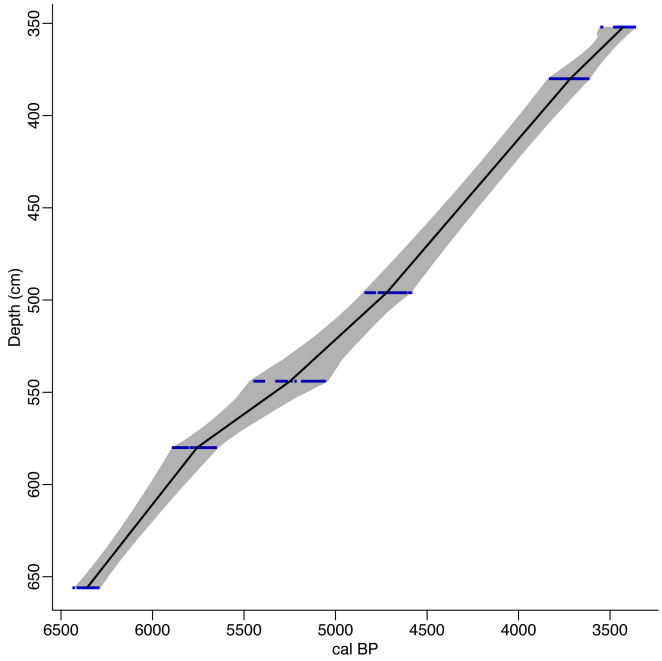

Figure 5.6 – Age-depth model for Raeburn Flow

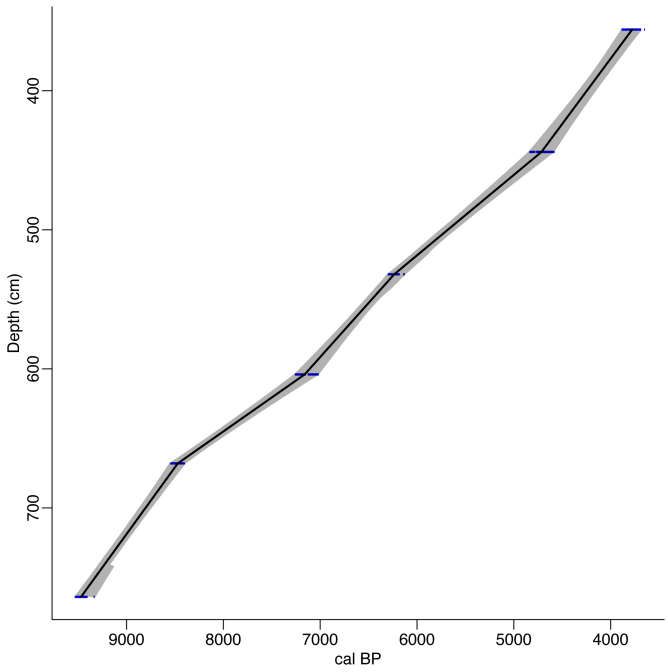

Figure 5.7 – Age-depth model for Tore Hill Moss

5.2.2 Chronological uncertainties

Given the possible age distributions of calibrated radiocarbon dates, there is an inherent uncertainty attached to each date reported in this thesis. This uncertainty arises from a combination of operational error and plateaus in the IntCal09 radiocarbon calibration curve (Reimer *et al.*, 2009). Throughout this thesis the value with the maximum likelihood based on its age-probability distribution was used to represent the age of an assay. Given the mean two-sigma error range for calibrated radiocarbon dates from this thesis an inherent dating error of ±110 years has to be taken into account.

Furthermore, as the dating of the changes in BSW throughout this thesis is based on interpolation of samples that are 4 cm apart and as some changes are only represented by a single sample, the dates presented have an additional possible error of approximately ±40 years (Langdon *et al.*, 2003). Each date should therefore be considered to have a possible age error of ±150 years attached to it. Possible future improvements to the chronological framework are suggested in Section 7.1.

5.3 Misten Bog, Belgium

5.3.1 Plant macrofossil remains

Core MIS-08-07 was analysed for plant macrofossil remains from the base of the core at 720 cm up to 360 cm at 4 cm intervals (**Figure 5.8**). **Figure 5.8** shows that the profile was largely dominated by *Sphagnum* spp., brown mosses, *Eriophorum vaginatum* and Ericaceae rootlets. The four main sections of *Sphagnum* communities were divided into zones MIS-1, MIS-2, MIS-3 and MIS-4. In each zone, sub-zones highlighted climatic and ecological shifts on a smaller time-scale. A detailed description of the ecological assemblage of the zones is provided in Table 5.3.

Table 5.3 - Summary of plant macrofossil zones from Misten Bog

Zone	Depth (cm)	Description	Age (cal yr BP)
MIS-1	720 - 654	Stable water table with *Sphagnum magellanicum* dominating the profile. Some *S. austinii* at the base and fragments of *Eriophorum vaginatum* throughout. Steady increase in *Sphagnum* dominance. Abrupt change from *S. magellanicum* to *S.* sect. *Acutifolia*.	7400 - 6600
MIS-2a	654 - 602	Start of long *S.* sect. *Acutifolia* dominated phase. Lowering of water-table and drying of site. Temporary disappearance of *E. vaginatum* towards the top and occurrences of *S. austinii*.	6600 - 6100
MIS-2b	602 - 554	Zone dominated by *S.* sect. *Acutifolia* and brown mosses. Temporary disappearance of *E. vaginatum*. Further drying of the bog. Prolonged spike in non-*Sphagnum* bryophyte components.	6100 - 5550
MIS-2c	554 - 522	Reappearance of *E. vaginatum*, which becomes fairly dominant at start of zone. Dominance of *S.* sect. *Acutifolia* declines alongside a drop in non-*Sphagnum* bryophytes. End of dry phase and start of wet phase.	5550 - 5150
MIS-3a	522 - 502	First of two pool phases indicated by emergence and prolonged presence of *S.* sect. *Cuspidata*. Spike in UOM, which is probably algal matter and disappearance of non-*Sphagnum* bryophytes.	5150 - 4900
MIS-3b	502 - 478	Dry phase separating the two pool phases indicated by a sharp rise in non-*Sphagnum* bryophytes, *E. vaginatum* and *Trichophorum cespitosum*. Further increase in Ericaceae rootlets and sharp drop in *Sphagnum* presence.	4900 - 4550
MIS-3c	478 - 454	Second and most pronounced pool phase of the record, indicated by large *S.* sect. *Cuspidata* dominance and almost complete disappearance of Ericaceae species, *E. vaginatum* and non-*Sphagnum* bryophytes.	4550 - 4400
MIS-4a	454 - 430	Drying of the bog with emergence of *E. vaginatum* and large proportion of Ericaceae rootlets. *T. cespitosum* present and *Sphagnum* almost entirely absent. This zone represents a dry phase of the bog.	4400 - 4250
MIS-4b	430 - 400	Hummocky zone with stabilised water table. Start of prolonged *S. austinii* dominance (Persch, 1950). Indications of moderate conditions with traces of non-*Sphagnum* bryophytes, Ericaceae rootlets and sparse *S.* sect. *Acutifolia*.	4250 - 3950

Figure 5.11 demonstrates clear shifts in bog surface wetness and long-term trends in surface conditions. Misten Bog began as an intermediately wet bog with stable water table conditions and a *Sphagnum magellanicum* / *Eriophorum vaginatum* community from *c*. 7400 BP to *c*. 6600 BP (720 cm - 654 cm). From *c*. 6600 BP until *c*. 5150 BP (654 cm - 522 cm) a prolonged phase of dry bog surface conditions prevailed, with *S*. section *Acutifolia* dominating. The dry phase climaxed with a spike in non-*Sphagnum* bryophytes and the disappearance of *E. vaginatum*, which indicated very dry conditions between *c*. 6100 BP to *c*. 5550 BP (602 cm - 554 cm).

A series of wet pool phases in zone MIS-3, occurred from *c*. 5150 BP until *c*. 4400 BP (522 cm - 454 cm). The first of these wet phases lasted from *c*. 5150 BP until *c*. 4900 BP (522 cm - 502 cm) and was characterised by a spike in hygrophilous *S*. section *Cuspidata*, the disappearance of non-*Sphagnum* bryophytes and the decreased presence of Ericaceae rootlets. This pool phase was relatively short lived and dry conditions returned on Misten Bog until *c*. 4550 BP (478 cm). Zone MIS-3b marked this drying and is characterised by a large drop in *Sphagnum* and a rise in non-*Sphagnum* bryophytes and *E. vaginatum*. The increased presence of Ericaceae wood and *Trichophorum cespitosum* supports the interpretation of a drying of the bog. Following this dry phase, the second pronounced pool phase (zone MIS-3c) took place between *c*. 4550 BP and *c*. 4400 BP (478 cm - 454 cm). This wet-shift was the most dominant wetting of the bog throughout the entire profile with an 80% dominance of *S*. section *Cuspidata* and sharp declines in Ericaceae species and *E. vaginatum,* accompanied by the complete disappearance of non-*Sphagnum* bryophytes and *T. cespitosum*. Zone MIS-3c also marked the gradual reappearance of *S. austinii*.

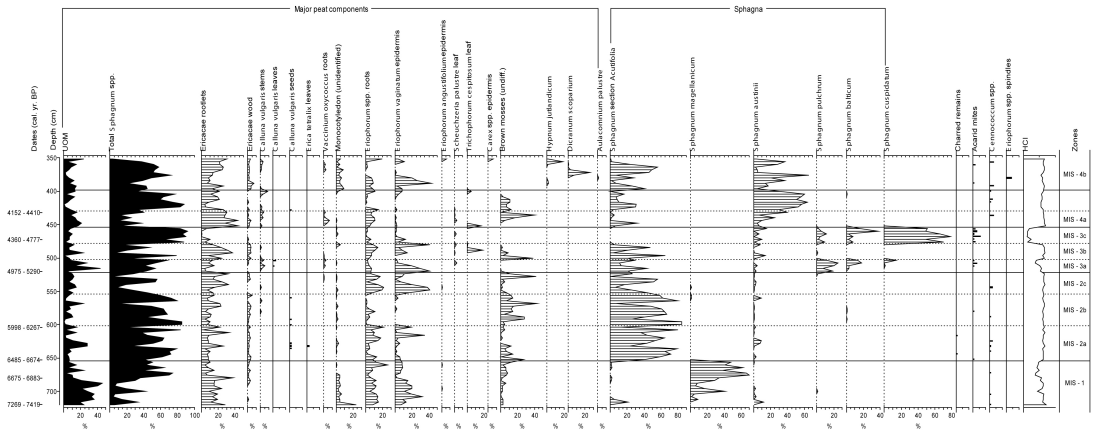

Figure 5.8 - Plant macrofossil composition of peat core MIS-08-07.

The fourth shift in plant communities occurred at *c*. 4400 BP (454 cm) and extended to the top of the analysed profile. Zone MIS-4 described the return to relatively drier hummocky conditions characterised initially by *Vaccinium oxycoccus*, *Eriophorum vaginatum* and brown moss domination, accompanied by a spike in *T. cespitosum*. At approximately 4250 BP (430 cm), Ericaceae species and *E. vaginatum* were largely replaced by *S. austinii* and a low percentage of *S.* section *Acutifolia*. A similar mid-Holocene dominance by *S. austinii* has been documented by Persch (1950), whose profile started at 420 cm.

5.3.2 Testate amoebae remains

Testate amoebae were sampled at the same depths as the plant macrofossils over the same core section as the plant macrofossils analysis. The peat profile was largely dominated by *Amphitrema flavum* and *Difflugia pulex* (Figure 5.9), which were, respectively, good indicators of wet and intermediate dry bog surface conditions. Key hydrological indicator species, such as the hydrophobic *Hyalosphenia subflava* and hygrophilous *Heleopera petricola* were rare. As with the plant macrofossil data the testate amoebae assemblages were separated into four zones. Testate amoebae data showed that Misten Bog started out with moderate to wet surface conditions, followed by a prolonged dry to very dry phase. At *c*. 5200 BP (524 cm) the start of two large pool phases, interrupted by a considerable dry phase, occurred before moderate to dry conditions returned. The peat record was therefore divided into four broad zones MIS-1 to MIS-4, with zones MIS-1 to MIS-3 being subdivided further.

Zone MIS-1 was dominated by *A. flavum* with relatively high levels of *Arcella discoides* and *Assulina muscorum* towards the top of the zone, which indicated

moderate to wet conditions on the bog. The wet phase, however, was briefly interrupted by a dry excursion at *c*. 6900 BP (688 cm), characterised by a spike in the abundance of *D. pulex* and decreased levels of hygrophilous *A. flavum* and *A. discoides*. At *c*. 6650 BP (660 cm) a clear shift in testate amoebae assemblage occurred with the disappearance of *A. discoides* and a sharp drop in *A. flavum* and *Hyalosphenia papilio* levels. This shift in ecology marked a change to dry surface conditions, preceding evidence from plant macrofossil data. This prolonged dry phase was briefly interrupted by a short-lived wet phase from approximately 6250 BP (620 cm), indicated by spikes in *A. flavum*, *H. papilio* and *A. discoides*, before dry conditions set in from *c*. 5950 BP until *c*. 5200 BP (590 cm - 524 cm) (Zone MIS-2c). *D. pulex* dominated the profile throughout the dry phase and hydrophobic *Cyclopyxis arcelloides* type first appeared on the site.

During the next *c*. 900 years, the testate amoebae assemblage of Misten Bog abruptly changed on four occasions. At *c*. 5200 BP (524 cm), *D. pulex* was largely replaced by *A. flavum* and wet indicators such as *A. discoides* reappeared in the profile. This phase (Zone MIS-3a) marked the first of two major wet phases and was relatively short-lived. By *c*. 4900 BP (502 cm) *D. pulex* replaced *A. flavum* and there was an increased abundance of *C. arcelloides* type, indicating a shift to dry bog surface conditions. The most pronounced wet phase on the site occurred between *c*. 4550 BP and *c*. 4400 BP (478 cm - 454 cm). This phase was characterised by the complete disappearance of dry species, such as *D. pulex*, *C. arcelloides* type and *Trigonopyxis arcula* type, and a dominance of *A. flavum*. There was a notable increase in the abundance of other hygrophilous species, such as *H. petricola*, *Heleopera sphagni*

and *Arcella artocrea*. The timing of this wet-shift was in line with evidence from the plant macrofossil analysis, suggesting a very abrupt event.

At *c*. 4400 BP (454 cm), Misten Bog suddenly reverted to dry surface conditions, indicated by the return of *C. arcelloides* type alongside a decrease in hygrophilous species. Descriptions of the different ecological zones based on testate amoebae evidence are summarised in Table 5.4.

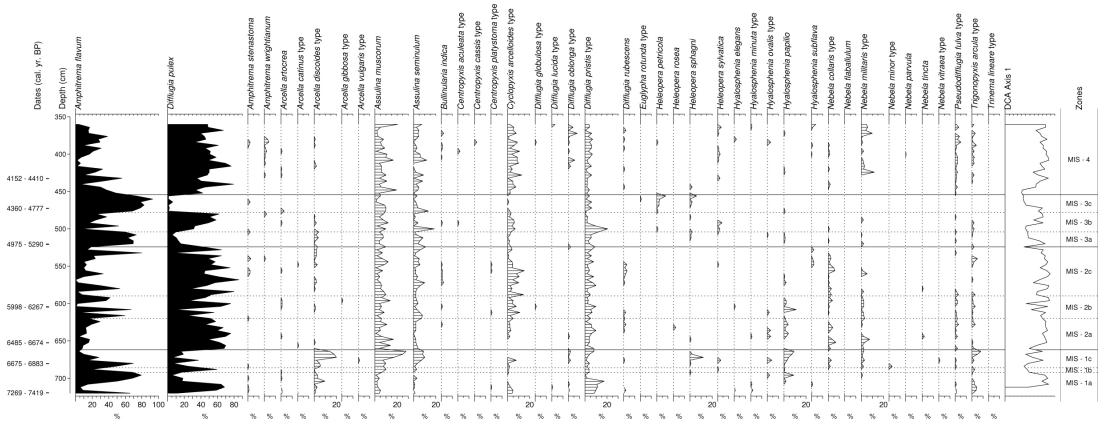

Figure 5.9 - Testate amoebae assemblage for MIS-08-07

Table 5.4 - Summary of testate amoebae zones from Misten Bog

Zone	Depth (cm)	Description	Age (cal yr BP)
MIS-1a	720 - 660	Wet period dominated by *A. flavum*, which gets replaced by *D. pulex*, *A. discoides* type and *Assulina* spp. towards the top of the zone. Interrupted by dry zone MIS-1b.	7400 - 6650
MIS-1b	692 - 684	Dry phase interrupting relatively wet zone MIS-1a indicated by sudden drop in *A. flavum*, *H. papilio* and *A. discoides* type accompanied by a sharp increase in *D. pulex*.	6950 - 6850
MIS-2a	660 - 620	Start of prolonged dry phase with dominance of *D. pulex*. Zone contains *Nebela militaris*, a sharp drop in *A. discoides*, and gradual declines in *H. papilio* and *A. muscorum*.	6650 - 6250
MIS-2b	620 - 590	Only wet phase interrupting prolonged dry zone MIS-2. Return of *A. flavum*, *A. discoides* type and spike in *H. papilio*. The sudden drop in *D. pulex* is also indicative of a wetting of the bog.	6250 - 5950
MIS-2c	590 - 524	Very dry conditions on the bog with fluctuations in wetness, however, always within the 'dry' range. Zone is dominated by *D. pulex* with a distinct dip in of *Amphitrema* spp. abundance. Conditions became dry enough for *Hyalosphenia subflava* to appear.	5950 - 5200
MIS-3a	524 - 502	First of two pool phases on the bog with dominance of *A. flavum* and first occurrence of *Amphitrema wrightianum*. Relative absence of *D. pulex* and the return of higher levels of *A. discoides* type support a shift to wetter conditions.	5200 - 4900
MIS-3b	502 - 478	Dry shift interrupting the two pool phases of zone MIS-3. Re-establishment of *D. pulex*, relative drop in *A. flavum*. Initial spikes and tailing off of *Difflugia pristis* type support a drying of the bog.	4900 - 4550
MIS-3c	478 - 454	Major wet phase of the bog with almost complete dominance of *A. flavum*, disappearance of *D. pulex*, spike in *D. pristis* type and gradual establishment of *H. petricola* and *Heleopera sphagni*.	4550 - 4400
MIS-4	454 - 400	Moderate to dry conditions with a prominent *D. pulex*, *A. muscorum* and *C. arcelloides* type community. Relatively low values of *Amphitrema* spp. dropping off towards the top of the zone. Short-lived wetting of the site around 432 cm.	4400 - 3950

The result of a detrended correspondence analysis performed on testate amoebae data is presented in Figure 5.10. Species and samples were both plotted in relation to their respective DCA Axis 1 and DCA Axis 2 scores. Rare and ecologically ambivalent species were excluded from the analysis. The eigenvalue score for Axis 1 shows that almost 60 per cent of variation in the species distribution is accounted for by the ecological variable represented by ordination Axis 1.

Analysis of species distribution along Axis 1 in relation to their known ecologically niches shows that Axis 1 represents a BSW gradient. Hygrophilous species that represent wet bog surface conditions, such as *Heleopera petricola*, *Heleopera sphagni*, *Amphitrema flavum*, *Arcella discoides* and *Hyalosphenia papilio,* were associated with high DCA Axis 1 scores. Hydrophobic species such as *Hyalosphenia subflava* and *Trigonopyxis sensu lato,* on the other hand, had low Axis 1 scores.

Axis 2 plots a further environmental gradient with *Arcella artrocrea* and *A. flavum* at one end and *A. discoides* and *Nebela minor* at the other. No environmental gradient could be determined that separates these species on either end of Axis 2. DCA Axis 2 scores were therefore not analysed further.

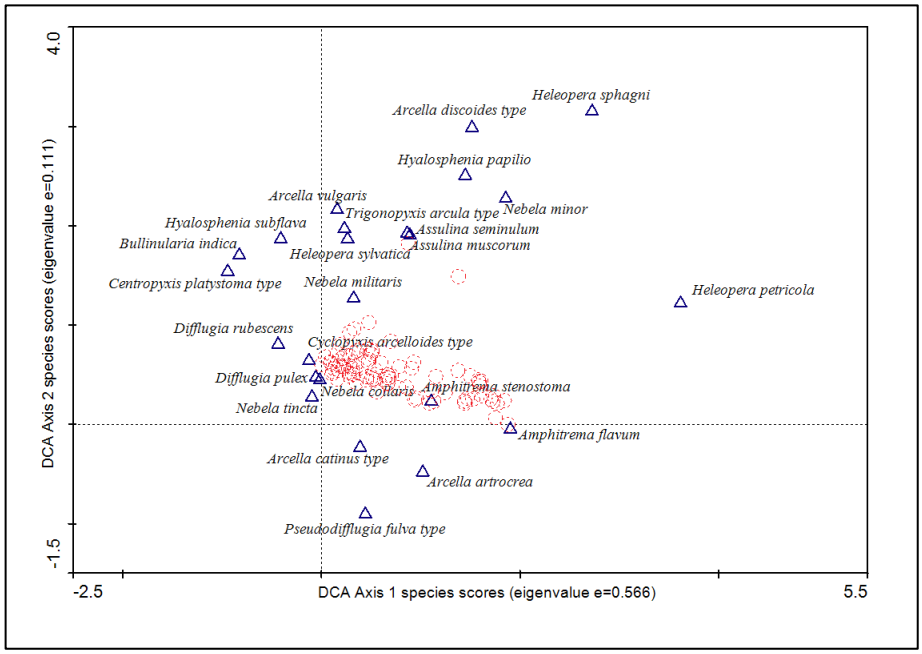

Figure 5.10 - Species versus samples plot of testate amoebae data for Misten Bog. Blue triangles represent species; red circles show samples scores.

5.3.3 Bog surface wetness

BSW reconstructions from both plant macrofossil and testate amoebae analysis have been standardised, normalised and averaged to give a composite signal of BSW changes (Figure 5.11). The composite signal showed wetting of the site as negative excursions and drying as positive ones. Four major zones became apparent, in line with results presented above. The immediate changes in BSW were the two major shifts to wetter conditions at *c*. 5200 BP and *c*. 4600 BP. The early part of the record shows that the bog started out with wet conditions followed by a shift to dry conditions at *c*. 6600 BP, which lasted until *c*. 5200 BP. Figure 5.11 shows that this prolonged dry phase was interrupted by a series of BSW fluctuations, most notable between *c*. 6250 BP and *c*. 5800 BP.

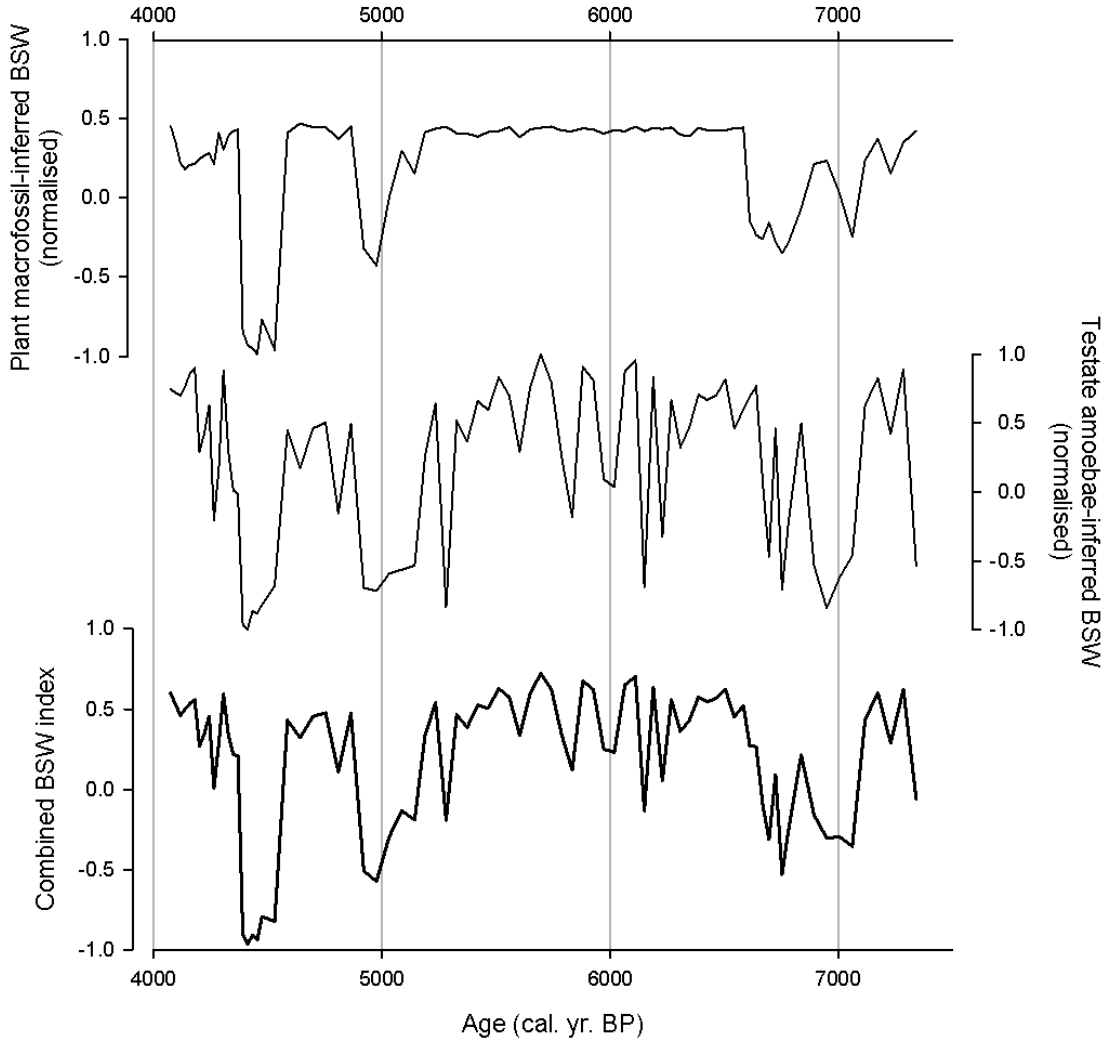

Figure 5.11 - BSW reconstructions based on testate amoebae and plant macrofossil data from Misten Bog. The thick black line represents averaged values from both proxies.

5.4 Raeburn Flow, Scotland

5.4.1 Plant macrofossil remains

Figure 5.12 and Table 5.5 shows the components that make up the peat stratigraphy at Raeburn Flow from 708 cm to 316 cm. The diagram demonstrates that Raeburn Flow has a very diverse history with a large burning event from 708 cm to 652 cm. The floristic composition of the peat matrix in this section was greatly impacted by this fire and a lot of material was burned, which made identification to species level, especially for monocotyledon and Ericaceae species very difficult. Following the burning, the site was largely dominated by *Sphagnum* spp., Ericaceae rootlets, and *E. vaginatum*. The stratigraphy of Raeburn Flow was broken down into five main zones, with zones RBF-1 and RBF-2 broken down into further sub-zones. Each zone and sub-zone highlighted shifts in ecology on the bog, which in turn reflected changes in bog surface wetness and corresponding changes in atmospheric moisture availability.

The site started out with dry bog surface conditions dominated by monocotyledons, especially *E. vaginatum* (zones RBF-1a and RBF-1b) comparable to records from Cumbria (Barber *et al.*, 1994; Hughes *et al.*, 2000a), and high concentrations of charred remains and charcoal, which resulted from a large-scale on-site fire. However, it is unclear if there was one burning event or if a series of fires occurred. At *c*. 5750 BP (582 cm) the amount of monocotyledons on the site sharply decreased and BSW conditions changed to more intermediate ones. A long phase of Ericaceae rootlet and *S.* section *Acutifolia*-dominated peat formation began. *E. vaginatum* was

also present, albeit in reduced abundance, throughout this period. With the exception of the period at *c*. 4450 BP (465 cm), abundance of other monocotyledons was relatively sparse. However, this long period of dry conditions was interrupted by a series of wet phases (zones RBF-2b and RBF-2c). A rapid increase in the abundance of *S*. section *Cuspidata* and *R. alba* alongside a decreased number of monocotyledons pointed towards pronounced lawn/pool phases and an increase in bog surface wetness. The first of these shifts occurred at *c*. 5350 BP (550 cm) and the second at *c*. 4750 BP (498 cm). Both events were relatively short-lived, only occupying approximately 10 cm (about 100 years) of stratigraphy.

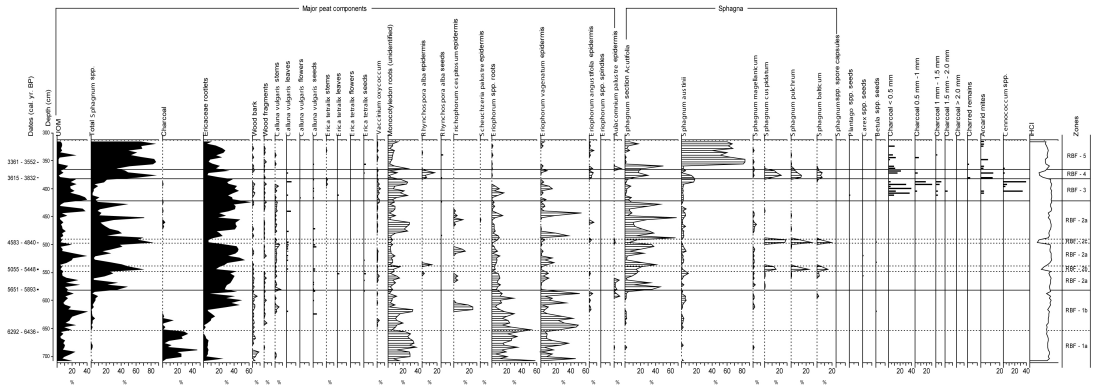

Figure 5.12 - Plant macrofossil composition of peat core RBF-08-01.

Table 5.5 - Summary of plant macrofossil zones from Raeburn Flow

Zone	Depth (cm)	Description	Age (cal a BP)
RBF-1a	708 - 656	Zone dominated by monocotyledons, particularly by *E. vaginatum*. Undifferentiated monocotyledon roots are abundant. Large scale burning event with charcoal making up > 40% of profile. The trophic status of this zone is unclear, although the presence of *S. austinii* suggests ombrotrophy.	7000 - 6350
RBF-1b	656 - 582	End of *E. vaginatum* dominated zone with gradual rise in Ericaceae rootlets. Drop in undifferentiated monocotyledon roots. Peak in *T. cespitosum* suggests dry bog surface conditions.	6350 - 5750
RBF-2a	582 - 424	Prolonged dry phase dominated by Ericaceae rootlets and *S.* sect. *Acutifolia*. The zone is interrupted by two wet phases RBF-2b and RBF-2c.	5750 - 4100
RBF-2b	550 - 538	First major wet-shift indicated by peak in *S.* sect. *Cuspidata* accompanied by drop in *E. vaginatum*. First occurrence of *R. alba* supports wetting of the bog.	5350 - 5200
RBF-2c	498 - 488	Second major wet-shift of the bog with second spike in *S.* sect. *Cuspidata* accompanied with large drop in Ericaceae rootlets, UOM and *E. vaginatum*.	4750 - 4650
RBF-3	424 - 382	Major drying of the bog characterised by near-absence of *Sphagnum* spp. and other bryophytes. Strong increase in Ericaceae rootlets, UOM and monocotyledons.	4100 - 3750
RBF-4	382 - 356	Prolonged wet phase shown by spike in *S.* sect. *Cuspidata*, *R. alba* and drop in Ericaceae rootlets, UOM and *E. vaginatum*. Reappearance of *S.* sect. *Acutifolia* and rise of *S. austinii*.	3750 – 3450
RBF-5	356 - 316	Hummocky phase of the bog with dominance of *S. austinii* and very little UOM, *E. vaginatum* and other *Sphagnum* spp. Return to more intermediate moisture conditions.	3450 – 3050

Following the intermediate dry period in Zone RBF-2, dry conditions returned to Raeburn Flow, as shown in Zone RBF-3, from *c*. 4100 BP until *c*. 3750 BP. (424 cm - 382 cm). The zone was dominated by non-algal UOM, Ericaceae rootlets and

monocotyledons. Conditions were too dry for *E. vaginatum* to establish with any dominance and *S.* section *Acutifolia* was almost completely absent during the phase. The end of the phase was marked by a gradual increase in *Sphagnum* spp. and a decrease in the amount of Ericaceae rootlets and UOM. The rapid appearance of very wet ecological indicators in the peat stratigraphy suggests a third major wet phase on the bog from *c*. 3750 BP until *c*. 3450 BP (382 cm - 356 cm). The pool phase was characterised by large spikes in *S.* section *Cuspidata*, *E. angustifolium*, *R. alba* and a pronounced drop in UOM, Ericaceae rootlets and *E. vaginatum*. The low concentration of UOM suggested a wet lawn phase on the edge of a bog pool. Following the third major wet phase, a return to moderately dry and hummock building conditions is suggested in Zone RBF-5, by the appearance and dominance of *S. austinii* and the moderate abundance of Ericaceae from 3450 BP (356 cm) onwards.

5.4.2 Testate amoebae data

Testate amoebae samples were analysed every 4 cm, matching the resolution of the plant macrofossil analysis. As a result of the large burning event at the base of the profile, testate amoebae preservation was too poor for accurate counting and consequently no testate amoebae data are present before *c*. 6250 BP (640 cm) (Zone RBF-1). The remainder of the profile has been divided into four main zones, with Zones RBF-3 and RBF-4 divided into further sub-zones, to indicate short-lived ecological change within zones of long-term bog surface conditions (Figure 5.13 and Table 5.6). The most dominant species were *A. flavum* and *D. pulex* alongside other important indicator species, which were less abundant throughout the profile. *A.*

muscorum is eurytopic in its ecological range and its abundance does not provide information about BSW.

Table 5.6 - Summary of testate amoebae zones from Raeburn Flow

Zone	Depth (cm)	Description	Age (cal yr BP)
RBF-1	700 - 640	Burned zone, testate preservation too poor to count.	6850 - 6250
RBF-2	640 - 584	Dry bog conditions indicated by dominance of *D. pulex* and *C. arcelloides* type and sharp drop in *A. flavum*. Presence of hydrophobic *Pseudodifflugia fulva* type.	6250 - 5800
RBF-3a	584 - 432	Moderate wetting of the bog and move to intermediate to dry conditions. Dominance of *D. pulex* with presence of *D. pristis* type, *P. fulva* type and *T. arcula* type. Zone is interrupted by two wet shifts, RBF-3b and RBF-3c.	5800 - 4150
RBF-3b	542 - 528	First short-lived wet phase on bog supported by dominance of *A. flavum* and relative peak in wet loving *Assulina seminulum* and *H. sphagni* alongside a sharp drop in *D. pulex*.	5250 - 5050
RBF-3c	496 - 482	Second short-lived wet phase indicated by peaks in *A. flavum* and drops in *A. muscorum*, *C. arcelloides* type and *D. pulex*. First appearance of *A. wrightianum*.	4700 - 4600
RBF-4a	432 - 316	Intermediate conditions shown by diverse community of hydrophobic and hygrophilous species. The zone is interrupted by two wet phases, RBF-4b and RBF-4c. Zone marks the establishment of *A. wrightianum*.	4150 - 3050
RBF-4b	416 - 408	Very brief wet shift indicated by spike in *A. wrightianum* and drop in *D. pulex*.	4050 - 3950
RBF-4c	384 - 370	Final wet phase shown by sharp drop in *D. pulex* and *C. arcelloides* type alongside a rise in *A. flavum* and rise in *A. wrightianum*.	3750 - 3600

Zone RBF-2 indicated dry bog conditions until 5800 BP (584 cm), which was in line with the evidence of the plant macrofossil analysis. The profile was largely dominated by hydrophobic *D. pulex*. The sharp drop in *A. flavum* supports a drying of the bog. The dry species *C. arcelloides* type and *P. fulva* type increase in abundance throughout the level. Zone RBF-3 indicates a shift to intermediate surface conditions lasting from *c*. 5800 BP until *c*. 4150 BP (584 cm - 432 cm) during which time dry species such as *D. fulva* type and *T. arcula* type were present in addition to the dominant *D. pulex*. The presence of *A. flavum* and *D. pristis* type suggests that conditions were less dry than in Zone RBF-2. This intermediate phase on the bog, however, was interrupted by a series of wet phases, similar to those detected in the plant macrofossil record. The first of the major wet phases (Zone RBF-3b) was relatively short-lived and lasted from *c*. 5250 BP until *c*. 5050 BP (542 cm - 528 cm). This wetting of the site was supported by the dominance of *A. flavum*, a small peak in *A. seminulum* and the presence of *H. sphagni* alongside a strong drop in *D. pulex* levels. The second short-lived wet-shift occurred from approximately 4700 BP until *c*. 4600 BP (496 cm - 482 cm), as shown by Zone RBF-3c. In addition to the peak in *A. flavum* levels and drops in *A. muscorum*, *C. arcelloides* type and *D. pulex*, this wet-shift was supported by the first emergence of hygrophilous *A. wrightianum*.

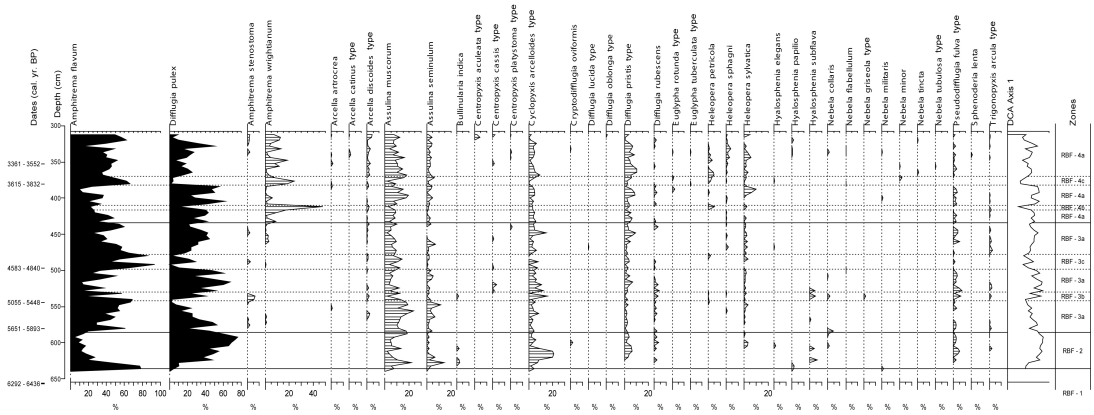

Figure 5.13 - Testate amoebae assemblages from RBF-08-01

Zone RBF-4 highlighted the emergence and establishment of *A. wrightianum*. Contrary to the plant macrofossil evidence, this suggested a wetting of the site. Two major wetting phases at *c*. 4050 BP (416 cm) and between *c*. 3750 BP and *c*. 3600 BP (384 cm - 370 cm) were highlighted in zones RBF-4b and RBF-4c, respectively. Both phases were characterised by a drop in *D. pulex* and a spike in the levels of *A. wrightianum* and *A. flavum*, respectively. The wet phase at *c*. 4050 BP is not registered in the plant macrofossil record and it is suggested that it was too short-lived to provoke a change in the plant community composition. Following the final wet phase on the bog, fluctuating hydrological conditions were characterised by a diverse community of wet and dry species, in correspondence with the plant macrofossil evidence.

5.4.3 Multi-proxy comparison

The averaged BSW reconstructions from plant macrofossil and testate amoebae analyses are shown in Figure 5.14 (solid black line). As a result of the early burning phase no testate amoebae sample scores were present below 640 cm. In line with the evidence from the individual biostratigraphic analyses outlined above, Raeburn Flow shows relatively stable moderately dry BSW conditions punctuated by temporary wet phases. The most notable of these occurred from *c*. 5300 BP to *c*. 5100 BP (542 cm - 528 cm), *c*. 4800 BP to *c*. 4600 BP (500 cm - 482 cm) and *c*. 4200 BP to *c*. 4000 BP (412 cm - 404 cm). After *c*. 3750 BP, BSW remains variable but generally wetter than previously.

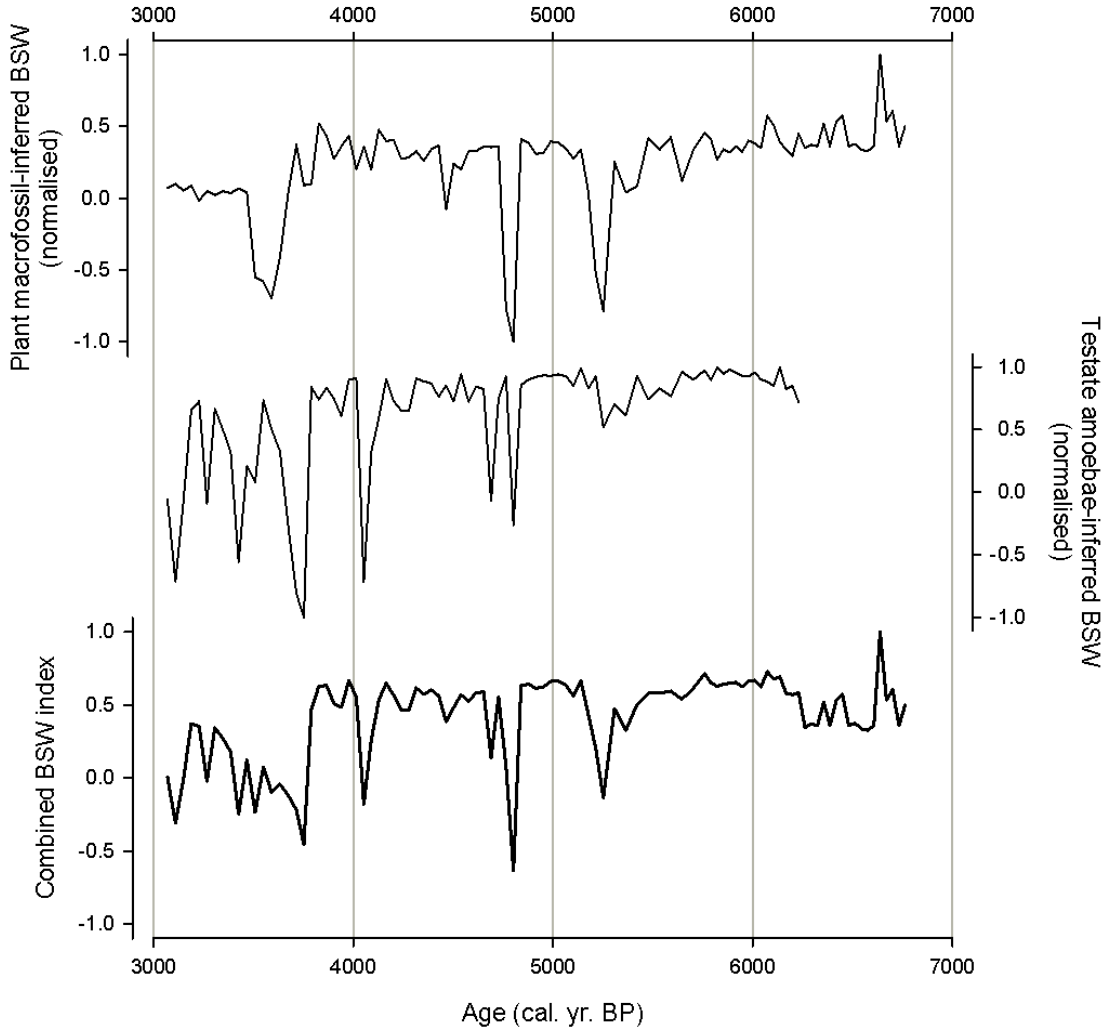

Figure 5.14 - BSW reconstructions based on testate amoebae and plant macrofossil data from Raeburn Flow. The thick black line represents averaged values from both proxies.

5.5 Tore Hill Moss, Scotland

5.5.1 Plant macrofossil remains

Using evidence from the plant macrofossil analysis, the peat stratigraphy from Tore Hill Moss was divided into four main zones TOR-1 to TOR-4 (Table 5.7 and **Figure 5.15**). Each zone represented different bog surface wetness conditions. Zones TOR-3 and TOR-4 were further divided into three sub-zones to highlight smaller-scale variations in BSW.

The presence of *Sphagnum palustre*, *Menyanthes trifoliate*, *Carex* spp., *Equisetum spp.* and a relatively large abundance of *Polytrichum strictum* indicated nutrient enriched and minerotrophic conditions. This suggested that the profile was part of a fen system before the bog turned ombrotrophic at approximately 9450 BP (762 cm). A direct relationship between surface wetness and atmospheric moisture availability is difficult to establish for a fen as factors such as ground water seepage influence the hydrology of the site. Therefore, the 132 cm section of the core below 796 cm was not analysed in greater detail for plant macrofossil remains.

Zone TOR-2 summarised the initial ombrotrophic phase of the bog with a stabilising water table and the emergence of hummock building *S. austinii*. In addition to *S. austinii*, *E. vaginatum* first appeared and Ericaceae rootlets became a considerable component of the peat profile. The profile was dominated by *S.* section *Acutifolia* and the brown mosses began to increase. At *c*. 8400 BP (664 cm), conditions on the bog became drier (Zone TOR-3a) with a steady decline in total *Sphagnum* spp., a peak in *E. vaginatum* and a large increase in Ericaceae rootlets. Following *c*. 1,250

years of dry conditions, bog surface conditions became even drier at *c*. 7150 BP (604 cm). Total *Sphagnum* spp. was at its lowest abundance and hydrophobic *Dicranum scoparium* dominated the peat profile. *E. vaginatum* almost entirely disappeared, indicating a strong drying out of the site. The *D. scoparium* dominated phase (zone TOR-3b) lasted for *c*. 800 years before more moderate conditions returned at *c*. 6350 BP (540 cm).

Table 5.7 - Summary of plant macrofossil zones from Tore Hill Moss

Zone	Depth (cm)	Description	Age (cal yr BP)
TOR-1	792 - 762	Wet fen section of the profile characterised by presence of *S. palustre*, *M. trifoliate* and *Equisetum spp*.	9750 - 9450
TOR-2	762 - 664	Initial ombrotrophic phase of the bog with fluctuating moisture conditions. Short-lived phase of *S. austinii* growth. Alternating *Sphagnum* spp. and Ericaceae rootlet dominance.	9450 - 8400
TOR-3a	664 - 604	First drying of the site shown by steady drop in *S.* sect. *Acutifolia*, rise of *E. vaginatum* and increased presence of brown mosses. Ericaceous rootlets levels are consistent and dominant.	8400 - 7150
TOR-3b	604 - 540	Major dry phase on the bog dominated by *D. scoparium* and low point in *Sphagnum* spp. cover accompanied by a reduction in *E. vaginatum* and minor drop in Ericaceae rootlets.	7150 - 6350
TOR-3c	540 - 448	Return to moderately dry conditions indicated by reappearance of *S.* sect. *Acutifolia* and *E. vaginatum*. First considerable presence of undifferentiated monocotyledon roots.	6350 - 4800
TOR-4a	448 - 368	Intermediate moisture conditions and dominance of *S.* sect. *Acutifolia*. Gradual wetting of the profile towards the top of the zone.	4800 - 3900
TOR-4b	368 - 348	Short-lived wet phase shown by sharp spike in *S. balticum* and drop in monocotyledons and UOM.	3900 - 3700
TOR-4c	348 - 308	Return to intermediate to dry conditions with established *S.* sect. *Acutifolia* and *E. vaginatum*.	3700 - 3250

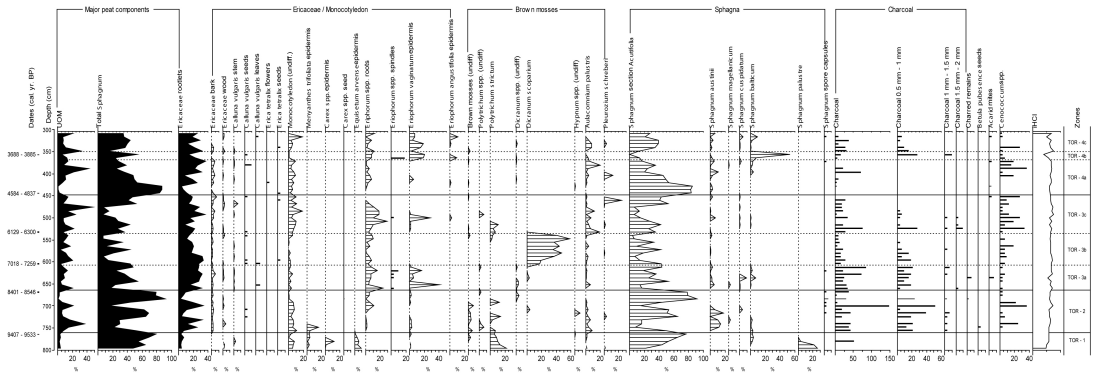

Figure 5.15 - Plant macrofossil composition of TOR-08-01.

The disappearance of *D. scoparium*, re-emergence of *S.* section *Acutifolia* and *E. vaginatum* and the increase in monocotyledons was described in zone TOR-3c. A peak in *Pleurozium schreberi* and the disappearance of *E. vaginatum* at *c*. 4800 BP (448 cm) marked the return of intermediate to dry conditions. Once more *S.* section *Acutifolia* and Ericaceae rootlets dominated (Zone TOR-4a) the peat stratigraphy, *E. vaginatum* rapidly disappeared along with most brown mosses, with the exception of *Aulacomnium palustre*. Surface conditions gradually became wetter, as highlighted by the emerging presence of *S.* section *Cuspidata* until conditions turned wet on the bog at *c*. 3900 BP (368 cm). A spike *S. balticum*, which has become nearly extinct in the UK at present, alongside *E. angustifolium,* accompanied by a drop in Ericaceae rootlets and UOM, supported the presence of a wet phase. Following the pool phase (Zone TOR-4b), dry to intermediate conditions returned to the site, as demonstrated by an increase in *E. vaginatum*, drop in *S.* section *Cuspidata* and the return of *S.* section *Acutifolia* at *c*. 3700 BP.

5.5.2 Testate amoebae remains

Evidence from the testate amoebae analysis show that the peat profile could be divided into three major zones of differing ecological and water table conditions (Figure 5.17). The profile was largely dominated by a *D. pulex*, *A. muscorum* and *C. arcelloides* type community interrupted by prolonged phases of *A. flavum* dominance. Zone TOR-1 corresponded to the fen part of the profile and showed very wet conditions dominated by *A. flavum*, *A. catinus* type and *H. papilio*. At *c*. 9450 BP (762 cm), when the site became ombrotrophic, *A. flavum*, *H. papilio* and *A. catinus* type disappeared and the site became dry (Zone TOR-2). This drying of the

site was supported by the emergence of *C. arcelloides* type and *D. pulex* community and the presence of *T. arcula* type.

Zone TOR-3 highlighted the site's return to wetter surface conditions with a high proportion of *A. flavum* and drop in *D. pulex*, *C. arcelloides* and *A. muscorum* from *c*. 8400 BP (664 cm) until *c*. 7150 BP (604 cm). This intermediate- to wet-shift was supported by the absence of *T. arcula* type and the disappearance of hydrophobic *Nebela militaris*. Following the wet phase, the bog returned to a prolonged phase of dry bog surface conditions with a dominance of *D. pulex* and the returned presence of *T. arcula* type. Wet indicator species such as *Amphitrema* spp. and *Arcella* spp. were either completely absent throughout Zone TOR-3b or at minimum abundance levels.

At approximately 4800 BP (448 cm), intermediate moisture conditions and a fluctuating water table set in on the site (Zone TOR-3c). The zone was characterised by a dominance of *A. flavum*, punctuated by dry episodes at *c*. 4350 BP and *c*. 3950 BP (412 cm and 372 cm). During the dry excursions, the profile was dominated by *D. pulex* and *T. arcula* type, and *A. flavum* dropped sharply in abundance. A summarised description of the ecological zones is given in Table 5.8.

Table 5.8 - Summary of testate amoebae zones for Tore Hill Moss

Zone	Depth (cm)	Description	Age (cal yr BP)
TOR-1	792 - 762	Wet fen phase dominated by hygrophilous species such as *A. flavum*, *Arcella catinus* type and *Hyalosphenia papilio*.	9750 - 9450
TOR-2	762 - 664	Initial dry phase dominated by communities of the hydrophobic species *D. pulex* and *C. arcelloides* type. Presence of *Trigonopyxis arcula* type.	9450 - 8400
TOR-3a	664 - 604	Dominance of *A. flavum* and *Assulina seminulum* coupled with the drop in *D. pulex* and *C. arcelloides* type abundance indicates wet phase. This is supported by brief reappearance of *H. papilio*.	8400 - 7150
TOR-3b	604 - 448	Driest phase of the profile with dominance of *D. pulex*. The prolonged presence of *T. arcula* type and *Pseudodifflugia fulva* type alongside the major dip in abundance and partial disappearance of *A. flavum* suggest very dry conditions.	7150 – 4800
TOR-3c	448 - 308	Return to dry to intermediate bog surface wetness conditions. Fluctuation between *D. pulex* and *T. arcula* type dominated communities and *Amphitrema* spp.	4800 - 3250

5.5.3 Multi-proxy comparison

BSW reconstructions from testate amoebae and plant macrofossil data are shown in Figure 5.16 alongside their combined average. The thick black line represents the mean index of bog surface wetness derived from both proxy sources. Surface wetness conditions on Tore Hill Moss showed a general drying of the bog until approximately 5300 BP (480 cm) at which time the bog slowly began to get wetter. This major dry period is, however, punctuated by a clear wetting phase, which started at *c*. 8100 BP (670 cm) and lasted until *c*. 7300 BP (615 cm). The wettest

surface conditions on the site occurred at *c*. 7800 BP (650 cm). After *c*. 5300 BP a series of wet excursions at *c*. 4800 BP (450 cm), *c*. 4200 BP (395 cm) and *c*. 3800 BP (360 cm) interrupted the general wetting trend of the bog surface.

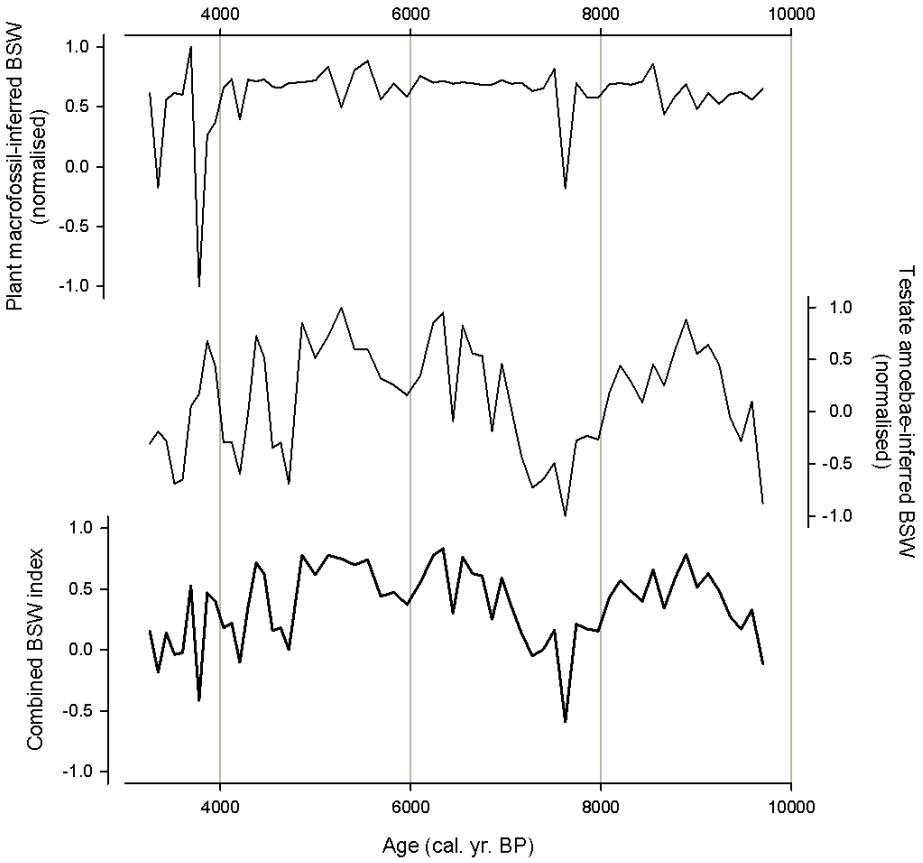

Figure 5.16 - BSW reconstructions based on testate amoebae and plant macrofossil data from Tore Hill Moss. The thick black line represents averaged values from both proxies.

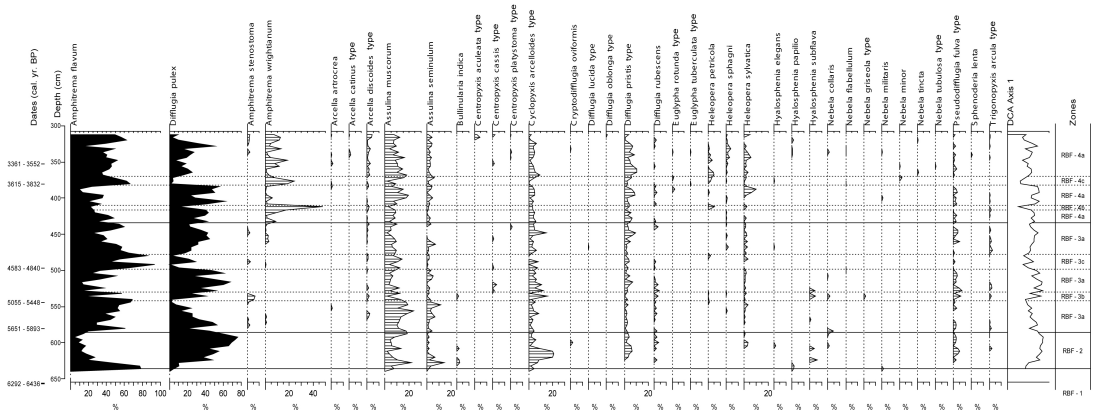

Figure 5.17 - Testate amoebae assemblages for TOR-08-01

5.6 Kortlandamossen, Sweden

5.6.1 Plant macrofossil remains

The peat stratigraphy from Kortlandamossen was analysed at 4 cm resolution from 574 cm to 346 cm. Data from the plant macrofossil analysis revealed that the stratigraphy could be divided into the three broad zones KOR-1 to KOR-3 (Figure 5.18 and Table 5.9). Each zone displayed unique BSW conditions and all were divided further into sub-zones.

Zone KOR-1 described fluctuating water table conditions, which were characterised by an interchange of wet and dry adapted species. KOR-1a showed a relatively dry bog plant community made up of *E. vaginatum*, monocotyledons and UOM alongside remains of Ericaceae wood. The almost complete absence of *Sphagnum* spp. indicated that conditions on the site were dry until approximately 6950 BP (558 cm). Following the initial dry phase, a sudden swing to intermediate wet conditions is inferred in Zone KOR-1b characterised by a strong emergence of *Sphagnum* spp. and the disappearance of *E. vaginatum,* alongside a drop in monocotyledons. *S.* section *Cuspidata* was the first *Sphagnum* species to become abundant; it was, however, quickly replaced by *S.* section *Acutifolia* and *S. magellanicum*. This indicated a quick wetting and gradual stabilising of surface moisture conditions. At *c*. 6850 BP (552 cm) the site suddenly dried out again, as indicated by the rapid collapse of the *Sphagnum* spp. community and its replacement by *E. vaginatum*, Ericaceae rootlets and monocotyledons. At the end of this dry zone (KOR-1c), *S.*

section *Acutifolia* became dominant once again, pushing out most other plants from the profile by *c*. 6450 BP (526 cm).

Zone KOR-2 encompassed a prolonged phase of *S.* section *Acutifolia* dominance. Initially, small amounts of *S. magellanicum* and *S.* section *Cuspidata* replaced the remnants of undifferentiated monocotyledons and *E. vaginatum* (Zone KOR-1a), but by 6050 BP (502 cm), *S*. section *Acutifolia* dominated the profile and only small traces of Ericaceae rootlets and undifferentiated monocotyledons compliment the profile alongside occasional occurrences of *E. vaginatum*. Because of the wide range of ecological habitats occupied by the different species of *S*. section *Acutifolia*, it was difficult to infer BSW conditions from the plant macrofossil data. Given the small traces of monocotyledons and Ericaceae species, it was estimated that conditions were intermediate to wet throughout this period and that *S. fuscum* was likely to have been the dominant species. A brief drying of the site at *c*. 5050 BP (438 cm) was indicated by a sudden spike in Ericaceae, accompanied by a drop in the total *Sphagnum* spp. abundance.

At approximately 4350 BP (386 cm), the emergence of *R. alba* and *E. angustifolium* alongside a decline in *Sphagnum* spp. indicated that surface conditions at Kortlandamossen become wetter (Zone KOR-3a). The presence of *E. vaginatum* roots appeared to contradict this wetting shift, but these roots are very likely to have grown down into the profile and are therefore not representative of surface conditions at the time. At *c*. 4200 BP (372 cm), *R. alba* and *E. angustifolium* were replaced by *S*. section *Acutifolia*, *S.* section *Cuspidata* and a brief occurrence of *S. magellanicum*, indicating that surface conditions became even wetter on Kortlandamossen, in line with evidence from peat bogs across Europe (Hughes *et al.*,

2000a; Langdon *et al.*, 2003). A summary of the ecological zones of Kortlandamossen is presented in Table 5.9.

Table 5.9 - Summary of plant macrofossil zones for Kortlandamossen

Zone	Depth (cm)	Description	Age (cal yr BP)
KOR-1a	574 - 558	Profile is dominated by *E. vaginatum*, monocotyledons and UOM, indicating dry bog surface conditions. This is supported by the general lack of *Sphagnum* spp.	7150 - 6950
KOR-1b	558 - 552	First major shift to *Sphagnum* spp. dominated peat with major drop in *E. vaginatum*. Initial *S.* sect. *Cuspidata* is quickly replaced by *S.* section *Acutifolia* and consequently by *S. magellanicum*.	6950 - 6850
KOR-1c	552 - 526	Second dry shift of the profile indicated by re-emergence of *E. vaginatum*, Ericaceae, monocotyledons and drop in *Sphagnum* spp. abundance.	6850 – 6450
KOR-2a	526 - 502	Start of *Sphagnum* dominance of the site. Initial *S.* section *Acutifolia*, *S.* section *Cuspidata* and *S. magellanicum* community replaces monocotyledon-dominated community. Change in ecology suggests a shift to wetter bog surface conditions.	6450 - 6050
KOR-2b	502 - 386	Long phase of *S.* section *Acutifolia* dominance and lack of monocotyledons and Ericaceae suggests wet surface conditions. Brief dry period around 438 cm.	6050 - 4350
KOR-3a	386 - 372	Major shift to wetter surface conditions as indicated by appearance of *R. alba*, *E. angustifolium* and drop in *S.* section *Acutifolia*.	4350 – 4200
KOR-3b	372 - 346	*Eriophorum* spp. and *R. alba* get replaced by *S.* section *Acutifolia* and *S.* sect. *Cuspidata* community, indicating further shift to wetter surface conditions.	4200 - 3900

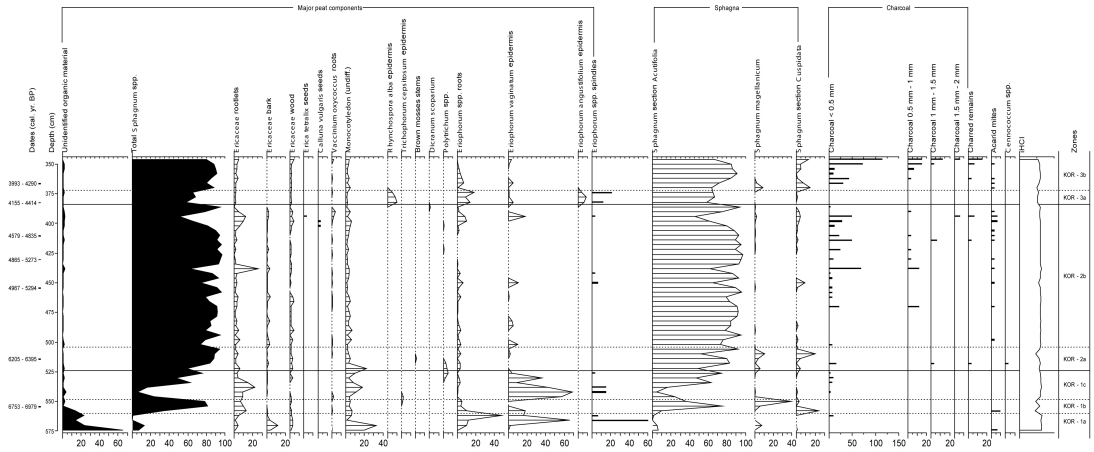

Figure 5.18 - Plant macrofossil composition of KOR-09-01.

5.6.2 Testate amoebae remains

As with the plant macrofossil record, the testate amoebae assemblage in the peat profile from Kortlandamossen was divided into three main zones, KOR-1 to KOR-3, with each zone representing major shifts in surface wetness conditions (Table 5.10 and Figure 5.19). Zones KOR-1 and KOR-3 were divided into further sub-zones, which indicated brief changes in ecological assemblage and associated changes in moisture availability.

Zone KOR-1a described an intermediate to dry phase of the bog with a presence of 'dry species' such as *T. arcula* type and *D. pulex*. However, the presence of more wet loving species such as *A. seminulum*, *A. discoides* type, *A. catinus* and *Difflugia rubescence* indicated that conditions were moderately dry.

At *c*. 6950 BP (558 cm) conditions on Kortlandamossen became much drier, according to the testate amoebae data, contradicting evidence from the plant macrofossil analysis. This dry phase was characterised by a drop in *A. flavum* and *D. pulex* and their replacement with the hydrophobic *T. arcula* type. This dry phase, however, was relatively short-lived and at approximately 6700 BP (542 cm) *T. arcula* type was replaced by *D. pulex*. The continued presence of *A. seminulum* and the tailing off of *C. arcelloides* type indicated a move to more intermediate to dry conditions on the bog (Zone KOR-1c).

Table 5.10 - Summary of testate amoebae zones from Kortlandamossen

Zone	Depth (cm)	Description	Age (cal yr BP)
KOR-1a	574 - 558	Profile dominated by *A. flavum* with presence of *A. seminulum* and *A. discoides* type indicating intermediate conditions.	7150 - 6950
KOR-1b	558 - 542	Shift to dry conditions as indicated by dominance of *T. arcula* type and major drop in *A. flavum*.	6950 - 6700
KOR-1c	542 - 516	Dominance of *D. pulex*, rise in *C. arcelloides* type and increase in *T. arcula* type indicate a return to moderately dry bog surface conditions.	6700 - 6300
KOR-2	516 - 466	Gradual drying out of the bog indicated by increases in *D. pulex* coupled with steady drop in *A. flavum*. Presence of *H. papilio* and *A. catinus* type indicate moderate conditions.	6300 - 5400
KOR-3a	466 - 346	Established wet surface conditions on Kortlandamossen as indicated by dominance of *A. flavum* and presence of *Hyalosphenia* spp. and *H. petricola*. This phase is interrupted by two drying shifts (KOR-3b and KOR-3c).	5400 – 3900
KOR-3b	442 - 430	First of two abrupt dry shifts on Kortlandamossen supported by sudden rise in *D. pulex* alongside a large drop in *A. flavum*.	5050 - 5000
KOR-3c	396 - 384	Second major shortlived dry shift shown by the replacement of *A. flavum* by *D. pulex*. Disappearance of *Hyalosphenia* spp. and *Heleopera* spp. support a shift to very dry conditions.	4500 - 4350

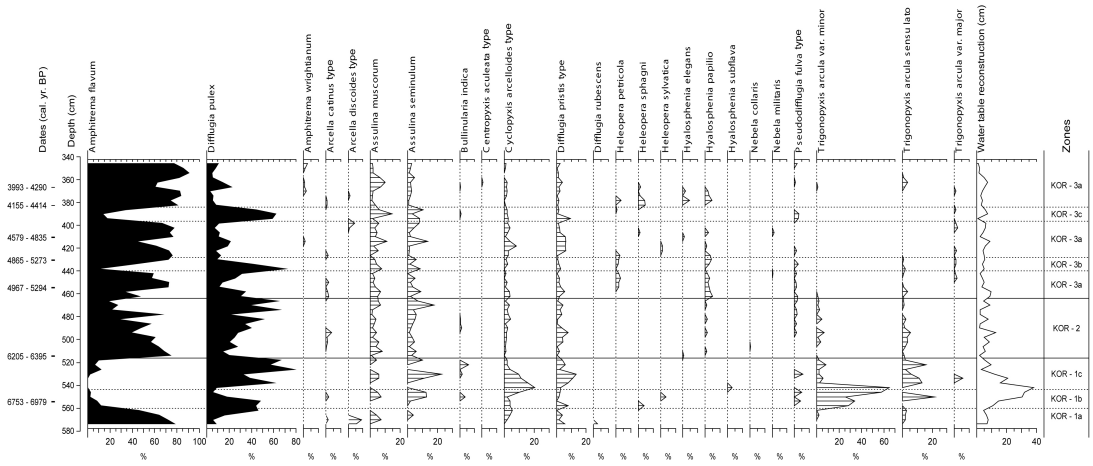

Figure 5.19 - Testate amoebae assemblages from KOR-09-01

Towards the top of zone KOR-1c, *A. flavum* began to increase at the same time that *D. pulex* sharply decreased and *C. arcelloides* type almost fully disappeared. This was coupled with a large drop in *T. arcula* type, which indicated a sudden shift to much wetter conditions at *c*. 6300 BP (516 cm). Following this sudden wetting of the site, a long phase of gradually drying surface conditions ensued, as indicated by a steady drop in *A. flavum,* coupled with a steady rise in *D. pulex* until *c*. 5400 BP (466 cm). At *c*. 5400 BP, wet conditions took hold on Kortlandamossen (KOR-4a) with a prominent *A. flavum*, *A. seminulum*, *H. petricola* and *H. papilio* community. However, the wet phase on Kortlandamossen was periodically interrupted by short-lived shifts to drier conditions. A sharp rise in *D. pulex* and a drop in *A. flavum* and *H. Papilio* from *c*. 5100 BP (442 cm) until *c*. 5000 BP (430 cm) indicated a short-lived shift to much drier conditions. At *c*. 5000 BP (430 cm), however, wet bog surface wetness conditions quickly returned. A second shift to drier conditions occurred between *c*. 4500 BP (396 cm) and *c*. 4350 BP (384), again indicated by a sudden drop in *A. flavum*, *Arcella* spp., *Heleopera* spp. and *Hyalosphenia* spp., alongside a sharp rise in *D. Pulex*. By *c*. 4350 BP (384 cm) the profile was once again dominated by *A. flavum*, supporting the interpretation of wet surface conditions on the site. A summary of the ecological zones of testate amoebae assemblages is presented in Table 5.10.

5.6.3 Multi-proxy comparison

A mean BSW index derived from testate amoebae and plant macrofossil data from Kortlandamossen (Figure 5.20) showed that dry bog surface conditions were present during the early peat formation phase from *c*. 7100 BP until *c*. 6500 BP (565 cm - 525 cm). Following the initial dry phase, conditions rapidly changed and the bog

surface became wet for the remainder of the profile. Figure 5.20 suggests there were stable BSW conditions at Kortlandamossen for most of the mid-Holocene, interrupted by brief and minor fluctuations. A pool phase, indicative of strong wetting of the bog, occurred between *c*. 4350 BP and *c*. 4150 BP (385 cm – 365 cm).

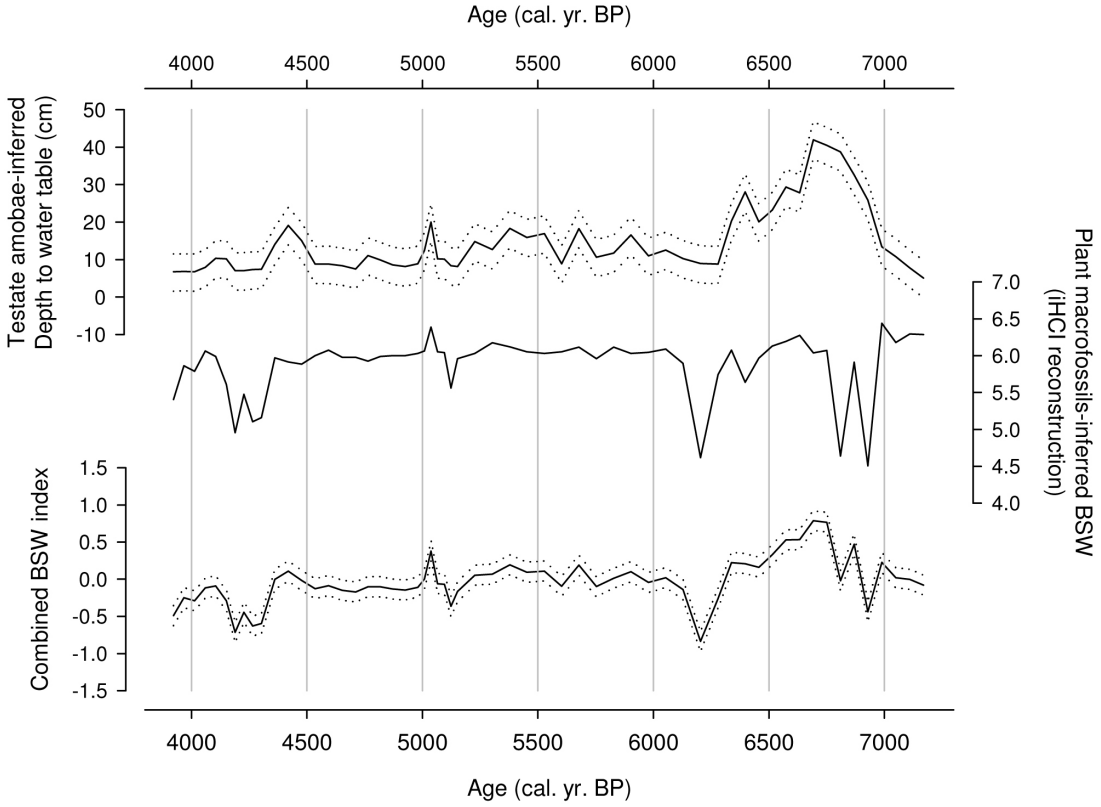

Figure 5.20 - BSW reconstructions based on testate amoebae and plant macrofossil data from Kortlandamossen.

5.7 Gällseredsmossen, Sweden

5.7.1 Plant macrofossil remains

Evidence from the plant macrofossil analysis of Gällseredsmossen showed that the site was relatively dry during the early- to mid-Holocene (Figure 5.21 and Table 5.11). The profile was divided into the three main ecological Zones GAL-1 to GAL-3, with the latter two further divided into sub-zones to reflect short-lived changes in bog surface wetness.

Zone GAL-1 represented a *Phragmites* fen stage, characterised by a large dominance of *P. australis* suggesting initial wet conditions. At *c*. 7350 BP (536 cm) Gällseredsmossen turned ombrotrophic and a period of dry surface conditions ensued. The combination of *S.* section *Acutifolia* and *E. vaginatum,* coupled with the gradual increase in Ericaceae, exemplified the gradual drying of the site. This was supported by the emergence of *T. cespitosum* towards the top of Zone GAL-2a. At *c*. 5500 BP (472 cm), a sudden increase in *S.* section *Cuspidata* and a drop in *T. cespitosum* and Ericaceae suggested a wetting of the site (Zone GAL-2b). This wet phase however, was short-lived and by *c*. 5400 BP (462 cm) dry surface conditions returned. Until *c*. 4800 BP (412 cm), a *S.* section *Acutifolia* and *E. vaginatum* community continued to dominate the profile.

From approximately 4800 BP (412 cm), *E. vaginatum* disappeared from the profile and the presence of undifferentiated monocotyledon roots returned to minimal background levels. The profile became dominated by *S*. section *Acutifolia* and Ericaceae, an indication of continuing dry bog surface wetness conditions. From *c*.

4800 BP until *c*. 4550 BP (396 cm), *S. austinii* made its first pronounced appearance, though it was quickly replaced by *S.* section *Acutifolia*. The dominance of this *S.* section *Acutifolia* and Ericaceae community was uninterrupted until *c*. 3900 BP (352 cm) (zone GAL-3b). By *c*. 3900 BP *S. austinii* made a gradual recovery and became dominant alongside *S.* section *Acutifolia* until the top of the profile, indicating intermediate to wet conditions on Gällseredsmossen. A brief spike in Ericaceae and *E. vaginatum* together with a sharp decrease in *Sphagnum* spp. abundance suggested a drying of the bog surface at approximately 3700 BP (334 cm).

Table 5.11 - Summary of plant macrofossil zones from Gällseredsmossen

Zone	Depth (cm)	Description	Age (cal yr BP)
GAL-1	546 - 536	*Phragmites australis* dominated fen section.	7650 - 7350
GAL-2a	536 - 412	Dry surface conditions, indicated by continuous change between *S.* sect. *Acutifolia* and *E. vaginatum*-dominated sections. The presence of *T. cespitosum* supports dry conditions.	7350 - 4800
GAL-2b	472 - 462	Short-lived wet phase interrupting dry conditions. A shift to wetter conditions is highlighted by the emergence of *S.* sect. *Cuspidata*, the large drop in *E. vaginatum* and the disappearance of *T. cespitosum*.	5500 - 5400
GAL-3a	412 - 396	Shift to *Sphagnum* dominated peat profile. First dominance of hummock building *S. austinii*. Disappearance of *E. vaginatum*.	4800 – 4550
GAL-3b	396 - 352	Continuing dry phase. Zone dominated by *S.* sect. *Acutifolia*, which gradually replaced *S. austinii*.	4550 - 3900
GAL-3c	352 - 322	Return to hummock building phase with a *S. austinii* and *S.* sect. *Acutifolia* community. Brief period of very dry conditions interrupt the zone around 334 cm.	3900 - 3550

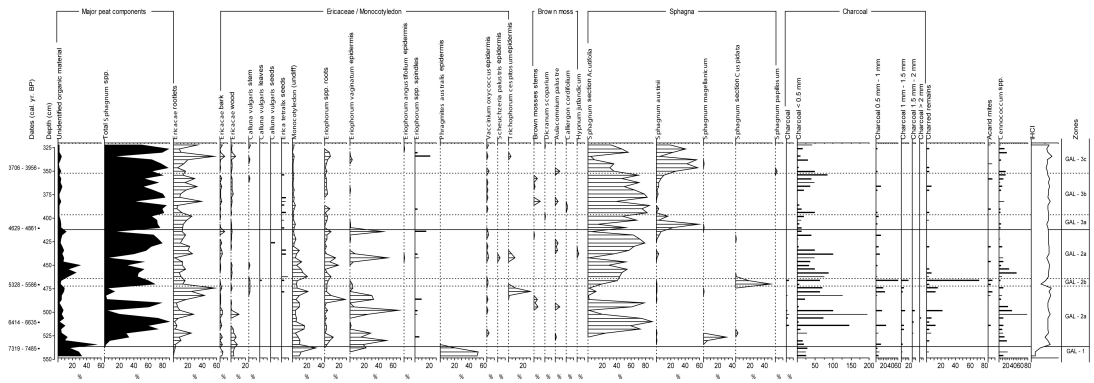

Figure 5.21 - Plant macrofossil composition of GAL-09-01

5.7.2 Testate amoebae remains

Evidence from the testate amoebae analysis supported the results from the plant macrofossil analysis, suggesting that the site was dry during the early- to mid-Holocene. The peat profile was divided into three main zones GAL-1 to GAL-3, with each representing different palaeohydrological conditions (Figure 5.22).

Zone GAL-1 characterised a gradual shift to wetter BSW conditions. This is supported by a steadily decreasing dominance of *D. pulex* and an increase in *A. muscorum* and *A. flavum*. The presence of *P. fulva* type and *T. arcula* type alongside *A. catinus* type indicated that conditions were initially moderately dry. At *c*. 5500 BP (470 cm) *A. flavum* became the dominant testate amoebae species. Simultaneously a sharp drop in *D. pulex* and *C. arcelloides* type abundance and the disappearance of *P. fulva* type suggested a shift to very wet conditions. This wet phase, however, was very short-lived and by *c*. 5400 BP (462 cm), dry surface conditions returned to Gällseredsmossen.

Surface conditions remained dry, which was highlighted by the continued dominance of a *D. pulex – C. arcelloides* type community. Hydrophobic *N. militaris* was found throughout the remainder of the profile. Dry surface conditions on Gällseredsmossen were briefly interrupted by a marked wet phase, which lasted from *c*. 4450 BP until *c*. 4250 BP (390 cm - 376 cm). During this phase, *A. flavum* became dominant, *H. papilio* reappeared and abundances of *D. pulex*, *C. arcelloides* type and *N. militaris* decreased. *T. arcula* type disappeared altogether from the profile during this wet phase. Characteristic features of the ecological zones and subzones from Gällseredsmossen are presented in Table 5.12.

Table 5.12 - Summary of testate amoebae zones at Gällseredsmossen

Zone	Depth (cm)	Description	Age (cal yr BP)
GAL-1a	546 - 534	Zone dominated by *D. pulex* with presence of *Trinema lineare* indicating dry conditions at the base.	7650 - 7300
GAL-1b	534 - 470	Stable dry conditions indicated by *D. pulex* - *A. muscorum* community. Presence of *P. fulva* type and *T. arcula* type supports evidence for dry conditions. Towards the end of the zone conditions become wetter with emergence of *A. flavum* and drop in dry indicator species.	7300 - 5500
GAL-2	470 - 462	Major peak in *A. flavum,* coupled with abrupt drop in *D. pulex* abundance, is evidence for a rapid, but short-lived change to wet conditions. This is supported by the presence of *A. catinus* type and the disappearance of *P. fulva* type.	5500 - 5400
GAL-3a	462 - 390	Profile becomes dominated by *D. pulex* and *C. arcelloides* type, suggesting dry conditions. *N. militaris* becomes more abundant and local spikes in *T. arcula* type support a dry phase.	5400 - 4450
GAL-3b	390 - 376	Temporary re-establishment of *A. flavum* and *H. papilio* suggest wetting of the bog. The continued presence of *D. pulex, C. arcelloides* type and *N. militaris* suggest that this wetting is not a pool phase.	4450 - 4250
GAL-3c	376 - 322	Return to very dry conditions as indicated by the dominance of *D. pulex* and *C. arcelloides* types, coupled with the disappearance of *A. flavum* and *H. papilio*. Dry phase is further supported by continued presence of *T. arcula* type and *P. fulva* type.	4250 - 3550

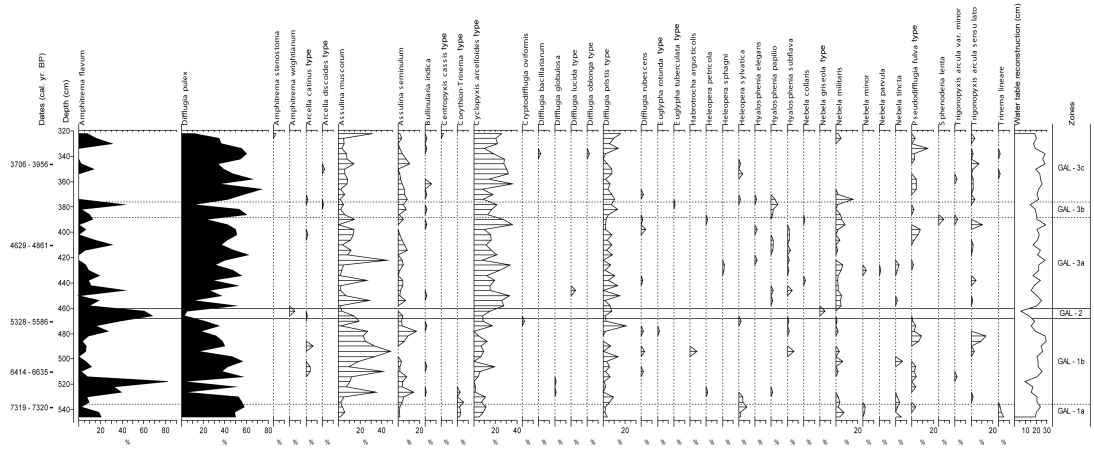

Figure 5.22 - Testate amoebae assemblages for GAL-09-01.

5.7.3 Multi-proxy comparison

Figure 5.23 shows BSW reconstructions from testate amoebae and plant macrofossil data. The mean sample score from both proxies is presented as a solid black line. From the graph, it is evident that Gällseredsmossen began as a site with relatively wet surface conditions, punctuated by a series of drying phases. Following this initial wet phase, the bog started to dry out until *c*. 5550 BP (470 cm) when a series of strong BSW oscillations occurred. These fluctuations in BSW lasted until approximately 4800 BP (400 cm) after which relatively stable BSW conditions returned to Gällseredsmossen. It is worth noting that the strong wetting of the bog at *c*. 5550 BP occurred in the plant macrofossil and testate amoebae data simultaneously.

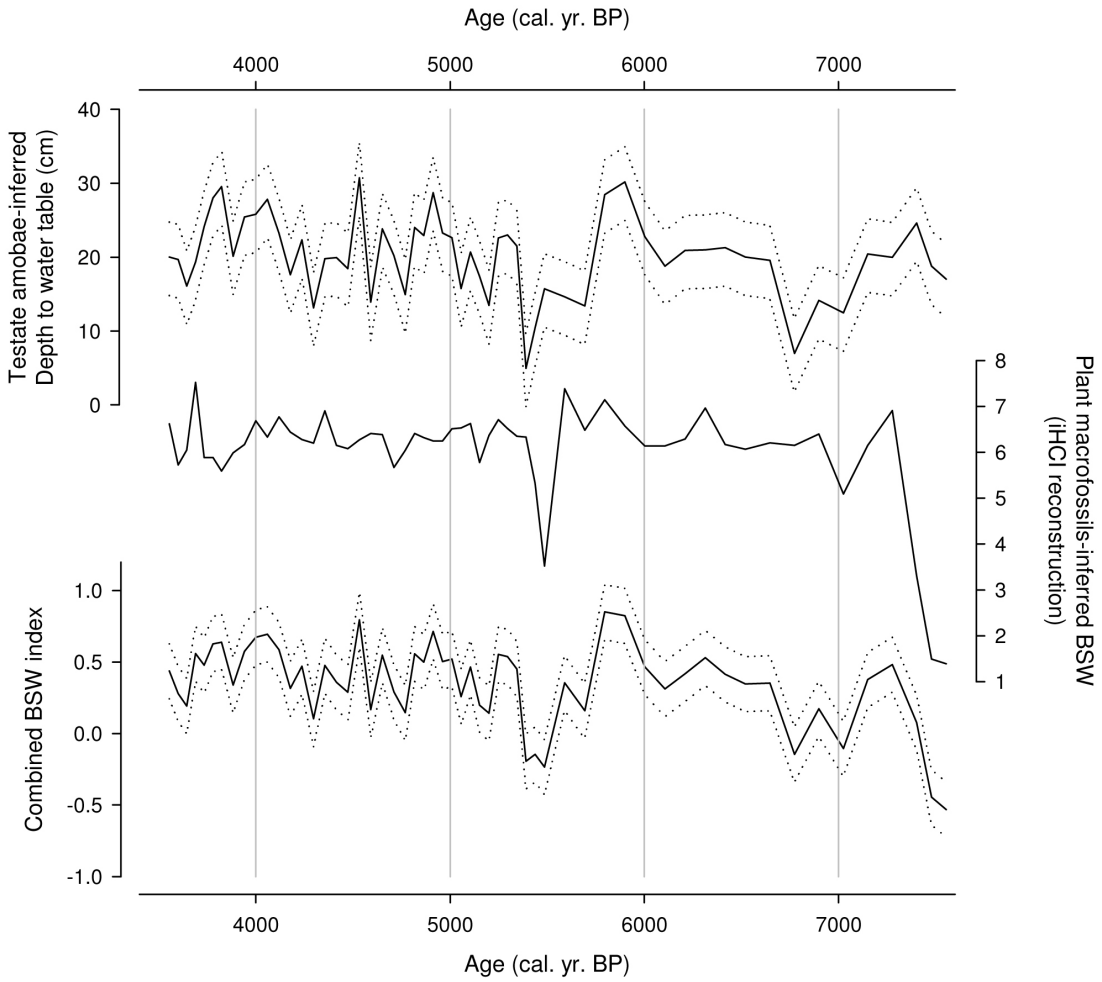

Figure 5.23 - BSW reconstructions based on testate amoebae and plant macrofossil data from Gällseredsmossen.

6 Discussion

6.1 Introduction

Relatively little is known about early- to mid-Holocene atmospheric moisture availability across northwest Europe as only limited evidence is available from many regions. By comparing and contrasting evidence from BSW reconstructions with existing evidence of palaeoclimatic change from other proxies, more light can be shed on climatic changes that took place during the mid-Holocene. Changes in BSW from five northwest European sites have been reconstructed using a multi-proxy approach, basing the chronological constraints on ^{14}C dating (Chapter 5). A series of wet and dry shifts on the bog surfaces along with periods of relatively stable dry conditions have been identified and are summarised in Table 6.1. These shifts in BSW represent a response to a combination of external factors, such as climate change (Barber and Langdon, 2007; Charman *et al.*, 2009), and autogenic processes, such as stabilisation of the water table once the sites have become ombrotrophic (Hughes, 2000; Hughes and Barber, 2003; Hughes and Barber, 2004). For each event an interpretation as to the origin of the change will be provided in the discussion below. Clear phases of hydroclimatic change on the peat bogs, corresponding to changes in the palaeo-record from other sites, will be highlighted and discussed.

The bogs in Table 6.1 have been ordered in latitudinal sequence to highlight regional and continental patterns of palaeohydrological change. This discussion will focus on each bog from this study in relation to the existing literature followed by

comparisons of BSW variability between the bogs. The second part of the chapter will focus on the link between atmospheric moisture availability across northwest Europe and its link to episodes of intensified North Atlantic ice rafting (Bond *et al.*, 2001). The identification and discussion of climate patterns in northwest Europe will help to fill the gaps in knowledge highlighted in Chapter 2.

Table 6.1 - Timing of changes in BSW on study sites. All dates are in cal. yr. BP

BSW	Kortlanda-mossen	Tore Hill Moss	Gällsereds-mossen	Raeburn Flow	Misten Bog
Wetting		3850 – 3750		3850 – 3400	
				4150 – 4050	
	4400 – 4250	4350 – 4050	4400 – 4150		
					4600 – 4400
		4850 - 4550		4850 – 4700	
			5050 – 4900		
			5250 – 5100		5250 – 4900
			5400 – 5350	5400 – 5250	
			5600 – 5500		
					7150 – 7000
		8100 – 7200 (7700 – 7500)			
Drying	7000 – 6400			6700 - 6650	
Relatively stable / dry	6400 – 4400	7150 - 4850	7250 – 5600	6650 – 5400	6650 – 5350
MHT	4400	4850	4750	5300	5250

6.1.1 Plant responses to ombrotrophy

Plant macrofossil analysis of all bogs from this study, with the exception of Misten Bog, show a distinct *Eriophorum vaginatum*-dominated phase of the bog surface shortly following the fen-bog-transition. Hughes and Barber (2004) suggested that this is a common feature on oceanic peat bogs and a common pathway to fully ombrotrophic conditions. A similar early dry phase dominated by *E. vaginatum* has been identified at the base of Walton Moss and Bolton Fell Moss in Cumbria (Barber *et al.*, 1994; Barber *et al.*, 1998; Hughes *et al.*, 2000a; Hughes and Barber, 2004) as well as Abbeyknockmoy Bog in Ireland (Hughes and Barber, 2004). It is therefore important to note that an *E. vaginatum* phase immediately following the fen-bog transition can represent a climatically-induced drying shift, a time-lag effect relating to the separation from the water table, as well as an autogenic process (c.f. Swindles et al., 2012). On Misten Bog a wet transition to ombrotrophy, characterised by a direct *Sphagnum* section *Acutifolia* and *Sphagnum magellanicum* phase, occurred without an initial dry *E. vaginatum* stage. Hughes and Barber (2004) pointed out that a transition to wet raised bog, as seen on Misten Bog, is at least as common as a dry transition characterised by an early *E. vaginatum* phase.

Another important plant species that is frequently found near the fen-bog transition in Holocene peat profiles is *S. magellanicum*. Plant macrofossil analyses from Gällseredsmossen, Misten Bog and Kortlandamossen show a high abundance of *S. magellanicum* at the base of the reconstructions. In contrast to the Belgian and Swedish bogs, *S. magellanicum* occurred only in very small quantities in the palaeoecological record from Tore Hill Moss and Raeburn Flow. This supports the findings by Hughes *et al.* (2007), who showed that *S. magellanicum* was only

present in small quantities on bogs in the British Isles throughout the Holocene. Daniels and Eddy (1990) suggested that *S. magellanicum* can be found in wooded sites in Europe, while Rodwell (1991) showed that although it is most abundant on raised mires (NVC classification – M18), it can also be found in relative abundance on blanket mires (NVC classification – M7a & M17a,b) and valley mires (NVC classification – M21a). The presence of *S. magellanicum* near the fen-bog transition may therefore indicate an autogenic transitional phase to fully ombrotrophic conditions as well as a manifestation of changes in climate. At present, *S. magellanicum* is found in greater abundance in the British Isles and forms an important part of the vegetation of raised mires (NVC classification – M18).

6.2 Patterns of atmospheric moisture availability

A key aim of this research is to establish patterns of atmospheric moisture availability across northwest Europe. In order to highlight climate patterns, evidence from BSW variability firstly needs to be compared with evidence of climate change from the wider literature before being compared with each other.

6.2.1 Kortlandamossen, Sweden

BSW reconstructions from Kortlandamossen (Figure 6.1) show that little variation in surface hydrology occurred during the mid-Holocene on the bog. The record from KOR-09-01 starts at *c*. 7200 BP with an initial shift to dry conditions, reflected in the high *E. vaginatum* content of the peat profile and the high abundance of hydrophobic *Trigonopyxis arcula* var. *minor* and *T. arcula sensu lato* (Zones KOR-1

a, b, c). Borgmark (2005) analysed a core from Kortlandamossen and found that peat accumulation started around 10,000 BP. The 2800-year age difference between Borgmark's basal peat and that of this thesis suggests that the *E. vaginatum* phase at the base of KOR-09-01 is a result of climatically induced drying of the site rather than an autogenic phase of early ombrotrophy (Hughes and Barber, 2004). Borgmark, however, did not analyse the plant macrofossil assemblage or establish the timing of the fen-bog transition for Kortlandamossen. It is therefore possible that a fen stage existed at the site until *c*. 7200 BP, at which point ombrotrophy occurred with an initial *E. vaginatum* stage (Section 6.1.1). Unfortunately no deeper material was collected from KOR-09-01 as a result of the impenetrable nature of the *E. vaginatum* layer and so it was not possible to establish the nature of peat that accumulated prior to *c*. 7200 BP.

For most of the record, BSW reconstructions from Kortlandamossen show a prolonged phase with little water table and floristic change, largely in line with a period of glacial absence and retreat in Scandinavia identified by Bakke *et al.* (2010). The evidence of a stable mid-Holocene phase without wet or dry excursions is likely to be a response to the HTM (e.g. Seppä *et al.*, 2009; Weckström *et al.*, 2010; Brown *et al.*, 2012) (Section 2.4.2). Seppä *et al.* (2009) demonstrated that temperatures in northern Europe were on average 1.5 ºC higher than present from *c*. 8000 BP until *c*. 4800 BP, making it the primary control on the length and severity of the summer water deficit on Kortlandamossen. Contrary to the humification records from Borgmark (2005), Gunnarson *et al.* (2003) and Aaby (1976) and Scandinavian glacial mass balance reconstructions (Matthews *et al.*, 2005; Nesje, 2009), no wet shifts were detected in the record between *c*. 5500 BP and *c*. 4800 BP.

During this time period, the surface vegetation of Kortlandamossen was largely dominated by eurytopic *Sphagnum fuscum*. *S. fuscum* can tolerate a large range of bog surface moisture conditions (Daniels and Eddy, 1990; Smith, 2004). Wetting of the bog surface, which would register in the peat humification record, does not always trigger a plant community change when *S. fuscum* is the dominant plant species (Barber, 1994). It is, therefore, likely that small BSW changes went undetected during the HTM.

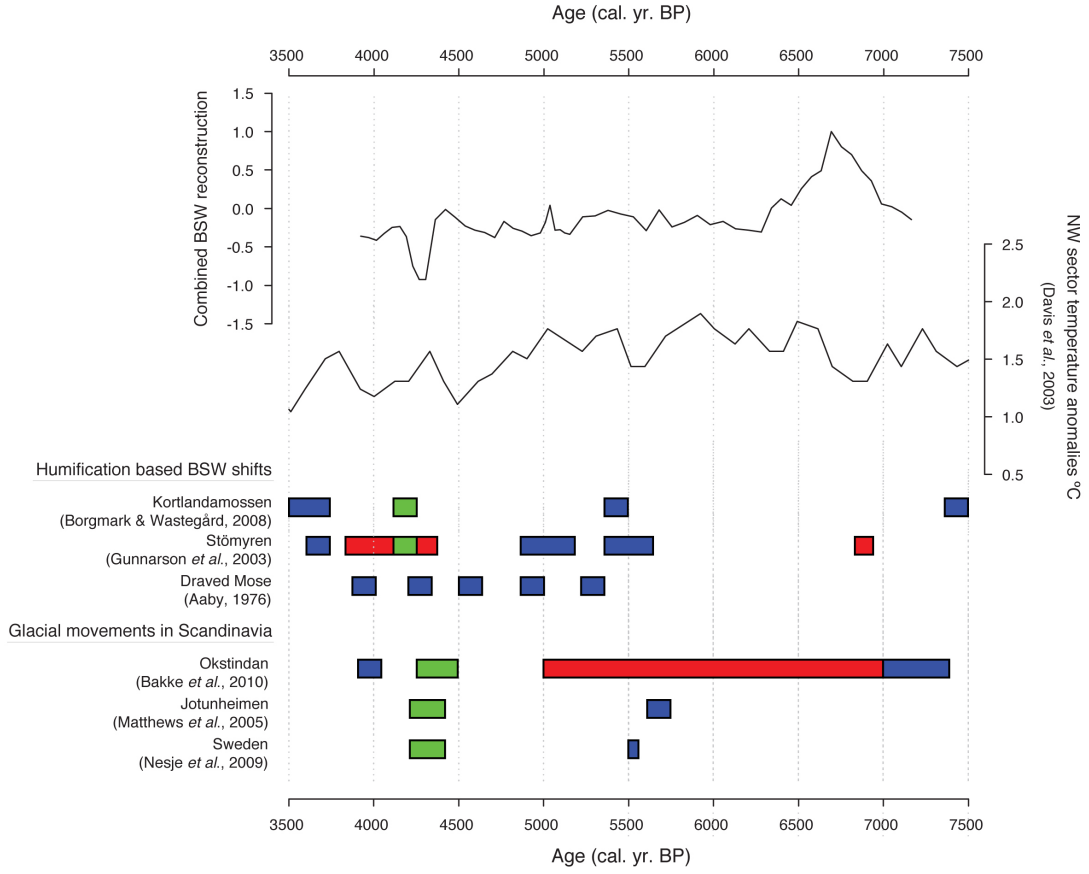

Figure 6.1 - Comparison of BSW reconstruction from Kortlandamossen with temperature, glacial mass balance and BSW reconstructions from published sources. High BSW values represent drying of the bog. Red coloured boxed indicate dry bog surface conditions or glacial retreats, blue boxes represent wetting of the bog surface or glacial advances and green boxes indicate significant wetting events or strong glacial advances.

The first major wetting of the bog surface occurred from *c*. 4400 to *c*. 4250 BP, indicated by an increase in the abundance of *Rhynchospora alba*, *Eriophorum angustifolium*, *Pseudodifflugia fulva* type and *Heleopera petricola*. This wet shift coincides with regional reconstructions of decreased peat humification (Aaby, 1976; Gunnarson *et al.*, 2003; Borgmark, 2005; Borgmark and Wastegård, 2008) and records of glacial advances in Scandinavia (Matthews *et al.*, 2000; Matthews *et al.*, 2005; Nesje, 2009; Bakke *et al.*, 2010) and the Alps (Joerin *et al.*, 2006). BSW reconstructions from Cumbria (Barber *et al.*, 1994; Hughes *et al.*, 2000a), Ireland (Barber *et al.*, 2003; Swindles *et al.*, 2010) and Scotland (Tipping, 1995a; Mauquoy and Barber, 2002; Langdon *et al.*, 2003; Langdon and Barber, 2004; Langdon and Barber, 2005; Mauquoy *et al.*, 2008) also show increased surface wetness between *c*. 4400 BP and *c*. 4000 BP. The shift marks the end of the prolonged phase of unchangeable mid-Holocene BSW conditions (Figure 6.1) and hence the end of the HTM. The overwhelming evidence for an abrupt climate anomaly between *c*. 4400 BP and *c*. 4000 BP from a wide range of palaeoclimatic proxy sources points to a large-scale event, the so-called '4.2k' event. This event has been identified in all of the bogs within this study and its extent will be discussed in more detail in Section 6.2.8 in relation to changes in North Atlantic SST and Westerly storm tracks.

6.2.2 Gällseredsmossen, Sweden

In contrast to Kortlandamossen, the BSW record of Gällseredsmossen is considerably more variable with more pronounced fluctuations in water table (Figure 6.2). Plant macrofossil analysis for Gällseredsmossen shows that an *E. vaginatum* and *S. magellanicum* community replaced an initial *Phragmites* fen at *c*. 7200 BP. As discussed in Section 6.1.1, this shift in plant community is likely to indicate a

shift to fully ombrotrophic conditions. By *c*. 7000 BP, *S. magellanicum* had been replaced by *S.* section *Acutifolia*, suggesting a drying of the bog surface, and a long phase of alternating *E. vaginatum* and *S*. s. *Acutifolia*-dominated surface conditions followed. This long phase of low BSW was only briefly interrupted by very wet conditions from *c*. 5600 BP to *c*. 5400 BP, which were characterised by a first major dominance of *Sphagnum* section *Cuspidata* together with increased abundance of wet-loving testate amoebae species *Cryptodifflugia oviformis* and *Heleopera sylvatica* (Charman *et al.*, 2000). The change to increased BSW corresponds very well with other palaeoclimatic records from the region. Humification records from three Swedish bogs (Gunnarson *et al.*, 2003; Borgmark, 2005; Borgmark and Wastegård, 2008) indicate sudden wetting of the bogs between *c*. 5600 BP and *c*. 5400 BP. Minor glacial advances recorded in southern Sweden (Nesje, 2009) at *c*. 5550 BP and Norwegian Jotunheimen (Matthews *et al.*, 2005) at *c*. 5700 BP corroborate the evidence for a large-scale yet short-lived climate anomaly rather than a local or autogenic signal (Swindles *et al.*, 2012a). Pollen-based temperature reconstructions by Davis *et al.* (2003) for the northwest European region show a slight drop in temperature at *c*. 5750 BP, in line with glacial advance and increased BSW records. It is likely that the decrease in BSW is the result of a drop in atmospheric and North Atlantic sea surface temperatures (Section 6.2.7), the so-called '5.3k' event.

Following the wetting of the bog surface between *c*. 5600 BP and *c*. 5400 BP a series of short-lived water table fluctuations ocurred until *c*. 4900 BP, characterised by an *E. vaginatum* and *S*. s. *Acutifolia* community. Wein (1973) demonstrated that *E. vaginatum* thrives in conditions of fluctuating water tables, which supports the

findings from the palaeoecological reconstruction. At approximately *c*. 4750 BP, *E. vaginatum* largely disappeared from the peat profile and *Sphagnum austinii* first appeared in abundance. This shift in surface vegetation is accompanied by increases in the abundance of hydrophilic *Nebela militaris* and *Pseudodifflugia fulva* type and marks a transition to wetter surface conditions that last until the top of the profile. The rise of *S. austinii* marks the distinct change to modern and more maritime climatic conditions. Kortlandamossen only registers a very slight decrease in BSW at *c*. 4750 BP. It is, therefore, likely that plant communities at Gällseredsmossen might have been closer to their environmental tolerance thresholds and the decrease in summer water deficit resulting from the decreasing temperature may have induced the plant community change. The timing of the wet phase also does not coincide with other climatic events in the region other than a slight wet-shift in Draved Mose from *c*. 4800 BP to *c*. 4700 BP (Aaby, 1976) and a slight cooling anomaly in the stacked record of pollen-based temperature reconstructions (Davis *et al.*, 2003; Seppä *et al.*, 2009). Seppä *et al.* (2009) suggest that the drop in temperatures could be linked with a decrease in the strength of Atlantic Westerlies.

Similarly to the other bogs in this study, increased BSW at Gällseredsmossen occurred between *c*. 4450 BP and *c*. 4150 BP. The timing of this wet phase on the bog in relation to other palaeoclimatic records suggests that it is part of a large-scale climate anomaly and is discussed in greater detail in Sections 6.2.8 and 6.3.

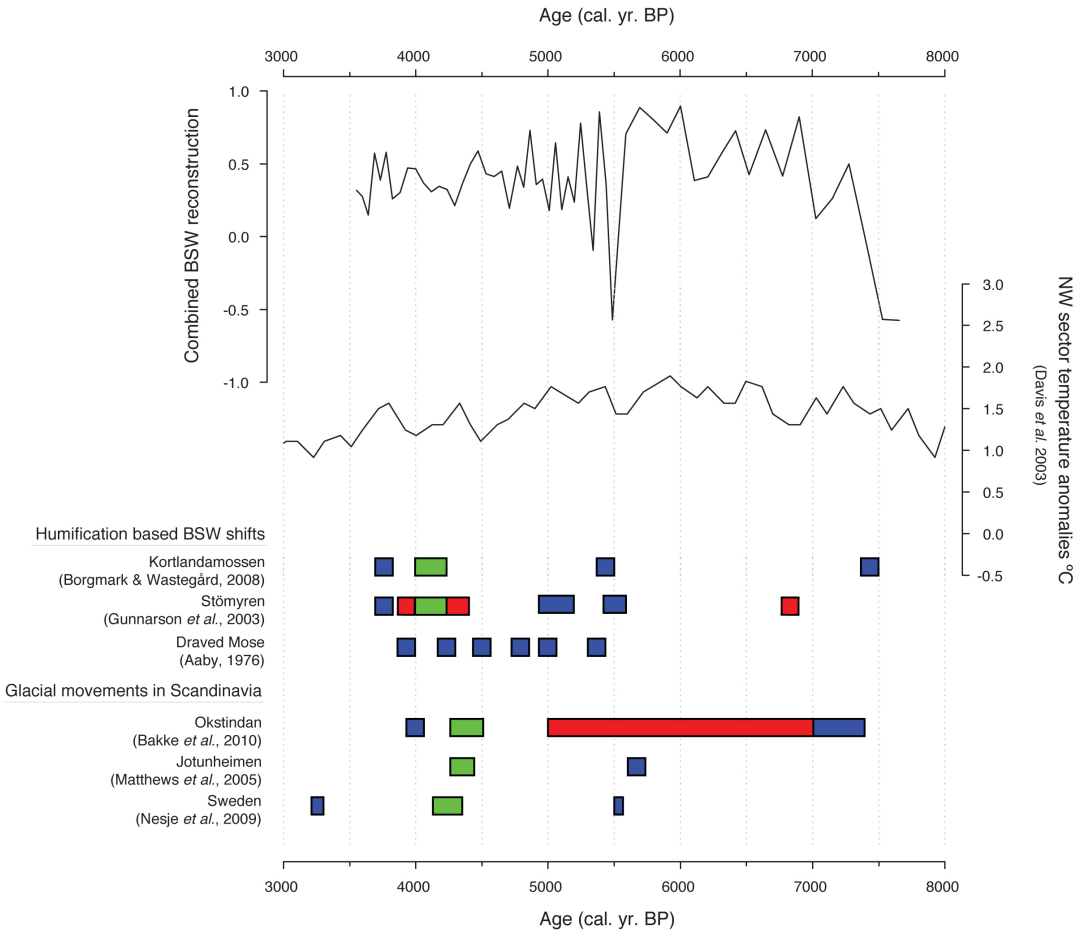

Figure 6.2 - Comparison of BSW reconstruction from Gällseredsmossen with other palaeoenvironmental reconstructions. Legend to the figure is the same as Figure 6.1.

6.2.3 Tore Hill Moss, Scotland

Plant macrofossil analyses show that Tore Hill Moss became ombrotrophic at *c*. 9400 BP and consequently dried out. Following the initial drying of the site, BSW increased from *c*. 8200 BP until *c*. 7600 BP, characterised by a rise in *Sphagnum cuspidatum* and *Sphagnum balticum*, both of which are species found in wet habitats. This phase of wet conditions on Tore Hill Moss coincided with increased BSW at Walton Moss (Hughes *et al.*, 2000a) and Bolton Fell Moss (Barber *et al.*, 1994) both

of which show a wetting trend around *c*. 8000 BP. A similar increase in BSW from *c*. 8300 BP until *c*. 8100 BP is also recorded in the humification record from Kortlandamossen Core 1 (Borgmark and Wastegård, 2008). However, it is not replicated in Borgmark and Wastegård's reconstruction from Core 2, making this the only period in the humification records from Kortlandamossen where the two reconstructions do not agree with one another. Evidence from the auxiliary core (MIS-08-08) from Misten Bog (Hughes *et al.*, in prep.) indicates that surface conditions were wet at approximately *c*. 7800 BP. Within the error margins of the chronology (Section 5.2.2), the wet excursion at *c*. 8000 BP coincides with the lowest temperatures since the start of the core (Davis *et al.*, 2003; Antonsson and Seppa, 2007; Seppä *et al.*, 2009). This implies a large-scale climatic anomaly that is likely to have been the result of a drop in atmospheric temperatures and changes in North Atlantic SST (BE5). A more detailed discussion of the event in relation to North Atlantic ice rafting and Bond Event BE5 is found in Section 6.3. Unfortunately the records from Temple Hill Moss and other Scandinavian BSW reconstructions do not stretch back far enough for comparisons.

From *c*. 7200 BP until *c*. 4850 BP, the surface of Tore Hill Moss was relatively dry with minor fluctuations in BSW, largely following the trends of the temperature reconstruction by Davis *et al.* (2003) for the NW sector (Figure 6.3). Between *c*. 4850 BP and *c*. 3250 BP, however, conditions changed and the site progressively became wetter with a series of pronounced wet-shifts. This change in BSW conditions marks the end of the HTM and the onset of modern climatic conditions. Reconstructions of BSW from published records from Scotland do not, however, support a widespread wetting event at *c*. 4850 BP, with Temple Hill Moss (Langdon

et al., 2003) indicating a phase of pronounced dry surface conditions from *c*. 4850 BP until *c*. 4700 BP. Other Scottish and Irish BSW records are unchanged during the period and show neither wetting or drying trends (Barber *et al.*, 1994; Mauquoy and Barber, 2002; Barber *et al.*, 2003; Hughes and Barber, 2004; Langdon and Barber, 2005; Mauquoy *et al.*, 2008). Evidence from Raeburn Flow, however, supports a strong wet phase around *c*. 4850 BP as shown in Section 6.2.4. It is therefore likely that the change in climatic conditions was a regional phenomenon, possibly as a result of changing Atlantic storm tracks.

At the time of the '4.2k' event, BSW at Tore Hill Moss increased in line with the other bogs from this study and many palaeoclimatic records for the period (Section 6.2.8). This wetting phase on Tore Hill Moss lasted from *c*. 4350 BP until *c*. 4000 BP and was characterised by the pronounced increase in the abundance of *Arcella discoides* type and *Euglypha* spp. This evidence of a pronounced wetting of the bog surface strengthens the argument for a large-scale climatic event during Bond Event BE3 and is discussed in more detail in Section 6.2.8.

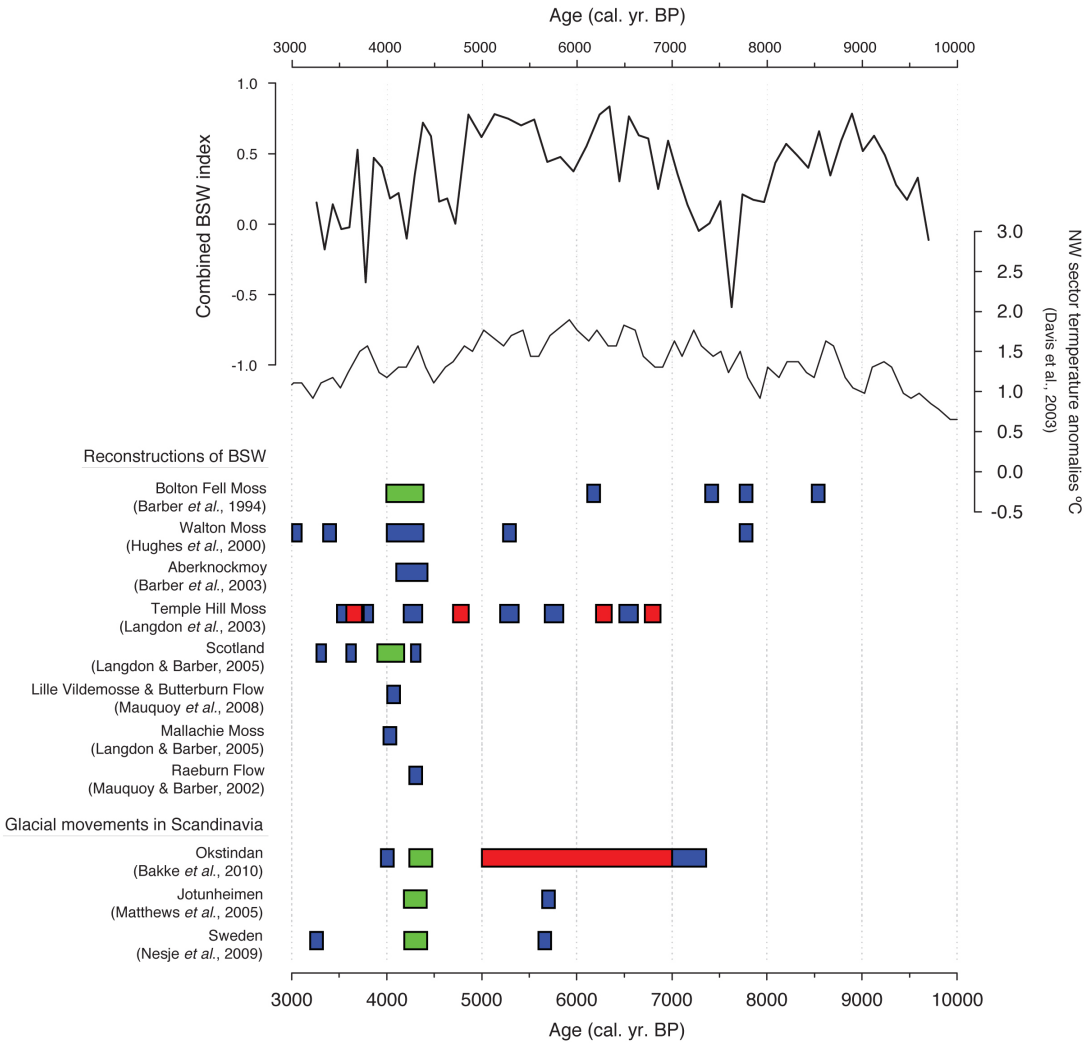

Figure 6.3 - Reconstructions of BSW from Tore Hill Moss compared against other palaeoenvironmental reconstructions. Legend to colours and trends is the same is in Figure 6.1.

6.2.4 Raeburn, Scotland

Interpretation of the lower part of peat stratigraphy from Raeburn Flow requires special attention as a large part of the peat matrix is comprised of charcoal and charred remains, indicating a large on-site fire. Such large fires burn plant fragments

beyond recognition and only tougher and more fire resistant plant fragments will remain in an identifiable state. This selective preservation of major peat building species can result in skewed results from BSW reconstructions. Plant macrofossil data from the core section below 654 cm (*c*. 6350 BP) were, therefore, excluded from hydroclimatic reconstructions from Raeburn Flow.

Similar to the nearby Walton Moss and Bolton Fell Moss, the base of Raeburn Flow is dominated by *E. vaginatum* indicating dry conditions that lasted until c. 5750 BP (Hughes and Barber, 2004). The first major wetting of the site occurred around *c*. 5300 BP (Figure 6.4), indicated by a abrupt rise in *S.* section *Cuspidata* and *Amphitrema stenostoma*, in line with evidence from Walton Moss (Hughes *et al.*, 2000a) and Temple Hill Moss (Langdon *et al.*, 2003), which both showed wetting trends at *c*. 5300 BP. Palaeoecological reconstructions by Mauquoy and Barber showed a switch from *S.* section *Acutifolia* to *S. austinii* accompanied by a disappearance of *E. vaginatum* at *c*. 5300 BP. This shift in plant community assemblage indicates a slight wetting of the bog surface (Stoneman, 1993; Stoneman *et al.*, 1993), in line with evidence from core RBF-08-01 and evidence from Tore Hill Moss. Given the variability in bog topography, a change in moisture availability will have different impacts on BSW, depending on the contemporary plant community. Low hummock / lawn microforms will show a considerable swing to pool species during a wetting phase, while changes to high hummock plant communities might only be marginal for the same change in moisture availability. It is likely that the starting position of the plant community at Raeburn Flow dictated the differences in BSW reconstructions between this study and Mauquoy and

Barber's work. The shift in BSW clearly marks the end of stable mid-Holocene conditions and the termination of the HTM.

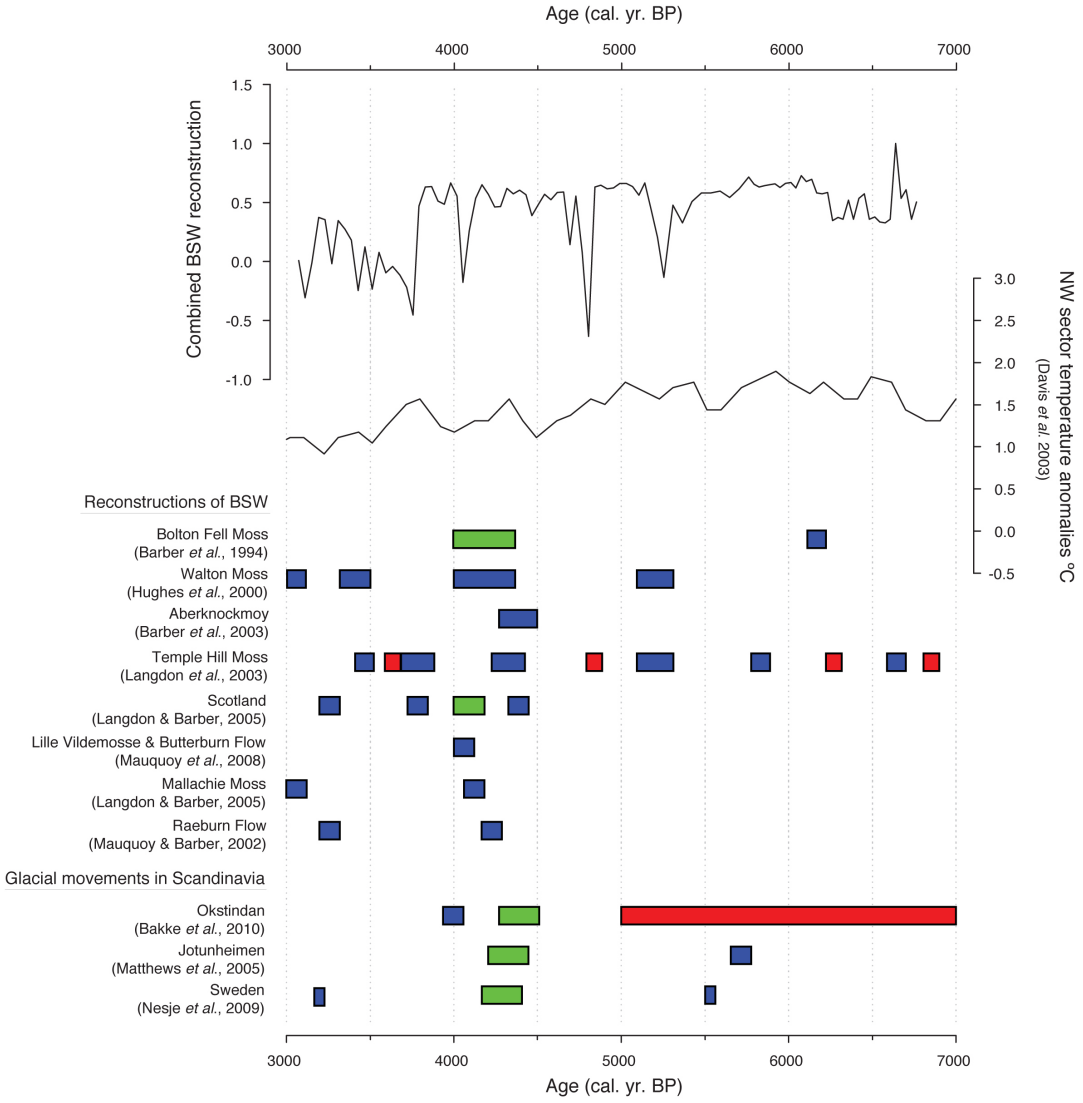

Figure 6.4 - Comparison of BSW reconstruction from Raeburn Flow to other sources of palaeoenvironmental data. Legend to colours and trends is the same as in Figure 6.1.

Following the end of the HTM, two pronounced wet shifts were recorded in the peat record from Raeburn Flow between *c*. 4850 BP – *c*. 4700 BP and *c*. 4150 BP – *c*. 4050 BP. In both cases, increased BSW conditions were characterised by a sharp rise in *S.* section *Cuspidata*, indicating very wet and near pool conditions. As discussed in Section 6.2.3 the synchronous increase in BSW between *c*. 4850 BP and *c*. 4700 BP at Raeburn Flow and Tore Hill Moss but absence from Temple Hill Moss (Langdon *et al.*, 2003) and other Scottish bogs (e.g. Tipping, 1995a; Langdon and Barber, 2005) suggests that the event was localised in nature.

The well-documented large-scale wet / cold event that has largely been observed in the palaeo-record between *c*. 4400 BP and *c*. 4000 BP (Section 6.2.8) took place at Raeburn Flow from *c*. 4150 BP – *c*. 4050 BP. The timing of the shift in BSW suggests that it is in response to the same climatic mechanisms responsible for triggering increases in BSW in the other bogs studied in this thesis (Section 6.2.8).

At *c*. 3850 BP a change in surface vegetation to a *S.* section *Cuspidata* and *Rhynchospora alba* community indicated a strong wetting of the site with consequent wet conditions persisting until the top of the reconstruction. Similar wet shifts occurred between *c*. 3850 BP and *c*. 3700 BP on Temple Hill Moss (Langdon *et al.*, 2003) and between *c*. 3850 BP and *c*. 3750 BP on Tore Hill Moss. However, no hydrological excursions at the time were recorded in the Cumbrian sites or in the wider palaeo-record of northwest Europe. It is therefore likely that the event was regional in nature and possibly the result of a prolonged period of Atlantic storm tracks making landfall across Scotland.

6.2.5 Misten Bog, Belgium

Because of the tough and sometimes impenetrable nature of *E. vaginatum* in the peat profile, the core from Misten Bog (MIS-08-07) does not contain the transition to ombrotrophic conditions. Instead the base of the core represents fully ombrotrophic conditions. A palaeoecological reconstruction from the auxiliary core (MIS-08-08) shows that the bog became ombrotrophic at around *c*. 7800 BP without the initial *E. vaginatum* phase (Hughes *et al.*, in prep) that has been observed on the other bogs in this study. Climatic reconstructions from Misten Bog largely follow the four distinct *Sphagnum* communities that made up the peat surface from *c*. 7350 BP until *c*. 4100 BP. Prolonged wet conditions started at *c*. 7150 BP and lasted until *c*. 6650 BP (Figure 6.5), characterised by a dominance of *S. magellanicum* (Section 6.1.1). This wet shift is not detected in other palaeoclimatic reconstruction from northwest Europe or the Alps and most likely represents localised changes in climate.

A sudden switch to a *S.* s. *Acutifolia* and brown moss-dominated plant community, indicating dry BSW conditions, occurred at *c*. 6650 BP and lasted until *c*. 5200 BP. This prolonged phase of dry conditions represents the HTM and is in line with records of Scandinavian (e.g. Nesje, 2009) and Swiss (e.g. Joerin *et al.*, 2006) glacial advance records and reconstructions from British bogs (e.g. Tipping, 1995a; Langdon *et al.*, 2003). Temperature reconstructions by Davis *et al.* (2003) show that temperatures for the central-west sector of Europe were relatively high but fairly steady (Figure 6.5). During the prolonged phase of relatively stable conditions from *c*. 6650 BP until *c*. 5200 BP, a series of short-lived increased BSW excursions occurred on the bog, largely characterised by changes in the testate amoebae community. This suggests that the small-scale and low-magnitude water table

fluctuations on Misten Bog during this period were precipitation rather than temperature-driven (Charman, 2007).

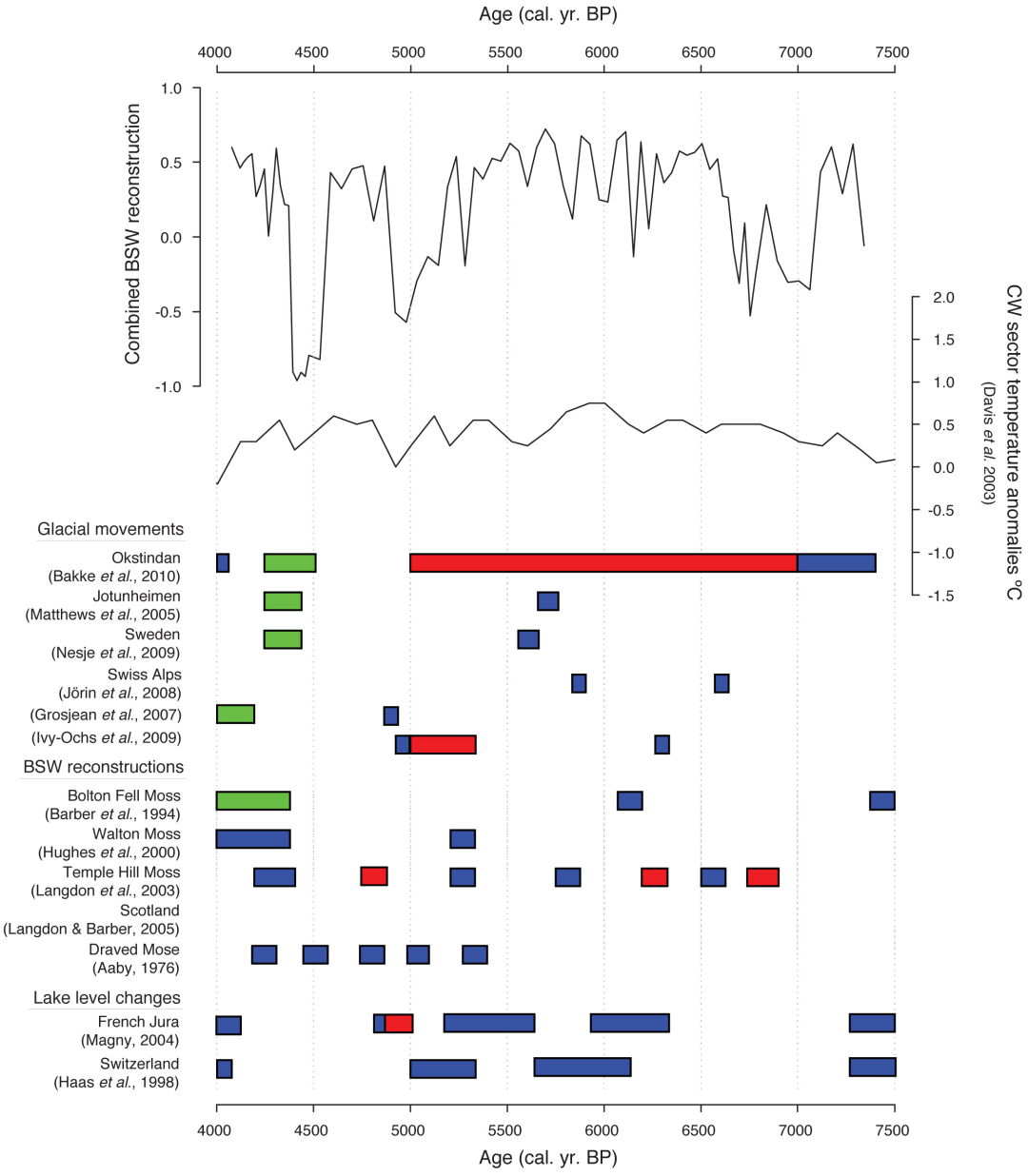

Figure 6.5 - Comparison of BSW reconstruction from Misten Bog with other sources of palaeoenvironmental information. Legend to the graph is the same as in Figure 6.1.

The first major wet shift since the onset of the HTM occurred at *c*. 5200 BP and lasted until *c*. 4900 BP, marking the end of the HTM. A similar shift to wetter conditions has been detected in Scotland (Langdon *et al.*, 2003; Langdon and Barber, 2005), Cumbria (Hughes *et al.*, 2000a) and Denmark (Aaby, 1976) but not in the central Scandinavian sites, such as Kortlandamossen and Stömyren for this time period. Evidence from Scandinavian glacial mass balance reconstructions (Ivy-Ochs *et al.*, 2009; Bakke *et al.*, 2010) shows pronounced glacial retreats during the period supporting evidence that the event did not occur in southern Sweden. However, contrary to the evidence from published palaeoclimatic records, a clear shift to wetter conditions is recorded in the BSW record from Gällseredsmossen suggesting a possible climatic divide across southern Sweden (Section 6.2.2). A shift to colder and more humid conditions has also been reconstructed for the Swiss Alps (Haas *et al.*, 1998), in lake level reconstructions in the Jura regions (Magny, 2004; Magny and Haas, 2004) and through changes in the tree limit altitudes (Schmidt *et al.*, 2002). Davis *et al.*'s (2003) temperature reconstruction shows a declining trend during this time, which is likely to be the result of changes in the strength of the North Atlantic thermohaline circulation. The wider implications of this wet phase in relation to the prevailing positioning of North Atlantic Westerlies and North Atlantic SST is discussed in greater detail in Sections 6.2.7 and 6.3.

During the period from *c*. 4600 BP until *c*. 4400, Misten Bog experienced the most pronounced wet surface conditions with an open pool phase characterised by the virtual absence of Ericaceae and herbaceous plants and complete dominance of the peat profile by *S.* s. *Cuspidata*. The event in Misten Bog slightly precedes significant increased BSW conditions in Cumbria (e.g. Hughes *et al.*, 2000a) and Scotland (e.g.

Langdon *et al.*, 2003) but coincides with increased BSW on Draved Mose (Aaby, 1976). Given the possible error margins in the chronological framework (Section 5.2.2) for Misten Bog it is likely that the event is the manifestation of the '4.2k' event experienced across all bogs in this study centred around *c*. 4400 BP – *c*. 4000 BP (Section 6.2.8). In contrast to the wet shift around *c*. 5250 BP, strong glacial advances in Scandinavia (Matthews *et al.*, 2005; Nesje, 2009; Bakke *et al.*, 2010) and higher lake levels in France and Switzerland (Magny, 2004; Grosjean *et al.*, 2007) at the time suggest a pan-European event.

6.2.6 The Holocene Thermal Maximum

A summary of wet and dry shifts, as well as relatively stable dry conditions on all five bogs, is shown in Figure 6.6. The bogs are arranged in latitudinal sequence to highlight potential north-south climate patterns. By comparing down-core plant and testate amoebae communities in relation to the overall reconstructed BSW curves for each of the study sites (see Chapter 5) prolonged phases of dry surface conditions were identified. It is apparent that all sites experienced a prolonged phase of fairly stable and dry surface conditions throughout the mid-Holocene (yellow bar).

On Misten Bog, dry surface conditions are characterised by a prolonged phase of *Sphagnum* section *Acutifolia* and brown mosses dominance accompanied by an increase in abundance of *Difflugia pulex* and the absence of hygrophilous testate amoebae species. The flora on Raeburn Flow was dominated by *Eriophorum vaginatum*, Ericaceae rootlets and *Trichophorum cespitosum* throughout the dry phase. The presence of *Sphagnum austinii*, albeit limited, suggests that the site was ombrotrophic. Dry mire surface conditions are supported by high abundance of

Cyclopyxis arcelloides type and *Difflugia pulex* together with the absence of hygrophilous testate amoebae species. On Tore Hill Moss, the surface vegetation was dominated by brown mosses *Dicranum scoparium*, *Aulacomnium palustre* and *Pleurozium schreberi* was well as *E. vaginatum*, largely replacing *Sphagnum* species. The presence of *S. austinii*, however, suggest continued ombrotrophic conditions on the site. The dominance of brown mosses was accompanied by increased abundance in *D. pulex*, *Trigonopyxis arcula* type and *Pseudodifflugia fulva* type and the absence of hygrophilous testate amoebae species. Conditions on Kortlandamossen throughout the mid-Holocene dry phase were characterised by dominance of *S.* s. *Acutifolia* and virtual absence of wet loving species, such as *Rhynchospora alba*, *Eriophorum angustifolium* and *Sphagnum* section *Cuspidata*, all of which increase in abundance at the end of the dry phase. A dominance of *E. vaginatum* and *S.* s. *Acutifolia* and the presence of *Trichophorum cespitosum* alongside the absence of wet loving species characterised dry surface conditions on Gällseredsmossen. This dry phase, however, was interrupted briefly from c. 5450 BP until c. 5350 BP with the emergence of *S.* s. *Cuspidata*. Dry conditions throughout the mid-Holocene were further characterised by the presence of hydrophobic *Hyalosphenia subflava* and elevated abundance of *D. pulex*.

These dry phase are likely to be the result of a prolonged episode of high temperatures (Holocene Thermal Maximum – Section 2.4.2) with average summer temperatures between 1.5ºC (Davis *et al.*, 2003; Seppä *et al.*, 2009) and 1.7ºC (Seppä and Birks, 2001) warmer than present. Localised temperature reconstructions from southern Sweden (Antonsson and Seppa, 2007) demonstrated the HTM with temperatures between 2.5ºC and 3ºC higher than present from *c*. 8000 BP until *c*.

4800 BP. Both the onset and termination of the HTM, however, have been shown to be time-transgressive (Kaufman *et al.*, 2004; Kaplan and Wolfe, 2006; Salonen *et al.*, 2011) and strongly dependent on regional environmental factors (e.g. Seppä and Birks, 2001; Davis *et al.*, 2003; Kaufman *et al.*, 2004; Moros *et al.*, 2004).

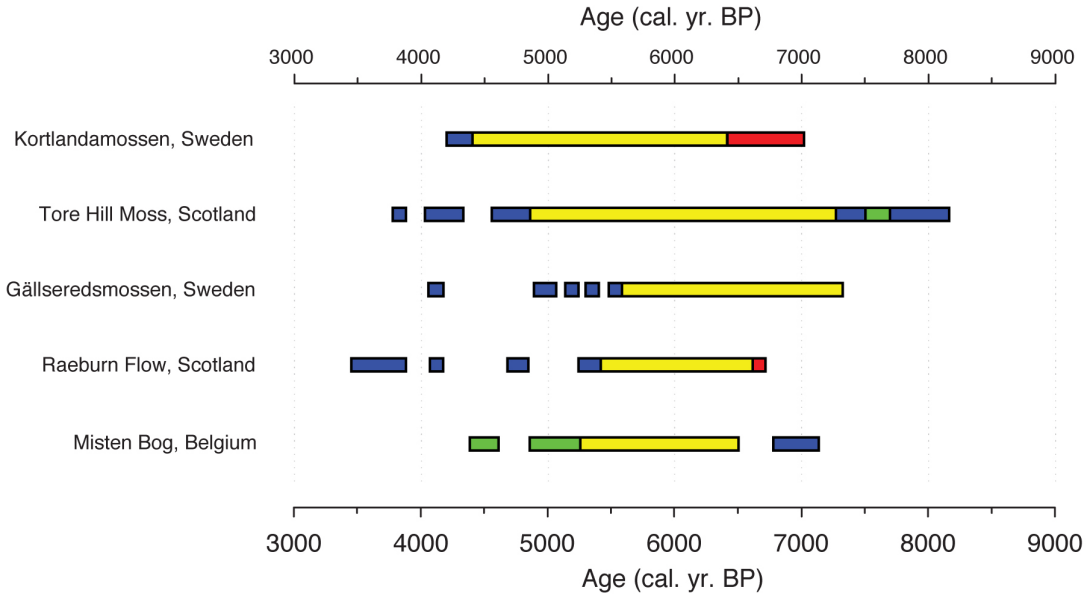

Figure 6.6 - Summary graph of changes in BSW from all study sites. Blue boxes indicate increased BSW, with green boxes showing extreme wetting events. Red boxes reflect periods of drying of the bog surface and yellow boxes show periods of relatively stable and dry conditions.

All bogs studied in this thesis, with the exception of Misten Bog and Raeburn Flow, experienced the onset of the HTM between *c*. 7250 BP and *c*. 7150 BP as shown above. The record from Raeburn Flow prior to the short-lived dry event at *c*. 6700 BP, however, proved unsuitable for palaeoclimatic reconstructions because of an on-

site fire and it is possible that the site was dry prior to *c*. 6700 BP, similar to Bolton Fell Moss (Barber *et al.*, 1994), although this remains to be established. Misten Bog was the last of the five bogs to show a response to the HTM, with dry conditions setting in at *c*. 6650 BP. As it is the most southern of the five bogs, it is likely that it experienced different regional environmental controls on climate (Seppä *et al.*, 2005) that the other bogs. The manifestation of the HTM at Kortlandamossen, Gällseredsmossen and Tore Hill Moss is in line with higher temperature reconstructions for Scandinavia (Antonsson and Seppa, 2007; Seppä *et al.*, 2009; Brown *et al.*, 2012) and the averaged northwest and centralwest European sectors (Davis *et al.*, 2003). Brown *et al.* (2012) and Antonsson *et al.* (2007) identified the onset of the HTM in Scandinavia at around c. 8000 BP, while Davis *et al.* (2003) determined its onset in the NW European sector at around c. 7900 BP. Seppä *et al.* (2005) suggested that predominantly blocking anti-cyclonic systems were responsible for the high mid-Holocene temperatures over Scandinavia between *c*. 8000 BP and *c*. 4800 BP.

Figure 6.6 suggests that there is a pattern in the termination of the HTM with Gällseredsmossen showing an end to the dry phase at *c*. 5600 BP before Raeburn Flow at *c*. 5400 BP and Misten Bog at *c*. 5350 BP. As described in Section 5.2.2, there is an uncertainty of ±150 years attached to ages from this research and it is possible that all three events occurred synchronously. Nonetheless, the pattern emerging from Figure 6.6 suggests that environmental and climatic changes at the end of the HTM were not spatially coherent across northwest Europe. Evidence for an early termination of the HTM at Gällseredsmossen is supported by Edvardsson *et al.* (2012), who identified the timing of the HTM as being between *c*. 7200 BP and *c*.

5750 BP for southern Sweden. Brown *et al.* (2012) also identified highest mid-Holocene temperatures in southern Scandinavia between *c*. 6700 BP and *c*. 5400 BP, in line with evidence for the HTM at Gällseredsmossen. Evidence of a termination at *c*. 5400 BP on Raeburn Flow is supported by other regional BSW reconstructions. BSW records from Temple Hill Moss (Langdon *et al.*, 2003) shows a return to wetter condition from *c*. 5400 BP onwards, while BSW reconstructions from Walton Moss identify the end of the HTM at *c*. 5300 BP (Hughes *et al.*, 2000a). Further research, such as tephrochronology (Langdon and Barber, 2004) and analysis of additional peat cores (Amesbury *et al.*, 2012a) from northwest Europe, is needed to determine the exact timing of the end of the HTM (Section 7.1).

The end of the HTM at Tore Hill Moss and Kortlandamossen occurred at *c*. 4850 BP and *c*. 4400 BP, respectively. Even taking into account the error margins attached to these dates (Section 5.2.2), it is clear that there is a distinct difference in timing between the terminations of the HTM at the two northern bogs compared with each other and the three southernmost ones. Given the proximity to the Scandes mountains, which form one of Europe's steepest climate barriers (Davis *et al.*, 2003), Kortlandamossen might have experienced blocking high-pressure systems for longer periods of time than other sites.

It is possible that a negative change in North Atlantic SST was responsible for the delayed termination of the HTM at Tore Hill Moss. Magny *et al.* (2004) hypothesised that SST anomalies in the North Atlantic strongly influence moisture availability across Europe by creating a mid-European wet zone (Section 6.2.7). A significant reduction in North Atlantic SST, indicated by an increase in the amount of drift ice (Bond *et al.*, 2001), occurred between *c*. 5600 BP and *c*. 5100 BP,

creating a tripartite division in the European climate system (Magny *et al.*, 2003b). It is likely that Tore Hill Moss lay north of this mid-European wet zone and therefore remained dry for a longer period than the more southerly bogs. The difference in timing between the termination of the HTM on Tore Hill Moss and the three southernmost bogs suggests that the northern location of Tore Hill Moss outside the mid-European wet zone resulted in dry conditions at Tore Hill Moss from *c*. 5600 BP until *c*. 5100 BP. This hypothesis is discussed in relation to the '5.3k' wet / cold event in Section 6.2.7.

It can be concluded that the mid-Holocene transition from a Holocene Thermal Maximum to wetter neoglacial conditions did not occur synchronously across northwest Europe. However, a general timing for the mid-Holocene transition for northwest Europe can be placed between *c*. 5600 BP and *c*. 4800 BP. It is likely that a change in atmospheric temperature (Davis *et al.*, 2003; Seppä *et al.*, 2009) coupled with a change in moisture transport (Magny *et al.*, 2003b), as a result of a drop in North Atlantic SST (Section 6.3), was responsible for the difference in timing of the HTM across northwest Europe.

6.2.7 Climatic division between *c*. 5600 BP – c. 5300 BP

As demonstrated by Magny *et al.* (2003b; 2006),decreases in North Atlantic SST and the strength of the thermohaline circulation do not elicit a uniform response in European climate with regards to moisture availability. Instead, a mid-European wet zone that is bordered by regions of dry conditions to the north and the south, exists during events of strong SST reduction (Magny *et al.*, 2006). The latitude and extent of this zone strongly depends on the severity of the SST anomaly in the North

Atlantic. Magny *et al.* (2003b) showed that the northern boundary of this zone was located at approximately 50ºN during the extreme '8.2k' cold event. During less severe climatic anomalies Magny *et al.* suggest a northern latitudinal limit of this mid-European wet zone at approximately 58ºN. Evidence of this northern latitudinal limit, however, is based on a limited number of data points and does not include any locations above 55ºN in the British Isles. Testing the existence of such a climatic boundary and refining its latitude will help to understand differences in response of BSW in northern peat bogs to changes in North Atlantic SST and the Atlantic Westerly Jet. Understanding the nature of a mid-European wet zone is important in order to establish a framework of palaeoclimatic changes and records of atmospheric moisture availability through the mid-Holocene. It will help to better differentiate between local, regional and large-scale climate change.

Evidence from this thesis supports the hypothesis of a tripartite climate system with a mid-European wet zone (Magny *et al.*, 2003b; Magny *et al.*, 2006) and demonstrates that a northern climatic divided existed at 57ºN during the '5.3k' event. BSW reconstructions from Misten Bog (50º33'N, 6º09'E), Raeburn Flow (55º20'N, 3º06'W) and Gällseredsmossen (56º10'N, 12º35'E) provide evidence that all three bogs became significantly wetter between *c*. 5600 BP and *c*. 5300 BP. In contrast, the two northernmost sites, Tore Hill Moss (57º14'N, 3º40'W) and Kortlandamossen (59º51'N, 12º17'E), both remained dry throughout this period. This partition in moisture availability centred on 57ºN supports the hypothesis of a mid-European wet zone.

A weakening of the thermohaline circulation (Keigwin, 1996; Bianchi and McCave, 1999) and reduction in North Atlantic Deep Water formation (Oppo *et al.*, 2003)

between *c*. 5600 BP and *c*. 5000 BP suggests that North Atlantic SST and changes in the Atlantic Westerly Jet were responsible for the climatic divide (Magny *et al.*, 2003b). The exact mechanisms behind the '5.3k' climatic event, however, are still not fully understood and a complex interaction between solar, orbital and ocean circulation driven forcing has been proposed (Magny *et al.*, 2006).

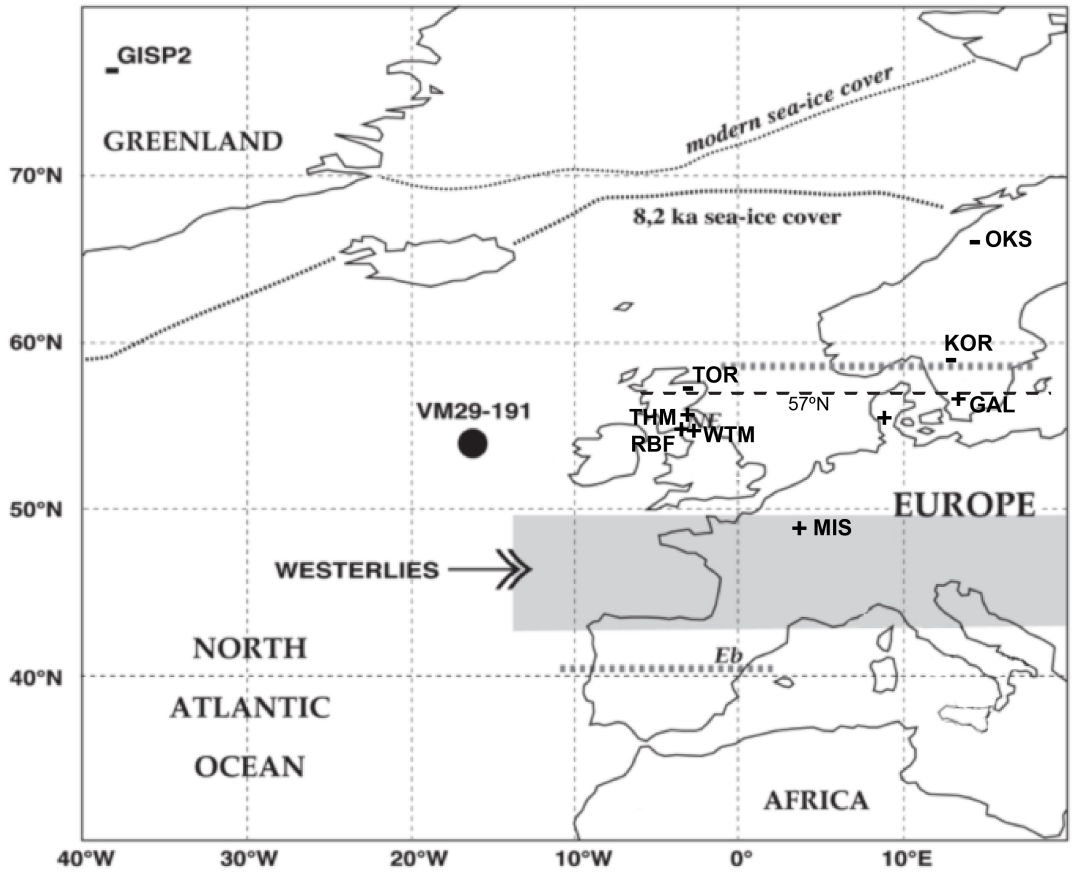

Figure 6.7 - Map showing increased (+) and decreased (-) atmospheric moisture availability during the 5.3k cold event. Dashed line indicates 57ºN climatic division. Gray bar indicates contracted mid-European wet zone during the '8.2k' event. [RBF=Raeburn Flow; WTM=Walton Moss (Hughes *et al*., 2000); THM=Temple Hill Moss (Langdon *et al*., 2003); TOR=Tore Hill Moss; MIS=Misten Bog; GAL=Gällseredsmossen; KOR=Kortlandamossen; OKS=Okstindan (Bakke *et al*., 2010)] (Adapted from Magny *et al*., 2003b).

6.2.8 The '4.2k' wet event

Similar to the climatic shift between *c*. 5600 BP and *c*. 5300 BP, sea surface temperatures in the North Atlantic dropped significantly around *c*. 4200 BP (Bond *et al.*, 1997 - BE3). Contrary to the '5.3k' event, however, no clear northern limit to the mid-European wet zone could be detected as all bogs became wet during the same time. The period between *c*. 4400 BP and *c*. 4000 BP is therefore of particular importance as it is the only time in the reconstructed record at which all five bogs show a quasi-synchronous shift to wet surface conditions.

Reconstructions from Kortlandamossen and Gällseredsmossen show increased BSW between *c*. 4400 and *c*. 4150 BP. Evidence of a wet shift on Kortlandamossen is supported by humification data by Borgmark and Wastegård (2008) that showed the most pronounced wetting of the site during the Holocene at *c*. 4200 BP. This wet period on Kortlandamossen and Gällseredsmossen is in agreement with evidence of a change to wetter / colder conditions from other Swedish peat bogs and Scandinavian glacial mass balance records. Gunnarson *et al.* (2003) identified a wet anomaly in surface conditions on Stömyren between *c*. 4200 BP and *c*. 4100 BP, while Mauquoy *et al.* (2008) showed a shift to wetter surface conditions on Lille Vildemossen in Denmark at *c*. 4100 BP. Records of glacial mass balance changes show prolonged glacial advances at Okstindan (Bakke *et al.*, 2010) between *c*. 4500 BP and *c*. 4250 BP and Jotunheimen at around *c*. 4420 BP (Matthews *et al.*, 2000; Matthews *et al.*, 2005). This evidence suggests that a shift to wetter / colder conditions occurred across most of Scandinavia between *c*. 4400 BP and *c*. 4100 BP.

Reconstructions from Tore Hill Moss show a distinct period of increased BSW between *c*. 4350 BP and *c*. 4050 and a similar shift to wetter conditions is recorded at Raeburn Flow from *c*. 4150 BP until *c*. 4050 BP. Mauquoy and Barber (2002) also identified an increase in BSW on Raeburn Flow, albeit 200 years earlier (Section 6.2.4). Furthermore, evidence from other peat-based palaeoclimatic constructions in Scotland suggests that a large-scale climatic shift occurred during the period. Records from Temple Hill Moss (Langdon *et al.*, 2003) show a significant wetting of the bog surface at *c*. 4400 BP. A synthesis of BSW conditions across Scotland for the last 5000 years (Langdon and Barber, 2005) highlighted that the majority of bogs underwent a wet shift between *c*. 4400 BP and *c*. 4150 BP, with the most pronounced shift to wet conditions at Longbridge Muir, in southern Scotland. Analyses from Kirkpatrick Fleming (Tipping, 1995a), Mallachie Moss (Langdon and Barber, 2005) and Butterburn Flow (Mauquoy *et al.*, 2008) all show increases in BSW between c. 4150 BP and c. 4100 BP. Both Cumbrian sites, Walton Moss (Hughes *et al.*, 2000a) and Bolton Fell Moss (Barber *et al.*, 1994), experienced increases in BSW between *c*. 4400 BP and *c*. 4000 BP, while reconstructions from Abbeyknockmoy Bog, Ireland, showed a sudden wetting at *c*. 4500 BP (Barber *et al.*, 2003). This evidence for a synchronous wet shift from the peat archive suggests a BSW response to a large-scale climatic event.

This period of climatic change (*c*. 4400 BP - *c*. 4000 BP) is also well documented in the literature and has been linked to drought events in the Middle East (Cullen *et al.*, 2000; Arz *et al.*, 2006) and North America (Viau *et al.*, 2002; Booth *et al.*, 2005) as well as the downfall of the Akkadian (deMenocal, 2001) and Indus valley civilisations (Staubwasser *et al.*, 2003). Furthermore, climatic anomalies during the

period have been recorded in Canada (Menounos *et al.*, 2008), tropical Africa (Thompson *et al.*, 2002b) and South America (Thompson *et al.*, 2000) suggesting that the increases in BSW recorded in the bogs in this thesis were part of a global climatic event (Bond *et al.*, 2001; Thompson *et al.*, 2002b), the so-called '4.2k' event. Staubwasser *et al.* (2003) hypothesised that it marks the start of modern climatic conditions and the Hypsithermal-Neoglaciation transition. However, as discussed above, the mid-Holocene transition in northwest Europe was centred on Bond Event BE4 rather than BE3.

6.3 Terrestrial response to episodes of increased ice rafting

Evidence from various reconstructions of North Atlantic SST have shown that changes in the North Atlantic have direct impacts on northwest European climate (Sutton and Hodson, 2005; Magny *et al.*, 2006). Episodes of increased sea drift ice in the North Atlantic have been linked to abrupt climatic changes in northwest Europe via the strength of the thermohaline circulation and the latitude of Atlantic Westerly storms (e.g. Magny *et al.*, 2003a; Niggemann *et al.*, 2003; Moros *et al.*, 2004; Charman, 2010). Bond *et al.* (1997) reconstructed the extent of ice rafted debris in the North Atlantic, which is linked to changes in sea surface temperatures. The strength of the thermohaline circulation and atmospheric temperatures have been shown to be linked to changes in North Atlantic SST and North Atlantic Deep Water formation (O'Brien *et al.*, 1995; Bond *et al.*, 2001; Oppo *et al.*, 2003). Chapman and Shackleton (2000) showed that decreased NADW production is linked with colder climatic conditions across Europe and that centennial- and millennial-scale fluctuations in North Atlantic thermohaline circulation have been an important factor

influencing European climate variability during the Holocene. Episodes of increased ice rafting in the North Atlantic (Bond Events) are therefore expected to trigger periods of wetter than long-term average surface conditions on northwest European peat bogs and should be identifiable in BSW reconstruction (Langdon *et al.*, 2003). However, the response of the European climate system is not uniform to changes in North Atlantic SST and a tripartite partition in moisture regime (Figure 2.4) has been established during strong SST anomalies (Magny *et al.*, 2006).

Bond *et al.* (1997) identified a series of significant paced events of increased IRD in the North Atlantic (Section 2.5.1) with a cyclic frequency of 1374±502 years throughout the Holocene. During the mid-Holocene these events occurred at *c*. 8100 BP (BE5), *c*. 5900 BP (BE4), and *c*. 4200 BP (BE3). Moreover, Bond *et al.* (1997) suggested that the pervasive millennial-scale pacing is the driver behind rapid climate change across Europe and is itself forced by changes in solar output (Bond *et al.*, 2001). Wanner and Bütikofer (2008), however, demonstrated that Bond Events were most likely not caused by a single forcing mechanism, such as solar variability, but that they were the result of a cocktail of environmental processes. In addition to the millennial-scale climate cycles, Bond *et al.* (2001) identified a succession of centennially-paced episodes of increased ice rafting in the North Atlantic, although, given the limited chronological constraints on their ocean core, they did not suggest a cyclic frequency for the centennial-scale episodes. Nonetheless, the identification of smaller faster-paced IRD episodes supports the evidence for centennial-scale periodicity in the intensity in North Atlantic Deep Water formation (Chapman and Shackleton, 2000). Similar centennial- and millennial-scale cycles of increased BSW have also been identified in the peat record (Hughes *et al.*, 2000a; Langdon *et al.*,

2003; Borgmark, 2005). It is therefore highly likely that cyclic changes in BSW and North Atlantic SST are closely linked and the later is expected to manifest itself in the peat archive.

Figure 6.8 shows a stacked record of North Atlantic drift ice in relation to BSW reconstructions from this study. Tore Hill Moss is the only record that stretches back far enough to be compare with IRD records during Bond Event 5 (BE5), which occurred at *c*. 8100 BP (Bond *et al.*, 1997; Bond *et al.*, 2001). Figure 6.3 shows that the early wetting phase at Tore Hill Moss (Section 6.2.3) started at *c*. 8200 BP (BE5), and that it reached its maximum extent during the period of strongly increasing sea ice cover at *c*. 7650 BP, suggesting a teleconnection between the two systems. It has been hypothesised that the '8.2k' event forms part of the millennial climate cycles (Bond *et al.*, 1997). However, overwhelming evidence (Barber *et al.*, 1999; Renssen *et al.*, 2001; Clarke *et al.*, 2004; Alley and Agustsdottir, 2005; Rohling and Palike, 2005; Wiersma and Renssen, 2006) points to a massive influx of glacial meltwater into the North Atlantic at *c*. 8400 BP, which slowed down North Atlantic Deep Water production and with it the thermohaline circulation. The consequent increase in North Atlantic ice rafting and increased BSW at Tore Hill may therefore have been a manifestation of the meltwater pulse rather than an underlying millennial-scale climate cycle. Evidence from Magny *et al.* (2003b) points to northern latitudes experiencing dry conditions during the '8.2k' event and it is therefore likely that the BSW anomaly at Tore Hill is a response to decreased temperatures rather than increased moisture availability (Magny *et al.*, 2003b). Hughes *et al.* (in prep.) are presently investigating the nature of the major wet

excursion on Tore Hill Moss centred on *c*. 7800 BP in relation to other sites across northwest Europe.

Figure 6.8 shows a reconstruction of increased amounts of drift ice between *c*. 5900 BP and *c*. 5200 BP, known as Bond Event BE4 in relation to BSW records from this study. During this period all bogs south of 57ºN (Gällseredsmossen, Raeburn Flow and Misten Bog) show a distinct wetting trend of bog surface conditions. As discussed in Section 6.2.7, however, the change to increased BSW conditions on the three bogs was likely to have been asynchronous. It is likely that regional environmental forcing mechanisms were responsible for the exact timing of the end of the HTM, marked by the wetting phase around BE4 (Davis *et al.*, 2003; Moros *et al.*, 2004). When compared to centennial-scale episodes of increased drift ice (blue bars in Figure 6.8), it becomes apparent that a climatic regime shift occurred after BE4. Prior to BE4, the two Scottish bogs did not show changes in BSW during centennial-scale period of increased ice rafting. However, after BE4, both bogs show wetting phases in line with smaller-scale variations in the amount of drift ice. This change in BSW response to changes in the North Atlantic, strongly suggests that modern climatic conditions had set in and that a more maritime climate controlled BSW. The slight temporal offset between ice rafting events and changes in BSW is possibly the result of the errors attached to the individual chronologies (Section 5.2.2) and the stacked nature of the drift ice record (Bond *et al.*, 2001). The patterns of atmospheric moisture availability and BSW changes between *c*. 5600 BP and *c*. 5300 BP are discussed in more detail in Section 6.2.7.

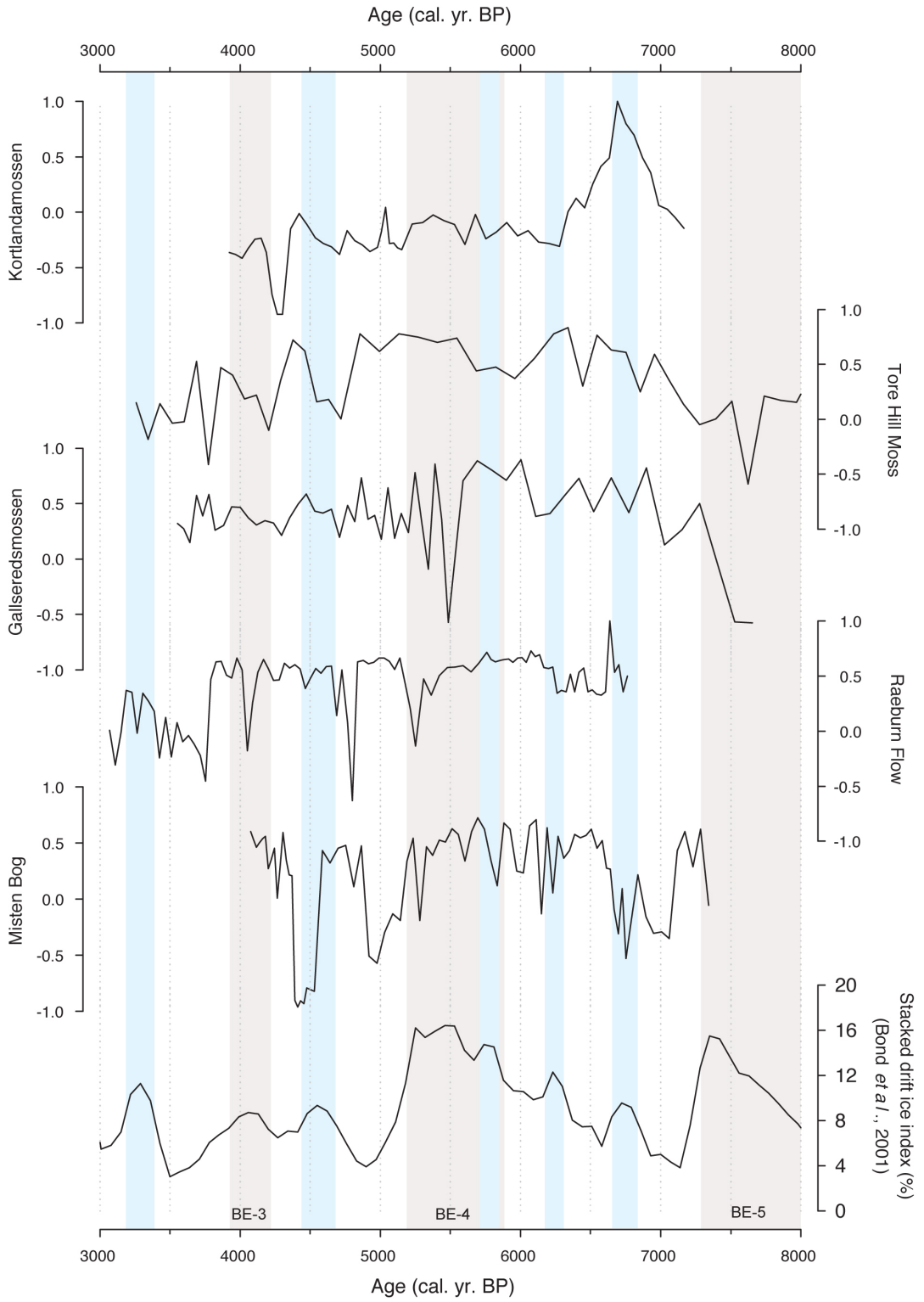

Figure 6.8 - Stack of BSW reconstruction from the peat bogs of this study and record of North Atlantic drift ice (Source: Bond *et al.*, 2001). Grey bands indicate Bond Events (BE) and blue bands highlight centennial increases in ice rafting.

Evidence from Misten Bog shows that changes in North Atlantic SST had a strong influence on local BSW conditions. Throughout the mid-Holocene record, both millennial- and centennial-scale changes in North Atlantic drift ice correspond to wet shifts in Misten Bog (Figure 6.8). However, it is possible that BSW changes and SST anomalies were independently driven by a common mechanism. Nonetheless, given the influence of SST and the thermohaline circulation on moisture transport to Europe, it is probable that changes in North Atlantic SST were the drivers for variation in BSW on Misten Bog.

As shown in Figure 6.8, all bogs show a distinct wet phase, within the error margins of the dating framework (Section 5.2.2) between *c*. 4400 BP and *c*. 4000 BP. This period coincides with the timing of Bond Event BE3 and it is likely that low North Atlantic SST were responsible for driving BSW change across Europe. BE3, however, is characterised by less ice rafting than compared with other mid-Holocene Bond Events, which did not trigger Europe-wide BSW changes (see above). It is therefore probable that other large-scale environmental and climatic forcing mechanisms were driving BSW across northwest Europe during the time. The manifestation of the synchronous increase in BSW across the bogs from this study during BE3 is discussed in greater detail in Section 6.2.8.

6.4 Conclusion

By comparing results from the BSW reconstructions with the wider literature, patterns of mid-Holocene climate change become apparent. All sites show a prolonged period of relatively stable and dry conditions during the mid-Holocene in

line with the Holocene Thermal Maximum. The transition to modern climatic conditions was not synchronous across all sites with the transition happening around the timing of the '5.3k' event at the three more southerly bogs and slightly later at Tore Hill Moss and Kortlandamossen. A clear climatic division exists at 57ºN (Magny *et al.*, 2003b) between *c*. 5600 BP and *c*. 5300 BP (Section 6.2.6). With the exception of Kortlandamossen, the timing for a mid-Holocene climatic transition can be placed between *c*. 5600 BP and *c*. 4800 BP.

Comparisons with episodes of increased North Atlantic ice rafting revealed that northwest European peat bogs generally show wetting trends during major periods of lower SST. Bond events BE3, BE4, and BE5 can be detected in the BSW reconstructions from the five peat bogs. Response to minor centennial-scale SST anomalies, however, is restricted to the three southern sites (Misten Bog, Raeburn Flow and Gällseredsmossen). Thus there exists a strong link between North Atlantic SST and northwest European BSW that is more pronounced after the mid-Holocene transition (Barber *et al.*, 1994; Langdon *et al.*, 2003).

7 Conclusions and future research

The main aim of this thesis was to reconstruct mid-Holocene patterns of changing BSW in a series of peat bogs and thereby to reconstruct changes in atmospheric moisture availability across northwest Europe. To address this aim, a series of research questions were raised in Chapter 1 and discussed throughout this thesis. BSW reconstructions from five bogs have demonstrated sensitivity to climate change and a direct link to large-scale environmental forcing factors. Comparisons of these reconstructions to other sources of palaeoclimatic proxy information have shown that atmospheric moisture availability across northwest Europe largely co-varies with fluctuations in sea surface temperatures and the position of Atlantic Westerly storms. Evidence from this thesis suggest that the degree to which atmospheric moisture availability is controlled by North Atlantic SST is latitude-dependent, with Misten Bog showing the greatest link between BSW and SST. BSW on Misten Bog was closely linked to North Atlantic SST throughout the Holocene, whereas Scottish sites only display such a relationship after the '5.3k' cold event.

Evidence from the BSW reconstructions in this thesis suggest that the BSW record is strongly linked to millennial-scale events of increased ice rafting (Section 6.3 - Research Question Q1). As hypothesised by Magny *et al.* (2003b), there existed a mid-European wet zone during periods of increased ice rafting in the North Atlantic. During the '5.3k' event, the northern extent of this zone was located at approximately 57ºN (Section 6.2.7). Based on the palaeoclimatic reconstruction from this thesis, Magny *et al.*'s original estimate of 58ºN could, therefore, be improved upon (Research Question Q2). More research is required to precisely

define the northern extent of the mid-European wet zone during SST anomalies of different magnitudes.

A Holocene thermal maximum that manifested itself as dry and relatively stable bog surface conditions (Research Question Q4) existed across northwest Europe. Similar to findings from Arctic Canada (Kaufman *et al.*, 2004) and Sweden (Seppä and Birks, 2001), show that the HTM did not occur synchronously and the exact timing of its onset and demise was controlled by regional and local environmental features, such as prevailing blocking anti-cyclonic system across Scandinavia. Four of the five bogs, with the exception of Kortlandamossen, showed a transition to wetter climatic conditions between *c*. 5300 BP and *c*. 4800 BP, marking the end of the HTM. This mid-Holocene transition to wetter / cooler conditions, or Hypsithermal-Neoglaciation transition, characterises a switch to modern climatic conditions, which see the length and severity of the summer water deficit being closely linked to changes in North Atlantic SST (Research Question Q3).

During the '4.2k' event, from *c*. 4400 BP until *c*. 4000 BP, all five peat bogs showed increases in BSW. The phase corresponds to Bond Event 3, within dating errors, and shows a period when northwest European bogs synchronously respond to changes in North Atlantic SST. The large geographical extent of proxy evidence for the '4.2k' event suggests that a bigger underlying climate driver might be responsible for climate change during the period. These climate drivers may have been amplified through a drop in SST.

All plant macrofossil-based reconstructions of BSW changes are based on an improved Hydroclimatic Index that was constructed for the purpose of this thesis. As

previously sensitive information about community assemblage and the indicative power of individual species was lost, a new dimension has been added. The new index takes the eurytopic or indicative nature of plant species into account when reconstructing BSW. However, further work is still needed to make the Hydroclimatic index even more robust (Section 7.1). As no adequate testate amoebae training set existed for Sweden, surface samples from ten raised bogs were used to create a transfer function for water table depth for south-central Sweden (Section 4.3).

7.1 Future research

With every new discovery in science a new world of possible research avenues opens up, as is the case with this research project. Given the time and financial constraints, however, there are a number of interesting research questions that could not be pursued, but which would make excellent ideas for future research projects.

The inclusion of tephrochronology would help to further constrain existing chronologies and to link the study sites at a fixed point in time (Langdon and Barber, 2004). With the recent discovery of far-travelled tephra from the Aleutian Isles in a peat core in Newfoundland (Pyne-O'Donnell *et al.*, 2012), finding far-travelled tephras from Alaska or Korea in European cores would enable cross-Atlantic or pan-hemispheric comparisons of past climate change. It would also provide a better basis for answering the question whether the origins of known climate events were atmospheric, oceanic, solar, orbital or a combination of the four.

All peat cores were analysed at the temporal resolution necessary to address the research questions outlined in Chapter 1. However, extending the analysis up to present and improving the temporal resolution to contiguous 1 cm slices, coupled with improvements to the chronology (e.g. tephra, additional ^{14}C dates) would enable more detailed research into new areas, such as time-series analysis of sub-millennial cyclicities. Finer resolution work would allow a stronger comparison with North Atlantic sea surface temperatures, shorter frequency oscillations, such as the Atlantic Multi-decadal Oscillation, and centennial-scale climate cycle (e.g. Chapman and Shackleton, 2000).

The accuracy of univariate indices of palaeohydrological information created from the complex and multi-dimensional palaeoecological data was limited by the predictive power of the statistical methods employed. Creating regional testate amoebae-based transfer functions for Scotland and the Belgian Ardennes would help to create more accurate palaeohydrological reconstructions. Furthermore, testing for spatial autocorrelation would help to improve the predictive power of the testate amoebae-based transfer functions. Sensitive ecological community assemblage information currently does not form part of testate-amoebae based transfer functions or the Hydroclimatic Index. The inclusion of species assemblage data in model constructions would allow for more eurytopic species to provide useful information about past hydrological conditions. Information about species with bi-modal distributions along the hydrological gradient could also be used more accurately.

As always, if time and money were not a constraint, reconstructions of triplicate cores from paired sites would address possible concerns about how representative a single core is of climatic change (Swindles *et al.*, 2012a). Furthermore, to constrain a

northern climatic division even further and to fully explore a time-transgressive nature of the HTM, the number of BSW reconstructions from new sites should be increased. However, the chosen number of sites was deemed sufficient in order to address the research questions posed in Chapter 1.

The purpose of this thesis, in addition to addressing its aims and answering its research questions, is to stimulate further palaeoenvironmental and palaeoecological research. It is important not to fall victim to ones discoveries and believe that all is known about the mid-Holocene European climate system. Further research over the coming years into the many different areas of palaeoclimatology will always be needed to fully understand the complexity of the environmental mechanisms governing European climate.

Appendix A – Raw data

1. Misten Bog

Plant macrofossils

Depth	400	404	408	412	416	420	424	428	432
UOM	14	3	13	8	5	1	2	8	16
Ericacae rootlets	21	11	19	21	9	4	5	26	30
Ericacae wood	0	0	0	0	1	0	0	2	0
Calluna vulgaris stems	9	3	0	0	0	0	2	1	4
Calluna vulgaris leaves	0	0	0	0	0	0	0	0	0
Calluna vulgaris seeds	0	0	0	0	0	0	0	1	0
Erica tetralix leaves	0	0	0	0	0	0	0	0	0
Vaccinium oxycoccus roots	0	0	0	0	0	0	0	0	2
Monocotyledon (unidentified)	2	0	0	0	0	0	0	0	0
Monocotyledon roots	0	0	0	0	0	0	0	0	0
Eriophorum spp. roots	11	1	2	0	1	0	0	15	7
Eriophorum vaginatum epidermis	8	4	1	0	0	0	0	2	0
Eriophorum angustifolium epidermis	0	0	0	0	0	0	0	0	0
Narthesium osifragum leaf	0	0	0	0	0	0	0	1	0
Trichophorum cespitosum leaf	5	0	0	0	0	0	0	0	0
Carex spp. epidermis	0	0	0	0	0	0	0	0	0
Brown mosses (undiff.)	0	0	3	11	11	7	7	12	1
Hypnum jutlandicum	0	0	0	0	0	0	0	0	0
Dicranum scoparium	0	0	0	0	0	0	0	0	0
Aulacomnium palustre	0	0	0	0	0	0	0	0	0
Total *Sphagnum* spp.	31	77	63	59	74	88	83	33	40
Sphagnum section *Acutifolia*	0	16	7	8	10	31	30	3	0
Sphagnum magellanicum	0	0	0	0	0	0	0	0	0
Sphagnum austinii	31	60	56	51	64	57	53	30	40
Sphagnum pulchrum	0	0	0	0	0	0	0	0	0
Sphagnum balticum	0	1	0	0	0	0	0	0	0
Sphagnum cuspidatum	0	0	0	0	0	0	0	0	0
Charred remains	0	0	0	0	0	0	0	0	0
Acarid mites	0	0	0	0	0	0	0	0	0
Cennococcum spp.	1	0	0	2	1	0	0	0	0
Eriophorum spindles	0	0	0	0	0	0	0	0	0

Depth	436	440	444	448	452	456	460	464	468
UOM	8	14	16	21	17	8	5	10	7
Ericacae rootlets	28	27	43	28	44	6	0	1	0
Ericacae wood	1	0	4	2	2	0	0	0	0
Calluna vulgaris stems	1	3	0	0	2	0	0	0	0
Calluna vulgaris leaves	0	0	0	0	0	0	0	0	0
Calluna vulgaris seeds	0	0	0	0	0	0	0	0	0
Erica tetralix leaves	0	0	0	0	0	0	0	0	0
Vaccinium oxycoccus roots	0	2	7	4	0	0	0	0	0
Monocotyledon (unidentified)	0	0	1	0	0	0	0	0	0
Monocotyledon roots	0	0	0	0	0	1	0	2	0
Eriophorum spp. roots	6	10	11	7	5	1	2	0	1
Eriophorum vaginatum epidermis	0	1	0	1	2	1	1	0	2

Eriophorum angustifolium epidermis	0	0	0	0	0	0	0	0	0
Narthesium osifragum leaf	1	0	3	0	0	0	0	2	0
Trichophorum cespitosum leaf	0	0	0	0	17	0	0	0	0
Carex spp. epidermis	0	0	0	0	0	0	0	0	0
Brown mosses (undiff.)	40	17	5	0	0	0	0	0	0
Hypnum jutlandicum	0	0	0	0	0	0	0	0	0
Dicranum scoparium	0	0	0	0	0	0	0	0	0
Aulacomnium palustre	0	0	0	0	0	0	0	0	0
Total *Sphagnum* spp.	11	25	10	37	11	83	92	86	90
Sphagnum section *Acutifolia*	5	1	0	32	6	0	0	0	0
Sphagnum magellanicum	0	0	0	0	0	0	0	0	0
Sphagnum austinii	6	25	10	4	6	15	0	6	0
Sphagnum pulchrum	0	0	0	0	0	2	5	11	4
Sphagnum balticum	0	0	0	0	0	16	38	2	8
Sphagnum cuspidatum	0	0	0	0	0	51	49	66	78
Charred remains	0	0	0	0	0	0	0	0	0
Acarid mites	0	0	0	0	0	2	3	1	6
Cennococcum spp.	3	0	0	0	0	0	0	0	0
Eriophorum spindles	0	0	0	0	0	0	0	0	0
Depth	**472**	**476**	**480**	**484**	**488**	**492**	**496**	**500**	**504**
UOM	7	2	12	6	7	23	1	7	8
Ericacae rootlets	10	4	14	23	31	37	8	24	13
Ericacae wood	1	0	3	4	3	4	0	4	1
Calluna vulgaris stems	0	0	0	1	0	0	0	1	4
Calluna vulgaris leaves	0	0	0	0	0	0	0	0	2
Calluna vulgaris seeds	0	0	0	0	0	0	0	0	0
Erica tetralix leaves	0	0	0	0	0	0	0	0	0
Vaccinium oxycoccus roots	0	0	0	0	0	0	1	1	3
Monocotyledon (unidentified)	0	0	5	0	0	0	0	0	0
Monocotyledon roots	0	0	0	0	0	0	0	0	0
Eriophorum spp. roots	6	1	9	14	11	7	7	4	2
Eriophorum vaginatum epidermis	12	3	41	4	8	14	0	0	2
Eriophorum angustifolium epidermis	0	0	0	0	0	0	0	0	0
Narthesium osifragum leaf	0	0	2	0	0	1	0	0	0
Trichophorum cespitosum leaf	0	0	1	0	19	0	0	0	0
Carex spp. epidermis	0	0	0	0	0	0	0	0	0
Brown mosses (undiff.)	0	0	0	2	0	9	3	38	0
Hypnum jutlandicum	0	0	0	0	0	0	0	0	0
Dicranum scoparium	0	0	0	0	0	0	0	0	0
Aulacomnium palustre	0	0	0	0	0	0	0	0	0
Total *Sphagnum* spp.	63	88	13	47	21	5	79	21	68
Sphagnum section *Acutifolia*	0	0	5	47	21	3	65	21	29
Sphagnum magellanicum	0	0	0	0	0	0	0	0	0
Sphagnum austinii	10	1	8	0	0	1	14	3	0
Sphagnum pulchrum	2	9	0	0	0	1	0	0	11
Sphagnum balticum	2	8	0	0	0	0	0	0	13
Sphagnum cuspidatum	49	70	0	0	0	0	0	0	14
Charred remains	0	0	0	0	0	0	0	0	0
Acarid mites	1	2	0	0	0	0	0	0	1
Cennococcum spp.	0	0	0	0	0	0	0	0	0
Eriophorum spindles	0	0	0	0	0	0	0	0	0
Depth	**508**	**512**	**516**	**520**	**524**	**528**	**532**	**536**	**540**
UOM	27	12	44	4	10	12	10	6	13
Ericacae rootlets	8	15	4	5	32	16	14	25	32
Ericacae wood	1	0	0	0	2	2	3	0	0
Calluna vulgaris stems	0	5	2	0	0	0	0	0	0
Calluna vulgaris leaves	0	1	0	0	0	0	0	0	0
Calluna vulgaris seeds	0	0	0	0	0	0	0	0	0
Erica tetralix leaves	0	0	0	0	0	0	0	0	0
Vaccinium oxycoccus roots	0	2	0	0	0	1	1	0	0
Monocotyledon (unidentified)	1	0	0	0	0	1	1	0	0
Monocotyledon roots	0	0	0	0	0	0	0	0	0

Eriophorum spp. roots	3	4	7	6	6	17	13	1	14
Eriophorum vaginatum epidermis	3	19	29	41	11	8	0	7	20
Eriophorum angustifolium epidermis	0	0	0	0	0	0	0	0	0
Narthesium osifragum leaf	3	0	0	0	0	0	0	0	0
Trichophorum cespitosum leaf	0	0	0	0	0	0	0	0	0
Carex spp. epidermis	0	0	0	0	0	0	0	0	0
Brown mosses (undiff.)	0	0	0	1	11	42	2	5	1
Hypnum jutlandicum	0	0	0	0	0	0	0	0	0
Dicranum scoparium	0	0	0	0	0	0	0	0	0
Aulacomnium palustre	0	0	0	0	0	0	0	0	0
Total *Sphagnum* spp.	54	41	54	43	28	1	56	54	19
Sphagnum section *Acutifolia*	11	13	44	21	26	0	56	51	17
Sphagnum magellanicum	0	0	0	0	0	0	0	0	0
Sphagnum austinii	0	4	0	3	1	1	0	3	2
Sphagnum pulchrum	25	20	7	19	1	0	0	0	0
Sphagnum balticum	18	3	3	0	0	0	0	0	0
Sphagnum cuspidatum	0	1	0	0	0	0	0	0	0
Charred remains	0	0	0	0	0	0	0	0	0
Acarid mites	3	1	0	0	0	0	0	0	0
Cennococcum spp.	0	0	0	0	0	0	0	0	0
Eriophorum spindles	0	0	0	0	0	0	0	0	0
Depth	**544**	**548**	**552**	**556**	**560**	**564**	**568**	**572**	**576**
UOM	15	4	11	6	3	2	23	6	8
Ericacae rootlets	16	7	14	15	7	8	22	23	8
Ericacae wood	0	0	0	5	0	0	2	4	3
Calluna vulgaris stems	1	0	0	0	0	2	0	0	0
Calluna vulgaris leaves	0	0	0	0	0	0	0	0	0
Calluna vulgaris seeds	0	0	0	0	1	0	0	0	0
Erica tetralix leaves	0	0	0	0	0	0	0	0	0
Vaccinium oxycoccus roots	0	0	0	0	0	0	0	0	0
Monocotyledon (unidentified)	0	2	0	1	0	0	0	2	0
Monocotyledon roots	0	0	0	0	0	0	0	0	0
Eriophorum spp. roots	21	19	8	0	0	1	1	0	4
Eriophorum vaginatum epidermis	38	41	16	0	3	0	0	0	2
Eriophorum angustifolium epidermis	1	0	0	0	0	0	0	0	0
Narthesium osifragum leaf	0	0	0	0	0	0	0	0	0
Trichophorum cespitosum leaf	0	0	0	0	0	0	0	0	0
Carex spp. epidermis	0	0	0	0	0	0	0	0	0
Brown mosses (undiff.)	2	0	7	12	14	7	43	15	12
Hypnum jutlandicum	0	0	0	0	0	0	0	0	0
Dicranum scoparium	0	0	0	0	0	0	0	0	0
Aulacomnium palustre	0	0	0	0	0	0	0	0	0
Total *Sphagnum* spp.	8	26	44	60	72	80	7	49	63
Sphagnum section *Acutifolia*	6	25	44	59	62	80	7	48	61
Sphagnum magellanicum	1	0	0	1	1	0	0	0	0
Sphagnum austinii	1	1	0	0	9	0	0	1	1
Sphagnum pulchrum	0	0	0	0	0	0	0	0	0
Sphagnum balticum	0	0	0	0	0	0	0	0	1
Sphagnum cuspidatum	0	0	0	0	0	0	0	0	0
Charred remains	0	0	0	0	0	0	0	0	0
Acarid mites	0	0	0	0	0	0	0	0	0
Cennococcum spp.	2	0	0	0	0	0	0	0	0
Eriophorum spindles	0	0	0	0	0	0	0	0	0
Depth	**580**	**584**	**588**	**592**	**596**	**600**	**604**	**608**	**612**
UOM	2	9	11	2	1	2	16	2	15
Ericacae rootlets	5	12	10	4	10	7	22	2	33
Ericacae wood	1	3	2	1	1	0	3	0	2
Calluna vulgaris stems	1	0	0	0	0	0	0	0	0
Calluna vulgaris leaves	0	0	0	0	0	0	0	0	0
Calluna vulgaris seeds	0	0	0	1	0	1	0	0	0
Erica tetralix leaves	0	0	0	0	0	0	0	0	0
Vaccinium oxycoccus roots	0	0	0	0	0	0	0	0	0

Monocotyledon (unidentified)	0	1	1	2	0	0	1	0	0
Monocotyledon roots	0	0	0	0	0	0	0	0	0
Eriophorum spp. roots	11	3	5	3	0	1	21	6	10
Eriophorum vaginatum epidermis	0	0	0	0	0	0	19	0	2
Eriophorum angustifolium epidermis	0	0	0	0	0	0	0	0	0
Narthesium osifragum leaf	0	0	0	0	0	0	0	0	0
Trichophorum cespitosum leaf	0	0	0	0	0	0	0	0	0
Carex spp. epidermis	0	0	0	0	0	0	0	0	0
Brown mosses (undiff.)	14	4	28	28	3	5	3	5	1
Hypnum jutlandicum	0	0	0	0	0	0	0	0	0
Dicranum scoparium	0	0	0	0	0	0	0	0	0
Aulacomnium palustre	0	0	0	0	0	0	0	0	0
Total *Sphagnum* spp.	65	68	42	59	85	85	15	84	37
Sphagnum section *Acutifolia*	64	67	41	26	85	85	13	80	36
Sphagnum magellanicum	0	0	0	0	0	0	0	0	0
Sphagnum austinii	0	1	1	1	0	0	2	0	1
Sphagnum pulchrum	0	0	0	0	0	0	0	0	0
Sphagnum balticum	1	0	0	1	0	0	0	0	0
Sphagnum cuspidatum	0	0	0	0	0	0	0	0	0
Charred remains	0	0	0	0	0	0	0	0	0
Acarid mites	1	0	0	0	0	0	0	0	0
Cennococcum spp.	0	0	1	0	0	0	0	0	0
Eriophorum spindles	0	0	0	0	0	0	0	0	0
Depth	**616**	**620**	**624**	**628**	**632**	**636**	**640**	**644**	**648**
UOM	2	3	11	28	28	6	9	4	6
Ericacae rootlets	9	7	8	8	26	4	10	7	8
Ericacae wood	2	3	2	1	2	1	1	1	4
Calluna vulgaris stems	0	0	0	0	0	0	0	0	0
Calluna vulgaris leaves	0	0	0	0	0	0	0	0	0
Calluna vulgaris seeds	0	0	0	1	1	1	0	0	0
Erica tetralix leaves	0	0	0	0	2	0	0	0	0
Vaccinium oxycoccus roots	0	0	0	0	0	0	0	0	0
Monocotyledon (unidentified)	0	0	1	3	1	0	1	0	0
Monocotyledon roots	0	0	0	0	0	0	0	0	0
Eriophorum spp. roots	8	18	14	3	4	5	0	3	13
Eriophorum vaginatum epidermis	35	3	1	5	2	0	2	0	5
Eriophorum angustifolium epidermis	0	0	0	0	0	0	0	0	0
Narthesium osifragum leaf	0	0	0	0	0	0	0	0	0
Trichophorum cespitosum leaf	0	0	0	0	0	0	0	0	0
Carex spp. epidermis	0	0	0	0	0	0	0	0	0
Brown mosses (undiff.)	0	2	0	0	12	5	7	14	1
Hypnum jutlandicum	0	0	0	0	0	0	0	0	0
Dicranum scoparium	0	0	0	0	0	0	0	0	0
Aulacomnium palustre	0	0	0	0	0	0	0	0	0
Total *Sphagnum* spp.	44	64	62	51	24	79	70	72	62
Sphagnum section *Acutifolia*	44	64	53	43	23	79	65	72	59
Sphagnum magellanicum	0	0	0	0	0	0	0	0	0
Sphagnum austinii	0	0	9	8	1	0	0	0	3
Sphagnum pulchrum	0	0	0	0	0	0	0	0	0
Sphagnum balticum	0	0	0	0	0	0	0	0	0
Sphagnum cuspidatum	0	0	0	0	0	0	0	0	0
Charred remains	1	0	0	0	0	0	0	1	0
Acarid mites	0	0	0	0	0	0	0	0	0
Cennococcum spp.	0	0	2	0	1	0	1	0	0
Eriophorum spindles	0	0	0	0	0	0	0	0	0
Depth	**652**	**656**	**660**	**664**	**668**	**672**	**676**	**680**	**684**
UOM	7	6	15	5	24	2	10	11	21
Ericacae rootlets	8	10	4	8	15	5	7	38	16
Ericacae wood	3	2	1	0	3	1	1	1	3
Calluna vulgaris stems	0	0	0	0	0	0	0	0	0
Calluna vulgaris leaves	0	0	0	0	0	0	0	0	0
Calluna vulgaris seeds	0	0	0	0	0	0	0	0	0

Erica tetralix leaves	0	0	0	0	0	0	0	0	0
Vaccinium oxycoccus roots	0	0	0	0	0	0	0	0	0
Monocotyledon (unidentified)	0	0	1	0	0	0	4	4	3
Monocotyledon roots	0	0	0	0	0	0	0	0	0
Eriophorum spp. roots	8	12	26	7	8	4	2	6	12
Eriophorum vaginatum epidermis	6	8	8	9	7	6	0	2	15
Eriophorum angustifolium epidermis	0	0	1	0	0	0	0	0	0
Narthesium osifragum leaf	0	0	0	0	0	0	0	0	0
Trichophorum cespitosum leaf	0	0	0	0	0	0	0	0	0
Carex spp. epidermis	0	0	0	0	0	0	0	0	0
Brown mosses (undiff.)	27	12	3	6	6	8	7	2	0
Hypnum jutlandicum	0	0	0	0	0	0	0	0	0
Dicranum scoparium	0	0	0	0	0	0	0	0	0
Aulacomnium palustre	0	0	0	0	0	0	0	0	0
Total *Sphagnum* spp.	41	50	42	64	38	74	70	36	30
Sphagnum section *Acutifolia*	41	1	1	2	0	0	0	2	1
Sphagnum magellanicum	0	48	41	62	38	66	70	34	29
Sphagnum austinii	0	1	0	0	0	0	0	0	0
Sphagnum pulchrum	0	0	0	0	0	0	0	0	0
Sphagnum balticum	0	0	0	0	0	0	0	0	0
Sphagnum cuspidatum	0	0	0	0	0	0	0	0	0
Charred remains	0	0	0	0	0	0	0	0	0
Acarid mites	1	0	0	0	0	0	0	0	0
Cennococcum spp.	0	0	0	0	0	1	0	0	0
Eriophorum spindles	0	0	0	0	0	0	0	0	0
Depth	**688**	**692**	**696**	**700**	**704**	**708**	**712**	**716**	**720**
UOM	46	40	21	28	36	33	36	19	24
Ericacae rootlets	15	15	24	9	19	13	19	11	28
Ericacae wood	2	0	0	0	0	0	1	0	0
Calluna vulgaris stems	0	0	0	0	0	0	0	0	0
Calluna vulgaris leaves	0	0	0	0	0	0	0	0	0
Calluna vulgaris seeds	0	0	0	0	0	0	0	0	0
Erica tetralix leaves	0	0	0	0	0	0	0	0	0
Vaccinium oxycoccus roots	0	0	0	0	0	0	0	0	0
Monocotyledon (unidentified)	4	5	2	3	6	3	4	4	23
Monocotyledon roots	0	0	0	0	0	0	0	0	0
Eriophorum spp. roots	7	12	10	5	12	14	13	15	8
Eriophorum vaginatum epidermis	12	20	20	11	19	32	9	13	7
Eriophorum angustifolium epidermis	0	0	1	0	0	0	0	0	0
Narthesium osifragum leaf	0	0	0	0	0	0	0	0	0
Trichophorum cespitosum leaf	0	0	0	0	0	0	0	0	0
Carex spp. epidermis	0	0	0	0	0	0	0	0	0
Brown mosses (undiff.)	6	2	2	2	0	1	3	3	3
Hypnum jutlandicum	0	0	0	0	0	0	0	0	0
Dicranum scoparium	0	0	0	0	0	0	0	0	0
Aulacomnium palustre	0	0	0	0	0	0	0	0	0
Total *Sphagnum* spp.	8	6	19	42	6	4	14	33	5
Sphagnum section *Acutifolia*	0	0	0	0	0	0	5	21	0
Sphagnum magellanicum	8	6	17	41	5	1	9	0	0
Sphagnum austinii	0	0	2	0	1	3	0	12	0
Sphagnum pulchrum	0	0	0	1	0	0	0	0	0
Sphagnum balticum	0	0	0	0	0	0	0	0	0
Sphagnum cuspidatum	0	0	0	0	0	0	0	0	0
Charred remains	0	0	0	0	0	0	0	0	0
Acarid mites	0	0	0	0	0	0	0	0	0
Cennococcum spp.	0	0	0	0	1	0	0	0	1
Eriophorum spindles	0	0	0	0	0	0	0	0	0

Testate amoebae

Depth	400	404	408	412	416	420	424	428	432	436	440
Amphitrema flavum	17	7	2	6	2	33	24	10	56	33	6
Amphitrema stenastoma	0	0	0	0	0	0	0	0	0	0	0
Amphitrema wrightianum	0	1	0	1	0	0	0	1	0	0	0
Arcella artocrea	0	0	0	0	0	1	0	1	0	0	0
Arcella catinus type	0	0	0	0	0	0	0	0	0	0	0
*Arcella discoide*s type	0	0	0	1	2	0	0	0	0	0	0
Arcella gibbosa type	0	0	0	0	0	0	0	0	0	0	0
Arcella hemispherica	0	0	0	0	0	0	0	0	0	0	0
Arcella vulgaris type	0	0	0	0	0	0	0	0	0	0	0
Assulina muscorum	11	9	17	4	6	6	6	10	4	11	4
Assulina seminulum	6	6	12	0	0	1	2	9	0	8	2
Bullinularia indica	0	1	0	0	0	0	0	0	0	0	0
Centropyxis aculeata type	0	0	0	0	0	0	0	0	0	0	0
Centropyxis cassis type	0	0	0	0	0	0	0	0	0	0	0
Centropyxis platystoma type	0	0	0	0	0	0	0	0	0	0	0
Corythion/Trinema type	0	0	0	0	0	0	0	0	0	0	0
Cryptodifflugia oviformis	0	0	0	0	0	0	0	0	0	0	0
Cyclopyxis arcelloides type	3	9	8	10	2	4	2	13	0	5	5
Difflugia globulosa type	0	0	0	0	0	0	0	0	0	0	0
Difflugia lucida type	0	0	0	0	0	0	0	0	0	0	0
Difflugia oblonga type	0	0	6	0	2	0	0	0	0	0	0
Difflugia pristis type	7	4	2	3	6	1	2	6	2	2	2
Difflugia pulex	51	58	49	70	76	50	50	48	35	40	80
Difflugia rubescens	0	0	0	0	0	1	0	0	0	0	0
Euglypha rotunda type	0	0	0	0	0	0	0	0	0	0	0
Euglypha stringosa type	0	0	0	0	0	0	0	0	0	0	0
Euglypha tuberculata type	0	0	0	0	0	0	0	0	0	0	0
Heleopera petricola	0	0	0	0	0	0	0	0	0	0	0
Heleopera rosea	0	0	0	0	0	0	0	0	0	0	0
Heleopera sphagni	0	0	0	0	0	0	0	0	0	0	0
Heleopera sylvatica	2	1	1	0	0	0	0	0	2	0	0
Hyalosphenia elegans	0	0	0	0	0	0	0	0	0	0	0
Hyalosphenia minuta type	0	0	0	0	0	0	0	0	0	0	0
Hyalosphenia ovalis type	0	0	0	0	0	0	0	0	0	0	0
Hyalosphenia papilio	0	0	0	0	0	1	1	0	0	0	0
Hyalosphenia subflava	0	0	0	0	0	0	0	0	0	0	0
Nebela collaris type	1	0	0	0	0	1	0	0	0	0	2
Nebela flaballulum	0	0	0	0	0	0	0	0	0	0	0
Nebela militaris type	0	0	1	2	3	2	12	0	0	0	0
Nebela minor type	0	0	0	0	0	0	0	0	0	0	0
Nebela parvula	0	0	0	0	0	0	0	0	0	0	0
Nebela tincta	0	0	0	0	0	0	0	0	0	0	0
Nebela vitraea type	0	0	0	0	0	0	0	0	0	0	0
Nebela wailesi type	0	0	0	0	0	0	0	0	0	0	0
Phryganella acropodia type	0	0	0	0	0	0	0	0	0	0	0
Placocista spinosa type	0	0	0	0	0	0	0	0	0	0	0
Pseudodifflugia fulva type	1	2	2	2	1	1	2	1	1	1	0
Trigonopyxis arcula type	0	2	1	2	0	0	0	2	0	1	0
Trinema lineare type	0	0	0	0	0	0	0	0	0	0	0

Depth	444	448	452	456	460	464	468	472	476	480	484
Amphitrema flavum	30	37	49	73	93	78	83	78	68	25	38
Amphitrema stenastoma	0	0	0	0	0	2	0	0	0	0	0
Amphitrema wrightianum	0	0	0	0	0	0	0	0	0	2	0
Arcella artocrea	0	0	0	0	0	0	0	0	3	0	0
Arcella catinus type	0	0	0	0	0	0	0	0	0	0	0
*Arcella discoide*s type	0	0	0	0	0	0	0	0	0	0	1

Arcella gibbosa type	0	0	0	0	0	0	0	0	0	0	0
Arcella hemispherica	0	0	0	0	0	0	0	0	0	0	0
Arcella vulgaris type	0	0	0	0	0	0	0	0	0	0	0
Assulina muscorum	6	20	4	5	2	1	9	10	10	8	4
Assulina seminulum	5	4	0	3	0	2	3	4	13	0	2
Bullinularia indica	0	0	0	0	0	0	0	0	0	0	0
Centropyxis aculeata type	0	0	0	0	0	0	0	0	0	0	0
Centropyxis cassis type	0	0	0	0	0	0	0	0	0	0	0
Centropyxis platystoma type	0	0	0	0	0	0	0	0	0	0	0
Corythion/Trinema type	0	0	0	0	0	0	0	0	0	0	0
Cryptodifflugia oviformis	0	0	0	0	0	0	0	0	0	0	0
Cyclopyxis arcelloides type	7	2	2	0	0	1	0	0	2	3	2
Difflugia globulosa type	0	0	0	0	0	0	0	0	0	0	0
Difflugia lucida type	0	0	0	0	0	0	0	0	0	0	0
Difflugia oblonga type	0	0	0	0	0	0	0	0	0	0	0
Difflugia pristis type	2	4	2	4	1	6	2	6	1	0	2
Difflugia pulex	45	33	42	1	1	6	1	2	1	62	50
Difflugia rubescens	1	0	0	0	0	0	0	0	0	0	0
Euglypha rotunda type	0	0	0	0	1	0	0	0	0	0	0
Euglypha stringosa type	0	0	0	0	0	0	0	0	0	0	0
Euglypha tuberculata type	0	0	0	0	0	0	0	0	0	0	0
Heleopera petricola	0	0	0	8	3	2	2	0	1	0	0
Heleopera rosea	0	0	0	0	0	0	0	0	0	0	0
Heleopera sphagni	2	0	0	6	0	2	1	0	0	0	1
Heleopera sylvatica	0	0	0	0	0	0	0	0	0	0	0
Hyalosphenia elegans	0	0	0	0	0	0	0	0	0	0	0
Hyalosphenia minuta type	0	0	0	0	0	0	0	0	0	0	0
Hyalosphenia ovalis type	0	0	0	0	0	0	0	0	0	0	0
Hyalosphenia papilio	0	0	0	0	0	0	0	0	1	0	0
Hyalosphenia subflava	0	0	0	0	0	0	0	0	0	0	0
Nebela collaris type	1	0	0	0	0	0	0	0	0	0	0
Nebela flaballulum	0	0	0	0	0	0	0	0	0	0	0
Nebela militaris type	0	0	0	0	0	0	0	0	0	0	0
Nebela minor type	0	0	0	0	0	0	0	0	0	0	0
Nebela parvula	0	0	0	0	0	0	0	0	0	0	0
Nebela tincta	0	0	0	0	0	0	0	0	0	0	0
Nebela vitraea type	0	0	0	0	0	0	0	0	0	0	0
Nebela wailesi type	0	0	0	0	0	0	0	0	0	0	0
Phryganella acropodia type	0	0	0	0	0	0	0	0	0	0	0
Placocista spinosa type	0	0	0	0	0	0	0	0	0	0	0
Pseudodifflugia fulva type	2	0	1	0	0	0	0	0	0	0	1
Trigonopyxis arcula type	0	0	0	0	0	0	0	0	0	0	0
Trinema lineare type	0	0	0	0	0	0	0	0	0	0	0
Depth	**488**	**492**	**496**	**500**	**504**	**508**	**512**	**516**	**520**	**524**	**528**
Amphitrema flavum	25	16	52	7	59	73	63	70	69	19	14
Amphitrema stenastoma	0	0	0	0	2	0	0	0	0	0	0
Amphitrema wrightianum	0	0	0	0	0	0	0	0	0	0	0
Arcella artocrea	0	1	0	0	0	0	0	0	0	0	0
Arcella catinus type	0	0	0	0	0	0	0	0	0	0	0
Arcella discoides type	0	2	0	0	4	1	4	1	0	3	2
Arcella gibbosa type	0	0	0	0	0	0	0	0	0	0	0
Arcella hemispherica	0	0	0	0	0	0	0	0	0	0	0
Arcella vulgaris type	0	0	0	0	0	0	0	0	0	0	0
Assulina muscorum	8	12	2	10	4	7	7	4	4	10	2
Assulina seminulum	0	4	0	19	1	3	8	6	4	11	6
Bullinularia indica	0	1	0	0	0	0	0	0	0	0	0
Centropyxis aculeata type	0	1	0	0	0	0	0	0	0	0	0
Centropyxis cassis type	0	0	0	0	0	0	0	0	0	0	0
Centropyxis platystoma type	0	0	0	0	0	0	0	0	0	0	0
Corythion/Trinema type	0	0	0	0	0	0	0	0	0	0	0
Cryptodifflugia oviformis	0	0	0	0	0	0	0	0	0	0	0
Cyclopyxis arcelloides type	6	6	4	7	3	2	0	2	1	3	4
Difflugia globulosa type	0	0	0	0	0	0	0	0	0	0	0

Difflugia lucida type	0	0	0	0	0	0	0	0	0	0	0
Difflugia oblonga type	0	0	0	0	0	0	0	0	0	2	0
Difflugia pristis type	2	2	10	21	12	5	6	3	4	9	6
Difflugia pulex	58	49	33	31	10	5	10	13	16	42	65
Difflugia rubescens	0	0	0	0	0	0	0	0	0	0	0
Euglypha rotunda type	0	0	0	0	0	0	0	0	0	0	0
Euglypha stringosa type	0	0	0	0	0	0	0	0	0	0	0
Euglypha tuberculata type	0	0	0	0	0	0	0	0	0	0	0
Heleopera petricola	0	0	0	1	0	0	0	0	0	0	0
Heleopera rosea	0	0	0	0	0	0	0	0	0	0	0
Heleopera sphagni	0	0	0	0	2	1	1	0	0	0	0
Heleopera sylvatica	0	4	0	2	1	0	0	0	0	0	0
Hyalosphenia elegans	0	0	0	0	0	0	0	0	0	0	0
Hyalosphenia minuta type	0	0	0	0	0	0	0	0	0	0	0
Hyalosphenia ovalis type	0	0	0	0	0	1	0	0	0	0	0
Hyalosphenia papilio	0	0	0	0	0	1	1	1	0	0	0
Hyalosphenia subflava	0	0	0	0	0	0	0	0	0	0	2
Nebela collaris type	0	0	0	1	0	0	0	1	0	0	0
Nebela flaballulum	0	0	0	0	0	0	0	0	0	0	0
Nebela militaris type	2	0	0	0	0	1	0	0	2	0	0
Nebela minor type	0	0	0	0	0	0	0	0	0	0	0
Nebela parvula	0	0	0	0	0	0	0	0	0	0	0
Nebela tincta	0	0	0	0	0	0	0	0	0	0	0
Nebela vitraea type	0	0	0	0	0	0	0	0	0	0	0
Nebela wailesi type	0	0	0	0	0	0	0	0	0	0	0
Phryganella acropodia type	0	0	0	0	0	0	0	0	0	0	0
Placocista spinosa type	0	0	0	0	0	0	0	0	0	0	0
Pseudodifflugia fulva type	0	0	0	0	1	0	0	1	0	0	0
Trigonopyxis arcula type	0	2	0	2	1	1	0	0	0	2	0
Trinema lineare type	0	0	0	0	0	0	0	0	0	0	0
Depth	**532**	**536**	**540**	**544**	**548**	**552**	**566**	**560**	**564**	**568**	**572**
Amphitrema flavum	80	22	24	10	13	10	12	33	10	0	3
Amphitrema stenastoma	0	0	3	0	0	0	2	2	0	0	0
Amphitrema wrightianum	0	0	1	0	0	0	0	0	0	0	0
Arcella artocrea	0	0	0	0	0	0	1	0	0	0	0
Arcella catinus type	0	0	0	0	1	0	0	0	0	0	0
*Arcella discoide*s type	2	2	1	0	3	0	0	0	0	2	2
Arcella gibbosa type	0	0	0	0	0	0	0	0	0	0	0
Arcella hemispherica	0	0	0	0	0	0	0	0	0	0	0
Arcella vulgaris type	0	0	0	0	0	0	0	0	0	0	0
Assulina muscorum	7	2	7	12	8	1	7	2	4	2	5
Assulina seminulum	2	1	5	4	6	1	2	2	3	2	10
Bullinularia indica	0	0	0	0	1	0	1	1	1	1	2
Centropyxis aculeata type	0	0	0	0	0	0	0	0	0	0	0
Centropyxis cassis type	0	0	0	0	0	0	0	0	0	0	0
Centropyxis platystoma type	0	0	0	0	1	0	1	0	0	0	0
Corythion/Trinema type	0	0	0	0	0	0	0	0	0	0	0
Cryptodifflugia oviformis	0	0	0	0	0	0	0	0	0	0	0
Cyclopyxis arcelloides type	0	1	1	4	5	4	15	8	10	5	10
Difflugia globulosa type	0	0	0	0	0	0	0	0	0	0	0
Difflugia lucida type	0	0	0	0	0	0	0	0	0	0	0
Difflugia oblonga type	0	0	0	0	0	0	0	0	0	0	0
Difflugia pristis type	2	6	2	8	2	3	4	2	8	2	7
Difflugia pulex	7	65	49	57	52	75	45	44	61	86	57
Difflugia rubescens	0	0	0	0	3	1	3	2	1	0	1
Euglypha rotunda type	0	0	0	0	0	0	0	0	0	0	0
Euglypha stringosa type	0	0	0	0	0	0	0	0	0	0	0
Euglypha tuberculata type	0	0	0	0	0	0	0	0	0	0	0
Heleopera petricola	0	0	0	0	0	0	0	0	0	0	0
Heleopera rosea	0	0	0	0	0	0	0	0	0	0	0
Heleopera sphagni	0	0	0	0	0	0	0	0	0	0	0
Heleopera sylvatica	0	0	0	0	1	0	0	0	0	0	0
Hyalosphenia elegans	0	0	0	0	0	0	0	0	0	0	0

Hyalosphenia minuta type	0	0	0	0	0	0	0	0	0	0	0
Hyalosphenia ovalis type	0	0	0	0	0	0	0	0	0	0	0
Hyalosphenia papilio	0	0	0	0	0	0	0	0	1	0	2
Hyalosphenia subflava	0	0	1	2	2	0	0	0	0	0	0
Nebela collaris type	0	2	3	1	2	5	6	0	1	0	1
Nebela flaballulum	0	0	0	0	0	0	0	0	0	0	0
Nebela militaris type	0	0	0	0	0	0	1	5	0	0	0
Nebela minor type	0	0	0	0	0	0	0	0	0	0	0
Nebela parvula	0	0	0	0	0	0	0	0	0	0	0
Nebela tincta	0	0	0	0	0	0	0	0	0	0	0
Nebela vitraea type	0	0	0	0	0	0	0	0	0	0	0
Nebela wailesi type	0	0	0	0	0	0	0	0	0	0	0
Phryganella acropodia type	0	0	0	0	0	0	0	0	0	0	0
Placocista spinosa type	0	0	0	0	0	0	0	0	0	0	0
Pseudodifflugia fulva type	1	0	0	0	0	0	0	0	0	0	0
Trigonopyxis arcula type	0	0	5	2	1	0	0	0	0	1	0
Trinema lineare type	0	0	0	0	0	0	0	0	0	0	0
Depth	**576**	**580**	**584**	**588**	**592**	**596**	**600**	**604**	**608**	**612**	**616**
Amphitrema flavum	29	53	2	8	42	37	2	1	67	4	59
Amphitrema stenastoma	0	0	0	0	0	0	0	0	0	0	0
Amphitrema wrightianum	0	0	0	0	0	0	0	0	0	0	0
Arcella artocrea	0	0	0	0	0	1	1	1	0	0	0
Arcella catinus type	0	0	0	0	0	0	0	0	0	0	0
Arcella discoides type	0	1	0	0	0	0	0	1	1	0	0
Arcella gibbosa type	0	0	0	0	0	1	0	0	0	0	0
Arcella hemispherica	0	0	0	0	0	0	0	0	0	0	0
Arcella vulgaris type	0	0	0	0	0	0	0	0	0	0	0
Assulina muscorum	6	5	8	10	6	14	4	6	4	8	2
Assulina seminulum	6	3	2	2	2	3	4	1	3	6	8
Bullinularia indica	0	0	0	0	0	0	0	1	0	0	0
Centropyxis aculeata type	0	0	0	0	0	0	0	0	0	0	0
Centropyxis cassis type	0	0	0	0	0	0	0	0	0	0	0
Centropyxis platystoma type	0	0	0	0	0	0	0	0	0	1	0
Corythion/Trinema type	0	0	0	0	0	0	0	0	0	0	0
Cryptodifflugia oviformis	0	0	0	0	0	0	0	0	0	0	0
Cyclopyxis arcelloides type	2	4	2	15	1	5	4	8	0	11	2
Difflugia globulosa type	0	0	0	0	0	0	0	1	0	0	0
Difflugia lucida type	0	0	0	0	0	0	0	0	0	0	0
Difflugia oblonga type	0	0	0	0	0	0	0	0	0	0	0
Difflugia pristis type	10	2	2	5	2	3	2	10	5	6	2
Difflugia pulex	47	28	80	52	46	26	76	64	9	56	24
Difflugia rubescens	0	0	0	0	0	0	0	0	0	2	0
Euglypha rotunda type	0	0	0	0	0	0	0	0	0	0	0
Euglypha stringosa type	0	0	0	0	0	0	0	0	0	0	0
Euglypha tuberculata type	0	0	0	0	0	0	0	0	0	0	0
Heleopera petricola	0	0	0	0	0	0	0	0	0	0	0
Heleopera rosea	0	0	0	0	0	0	0	0	0	0	0
Heleopera sphagni	0	0	0	0	0	0	0	0	0	0	0
Heleopera sylvatica	0	0	0	0	0	0	0	0	0	0	0
Hyalosphenia elegans	0	0	0	0	0	0	0	1	0	0	0
Hyalosphenia minuta type	0	0	0	0	0	0	0	0	0	0	0
Hyalosphenia ovalis type	0	0	0	0	0	0	0	0	0	2	0
Hyalosphenia papilio	0	0	0	0	0	2	2	0	11	0	0
Hyalosphenia subflava	0	0	0	0	0	0	0	0	0	0	0
Nebela collaris type	0	3	1	3	1	4	0	1	0	1	0
Nebela flaballulum	0	0	0	0	0	0	0	0	0	0	0
Nebela militaris type	0	0	2	0	1	2	2	2	0	2	2
Nebela minor type	0	0	0	0	0	0	0	0	0	0	0
Nebela parvula	0	0	0	0	0	0	0	0	0	0	0
Nebela tincta	0	1	0	0	0	0	0	0	0	0	0
Nebela vitraea type	0	0	0	0	0	0	0	0	0	0	0
Nebela wailesi type	0	0	0	0	0	0	0	0	0	0	0
Phryganella acropodia type	0	0	0	0	0	0	0	0	0	0	0

Placocista spinosa type	0	0	0	0	0	0	0	0	0	0	0
Pseudodifflugia fulva type	0	0	1	3	0	2	2	0	0	1	1
Trigonopyxis arcula type	0	0	0	3	0	1	1	3	0	1	0
Trinema lineare type	0	0	0	0	0	0	0	0	0	0	0
Depth	**620**	**624**	**628**	**632**	**636**	**640**	**644**	**648**	**652**	**656**	**660**
Amphitrema flavum	16	29	19	12	13	13	4	17	16	9	8
Amphitrema stenastoma	1	0	0	0	0	0	0	0	0	0	0
Amphitrema wrightianum	0	0	0	0	0	0	0	0	0	0	0
Arcella artocrea	0	0	0	0	0	0	1	0	0	0	0
Arcella catinus type	0	0	0	0	0	0	0	0	0	1	0
Arcella discoides type	0	0	0	0	0	0	0	0	1	0	0
Arcella gibbosa type	0	0	0	0	0	0	0	0	0	0	0
Arcella hemispherica	0	0	0	0	0	0	0	0	0	0	0
Arcella vulgaris type	0	0	0	0	0	0	0	0	0	0	0
Assulina muscorum	6	5	11	4	5	1	6	17	4	14	4
Assulina seminulum	7	2	2	2	2	0	1	2	2	3	4
Bullinularia indica	0	0	1	0	0	0	0	0	0	0	0
Centropyxis aculeata type	0	0	0	0	0	0	0	0	0	0	0
Centropyxis cassis type	0	0	0	0	0	0	0	0	0	0	0
Centropyxis platystoma type	0	0	0	0	0	0	0	0	0	0	0
Corythion/Trinema type	0	0	0	0	0	0	0	0	0	0	0
Cryptodifflugia oviformis	0	0	0	0	0	0	0	0	0	0	0
Cyclopyxis arcelloides type	5	1	2	2	3	0	2	0	0	0	0
Difflugia globulosa type	0	0	0	0	0	0	0	0	0	0	0
Difflugia lucida type	0	0	0	0	0	0	0	0	0	0	0
Difflugia oblonga type	0	0	0	0	0	0	1	0	0	0	0
Difflugia pristis type	5	1	6	6	10	6	4	4	4	2	8
Difflugia pulex	52	58	45	67	59	76	70	49	63	70	68
Difflugia rubescens	1	0	2	0	1	0	0	0	0	0	0
Euglypha rotunda type	0	0	0	0	0	0	0	0	0	0	0
Euglypha stringosa type	0	0	0	0	0	0	0	0	0	0	0
Euglypha tuberculata type	0	0	0	0	0	0	0	0	0	0	0
Heleopera petricola	0	0	0	0	0	0	0	0	0	0	0
Heleopera rosea	0	0	0	2	0	0	0	0	0	0	0
Heleopera sphagni	0	0	0	0	0	0	0	1	0	0	0
Heleopera sylvatica	0	0	0	0	0	0	0	0	0	0	0
Hyalosphenia elegans	0	0	0	0	0	0	0	0	0	0	0
Hyalosphenia minuta type	0	0	0	0	0	0	1	0	0	0	0
Hyalosphenia ovalis type	0	0	0	0	3	0	3	0	0	0	0
Hyalosphenia papilio	1	2	4	1	1	4	2	0	0	0	0
Hyalosphenia subflava	0	0	0	0	0	0	0	0	0	0	0
Nebela collaris type	0	0	2	4	2	0	0	4	7	0	2
Nebela flaballulum	0	0	0	0	0	0	0	0	0	0	0
Nebela militaris type	3	0	1	0	0	0	2	7	3	1	2
Nebela minor type	0	0	0	0	0	0	0	0	0	0	0
Nebela parvula	0	0	0	0	0	0	0	0	0	0	0
Nebela tincta	0	0	0	0	0	0	2	0	0	0	0
Nebela vitraea type	0	0	0	0	0	0	0	0	0	0	0
Nebela wailesi type	0	0	0	0	0	0	0	0	0	0	0
Phryganella acropodia type	0	0	0	0	0	0	0	0	0	0	0
Placocista spinosa type	0	0	0	0	0	0	0	0	0	0	0
Pseudodifflugia fulva type	2	1	3	0	1	0	2	0	0	0	2
Trigonopyxis arcula type	1	1	3	0	0	0	0	0	1	0	2
Trinema lineare type	0	0	0	0	0	0	0	0	0	0	0
Depth	**664**	**672**	**676**	**680**	**684**	**688**	**692**	**696**	**700**	**704**	**708**
Amphitrema flavum	4	28	15	70	49	19	68	79	68	50	15
Amphitrema stenastoma	0	0	0	0	1	0	0	0	1	0	0
Amphitrema wrightianum	0	0	0	0	0	0	0	0	0	0	0
Arcella artocrea	0	0	0	0	0	0	1	0	1	0	0
Arcella catinus type	0	0	0	0	0	0	0	0	0	0	0
Arcella discoides type	14	20	2	5	6	0	1	3	3	10	0

Arcella gibbosa type	0	0	0	0	0	0	0	0	0	0	0
Arcella hemispherica	0	0	0	0	0	0	0	0	0	0	0
Arcella vulgaris type	0	0	1	0	0	0	0	0	0	0	0
Assulina muscorum	28	17	7	10	8	10	6	1	4	2	2
Assulina seminulum	9	10	7	3	1	3	0	0	3	0	1
Bullinularia indica	0	0	0	0	0	0	0	0	0	0	0
Centropyxis aculeata type	0	0	0	0	0	0	0	0	0	0	0
Centropyxis cassis type	0	0	0	0	0	0	0	0	0	0	0
Centropyxis platystoma type	0	0	0	0	0	0	0	0	0	0	0
Corythion/Trinema type	0	0	0	0	0	0	0	0	0	0	0
Cryptodifflugia oviformis	0	0	0	0	0	0	0	0	0	0	0
Cyclopyxis arcelloides type	0	0	8	0	2	1	1	0	0	0	1
Difflugia globulosa type	0	0	0	0	0	0	0	0	0	0	0
Difflugia lucida type	0	0	0	0	0	0	0	0	0	0	0
Difflugia oblonga type	2	0	2	0	0	0	0	0	0	0	1
Difflugia pristis type	8	2	1	4	2	4	4	0	2	17	11
Difflugia pulex	16	6	37	7	25	59	17	5	18	17	64
Difflugia rubescens	0	0	1	0	0	0	0	0	0	0	0
Euglypha rotunda type	0	0	0	0	0	0	0	0	0	0	0
Euglypha stringosa type	0	0	0	0	0	0	0	0	0	0	0
Euglypha tuberculata type	0	0	0	0	0	0	0	0	0	0	0
Heleopera petricola	0	0	0	0	0	0	0	0	0	0	0
Heleopera rosea	0	0	0	0	0	0	0	0	0	0	0
Heleopera sphagni	0	12	0	1	0	0	1	0	0	0	0
Heleopera sylvatica	0	0	3	0	0	1	0	0	0	0	0
Hyalosphenia elegans	0	0	0	0	0	0	0	0	0	0	0
Hyalosphenia minuta type	0	0	0	0	0	0	0	0	0	0	1
Hyalosphenia ovalis type	0	0	4	0	0	0	0	2	0	0	0
Hyalosphenia papilio	9	4	3	1	0	1	0	9	0	2	0
Hyalosphenia subflava	0	0	0	0	0	0	0	0	0	0	1
Nebela collaris type	0	0	3	0	2	0	0	0	0	0	0
Nebela flaballulum	0	0	0	0	0	0	0	0	0	0	0
Nebela militaris type	2	1	3	0	2	0	0	1	0	0	0
Nebela minor type	0	0	0	0	3	0	0	0	0	0	0
Nebela parvula	0	0	0	0	0	0	0	0	0	0	0
Nebela tincta	0	0	0	0	0	0	0	0	0	0	0
Nebela vitraea type	0	0	1	0	0	0	0	0	0	0	0
Nebela wailesi type	0	0	0	0	0	0	0	0	0	0	0
Phryganella acropodia type	0	0	0	0	0	0	0	0	0	0	0
Placocista spinosa type	0	0	0	0	0	0	0	0	0	0	0
Pseudodifflugia fulva type	0	0	1	0	1	0	0	0	0	0	1
Trigonopyxis arcula type	8	0	2	0	0	3	1	0	0	2	2
Trinema lineare type	0	0	0	0	0	0	0	0	0	0	0

Depth	**712**	**716**	**720**
Amphitrema flavum	6	9	66
Amphitrema stenastoma	1	1	0
Amphitrema wrightianum	0	0	0
Arcella artocrea	0	1	1
Arcella catinus type	0	0	0
*Arcella discoide*s type	3	1	1
Arcella gibbosa type	0	0	0
Arcella hemispherica	0	0	0
Arcella vulgaris type	0	0	0
Assulina muscorum	3	5	4
Assulina seminulum	1	0	1
Bullinularia indica	0	0	0
Centropyxis aculeata type	0	0	0
Centropyxis cassis type	0	0	0
Centropyxis platystoma type	1	0	0
Corythion/Trinema type	0	0	0
Cryptodifflugia oviformis	0	0	0
Cyclopyxis arcelloides type	3	5	4
Difflugia globulosa type	0	0	0

Difflugia lucida type	1	0	0
Difflugia oblonga type	0	1	0
Difflugia pristis type	11	10	8
Difflugia pulex	69	58	12
Difflugia rubescens	0	2	0
Euglypha rotunda type	0	0	0
Euglypha stringosa type	0	0	0
Euglypha tuberculata type	0	0	0
Heleopera petricola	0	0	0
Heleopera rosea	0	0	0
Heleopera sphagni	0	0	0
Heleopera sylvatica	0	0	0
Hyalosphenia elegans	0	1	0
Hyalosphenia minuta type	0	2	0
Hyalosphenia ovalis type	0	0	0
Hyalosphenia papilio	0	0	0
Hyalosphenia subflava	0	0	0
Nebela collaris type	0	0	0
Nebela flaballulum	0	0	0
Nebela militaris type	0	0	0
Nebela minor type	0	0	0
Nebela parvula	0	0	0
Nebela tincta	0	0	0
Nebela vitraea type	0	0	0
Nebela wailesi type	0	0	0
Phryganella acropodia type	0	0	0
Placocista spinosa type	0	0	0
Pseudodifflugia fulva type	0	1	1
Trigonopyxis arcula type	4	4	1
Trinema lineare type	0	0	0

2. Raeburn Flow

Plant macrofossils

Depth	316	320	324	328	332	336	340	344	348
UOM	5	6	6	5	6	3	23	3	2
Ericaceae	10	4	17	27	32	28	16	26	9
Ericaceous rootlets	9	3	16	24	28	26	15	23	8
Bark fragments	0	0	0	1	0	0	0	1	0
Wood fragments	0	0	0	2	1	2	0	0	0
Calluna vulgaris stem	0	0	0	0	0	0	1	0	0
Calluna vulgaris leaves	0	0	0	0	0	0	0	0	0
Calluna vulgaris flower	0	0	0	0	0	0	0	0	0
Erica tetralix stem	0	0	0	0	1	0	0	0	0
Erica tetralix leaves	0	0	0	0	0	0	0	0	0
Erica tetralix flower	0	0	0	0	0	0	0	0	0
Vaccinium oxycoccus	1	1	1	0	2	0	0	2	1
Monocot roots (unidentified)	13	6	6	2	8	7	6	5	5
Charcoal	0	0	0	0	0	0	0	0	0
Rhynchospora alba	0	0	0	0	0	1	0	0	0
Trichophorum cespitosum	0	0	0	0	0	0	0	0	0
Scheuchzeria palustre	0	0	0	0	0	0	0	0	0
Eriophorum spp. Roots	0	0	2	0	0	0	2	0	0
Eriophorum vaginatum leaf	5	0	3	0	0	0	0	0	0
Eriophorum angustifolia leaf	1	0	1	0	6	0	1	0	0
Total brown moss	0	0	0	0	0	0	0	0	0
Aulacomnium palustre	0	0	0	0	0	0	0	0	0
Total *Sphagnum*	66	84	66	68	47	60	52	66	84
Sphagnum sec. *Acutifolia*	6	17	4	2	6	0	0	1	0
Sphagnum austinii	60	67	62	68	40	60	51	65	84
Sphagnum magellanicum	0	0	0	0	1	0	0	0	0
Sphagnum sec. *Cuspidata*	0	0	0	0	0	0	1	0	0
Sphagnum cuspidatum	0	0	0	0	0	0	0	0	0
Sphagnum pulchrum	0	0	0	0	0	0	1	0	0
Sphagnum balticum	0	0	0	0	0	0	0	0	0
Plantago seed	0	0	0	0	0	0	0	0	0
Rhynchospora seeds	0	0	0	0	0	0	2	0	0
Carex seeds	0	0	0	0	0	0	0	0	0
Calluna seeds	0	0	0	0	0	0	0	0	0
Erica seeds	0	0	0	0	0	0	0	0	0
Betula seeds	0	0	0	0	0	0	0	0	0
Charcoal < 0.5 mm	0	0	10	0	0	0	7	12	2
Charcoal 0.5 mm -1 mm	0	0	0	0	0	0	0	6	0
Charcoal 1 mm - 1.5 mm	0	0	0	0	0	0	2	0	0
Charcoal 1.5 mm - 2.0 mm	0	0	0	0	0	0	0	0	0
Charcoal > 2.0 mm	0	0	0	0	0	0	0	0	0
Charred remains	0	0	0	0	0	0	0	0	0
Arcarid mites	3	3	2	0	0	0	0	0	7
Cennococcum spp.	0	0	0	0	0	0	0	0	0
Eriophorum spp. spindles	0	0	0	0	0	0	0	0	0
Sphagnum spore capsule	0	0	0	0	0	0	0	0	0

Depth	352	356	360	364	368	372	376	380	384
UOM	2	2	14	10	4	8	2	4	24
Ericaceae	9	12	22	16	36	7	5	21	41

Ericaceous rootlets	6	11	20	15	31	6	4	19	37
Bark fragments	0	0	1	1	2	0	0	0	0
Wood fragments	3	0	1	0	1	0	0	2	0
Calluna vulgaris stem	0	1	0	0	0	0	0	0	0
Calluna vulgaris leaves	0	0	0	0	0	1	0	0	0
Calluna vulgaris flower	0	0	0	0	0	0	0	0	0
Erica tetralix stem	0	0	0	0	0	0	0	0	2
Erica tetralix leaves	0	0	0	0	0	0	0	0	0
Erica tetralix flower	0	0	0	0	0	0	0	0	0
Vaccinium oxycoccus	0	0	0	0	2	0	1	0	2
Monocot roots (unidentified)	3	2	8	27	1	12	1	4	17
Charcoal	0	0	0	0	0	0	0	0	0
Rhynchospora alba	0	0	0	0	5	17	4	6	0
Trichophorum cespitosum	0	0	0	0	0	0	0	0	0
Scheuchzeria palustre	0	0	0	0	0	0	0	0	0
Eriophorum spp. Roots	0	1	0	1	0	0	1	0	0
Eriophorum vaginatum leaf	0	0	3	0	9	1	0	0	0
Eriophorum angustifolia leaf	0	0	0	4	0	5	3	3	0
Total brown moss	0	0	1	10	0	0	0	0	0
Aulacomnium palustre	0	0	1	10	0	0	0	0	0
Total *Sphagnum*	86	82	51	32	45	49	84	61	21
Sphagnum sec. *Acutifolia*	1	0	50	23	18	17	30	13	3
Sphagnum austinii	84	82	2	2	5	0	13	16	17
Sphagnum magellanicum	1	0	0	1	1	0	1	0	0
Sphagnum sec. *Cuspidata*	0	1	0	6	21	32	40	31	1
Sphagnum cuspidatum	0	0	0	1	13	16	22	11	0
Sphagnum pulchrum	0	1	0	4	6	9	14	13	0
Sphagnum balticum	0	0	0	1	2	7	4	7	1
Plantago seed	0	0	0	0	0	0	0	0	0
Rhynchospora seeds	0	0	0	0	0	0	0	1	0
Carex seeds	0	0	0	0	0	0	0	0	0
Calluna seeds	0	1	0	0	0	0	0	0	1
Erica seeds	0	2	0	0	0	1	0	0	0
Betula seeds	0	0	0	0	0	0	0	0	0
Charcoal < 0.5 mm	0	0	9	11	21	15	0	0	0
Charcoal 0.5 mm -1 mm	0	0	0	0	0	4	0	0	0
Charcoal 1 mm - 1.5 mm	0	0	0	0	0	0	0	0	0
Charcoal 1.5 mm - 2.0 mm	0	0	0	0	0	0	0	0	0
Charcoal > 2.0 mm	0	0	0	0	0	0	0	0	0
Charred remains	0	1	0	0	0	0	0	2	0
Arcarid mites	0	0	3	2	0	13	0	12	0
Cennococcum spp.	0	0	0	2	0	2	0	0	0
Eriophorum spp. spindles	0	0	0	0	0	0	0	0	0
Sphagnum spore capsule	0	0	0	0	0	0	0	0	0
Depth	**388**	**392**	**396**	**400**	**404**	**408**	**412**	**416**	**420**
UOM	17	25	17	18	22	16	30	37	39
Ericaceae	36	44	49	47	49	47	35	41	41
Ericaceous rootlets	30	33	43	40	46	39	31	37	38
Bark fragments	0	3	1	1	0	3	1	0	0
Wood fragments	0	3	0	1	0	2	0	1	0
Calluna vulgaris stem	0	0	4	0	2	0	0	1	0
Calluna vulgaris leaves	5	0	0	0	0	0	1	0	0
Calluna vulgaris flower	0	0	0	0	0	0	0	1	0
Erica tetralix stem	0	2	0	0	0	0	0	0	0
Erica tetralix leaves	0	0	0	0	0	0	1	0	0
Erica tetralix flower	0	0	0	0	0	0	0	0	0
Vaccinium oxycoccus	1	3	1	5	1	3	1	1	3
Monocot roots (unidentified)	26	24	9	7	21	16	26	11	6
Charcoal	0	1	0	0	0	0	0	0	0
Rhynchospora alba	0	0	0	0	0	0	0	0	0
Trichophorum cespitosum	0	0	0	0	0	0	0	0	0
Scheuchzeria palustre	0	0	0	0	0	0	0	0	0

Eriophorum spp. Roots	0	0	5	10	3	16	8	1	0
Eriophorum vaginatum leaf	4	0	11	16	1	3	0	0	7
Eriophorum angustifolia leaf	0	0	0	0	0	0	0	0	0
Total brown moss	0	0	0	0	0	0	0	0	0
Aulacomnium palustre	0	0	0	0	0	0	0	0	0
Total *Sphagnum*	17	3	9	3	3	2	2	10	6
Sphagnum sec. *Acutifolia*	1	0	7	2	2	1	0	8	4
Sphagnum austinii	16	3	2	1	2	1	2	2	2
Sphagnum magellanicum	0	0	0	0	0	0	0	0	0
Sphagnum sec. *Cuspidata*	0	0	0	0	0	0	0	0	0
Sphagnum cuspidatum	0	0	0	0	0	0	0	0	0
Sphagnum pulchrum	0	0	0	0	0	0	0	0	0
Sphagnum balticum	0	0	0	0	0	0	0	0	0
Plantago seed	0	0	0	0	0	0	1	0	0
Rhynchospora seeds	0	0	0	0	0	0	0	0	0
Carex seeds	0	0	0	0	0	0	0	0	0
Calluna seeds	0	0	0	1	1	0	0	1	0
Erica seeds	0	0	0	0	0	0	0	0	0
Betula seeds	0	0	0	0	0	0	0	0	0
Charcoal < 0.5 mm	3	30	3	39	12	36	9	0	0
Charcoal 0.5 mm -1 mm	18	30	0	0	3	0	0	0	0
Charcoal 1 mm - 1.5 mm	9	6	0	0	3	0	3	0	0
Charcoal 1.5 mm - 2.0 mm	0	0	0	0	3	0	0	0	0
Charcoal > 2.0 mm	0	0	0	0	0	0	0	0	0
Charred remains	0	0	0	0	0	0	0	0	0
Arcarid mites	0	0	0	0	3	3	0	0	0
Cennococcum spp.	39	6	3	0	33	0	0	0	0
Eriophorum spp. spindles	0	0	0	0	0	0	0	0	0
Sphagnum spore capsule	0	0	0	0	0	0	0	0	0
Depth	**424**	**428**	**432**	**436**	**440**	**444**	**448**	**452**	**456**
UOM	9	5	3	34	37	5	12	3	4
Ericaceae	70	42	47	44	40	19	30	17	48
Ericaceous rootlets	60	39	42	41	33	19	28	16	47
Bark fragments	1	1	0	0	0	0	0	0	0
Wood fragments	3	0	2	1	0	0	0	0	0
Calluna vulgaris stem	3	2	2	1	3	0	1	0	1
Calluna vulgaris leaves	0	0	0	0	4	0	0	0	0
Calluna vulgaris flower	0	0	0	0	0	0	0	0	0
Erica tetralix stem	0	0	0	0	0	0	0	0	0
Erica tetralix leaves	0	0	0	0	0	0	0	0	0
Erica tetralix flower	0	0	0	0	0	0	0	0	0
Vaccinium oxycoccus	3	0	1	1	0	0	1	1	0
Monocot roots (unidentified)	8	2	9	9	7	1	10	2	3
Charcoal	1	0	0	0	1	0	0	0	0
Rhynchospora alba	0	0	0	0	0	0	0	0	0
Trichophorum cespitosum	0	0	0	0	2	0	4	0	12
Scheuchzeria palustre	0	0	0	0	0	0	0	0	1
Eriophorum spp. Roots	3	1	4	1	1	7	15	5	1
Eriophorum vaginatum leaf	0	4	6	0	5	54	19	2	0
Eriophorum angustifolia leaf	0	0	0	0	0	0	0	0	0
Total brown moss	0	0	0	0	0	0	0	0	0
Aulacomnium palustre	0	0	0	0	0	0	0	0	0
Total *Sphagnum*	9	46	30	12	8	13	10	71	30
Sphagnum sec. *Acutifolia*	8	46	30	6	6	9	3	68	29
Sphagnum austinii	1	0	0	6	1	4	5	3	1
Sphagnum magellanicum	0	0	0	0	0	1	1	0	0
Sphagnum sec. *Cuspidata*	0	0	0	0	1	0	1	0	0
Sphagnum cuspidatum	0	0	0	0	1	0	0	0	0
Sphagnum pulchrum	0	0	0	0	0	0	1	0	0
Sphagnum balticum	0	0	0	0	0	0	0	0	0
Plantago seed	0	0	0	0	0	0	0	0	0
Rhynchospora seeds	1	0	0	0	0	0	0	0	0

Carex seeds	0	0	0	0	0	0	0	0	0
Calluna seeds	0	0	0	0	0	0	0	0	0
Erica seeds	0	0	0	0	0	0	0	0	0
Betula seeds	0	0	0	0	0	0	0	0	0
Charcoal < 0.5 mm	0	0	0	0	0	0	0	0	0
Charcoal 0.5 mm -1 mm	0	0	0	0	0	0	0	0	0
Charcoal 1 mm - 1.5 mm	0	0	0	0	0	0	0	0	0
Charcoal 1.5 mm - 2.0 mm	0	0	0	0	0	0	0	0	0
Charcoal > 2.0 mm	0	0	0	0	0	0	0	0	0
Charred remains	0	0	0	0	0	0	0	0	0
Arcarid mites	0	0	0	0	0	0	0	0	0
Cennococcum spp.	0	0	0	0	0	0	0	0	0
Eriophorum spp. spindles	0	0	0	0	0	0	0	0	0
Sphagnum spore capsule	0	0	0	0	0	0	0	0	0
Depth	**460**	**464**	**468**	**472**	**476**	**480**	**484**	**488**	**492**
UOM	8	5	6	7	11	6	8	4	6
Ericaceae	43	46	45	43	21	21	25	13	8
Ericaceous rootlets	42	42	43	41	16	20	24	12	6
Bark fragments	0	0	0	1	0	0	1	0	0
Wood fragments	1	1	0	1	0	1	0	1	0
Calluna vulgaris stem	0	2	1	0	2	0	0	0	2
Calluna vulgaris leaves	0	0	0	0	2	0	0	0	0
Calluna vulgaris flower	0	0	0	0	0	0	0	0	0
Erica tetralix stem	0	0	0	0	0	0	0	0	0
Erica tetralix leaves	0	0	0	0	0	0	0	0	0
Erica tetralix flower	0	0	0	0	0	0	0	0	0
Vaccinium oxycoccus	0	1	1	0	1	0	0	0	0
Monocot roots (unidentified)	28	28	25	21	26	10	4	4	6
Charcoal	3	0	2	0	0	0	0	0	0
Rhynchospora alba	0	0	0	0	0	0	0	0	0
Trichophorum cespitosum	0	2	0	0	0	0	0	0	0
Scheuchzeria palustre	0	0	0	0	0	0	0	0	0
Eriophorum spp. Roots	0	3	3	3	5	2	9	10	8
Eriophorum vaginatum leaf	0	0	0	1	0	20	37	0	6
Eriophorum angustifolia leaf	6	0	0	0	0	0	0	0	3
Total brown moss	0	0	0	0	0	0	0	0	1
Aulacomnium palustre	0	0	0	0	0	0	0	0	1
Total *Sphagnum*	12	15	19	25	36	40	17	68	61
Sphagnum sec. *Acutifolia*	10	11	13	23	32	38	14	66	16
Sphagnum austinii	1	1	5	0	3	2	3	2	0
Sphagnum magellanicum	1	4	2	1	1	0	0	0	0
Sphagnum sec. *Cuspidata*	0	0	0	1	0	0	0	0	44
Sphagnum cuspidatum	0	0	0	0	0	0	0	0	28
Sphagnum pulchrum	0	0	0	1	0	0	0	0	12
Sphagnum balticum	0	0	0	0	0	0	0	0	4
Plantago seed	0	0	0	0	0	0	0	0	0
Rhynchospora seeds	0	0	0	0	0	0	1	0	0
Carex seeds	0	0	0	0	0	0	0	0	0
Calluna seeds	0	0	0	2	0	0	0	0	1
Erica seeds	0	0	0	0	0	0	0	0	0
Betula seeds	0	0	0	0	0	0	0	0	0
Charcoal < 0.5 mm	0	0	0	0	0	0	0	0	0
Charcoal 0.5 mm -1 mm	0	0	0	0	0	0	0	0	0
Charcoal 1 mm - 1.5 mm	0	0	0	0	0	0	0	0	0
Charcoal 1.5 mm - 2.0 mm	0	0	0	0	0	0	0	0	0
Charcoal > 2.0 mm	0	0	0	0	0	0	0	0	0
Charred remains	0	0	0	0	0	0	0	0	0
Arcarid mites	0	0	0	0	0	0	0	0	0
Cennococcum spp.	0	0	0	0	0	0	0	0	0
Eriophorum spp. spindles	0	0	0	0	0	0	0	0	0
Sphagnum spore capsule	0	0	0	0	0	0	0	0	0

Depth	496	500	504	508	512	516	520	524	528
UOM	4	18	4	7	6	19	38	21	19
Ericaceae	8	34	49	48	52	46	36	50	57
Ericaceous rootlets	6	26	43	46	45	42	30	47	53
Bark fragments	0	0	0	0	1	1	0	0	0
Wood fragments	0	0	1	0	1	0	3	0	0
Calluna vulgaris stem	0	6	4	1	1	2	1	1	2
Calluna vulgaris leaves	2	2	1	1	2	0	1	1	1
Calluna vulgaris flower	0	0	0	0	0	0	0	0	0
Erica tetralix stem	0	0	0	0	0	0	0	0	0
Erica tetralix leaves	0	0	0	0	0	0	0	0	0
Erica tetralix flower	0	0	0	0	0	0	0	0	0
Vaccinium oxycoccus	0	0	0	0	2	1	1	1	1
Monocot roots (unidentified)	3	6	3	3	4	4	9	4	6
Charcoal	0	0	0	0	0	0	0	0	0
Rhynchospora alba	0	0	0	0	0	0	0	0	0
Trichophorum cespitosum	0	0	0	11	15	3	0	0	0
Scheuchzeria palustre	0	0	0	0	0	0	0	0	0
Eriophorum spp. Roots	2	0	3	5	8	1	11	6	7
Eriophorum vaginatum leaf	0	2	0	0	3	1	1	16	6
Eriophorum angustifolia leaf	0	0	0	0	0	0	0	0	0
Total brown moss	2	0	0	0	0	0	1	0	0
Aulacomnium palustre	2	0	0	0	0	0	0	0	0
Total *Sphagnum*	80	37	41	26	13	25	6	3	5
Sphagnum sec. *Acutifolia*	5	35	38	20	6	25	3	2	2
Sphagnum austinii	0	1	2	4	6	0	2	1	3
Sphagnum magellanicum	0	0	0	2	1	0	1	0	1
Sphagnum sec. *Cuspidata*	74	1	1	0	0	0	0	0	0
Sphagnum cuspidatum	27	0	0	0	0	0	0	0	0
Sphagnum pulchrum	28	1	1	0	0	0	0	0	0
Sphagnum balticum	19	0	0	0	0	0	0	0	0
Plantago seed	0	0	0	0	0	0	0	0	0
Rhynchospora seeds	0	0	0	0	0	0	0	0	0
Carex seeds	0	0	0	0	0	0	1	0	0
Calluna seeds	0	2	3	0	0	0	0	0	0
Erica seeds	0	0	0	0	0	0	0	0	1
Betula seeds	1	0	0	0	0	0	0	0	0
Charcoal < 0.5 mm	0	0	0	0	0	0	0	0	0
Charcoal 0.5 mm -1 mm	0	0	0	0	0	0	0	0	0
Charcoal 1 mm - 1.5 mm	0	0	0	0	0	0	0	0	0
Charcoal 1.5 mm - 2.0 mm	0	0	0	0	0	0	0	0	0
Charcoal > 2.0 mm	0	0	0	0	0	0	0	0	0
Charred remains	0	0	0	0	0	0	0	0	0
Arcarid mites	0	0	0	0	0	0	0	0	0
Cennococcum spp.	0	0	0	0	0	0	0	0	0
Eriophorum spp. spindles	0	0	0	0	0	0	0	0	0
Sphagnum spore capsule	0	0	0	0	0	0	0	0	0

Depth	532	536	540	544	548	552	556	560	564
UOM	12	3	6	4	8	6	7	12	26
Ericaceae	32	28	22	17	45	39	45	45	40
Ericaceous rootlets	31	27	20	15	42	34	40	39	37
Bark fragments	0	1	0	1	0	1	0	2	1
Wood fragments	0	0	0	0	0	2	0	3	0
Calluna vulgaris stem	1	0	1	0	2	0	2	0	0
Calluna vulgaris leaves	0	0	0	1	0	0	0	0	0
Calluna vulgaris flower	0	0	0	0	0	0	0	0	0
Erica tetralix stem	0	0	0	0	0	0	0	0	0
Erica tetralix leaves	0	0	0	0	0	2	0	0	0
Erica tetralix flower	0	0	0	0	0	0	0	0	0
Vaccinium oxycoccus	0	0	1	0	1	0	3	1	2

Monocot roots (unidentified)	6	1	16	7	8	3	11	15	6
Charcoal	0	0	0	0	0	0	0	0	0
Rhynchospora alba	0	13	0	0	0	3	0	0	0
Trichophorum cespitosum	0	0	0	0	0	0	5	1	5
Scheuchzeria palustre	0	0	0	0	0	0	0	0	0
Eriophorum spp. Roots	6	5	3	5	0	9	10	11	9
Eriophorum vaginatum leaf	18	9	2	0	6	10	3	11	6
Eriophorum angustifolia leaf	0	0	0	0	0	1	0	0	0
Total brown moss	0	0	0	0	0	0	0	0	7
Aulacomnium palustre	0	0	0	0	0	0	0	0	7
Total *Sphagnum*	26	41	49	68	24	29	18	3	3
Sphagnum sec. *Acutifolia*	23	41	22	14	17	15	9	1	3
Sphagnum austinii	2	0	0	1	5	9	3	1	0
Sphagnum magellanicum	1	0	1	0	0	1	0	1	0
Sphagnum sec. *Cuspidata*	0	0	26	53	2	4	5	0	0
Sphagnum cuspidatum	0	0	12	15	0	1	1	0	0
Sphagnum pulchrum	0	0	8	24	0	1	1	0	0
Sphagnum balticum	0	0	6	14	2	2	3	0	0
Plantago seed	0	0	0	0	0	0	0	0	0
Rhynchospora seeds	0	0	0	0	0	0	0	0	0
Carex seeds	0	0	0	0	0	0	1	0	0
Calluna seeds	0	0	0	2	2	0	0	0	0
Erica seeds	0	0	0	0	1	2	0	0	1
Betula seeds	1	0	0	0	0	0	0	0	0
Charcoal < 0.5 mm	0	0	0	0	0	0	0	0	0
Charcoal 0.5 mm -1 mm	0	0	0	0	0	0	0	0	0
Charcoal 1 mm - 1.5 mm	0	0	0	0	0	0	0	0	0
Charcoal 1.5 mm - 2.0 mm	0	0	0	0	0	0	0	0	0
Charcoal > 2.0 mm	0	0	0	0	0	0	0	0	0
Charred remains	0	0	0	0	0	0	0	0	0
Arcarid mites	0	0	0	0	0	0	0	0	0
Cennococcum spp.	0	0	0	0	0	0	0	0	0
Eriophorum spp. spindles	0	0	0	0	0	0	0	0	0
Sphagnum spore capsule	0	0	0	0	0	0	0	0	0
Depth	**568**	**572**	**576**	**580**	**584**	**588**	**592**	**596**	**600**
UOM	9	28	9	14	12	21	10	14	11
Ericaceae	39	32	32	34	44	4	46	29	54
Ericaceous rootlets	35	30	29	27	41	3	39	27	49
Bark fragments	1	0	2	0	1	0	6	1	2
Wood fragments	2	0	1	0	2	0	1	0	3
Calluna vulgaris stem	1	2	0	7	0	0	0	1	0
Calluna vulgaris leaves	0	0	0	0	0	0	0	0	0
Calluna vulgaris flower	0	0	0	0	0	0	0	0	0
Erica tetralix stem	0	0	0	0	0	0	0	0	0
Erica tetralix leaves	0	0	0	0	0	0	0	0	0
Erica tetralix flower	0	0	0	0	0	0	0	0	0
Vaccinium oxycoccus	0	0	0	0	0	1	0	0	0
Monocot roots (unidentified)	10	6	3	6	4	1	11	5	5
Charcoal	0	0	0	0	0	0	0	0	0
Rhynchospora alba	0	0	0	0	0	0	0	0	0
Trichophorum cespitosum	0	0	0	0	0	0	0	0	0
Scheuchzeria palustre	0	0	0	0	0	0	0	0	0
Eriophorum spp. Roots	7	12	8	6	10	14	11	29	11
Eriophorum vaginatum leaf	1	1	0	1	25	52	6	16	11
Eriophorum angustifolia leaf	0	0	0	0	0	4	0	0	1
Total brown moss	2	2	2	4	0	3	11	0	0
Aulacomnium palustre	2	2	2	4	0	3	8	0	0
Total *Sphagnum*	33	19	47	35	5	1	9	6	6
Sphagnum sec. *Acutifolia*	33	11	46	35	4	1	1	1	0
Sphagnum austinii	0	3	0	0	1	0	5	4	6
Sphagnum magellanicum	0	3	0	0	0	0	1	1	0
Sphagnum sec. *Cuspidata*	0	1	1	0	0	0	2	0	0

Sphagnum cuspidatum	0	1	1	0	0	0	0	0	0
Sphagnum pulchrum	0	0	0	0	0	0	0	0	0
Sphagnum balticum	0	0	0	0	0	0	2	0	0
Plantago seed	0	0	0	0	0	0	0	0	0
Rhynchospora seeds	0	0	0	0	0	0	0	0	0
Carex seeds	0	0	0	0	0	0	0	0	0
Calluna seeds	1	1	0	1	2	0	0	0	1
Erica seeds	0	0	0	0	1	0	0	0	0
Betula seeds	0	0	0	0	0	0	0	0	0
Charcoal < 0.5 mm	0	0	0	0	0	0	0	0	0
Charcoal 0.5 mm -1 mm	0	0	0	0	0	0	0	0	0
Charcoal 1 mm - 1.5 mm	0	0	0	0	0	0	0	0	0
Charcoal 1.5 mm - 2.0 mm	0	0	0	0	0	0	0	0	0
Charcoal > 2.0 mm	0	0	0	0	0	0	0	0	0
Charred remains	0	0	0	0	0	0	0	0	0
Arcarid mites	0	0	0	0	0	0	0	0	0
Cennococcum spp.	0	0	0	0	0	0	0	0	0
Eriophorum spp. spindles	0	0	0	0	0	0	0	0	0
Sphagnum spore capsule	0	0	0	0	0	0	0	0	0
Depth	**604**	**608**	**612**	**616**	**620**	**624**	**628**	**632**	**636**
UOM	8	10	18	14	39	31	20	18	16
Ericaceae	36	51	37	7	9	13	16	10	13
Ericaceous rootlets	35	46	29	4	6	10	14	10	9
Bark fragments	0	3	3	1	0	1	1	0	1
Wood fragments	0	1	0	1	0	2	1	0	0
Calluna vulgaris stem	0	1	5	1	2	0	0	0	0
Calluna vulgaris leaves	0	0	0	0	1	0	0	0	0
Calluna vulgaris flower	0	0	0	0	0	0	0	0	0
Erica tetralix stem	0	0	0	0	0	0	0	0	0
Erica tetralix leaves	0	0	0	0	0	0	0	0	0
Erica tetralix flower	0	0	0	0	0	0	0	0	0
Vaccinium oxycoccus	1	0	0	0	0	0	0	0	3
Monocot roots (unidentified)	3	9	1	33	32	16	12	10	11
Charcoal	0	0	0	0	0	0	2	0	13
Rhynchospora alba	0	0	0	0	0	0	0	0	0
Trichophorum cespitosum	3	19	25	25	0	0	0	0	0
Scheuchzeria palustre	0	0	0	0	0	0	0	0	0
Eriophorum spp. Roots	13	7	5	11	17	30	20	14	22
Eriophorum vaginatum leaf	34	2	10	6	3	9	29	43	23
Eriophorum angustifolia leaf	0	0	1	2	0	0	0	0	0
Total brown moss	0	0	0	0	0	0	0	0	0
Aulacomnium palustre	0	0	0	0	0	0	0	0	0
Total *Sphagnum*	3	2	3	0	1	1	2	5	2
Sphagnum sec. *Acutifolia*	0	0	0	0	1	1	1	2	0
Sphagnum austinii	3	1	1	0	0	0	1	3	2
Sphagnum magellanicum	0	1	2	0	0	0	0	0	0
Sphagnum sec. *Cuspidata*	0	0	0	0	0	0	0	0	0
Sphagnum cuspidatum	0	0	0	0	0	0	0	0	0
Sphagnum pulchrum	0	0	0	0	0	0	0	0	0
Sphagnum balticum	0	0	0	0	0	0	0	0	0
Plantago seed	0	0	0	0	0	0	0	0	0
Rhynchospora seeds	0	0	0	0	0	0	0	0	0
Carex seeds	0	0	0	0	0	0	0	0	0
Calluna seeds	0	0	0	0	0	4	0	0	0
Erica seeds	0	0	0	0	0	0	0	0	0
Betula seeds	0	0	0	0	1	0	0	0	0
Charcoal < 0.5 mm	0	0	0	0	0	0	0	0	0
Charcoal 0.5 mm -1 mm	0	0	0	0	0	0	0	0	0
Charcoal 1 mm - 1.5 mm	0	0	0	0	0	0	0	0	0
Charcoal 1.5 mm - 2.0 mm	0	0	0	0	0	0	0	0	0
Charcoal > 2.0 mm	0	0	0	0	0	0	0	0	0
Charred remains	0	0	0	0	0	0	0	0	0

Arcarid mites	0	0	0	0	0	0	0	0	0
Cennococcum spp.	0	0	0	0	0	0	0	0	0
Eriophorum spp. spindles	0	0	0	0	0	0	0	0	0
Sphagnum spore capsule	0	0	0	0	0	0	0	0	0
Depth	**640**	**644**	**648**	**652**	**656**	**660**	**664**	**668**	**672**
UOM	10	23	8	18	4	8	4	5	10
Ericaceae	10	1	4	0	2	0	5	7	6
Ericaceous rootlets	4	0	2	0	0	0	2	3	6
Bark fragments	2	0	2	0	2	0	3	4	0
Wood fragments	4	0	0	0	0	0	0	0	0
Calluna vulgaris stem	0	0	0	0	0	0	0	0	0
Calluna vulgaris leaves	0	0	0	0	0	0	0	0	0
Calluna vulgaris flower	0	0	0	0	0	0	0	0	0
Erica tetralix stem	0	0	0	0	0	0	0	0	0
Erica tetralix leaves	0	0	0	0	0	0	0	0	0
Erica tetralix flower	0	0	0	0	0	0	0	0	0
Vaccinium oxycoccus	0	1	0	0	0	0	0	0	0
Monocot roots (unidentified)	20	11	10	5	23	30	26	28	33
Charcoal	1	0	3	0	29	33	25	26	9
Rhynchospora alba	0	0	0	0	0	0	0	0	0
Trichophorum cespitosum	0	0	0	0	0	0	0	0	0
Scheuchzeria palustre	0	0	0	0	0	0	0	0	0
Eriophorum spp. Roots	24	14	26	52	36	21	34	26	26
Eriophorum vaginatum leaf	32	50	47	25	6	9	8	8	16
Eriophorum angustifolia leaf	0	0	0	0	0	0	0	0	0
Total brown moss	0	0	0	0	0	0	0	0	0
Aulacomnium palustre	0	0	0	0	0	0	0	0	0
Total *Sphagnum*	2	0	2	0	0	0	0	0	0
Sphagnum sec. *Acutifolia*	1	0	0	0	0	0	0	0	0
Sphagnum austinii	1	0	2	0	0	0	0	0	0
Sphagnum magellanicum	0	0	0	0	0	0	0	0	0
Sphagnum sec. *Cuspidata*	0	0	0	0	0	0	0	0	0
Sphagnum cuspidatum	0	0	0	0	0	0	0	0	0
Sphagnum pulchrum	0	0	0	0	0	0	0	0	0
Sphagnum balticum	0	0	0	0	0	0	0	0	0
Plantago seed	0	0	0	0	0	0	0	0	0
Rhynchospora seeds	0	0	0	0	0	0	0	0	0
Carex seeds	0	0	0	0	0	0	0	0	0
Calluna seeds	0	0	0	0	0	0	0	0	0
Erica seeds	0	0	0	0	0	0	0	0	0
Betula seeds	0	0	0	0	0	0	0	0	0
Charcoal < 0.5 mm	0	0	0	0	0	0	0	0	0
Charcoal 0.5 mm -1 mm	0	0	0	0	0	0	0	0	0
Charcoal 1 mm - 1.5 mm	0	0	0	0	0	0	0	0	0
Charcoal 1.5 mm - 2.0 mm	0	0	0	0	0	0	0	0	0
Charcoal > 2.0 mm	0	0	0	0	0	0	0	0	0
Charred remains	0	0	0	0	0	0	0	0	0
Arcarid mites	0	0	0	0	0	0	0	0	0
Cennococcum spp.	0	0	0	0	0	0	0	0	0
Eriophorum spp. spindles	0	0	0	0	0	0	0	0	0
Sphagnum spore capsule	0	0	0	0	0	0	0	0	0
Depth	**676**	**680**	**684**	**688**	**692**	**696**	**700**	**704**	**708**
UOM	8	10	9	7	23	18	9	6	17
Ericaceae	6	5	5	6	13	11	8	23	3
Ericaceous rootlets	5	5	4	6	5	5	3	23	0
Bark fragments	1	0	0	0	8	5	4	0	3
Wood fragments	0	0	1	0	0	0	0	0	0
Calluna vulgaris stem	0	0	0	0	0	1	1	0	0
Calluna vulgaris leaves	0	0	0	0	0	0	0	0	0
Calluna vulgaris flower	0	0	0	0	0	0	0	0	0

Erica tetralix stem	0	0	0	0	0	0	0	0	0
Erica tetralix leaves	0	0	0	0	0	0	0	0	0
Erica tetralix flower	0	0	0	0	0	0	0	0	0
Vaccinium oxycoccus	0	0	0	0	0	0	0	0	0
Monocot roots (unidentified)	34	28	37	11	28	29	29	7	14
Charcoal	2	11	6	46	18	25	25	5	1
Rhynchospora alba	0	0	0	0	0	0	0	0	0
Trichophorum cespitosum	0	0	0	0	0	0	0	0	0
Scheuchzeria palustre	0	0	0	0	0	0	0	0	0
Eriophorum spp. Roots	15	17	35	13	19	5	21	11	58
Eriophorum vaginatum leaf	37	26	5	17	0	16	8	46	4
Eriophorum angustifolia leaf	0	0	0	0	0	0	0	0	0
Total brown moss	0	0	1	0	0	0	0	1	0
Aulacomnium palustre	0	0	1	0	0	0	0	0	0
Total *Sphagnum*	0	2	2	0	0	0	0	0	2
Sphagnum sec. *Acutifolia*	0	0	2	0	0	0	0	0	0
Sphagnum austinii	0	2	0	0	0	0	0	0	2
Sphagnum magellanicum	0	0	1	0	0	0	0	0	0
Sphagnum sec. *Cuspidata*	0	0	0	0	0	0	0	0	0
Sphagnum cuspidatum	0	0	0	0	0	0	0	0	0
Sphagnum pulchrum	0	0	0	0	0	0	0	0	0
Sphagnum balticum	0	0	0	0	0	0	0	0	0
Plantago seed	0	0	0	0	0	0	0	0	0
Rhynchospora seeds	0	0	0	0	0	0	0	0	0
Carex seeds	0	0	0	0	0	0	0	0	0
Calluna seeds	0	0	0	0	0	0	0	0	0
Erica seeds	0	0	0	0	0	0	0	0	0
Betula seeds	0	0	0	0	0	0	0	0	0
Charcoal < 0.5 mm	0	0	0	0	0	0	0	0	0
Charcoal 0.5 mm -1 mm	0	0	0	0	0	0	0	0	0
Charcoal 1 mm - 1.5 mm	0	0	0	0	0	0	0	0	0
Charcoal 1.5 mm - 2.0 mm	0	0	0	0	0	0	0	0	0
Charcoal > 2.0 mm	0	0	0	0	0	0	0	0	0
Charred remains	0	0	0	0	0	0	0	0	0
Arcarid mites	0	0	0	0	0	0	0	0	0
Cennococcum spp.	0	0	0	0	0	0	0	0	0
Eriophorum spp. spindles	0	0	0	0	0	0	0	0	0
Sphagnum spore capsule	0	0	0	0	0	0	0	0	0

Testate amoebae

Depth	**312**	**316**	**320**	**324**	**328**	**332**	**336**	**340**	**344**	**348**	**352**
Amphitrema flavum	49	57	62	39	13	49	35	41	39	52	45
Amphitrema stenostoma	2	2	2	1	0	0	2	0	0	0	0
Amphitrema wrightianum	7	12	12	4	3	13	1	2	4	19	8
Arcella artrocrea	1	0	0	0	0	0	0	1	0	0	1
Arcella catinus type	1	0	0	0	0	0	1	2	0	0	0
Arcella discoides type	4	4	1	0	1	3	1	1	0	1	3
Assulina muscorum	7	12	8	7	10	4	11	7	16	9	11
Assulina seminulum	2	4	1	4	4	1	3	2	4	3	3
Bullinularia indica	0	0	0	0	0	0	0	0	0	0	0
Centropyxis aculeata type	2	4	0	0	0	0	0	0	0	0	0
Centropyxis cassis type	2	0	0	0	0	0	0	0	0	0	1
Centropyxis platystoma type	1	0	0	0	0	0	1	0	0	0	0
Cyclopyxis arcelloides type	2	0	2	6	4	4	5	5	3	1	3
Cryptodifflugia oviformis	0	0	0	0	0	0	0	0	0	0	0
Difflugia oblonga type	1	0	0	0	0	0	0	0	0	0	0
Difflugia pristis type	4	1	1	5	7	6	4	8	2	5	5
Difflugia pulex	9	3	10	31	50	14	27	23	19	6	18

Difflugia rubescens	0	0	2	0	1	0	0	0	0	0	0
Euglypha rotunda type	0	0	0	0	0	0	1	0	0	0	0
Euglypha tuberculata type	0	0	0	0	0	0	0	0	0	0	0
Heleopera petricola	0	0	0	0	0	1	0	2	1	3	0
Heleopera sphagni	1	0	1	1	2	4	2	2	3	0	1
Heleopera sylvatica	5	0	0	0	2	0	3	4	6	2	1
Hyalosphenia elegans	0	0	0	0	0	0	0	0	0	0	0
Hyalosphenia papilio	0	0	2	0	0	0	0	1	0	0	0
Hyalosphenia subflava	0	0	0	0	0	0	0	0	0	0	0
Nebela collaris	0	0	0	0	0	0	1	0	0	0	0
Nebela flabellulum	0	0	0	0	0	0	0	0	0	0	0
Nebela griseola type	0	0	0	0	0	0	0	0	0	0	0
Nebela militaris	0	0	0	0	0	0	0	0	0	0	0
Nebela minor	0	0	0	0	0	0	0	0	0	0	0
Nebela tincta	0	0	1	0	0	0	0	0	0	0	0
Nebela tubulosa type	0	0	0	0	0	0	0	0	0	0	0
Pseudodifflugia fulva type	1	0	0	0	2	0	0	2	0	1	0
Sphenoderia lenta	0	0	0	0	0	0	0	1	0	0	0
Trigonopyxis arcula type	1	1	0	0	0	0	0	0	0	0	0
Depth	**356**	**360**	**364**	**368**	**372**	**376**	**380**	**384**	**388**	**392**	**396**
Amphitrema flavum	46	43	35	36	47	62	66	24	10	14	37
Amphitrema stenostoma	0	0	0	0	0	0	0	0	0	0	0
Amphitrema wrightianum	11	1	1	3	8	24	18	1	1	0	1
Arcella artrocrea	0	0	0	0	0	0	0	1	0	0	0
Arcella catinus type	0	0	0	0	0	0	0	0	0	0	0
Arcella discoides type	1	2	2	2	0	0	1	1	0	0	0
Assulina muscorum	10	15	10	18	16	2	9	6	15	10	20
Assulina seminulum	3	1	2	3	6	1	1	4	3	0	2
Bullinularia indica	0	0	0	0	0	0	0	0	0	0	0
Centropyxis aculeata type	0	0	0	0	0	0	0	0	0	0	0
Centropyxis cassis type	0	0	0	0	0	0	0	0	0	0	0
Centropyxis platystoma type	0	0	0	0	0	0	0	0	0	0	0
Cyclopyxis arcelloides type	4	5	6	10	5	1	0	3	4	5	5
Cryptodifflugia oviformis	0	0	0	0	0	0	0	0	0	0	0
Difflugia oblonga type	0	0	0	0	0	0	0	0	0	0	0
Difflugia pristis type	7	10	10	6	6	2	2	1	6	8	9
Difflugia pulex	13	20	25	15	3	4	1	55	46	50	23
Difflugia rubescens	1	0	0	0	0	0	0	1	0	2	0
Euglypha rotunda type	0	0	0	0	1	0	0	0	2	0	0
Euglypha tuberculata type	0	0	0	0	0	0	0	0	0	0	0
Heleopera petricola	0	1	5	5	3	2	0	0	0	1	0
Heleopera sphagni	1	0	1	0	0	1	0	0	0	0	0
Heleopera sylvatica	2	0	3	2	2	1	0	2	10	6	2
Hyalosphenia elegans	0	0	0	0	0	1	0	0	0	0	0
Hyalosphenia papilio	0	0	0	0	0	0	0	0	0	0	0
Hyalosphenia subflava	0	0	0	0	0	0	0	0	0	0	0
Nebela collaris	0	0	0	0	0	0	0	0	0	0	0
Nebela flabellulum	0	0	0	0	0	0	0	0	0	0	0
Nebela griseola type	0	0	0	0	0	0	0	0	0	0	0
Nebela militaris	0	0	0	0	0	0	0	0	0	0	0
Nebela minor	1	0	0	0	2	0	0	0	0	0	0
Nebela tincta	0	0	1	0	0	0	0	0	0	0	0
Nebela tubulosa type	1	0	0	0	0	0	0	0	0	0	0
Pseudodifflugia fulva type	1	3	0	1	0	0	0	0	2	3	0
Sphenoderia lenta	0	0	0	0	0	0	0	0	0	0	0
Trigonopyxis arcula type	0	0	0	0	0	0	0	0	0	0	0
Depth	**400**	**404**	**408**	**412**	**416**	**420**	**424**	**428**	**432**	**436**	**440**
Amphitrema flavum	35	20	34	22	26	27	42	48	30	54	60
Amphitrema stenostoma	0	0	0	0	0	0	0	0	0	0	0
Amphitrema wrightianum	6	1	2	48	18	9	1	2	9	2	0
Arcella artrocrea	0	0	0	0	0	0	0	0	0	0	0
Arcella catinus type	0	0	0	0	0	0	0	0	0	0	0

Arcella discoides type	0	1	0	2	1	0	0	0	0	2	0
Assulina muscorum	18	7	10	3	8	9	7	8	4	10	4
Assulina seminulum	5	2	3	1	1	0	1	3	1	3	0
Bullinularia indica	0	0	0	0	0	0	0	0	0	0	0
Centropyxis aculeata type	0	0	0	0	0	0	0	0	0	0	0
Centropyxis cassis type	0	0	0	0	0	0	0	0	0	0	0
Centropyxis platystoma type	0	0	0	0	0	0	0	0	0	0	1
Cyclopyxis arcelloides type	1	4	3	3	4	5	4	4	6	4	4
Cryptodifflugia oviformis	0	0	0	0	0	0	0	0	0	0	0
Difflugia oblonga type	0	0	0	0	0	0	0	0	0	0	0
Difflugia pristis type	2	3	4	4	1	5	3	7	5	2	3
Difflugia pulex	28	62	41	10	40	43	39	25	42	21	22
Difflugia rubescens	0	0	2	0	0	0	0	0	1	0	3
Euglypha rotunda type	0	0	0	0	0	0	0	0	0	0	0
Euglypha tuberculata type	0	0	0	0	0	0	0	0	0	0	0
Heleopera petricola	0	0	0	5	0	0	0	0	0	0	0
Heleopera sphagni	1	1	0	0	0	0	0	0	0	1	0
Heleopera sylvatica	0	0	0	2	0	0	0	2	0	2	1
Hyalosphenia elegans	0	0	0	0	0	0	0	0	0	0	0
Hyalosphenia papilio	0	0	0	0	0	0	0	0	0	0	0
Hyalosphenia subflava	0	0	0	0	0	0	0	0	0	0	0
Nebela collaris	0	0	0	0	0	0	0	0	0	0	0
Nebela flabellulum	0	0	0	0	0	0	0	0	0	0	0
Nebela griseola type	0	0	0	0	0	0	0	0	0	0	0
Nebela militaris	1	0	0	0	0	0	0	0	0	0	0
Nebela minor	0	0	0	0	0	0	0	0	0	0	0
Nebela tincta	0	0	0	0	0	0	0	0	0	0	0
Nebela tubulosa type	0	0	0	0	0	0	0	0	0	0	0
Pseudodifflugia fulva type	2	2	3	0	0	0	3	1	2	0	0
Sphenoderia lenta	0	0	0	0	0	0	0	0	0	0	0
Trigonopyxis arcula type	0	1	0	0	2	0	1	0	0	0	0
Depth	**444**	**448**	**452**	**456**	**460**	**464**	**468**	**472**	**476**	**480**	**484**
Amphitrema flavum	44	24	36	40	33	51	57	55	65	85	55
Amphitrema stenostoma	1	2	0	0	0	0	0	0	0	0	0
Amphitrema wrightianum	1	0	2	2	3	0	0	0	0	0	0
Arcella artrocrea	0	0	0	0	0	0	0	0	0	0	0
Arcella catinus type	0	0	0	0	0	0	0	0	0	0	0
Arcella discoides type	1	0	1	0	1	0	0	0	0	1	1
Assulina muscorum	5	2	5	8	10	6	6	9	9	7	14
Assulina seminulum	0	0	0	1	4	7	1	1	1	2	2
Bullinularia indica	0	0	0	0	0	0	0	0	0	0	0
Centropyxis aculeata type	0	0	0	0	0	0	0	0	0	0	0
Centropyxis cassis type	0	0	0	1	0	0	0	0	0	0	0
Centropyxis platystoma type	0	0	0	0	0	0	0	0	0	0	0
Cyclopyxis arcelloides type	5	15	3	1	4	3	2	7	3	0	0
Cryptodifflugia oviformis	0	0	0	0	0	0	0	0	0	0	0
Difflugia oblonga type	0	0	0	0	0	0	0	0	0	0	0
Difflugia pristis type	4	9	6	1	5	1	2	1	3	1	4
Difflugia pulex	35	43	41	44	32	32	24	24	17	2	21
Difflugia rubescens	0	0	0	0	0	0	0	0	0	0	0
Euglypha rotunda type	0	0	0	0	0	0	0	0	0	0	0
Euglypha tuberculata type	0	0	0	0	0	0	0	0	0	0	0
Heleopera petricola	0	0	0	0	0	0	0	0	0	2	0
Heleopera sphagni	0	0	1	0	0	0	2	0	0	0	0
Heleopera sylvatica	0	2	2	0	3	0	3	0	2	0	4
Hyalosphenia elegans	0	0	0	0	0	0	0	0	0	0	0
Hyalosphenia papilio	0	0	0	0	0	0	0	0	0	0	0
Hyalosphenia subflava	0	0	0	0	0	0	0	0	0	0	0
Nebela collaris	0	0	0	0	0	0	0	0	0	0	0
Nebela flabellulum	0	0	0	0	0	0	0	0	0	0	0
Nebela griseola type	0	0	0	0	0	0	0	0	0	0	0
Nebela militaris	0	0	0	0	0	0	0	0	0	0	0
Nebela minor	0	0	0	0	0	0	0	0	0	0	0

Nebela tincta	0	0	0	0	0	0	0	0	0	0	0
Nebela tubulosa type	0	0	0	0	0	0	0	0	0	0	0
Pseudodifflugia fulva type	4	4	2	0	5	0	0	0	1	0	0
Sphenoderia lenta	0	0	0	0	0	0	0	0	0	0	0
Trigonopyxis arcula type	1	0	0	1	2	0	1	3	1	0	0
Depth	**488**	**492**	**496**	**500**	**504**	**508**	**512**	**516**	**520**	**524**	**528**
Amphitrema flavum	43	94	65	33	23	51	32	12	14	37	11
Amphitrema stenostoma	3	0	0	0	0	0	0	0	0	0	0
Amphitrema wrightianum	0	0	0	0	0	0	0	0	0	0	0
Arcella artrocrea	0	0	0	0	0	0	0	0	0	0	0
Arcella catinus type	0	0	0	0	0	0	0	0	0	0	0
Arcella discoides type	0	0	0	0	0	0	0	0	0	1	0
Assulina muscorum	11	4	12	8	4	6	5	4	3	12	4
Assulina seminulum	0	1	0	3	1	5	4	1	0	2	1
Bullinularia indica	0	0	0	0	0	0	0	0	0	0	0
Centropyxis aculeata type	0	0	0	0	0	0	0	0	0	0	0
Centropyxis cassis type	0	0	1	0	0	0	0	0	3	0	1
Centropyxis platystoma type	0	0	0	0	0	0	0	0	0	0	0
Cyclopyxis arcelloides type	8	0	7	4	6	3	6	5	11	5	13
Cryptodifflugia oviformis	0	0	0	0	0	0	0	0	0	0	0
Difflugia oblonga type	0	0	0	0	0	0	0	0	0	0	0
Difflugia pristis type	4	1	3	2	1	4	1	7	5	2	3
Difflugia pulex	29	0	11	47	60	25	49	67	60	32	51
Difflugia rubescens	1	0	1	0	0	0	1	1	3	0	4
Euglypha rotunda type	0	0	0	0	0	0	0	0	0	0	0
Euglypha tuberculata type	0	0	0	0	0	0	0	0	0	0	0
Heleopera petricola	0	0	0	0	0	0	0	0	0	0	0
Heleopera sphagni	0	0	0	0	0	0	0	0	0	0	0
Heleopera sylvatica	0	0	0	1	2	1	1	1	0	2	0
Hyalosphenia elegans	0	0	0	0	0	0	0	0	0	0	0
Hyalosphenia papilio	0	0	0	0	0	0	0	0	0	0	0
Hyalosphenia subflava	0	0	0	0	0	0	0	0	0	0	4
Nebela collaris	0	0	0	0	0	0	0	0	0	0	0
Nebela flabellulum	0	0	0	0	0	0	0	0	0	0	0
Nebela griseola type	0	0	0	0	0	0	0	0	0	0	0
Nebela militaris	0	0	0	0	0	0	0	0	0	0	0
Nebela minor	0	0	0	0	0	0	0	0	0	0	0
Nebela tincta	0	0	0	0	0	0	0	0	0	0	0
Nebela tubulosa type	0	0	0	0	0	0	0	0	0	0	0
Pseudodifflugia fulva type	1	0	0	1	3	3	2	2	0	5	7
Sphenoderia lenta	0	0	0	0	0	0	0	0	0	0	0
Trigonopyxis arcula type	0	0	0	0	0	0	0	0	2	2	0
Depth	**532**	**536**	**540**	**544**	**548**	**552**	**556**	**560**	**564**	**568**	**572**
Amphitrema flavum	57	14	69	67	54	52	54	38	49	44	29
Amphitrema stenostoma	0	6	6	1	0	0	0	0	0	1	0
Amphitrema wrightianum	0	0	0	0	0	0	0	0	1	0	1
Arcella artrocrea	0	0	0	0	0	1	0	0	0	0	0
Arcella catinus type	0	0	0	0	0	0	0	0	0	0	0
Arcella discoides type	0	2	0	0	0	0	0	2	1	0	0
Assulina muscorum	12	2	13	18	19	10	24	19	13	13	11
Assulina seminulum	2	0	3	3	12	4	3	4	7	2	2
Bullinularia indica	0	2	0	0	0	0	0	0	0	0	0
Centropyxis aculeata type	0	0	0	0	0	0	0	0	0	0	0
Centropyxis cassis type	0	0	0	0	0	0	0	0	0	0	0
Centropyxis platystoma type	0	0	0	0	0	0	0	0	0	0	0
Cyclopyxis arcelloides type	1	16	2	6	2	4	4	8	1	4	3
Cryptodifflugia oviformis	0	0	0	0	0	0	0	0	0	0	0
Difflugia oblonga type	0	0	0	0	0	0	0	0	0	0	0
Difflugia pristis type	2	0	3	0	3	0	1	2	1	2	3
Difflugia pulex	22	41	3	2	7	24	12	25	25	33	48
Difflugia rubescens	0	3	0	1	0	2	0	2	0	1	0
Euglypha rotunda type	0	0	0	0	0	0	0	0	0	0	0

Euglypha tuberculata type	0	0	0	0	0	0	0	0	0	0	0
Heleopera petricola	0	0	0	1	0	0	0	0	0	0	0
Heleopera sphagni	0	0	0	0	0	0	1	0	0	0	0
Heleopera sylvatica	2	0	1	0	3	1	1	0	1	0	1
Hyalosphenia elegans	0	0	0	0	0	0	0	0	0	0	0
Hyalosphenia papilio	0	0	0	0	0	0	0	0	0	0	0
Hyalosphenia subflava	0	5	0	0	0	0	0	0	0	1	0
Nebela collaris	0	2	0	0	0	0	0	0	0	0	0
Nebela flabellulum	0	0	0	0	0	0	0	0	0	0	0
Nebela griseola type	0	2	0	0	0	0	0	0	0	0	0
Nebela militaris	0	0	0	0	0	0	0	0	0	0	0
Nebela minor	0	0	0	0	0	0	0	0	0	0	0
Nebela tincta	0	0	0	0	0	0	0	0	0	0	0
Nebela tubulosa type	0	0	0	0	0	0	0	0	0	0	0
Pseudodifflugia fulva type	1	6	0	1	0	3	0	0	0	0	2
Sphenoderia lenta	0	0	0	0	0	0	0	0	0	0	0
Trigonopyxis arcula type	0	2	0	0	0	0	0	0	0	0	0
Depth	**576**	**580**	**584**	**588**	**592**	**596**	**600**	**604**	**608**	**612**	**616**
Amphitrema flavum	29	61	20	14	4	13	9	17	13	12	17
Amphitrema stenostoma	2	0	0	0	0	0	0	0	0	0	0
Amphitrema wrightianum	0	0	0	0	0	0	0	0	0	0	0
Arcella artrocrea	0	0	0	0	0	0	0	0	0	0	0
Arcella catinus type	0	0	0	0	0	0	0	0	0	0	0
Arcella discoides type	0	0	0	0	0	0	0	0	0	0	0
Assulina muscorum	10	11	18	19	8	4	5	6	13	2	4
Assulina seminulum	1	2	4	0	2	0	2	0	2	0	2
Bullinularia indica	0	0	0	0	0	0	0	0	2	0	0
Centropyxis aculeata type	0	0	0	0	0	0	0	0	0	0	0
Centropyxis cassis type	0	0	0	0	0	0	0	0	0	0	0
Centropyxis platystoma type	0	0	0	0	0	0	0	0	0	0	0
Cyclopyxis arcelloides type	1	3	4	3	2	6	3	1	10	20	21
Cryptodifflugia oviformis	0	0	0	0	0	0	2	0	0	0	0
Difflugia oblonga type	0	0	0	0	0	0	0	0	0	0	0
Difflugia pristis type	2	1	2	3	4	2	2	6	6	7	4
Difflugia pulex	53	19	44	59	76	73	69	66	42	55	48
Difflugia rubescens	0	0	2	0	2	0	3	0	2	0	0
Euglypha rotunda type	0	0	0	0	0	0	0	0	0	0	0
Euglypha tuberculata type	0	0	0	0	0	0	0	0	0	0	0
Heleopera petricola	0	0	0	0	0	0	0	0	0	0	0
Heleopera sphagni	0	0	0	0	0	0	0	0	0	0	0
Heleopera sylvatica	0	0	0	1	0	0	3	3	0	0	0
Hyalosphenia elegans	0	0	0	0	0	0	0	1	0	0	0
Hyalosphenia papilio	0	0	0	0	0	0	0	0	0	0	0
Hyalosphenia subflava	0	0	0	0	0	0	0	0	4	0	0
Nebela collaris	0	0	4	1	0	0	0	1	0	0	0
Nebela flabellulum	0	0	0	0	0	0	0	0	0	0	0
Nebela griseola type	0	0	0	0	0	0	0	0	0	0	0
Nebela militaris	0	0	0	0	0	0	0	0	0	0	0
Nebela minor	0	0	0	0	0	0	0	0	0	0	0
Nebela tincta	0	0	0	0	0	0	0	0	0	0	0
Nebela tubulosa type	0	0	0	0	0	0	0	0	0	0	0
Pseudodifflugia fulva type	2	2	0	1	2	2	2	0	4	5	4
Sphenoderia lenta	0	0	0	0	0	0	0	0	0	0	0
Trigonopyxis arcula type	0	2	0	0	0	0	0	0	2	0	0

Depth	**620**	**624**	**628**	**632**	**636**
Amphitrema flavum	27	19	44	77	78
Amphitrema stenostoma	0	0	0	0	0
Amphitrema wrightianum	0	0	0	0	0
Arcella artrocrea	0	0	0	0	0
Arcella catinus type	0	0	0	0	0
Arcella discoides type	0	0	0	0	0
Assulina muscorum	7	10	22	5	8

Assulina seminulum	7	2	15	4	2
Bullinularia indica	0	2	2	0	0
Centropyxis aculeata type	0	0	0	0	0
Centropyxis cassis type	0	0	0	0	0
Centropyxis platystoma type	0	0	0	0	0
Cyclopyxis arcelloides type	20	8	7	2	5
Cryptodifflugia oviformis	0	0	0	0	0
Difflugia oblonga type	0	0	0	0	0
Difflugia pristis type	3	0	0	0	0
Difflugia pulex	37	48	10	11	5
Difflugia rubescens	0	2	0	0	0
Euglypha rotunda type	0	0	0	0	0
Euglypha tuberculata type	0	0	0	0	0
Heleopera petricola	0	0	0	0	0
Heleopera sphagni	0	0	0	0	0
Heleopera sylvatica	0	0	0	0	0
Hyalosphenia elegans	0	0	0	0	0
Hyalosphenia papilio	0	0	0	2	2
Hyalosphenia subflava	0	6	0	0	0
Nebela collaris	0	0	0	0	0
Nebela flabellulum	0	0	0	0	0
Nebela griseola type	0	0	0	0	0
Nebela militaris	0	0	0	0	2
Nebela minor	0	0	0	0	0
Nebela tincta	0	0	0	0	0
Nebela tubulosa type	0	0	0	0	0
Pseudodifflugia fulva type	0	2	0	0	0
Sphenoderia lenta	0	0	0	0	0
Trigonopyxis arcula type	0	0	0	0	0

3. Tore Hill Moss

Plant macrofossils

Depth	308	316	324	332	340	348	356	364	372
UOM	20	7	8	7	11	32	5	12	14
Ericacae rootlets	25	18	29	12	22	32	13	23	37
Ericacae bark	0	0	0	0	3	2	0	0	4
Ericacae wood	2	2	0	0	0	3	0	0	1
Calluna vulgaris stem	0	0	0	0	0	2	0	0	1
Monocotyledon (undiff.)	0	19	3	5	4	1	1	1	9
Menyanthes trifoliata	0	0	0	0	0	0	0	0	0
Carex spp.	0	0	0	0	0	0	0	0	0
Equisetum arvense	0	0	0	0	0	0	0	0	0
Eriophorum spp. roots	12	0	8	3	2	11	8	8	1
Eriophorum vaginatum epidermis	7	7	4	19	15	2	20	19	0
Eriophorum angustifolia epidermis	0	11	0	1	0	0	0	9	0
Polytrichum spp. (undiff)	0	0	0	0	0	0	0	0	0
Polytrichum strictum	0	0	0	0	0	0	0	0	0
Dicranum spp. (undiff)	0	0	0	2	0	0	0	1	1
Dicranum scoparium	0	0	0	0	0	0	0	0	0
Hypnum spp. (undiff)	0	0	0	0	0	0	0	0	0
Aulacomnium palustris	0	0	4	8	8	0	0	3	5
Pleurozium schreberi	0	0	0	3	0	0	0	0	0
Brown moss (undiff)	0	0	0	0	0	2	0	0	1
Total *Sphagnum*	34	35	44	40	37	13	53	23	27
Sphagnum section *Acutifolia*	27	21	39	39	34	13	0	13	17
Sphagnum austinii	6	0	4	0	2	0	0	2	5
Sphagnum magellanicum	0	0	0	0	0	0	0	0	0
Sphagnum cuspidatum	0	5	0	1	1	0	0	0	2
Sphagnum balticum	1	9	2	0	1	0	53	8	3
Sphagnum palustre	0	0	0	0	0	0	0	0	0
Calluna vulgaris leaves	0	3	0	0	0	0	0	0	0
Erica tetralix flowers	0	0	0	0	0	0	0	0	0
Carex spp. seed	0	0	0	0	0	0	0	0	0
Calluna vulgaris seeds	0	0	0	0	0	0	3	0	0
Erica tetralix seeds	0	0	0	0	3	0	0	0	0
Betula pubesence seeds	0	0	0	0	0	0	0	0	0
Charcoal < 0.5 mm	1	9	36	9	27	30	15	6	0
Charcoal 0.5 mm - 1 mm	0	6	3	0	9	15	27	0	0
Charcoal 1 mm - 1.5 mm	0	0	0	0	0	0	9	0	0
Charcoal 1.5 mm - 2 mm	0	0	0	0	0	0	0	0	0
Charred remains	0	0	0	0	0	0	0	0	0
Acarid mites	0	3	0	0	0	0	0	0	3
Cennococcum spp.	2	3	0	0	27	3	3	6	18
Eriophorum spp. spindles	0	0	0	0	0	0	0	18	0
Sphagnum spore capsules	0	3	0	0	0	0	0	0	3

Depth	380	388	396	404	412	420	428	436	444
UOM	8	42	22	10	11	6	1	1	2
Ericacae rootlets	26	22	31	7	19	25	4	6	11
Ericacae bark	3	1	3	4	1	3	0	0	2
Ericacae wood	0	0	0	1	0	0	0	0	0
Calluna vulgaris stem	1	0	0	0	1	0	0	0	0
Monocotyledon (undiff.)	4	3	7	9	4	7	4	5	2
Menyanthes trifoliata	0	0	0	0	0	0	0	0	0

Carex spp.	0	0	0	0	0	0	0	0	0
Equisetum arvense	0	0	0	0	0	0	0	0	0
Eriophorum spp. roots	1	5	2	6	8	3	2	0	0
Eriophorum vaginatum epidermis	0	0	0	0	5	0	0	0	0
Eriophorum angustifolia epidermis	0	0	0	0	0	1	0	0	0
Polytrichum spp. (undiff)	0	0	0	0	0	0	0	0	0
Polytrichum strictum	0	0	0	0	0	0	0	0	0
Dicranum spp. (undiff)	0	0	0	0	1	0	0	0	0
Dicranum scoparium	0	0	0	0	0	0	0	0	0
Hypnum spp. (undiff)	0	0	0	0	0	0	1	0	0
Aulacomnium palustris	20	3	1	4	1	2	0	0	0
Pleurozium schreberi	0	0	0	12	0	0	0	0	0
Brown moss (undiff)	0	0	0	0	0	1	0	0	0
Total *Sphagnum*	38	24	35	48	49	53	87	87	84
Sphagnum section *Acutifolia*	35	24	20	45	49	53	85	83	84
Sphagnum austinii	1	0	11	3	0	0	2	3	0
Sphagnum magellanicum	1	0	0	0	0	0	0	0	0
Sphagnum cuspidatum	0	0	0	0	0	0	0	0	0
Sphagnum balticum	2	0	4	0	0	0	0	0	0
Sphagnum palustre	0	0	0	0	0	0	0	0	0
Calluna vulgaris leaves	0	0	0	0	0	0	0	0	0
Erica tetralix flowers	0	0	0	0	0	3	0	0	0
Carex spp. seed	0	0	0	0	0	0	0	0	0
Calluna vulgaris seeds	9	0	0	0	0	0	0	0	0
Erica tetralix seeds	0	0	0	0	0	0	0	0	3
Betula pubesence seeds	0	0	0	0	0	0	0	0	0
Charcoal < 0.5 mm	0	21	69	0	9	3	6	0	0
Charcoal 0.5 mm - 1 mm	0	0	0	0	0	0	0	0	0
Charcoal 1 mm - 1.5 mm	0	0	0	0	0	0	0	0	0
Charcoal 1.5 mm - 2 mm	0	0	0	0	0	0	0	0	0
Charred remains	0	0	0	0	0	0	0	0	0
Acarid mites	0	0	0	0	0	0	3	0	0
Cennococcum spp.	15	36	3	18	0	0	0	0	0
Eriophorum spp. spindles	0	0	0	0	0	0	0	0	0
Sphagnum spore capsules	0	0	0	0	0	0	0	0	0
Depth	**452**	**460**	**468**	**476**	**484**	**492**	**500**	**508**	**516**
UOM	14	11	7	48	12	24	8	8	10
Ericacae rootlets	19	17	13	28	20	36	15	21	8
Ericacae bark	7	2	2	0	4	2	3	0	1
Ericacae wood	1	1	3	2	0	0	0	0	0
Calluna vulgaris stem	0	0	6	0	0	1	0	0	0
Monocotyledon (undiff.)	10	3	11	4	19	6	4	10	9
Menyanthes trifoliata	0	0	0	0	0	0	0	0	0
Carex spp.	0	0	0	0	0	0	0	0	0
Equisetum arvense	0	0	0	0	0	0	0	0	0
Eriophorum spp. roots	0	0	5	11	18	18	10	29	10
Eriophorum vaginatum epidermis	0	0	0	0	0	1	28	1	1
Eriophorum angustifolia epidermis	0	0	0	0	0	0	2	0	0
Polytrichum spp. (undiff)	0	0	0	0	0	6	0	0	0
Polytrichum strictum	0	0	0	0	0	0	0	0	11
Dicranum spp. (undiff)	0	0	0	0	0	0	0	0	0
Dicranum scoparium	0	0	0	0	0	0	0	0	0
Hypnum spp. (undiff)	0	0	0	0	0	0	0	0	0
Aulacomnium palustris	2	0	2	1	12	1	7	2	4
Pleurozium schreberi	0	24	1	0	0	0	0	0	2
Brown moss (undiff)	1	0	0	0	0	0	0	0	0
Total *Sphagnum*	47	41	52	7	15	6	23	27	43
Sphagnum section *Acutifolia*	43	41	52	6	13	6	15	27	42
Sphagnum austinii	3	0	0	0	1	0	7	0	0
Sphagnum magellanicum	0	0	0	0	0	0	0	0	0
Sphagnum cuspidatum	1	0	0	1	0	0	1	0	1
Sphagnum balticum	0	0	0	0	0	0	1	0	1
Sphagnum palustre	0	0	0	0	0	0	0	0	0

Calluna vulgaris leaves	0	0	0	0	0	0	0	0	0
Erica tetralix flowers	0	0	0	0	0	0	0	0	0
Carex spp. seed	0	0	0	0	0	0	0	0	0
Calluna vulgaris seeds	3	0	0	0	0	0	0	0	0
Erica tetralix seeds	0	3	0	0	0	0	0	0	0
Betula pubesence seeds	0	0	0	0	0	0	0	0	0
Charcoal < 0.5 mm	0	27	18	18	21	3	33	0	21
Charcoal 0.5 mm - 1 mm	0	0	0	0	3	6	3	0	3
Charcoal 1 mm - 1.5 mm	0	0	0	0	0	0	3	0	0
Charcoal 1.5 mm - 2 mm	0	0	0	0	0	0	3	0	3
Charred remains	0	0	0	0	0	0	0	0	0
Acarid mites	3	0	0	0	0	0	0	0	0
Cennococcum spp.	27	9	12	3	3	12	27	18	6
Eriophorum spp. spindles	0	0	0	0	0	0	3	0	0
Sphagnum spore capsules	0	0	0	0	0	0	0	0	0
Depth	**524**	**532**	**540**	**548**	**556**	**564**	**572**	**580**	**588**
UOM	22	7	14	11	7	17	3	11	14
Ericacae rootlets	22	19	14	11	18	20	19	17	32
Ericacae bark	2	1	0	1	2	0	1	1	1
Ericacae wood	1	1	3	0	0	0	0	0	0
Calluna vulgaris stem	0	0	0	0	0	1	0	0	1
Monocotyledon (undiff.)	7	5	5	0	1	0	0	2	0
Menyanthes trifoliata	0	0	0	0	0	0	0	0	0
Carex spp.	0	0	0	0	0	0	0	0	0
Equisetum arvense	0	0	0	0	0	0	0	0	0
Eriophorum spp. roots	7	4	9	10	2	6	0	1	5
Eriophorum vaginatum epidermis	1	0	0	0	0	0	0	0	0
Eriophorum angustifolia epidermis	0	0	0	0	0	0	0	0	0
Polytrichum spp. (undiff)	0	0	0	0	0	0	0	0	0
Polytrichum strictum	4	7	3	2	0	0	0	0	0
Dicranum spp. (undiff)	0	0	0	0	0	0	0	0	0
Dicranum scoparium	0	0	41	58	37	44	35	47	37
Hypnum spp. (undiff)	0	0	0	0	0	0	0	0	0
Aulacomnium palustris	6	19	2	0	0	4	0	0	3
Pleurozium schreberi	0	0	0	0	0	0	0	1	0
Brown moss (undiff)	1	0	2	0	0	0	0	0	0
Total *Sphagnum*	26	36	7	7	33	9	43	21	7
Sphagnum section *Acutifolia*	26	35	4	6	33	9	42	19	7
Sphagnum austinii	0	1	2	0	0	0	1	1	0
Sphagnum magellanicum	0	0	0	0	0	0	0	0	0
Sphagnum cuspidatum	0	0	0	0	0	0	0	0	0
Sphagnum balticum	0	0	0	0	0	0	0	0	0
Sphagnum palustre	0	0	0	0	0	0	0	0	0
Calluna vulgaris leaves	0	0	0	0	0	0	0	0	0
Erica tetralix flowers	0	0	0	0	0	0	0	0	0
Carex spp. seed	0	0	0	0	0	0	0	0	0
Calluna vulgaris seeds	0	3	3	0	0	0	0	0	0
Erica tetralix seeds	0	0	0	0	0	0	0	0	0
Betula pubesence seeds	0	0	0	0	0	0	0	0	0
Charcoal < 0.5 mm	75	27	9	9	12	6	21	15	15
Charcoal 0.5 mm - 1 mm	27	0	0	0	3	0	6	15	6
Charcoal 1 mm - 1.5 mm	3	0	0	0	0	0	3	0	0
Charcoal 1.5 mm - 2 mm	9	0	0	0	0	0	0	0	0
Charred remains	0	0	0	0	0	0	0	0	0
Acarid mites	0	0	0	0	0	0	0	0	0
Cennococcum spp.	33	3	0	6	0	18	6	6	9
Eriophorum spp. spindles	0	0	0	0	0	0	0	0	0
Sphagnum spore capsules	0	0	0	0	0	0	0	0	0
Depth	**596**	**604**	**612**	**620**	**628**	**636**	**644**	**652**	**660**
UOM	20	4	8	13	8	9	4	5	20
Ericacae rootlets	34	27	27	26	32	29	27	15	31
Ericacae bark	0	1	1	2	5	1	1	2	1

Ericacae wood	0	1	0	1	1	2	0	0	0
Calluna vulgaris stem	0	0	0	1	1	0	1	0	1
Monocotyledon (undiff.)	2	2	2	0	5	1	3	0	4
Menyanthes trifoliata	0	0	0	0	0	0	0	0	0
Carex spp.	0	0	0	0	0	0	0	0	0
Equisetum arvense	0	0	0	0	0	0	0	0	0
Eriophorum spp. roots	8	3	8	16	7	7	5	4	24
Eriophorum vaginatum epidermis	0	0	2	16	4	5	0	41	0
Eriophorum angustifolia epidermis	0	0	0	0	0	0	0	0	0
Polytrichum spp. (undiff)	0	0	2	0	0	0	0	0	0
Polytrichum strictum	0	0	0	0	0	0	0	0	0
Dicranum spp. (undiff)	0	0	2	0	0	0	3	3	1
Dicranum scoparium	19	17	0	0	1	3	0	0	0
Hypnum spp. (undiff)	0	0	0	0	0	0	0	0	0
Aulacomnium palustris	2	1	0	2	1	1	0	6	0
Pleurozium schreberi	0	0	0	0	0	0	0	0	0
Brown moss (undiff)	0	0	0	0	0	0	0	0	0
Total *Sphagnum*	14	44	48	23	36	44	54	23	17
Sphagnum section *Acutifolia*	14	43	44	19	36	26	52	14	16
Sphagnum austinii	0	1	3	1	0	2	2	5	0
Sphagnum magellanicum	0	0	0	0	0	0	0	2	0
Sphagnum cuspidatum	0	0	0	0	0	9	0	1	1
Sphagnum balticum	0	0	1	2	0	7	0	1	0
Sphagnum palustre	0	0	0	0	0	0	0	0	0
Calluna vulgaris leaves	0	6	0	0	0	0	0	6	0
Erica tetralix flowers	0	0	0	0	0	0	0	0	0
Carex spp. seed	0	0	0	0	0	0	0	0	0
Calluna vulgaris seeds	3	3	0	0	0	0	0	0	0
Erica tetralix seeds	3	0	0	0	0	0	0	0	0
Betula pubesence seeds	0	0	0	0	0	0	0	0	0
Charcoal < 0.5 mm	27	15	84	21	72	24	21	30	33
Charcoal 0.5 mm - 1 mm	18	0	21	9	18	15	9	18	3
Charcoal 1 mm - 1.5 mm	0	0	6	0	3	0	0	0	0
Charcoal 1.5 mm - 2 mm	0	0	0	0	0	0	0	0	3
Charred remains	0	0	0	0	0	6	0	0	0
Acarid mites	0	0	0	0	0	6	0	0	0
Cennococcum spp.	0	6	3	0	6	3	3	0	3
Eriophorum spp. spindles	0	0	0	9	3	3	0	0	3
Sphagnum spore capsules	0	0	0	3	0	0	0	0	0
Depth	**668**	**676**	**684**	**692**	**700**	**708**	**716**	**724**	**732**
UOM	2	2	1	6	21	6	5	7	16
Ericacae rootlets	9	6	2	19	34	11	6	4	32
Ericacae bark	1	2	0	2	1	3	2	1	1
Ericacae wood	0	0	1	0	2	0	0	0	0
Calluna vulgaris stem	0	0	0	0	0	0	0	0	0
Monocotyledon (undiff.)	0	1	1	6	7	8	5	3	6
Menyanthes trifoliata	0	0	0	0	0	0	0	0	0
Carex spp.	0	0	0	0	0	0	0	0	0
Equisetum arvense	0	0	0	0	0	0	0	0	0
Eriophorum spp. roots	5	5	0	6	11	4	0	0	1
Eriophorum vaginatum epidermis	1	2	0	1	0	0	0	0	2
Eriophorum angustifolia epidermis	0	0	0	0	0	0	0	0	0
Polytrichum spp. (undiff)	2	0	0	0	0	0	0	0	0
Polytrichum strictum	0	0	0	12	0	0	0	14	3
Dicranum spp. (undiff)	1	4	2	0	0	0	0	0	0
Dicranum scoparium	0	0	0	0	0	4	0	0	0
Hypnum spp. (undiff)	0	0	0	0	0	0	7	0	0
Aulacomnium palustris	0	0	0	2	1	3	1	3	6
Pleurozium schreberi	0	0	0	0	0	0	0	3	0
Brown moss (undiff)	0	0	0	0	7	0	3	3	4
Total *Sphagnum*	79	78	92	44	15	63	69	65	29
Sphagnum section *Acutifolia*	78	79	92	44	15	53	51	65	16
Sphagnum austinii	0	0	0	0	0	6	18	0	10

Sphagnum magellanicum	0	0	0	0	0	0	0	0	2
Sphagnum cuspidatum	0	0	0	0	0	4	0	0	0
Sphagnum balticum	0	0	0	0	0	0	0	0	2
Sphagnum palustre	0	0	0	0	0	0	0	0	0
Calluna vulgaris leaves	0	0	0	0	0	0	0	0	0
Erica tetralix flowers	0	0	0	0	0	0	0	0	0
Carex spp. seed	0	0	1	0	0	0	0	0	0
Calluna vulgaris seeds	0	0	0	0	0	3	0	3	0
Erica tetralix seeds	0	0	0	0	0	0	0	0	0
Betula pubesence seeds	0	0	0	0	0	0	0	0	0
Charcoal < 0.5 mm	36	3	30	6	147	18	42	18	0
Charcoal 0.5 mm - 1 mm	0	0	24	0	51	3	39	18	0
Charcoal 1 mm - 1.5 mm	0	0	3	0	0	0	6	3	0
Charcoal 1.5 mm - 2 mm	0	0	0	0	0	0	0	0	0
Charred remains	0	0	3	0	0	0	0	0	0
Acarid mites	0	0	0	0	0	0	0	0	0
Cennococcum spp.	3	3	0	21	36	0	3	6	0
Eriophorum spp. spindles	0	0	0	0	0	0	0	0	0
Sphagnum spore capsules	3	0	6	3	3	0	3	0	0

Depth	**740**	**748**	**756**	**764**	**772**	**780**	**788**	**796**
UOM	37	15	8	3	4	2	3	4
Ericacae rootlets	11	25	7	3	7	4	3	4
Ericacae bark	2	2	2	0	0	0	0	0
Ericacae wood	4	0	0	0	0	0	3	2
Calluna vulgaris stem	0	0	0	0	0	3	0	0
Monocotyledon (undiff.)	7	5	11	3	0	8	6	5
Menyanthes trifoliata	0	16	4	3	4	1	3	1
Carex spp.	0	0	0	0	0	12	1	0
Equisetum arvense	0	0	0	1	3	6	4	9
Eriophorum spp. roots	2	2	0	0	0	0	0	0
Eriophorum vaginatum epidermis	2	3	0	2	0	0	1	1
Eriophorum angustifolia epidermis	0	0	0	0	0	0	0	0
Polytrichum spp. (undiff)	2	6	0	0	0	0	0	0
Polytrichum strictum	0	0	7	5	8	10	13	22
Dicranum spp. (undiff)	0	0	0	0	0	0	0	0
Dicranum scoparium	0	0	0	0	0	0	0	0
Hypnum spp. (undiff)	0	0	0	1	0	0	0	0
Aulacomnium palustris	2	4	9	2	2	0	0	2
Pleurozium schreberi	0	0	0	0	0	0	0	2
Brown moss (undiff)	1	0	5	0	3	0	0	0
Total *Sphagnum*	30	21	52	79	69	54	64	48
Sphagnum section *Acutifolia*	16	8	49	77	65	52	44	22
Sphagnum austinii	14	12	0	0	0	0	0	0
Sphagnum magellanicum	0	0	0	0	0	0	0	0
Sphagnum cuspidatum	0	0	0	0	0	0	0	0
Sphagnum balticum	1	1	3	2	4	2	0	0
Sphagnum palustre	0	0	0	0	0	3	21	26
Calluna vulgaris leaves	0	0	0	0	0	0	0	0
Erica tetralix flowers	0	0	0	0	0	0	0	0
Carex spp. seed	0	0	0	0	0	0	0	0
Calluna vulgaris seeds	0	0	0	0	0	0	0	0
Erica tetralix seeds	0	0	0	0	0	0	0	0
Betula pubesence seeds	0	3	0	0	0	0	0	0
Charcoal < 0.5 mm	42	36	42	0	0	51	0	0
Charcoal 0.5 mm - 1 mm	21	12	21	0	0	0	0	0
Charcoal 1 mm - 1.5 mm	3	0	3	0	0	0	0	0
Charcoal 1.5 mm - 2 mm	0	0	0	0	0	0	0	0
Charred remains	0	0	0	0	0	0	0	0
Acarid mites	0	0	0	0	0	0	0	0
Cennococcum spp.	24	3	0	0	0	0	0	0
Eriophorum spp. spindles	0	0	0	0	0	0	0	0
Sphagnum spore capsules	0	0	0	0	0	0	0	0

Testate amoebae

Depth	308	316	324	332	340	348	356	364	372	380	388
Amphitrema flavum	34	39	43	68	64	31	25	8	9	29	26
Amphitrema stenostoma	1	2	0	0	0	0	0	0	0	0	0
Amphitrema wrightianum	0	0	0	1	0	0	0	0	0	2	0
Arcella catinus type	0	0	0	0	0	0	0	0	0	0	0
Arcella discoides type	0	0	1	0	0	0	0	4	0	2	0
Assulina muscorum	23	9	14	9	3	8	16	8	12	8	7
Assulina seminulum	9	4	5	1	0	0	3	0	9	2	13
Bullinularia indica	0	0	0	1	0	0	0	0	0	0	0
Centropyxis platystoma type	0	0	0	0	0	0	0	0	0	0	0
Cyclopyxis arcelloides type	14	15	9	5	17	15	3	8	12	29	31
Difflugia lucida type	0	0	0	0	0	0	0	0	0	0	0
Difflugia oblonga type	0	0	0	0	0	0	0	4	0	0	0
Difflugia pristis type	3	1	3	4	6	8	13	4	6	20	11
Difflugia pulex	14	27	22	11	11	38	41	58	48	8	11
Euglypha strigosa	0	0	0	0	0	0	0	0	0	0	0
Euglypha tuberculata type	0	0	0	0	0	0	0	0	0	0	0
Heleopera sphagni	0	0	0	0	0	0	0	0	0	0	0
Heleopera sylvatica	0	0	0	0	0	0	0	0	0	0	0
Hyalosphenia ovalis	0	0	0	0	0	0	0	0	0	0	0
Hyalosphenia papilio	0	0	0	0	0	0	0	0	0	0	0
Hyalosphenia subflava	1	0	0	0	0	0	0	0	0	0	0
Nebela collaris	0	0	0	0	0	0	0	0	0	0	0
Nebela militaris	0	0	0	0	0	0	0	0	0	0	0
Nebela tincta	0	0	0	0	0	0	0	0	0	0	0
Pseudodifflugia fulva type	1	4	3	0	0	0	0	0	0	0	0
Trigonopyxis arcula var. *minor*	0	0	0	0	0	0	0	0	0	0	0
Trigonopyxis arcula sensu *lato*	0	0	0	0	0	0	0	4	3	0	0
Trigonopyxis arcula var. *major*	0	0	0	0	0	0	0	0	0	0	0
Trinema lineara	0	0	0	0	0	0	0	0	0	0	0

Depth	396	404	412	420	428	436	444	452	460	468	476
Amphitrema flavum	52	17	0	6	35	33	71	0	3	4	0
Amphitrema stenostoma	0	0	0	0	0	0	0	0	0	0	0
Amphitrema wrightianum	0	0	0	0	0	0	0	0	0	0	0
Arcella catinus type	0	0	0	0	5	0	0	0	0	0	0
Arcella discoides type	0	0	0	0	0	0	0	0	0	0	0
Assulina muscorum	8	22	18	21	40	26	12	14	22	7	4
Assulina seminulum	0	22	6	3	5	13	2	0	0	2	0
Bullinularia indica	0	0	0	0	0	0	0	0	0	0	0
Centropyxis platystoma type	0	0	0	0	0	0	0	0	0	0	0
Cyclopyxis arcelloides type	12	9	12	9	4	0	2	3	8	9	7
Difflugia lucida type	0	0	0	0	0	0	0	0	0	0	0
Difflugia oblonga type	0	0	0	0	0	0	0	0	0	0	0
Difflugia pristis type	8	4	18	9	2	7	2	8	19	13	4
Difflugia pulex	8	26	18	53	6	13	12	75	41	55	66
Euglypha strigosa	4	0	0	0	0	0	0	0	0	0	0
Euglypha tuberculata type	8	0	0	0	0	0	0	0	0	0	0
Heleopera sphagni	0	0	0	0	0	0	0	0	0	0	0
Heleopera sylvatica	0	0	0	0	0	0	0	0	0	0	0
Hyalosphenia ovalis	0	0	0	0	0	0	0	0	0	0	0
Hyalosphenia papilio	0	0	0	0	0	9	0	0	0	0	0
Hyalosphenia subflava	0	0	0	0	0	0	0	0	0	0	0
Nebela collaris	0	0	0	0	0	0	0	0	0	2	4
Nebela militaris	0	0	0	0	1	0	0	0	0	0	0
Nebela tincta	0	0	0	0	0	0	0	0	0	0	0
Pseudodifflugia fulva type	0	0	0	0	0	0	0	0	8	4	0

Trigonopyxis arcula var. *minor*	0	0	0	0	0	0	0	0	0	0	7
Trigonopyxis arcula sensu *lato*	0	0	29	0	1	0	0	0	0	5	4
Trigonopyxis arcula var. *major*	0	0	0	0	0	0	0	0	0	0	5
Trinema lineara	0	0	0	0	0	0	0	0	0	0	0
Depth	**484**	**492**	**500**	**508**	**516**	**524**	**532**	**540**	**548**	**556**	**564**
Amphitrema flavum	15	14	21	22	16	21	4	0	33	0	0
Amphitrema stenostoma	0	0	0	0	0	0	0	0	0	0	0
Amphitrema wrightianum	0	0	0	0	0	0	0	0	0	0	0
Arcella catinus type	0	0	0	0	0	0	0	0	0	0	0
Arcella discoides type	0	0	0	0	0	0	0	0	0	0	0
Assulina muscorum	10	11	0	6	6	7	7	3	3	7	33
Assulina seminulum	0	0	7	6	3	0	0	3	0	4	0
Bullinularia indica	0	0	7	0	0	0	0	0	0	0	0
Centropyxis platystoma type	0	0	0	0	0	0	0	0	0	0	0
Cyclopyxis arcelloides type	5	3	7	11	19	14	7	5	23	7	11
Difflugia lucida type	0	0	0	0	0	0	0	0	0	0	0
Difflugia oblonga type	0	0	0	0	0	0	0	0	0	0	0
Difflugia pristis type	0	8	7	6	19	4	0	3	8	7	6
Difflugia pulex	70	62	43	50	29	50	76	84	31	67	50
Euglypha strigosa	0	0	0	0	0	0	0	0	0	0	0
Euglypha tuberculata type	0	0	0	0	0	0	0	0	0	0	0
Heleopera sphagni	0	0	0	0	0	0	0	0	0	0	0
Heleopera sylvatica	0	0	0	0	0	0	0	0	0	0	0
Hyalosphenia ovalis	0	0	0	0	0	0	0	0	0	0	0
Hyalosphenia papilio	0	0	0	0	0	0	0	0	0	0	0
Hyalosphenia subflava	0	0	0	0	0	0	0	0	0	0	0
Nebela collaris	0	0	0	0	0	0	0	3	0	0	0
Nebela militaris	0	0	0	0	0	0	0	0	0	0	0
Nebela tincta	0	0	0	0	0	0	0	0	0	0	0
Pseudodifflugia fulva type	0	0	0	0	6	0	2	0	0	4	0
Trigonopyxis arcula var. *minor*	0	0	0	0	0	0	0	0	0	0	0
Trigonopyxis arcula sensu *lato*	0	3	7	0	0	4	2	0	0	4	0
Trigonopyxis arcula var. *major*	0	0	0	0	0	0	0	0	0	0	0
Trinema lineara	0	0	0	0	0	0	2	0	3	0	0
Depth	**572**	**580**	**588**	**596**	**604**	**612**	**620**	**628**	**636**	**644**	**652**
Amphitrema flavum	2	18	4	32	60	70	63	44	80	33	32
Amphitrema stenostoma	0	0	0	0	0	0	0	0	0	0	0
Amphitrema wrightianum	0	0	0	0	0	0	0	0	0	0	0
Arcella catinus type	0	0	0	0	0	0	0	0	0	0	0
Arcella discoides type	0	0	0	0	0	0	0	0	0	0	0
Assulina muscorum	40	36	23	11	11	0	4	22	0	29	16
Assulina seminulum	2	22	15	11	0	3	2	15	9	10	12
Bullinularia indica	0	0	4	0	0	0	0	2	2	0	0
Centropyxis platystoma type	0	0	0	0	0	0	0	0	0	0	4
Cyclopyxis arcelloides type	2	8	0	5	0	15	19	7	4	10	8
Difflugia lucida type	0	0	0	0	0	0	0	0	0	0	0
Difflugia oblonga type	0	0	0	0	0	0	0	0	0	0	0
Difflugia pristis type	6	2	4	3	6	0	0	0	0	5	4
Difflugia pulex	48	12	50	39	23	13	13	10	2	14	20
Euglypha strigosa	0	0	0	0	0	0	0	0	0	0	0
Euglypha tuberculata type	0	0	0	0	0	0	0	0	0	0	0
Heleopera sphagni	0	0	0	0	0	0	0	0	0	0	0
Heleopera sylvatica	0	2	0	0	0	0	0	0	0	0	0
Hyalosphenia ovalis	0	0	0	0	0	0	0	0	0	0	0
Hyalosphenia papilio	0	0	0	0	0	0	0	0	2	0	0
Hyalosphenia subflava	0	0	0	0	0	0	0	0	0	0	0
Nebela collaris	0	0	0	0	0	0	0	0	0	0	0
Nebela militaris	0	0	0	0	0	0	0	0	0	0	0
Nebela tincta	0	0	0	0	0	0	0	0	0	0	4
Pseudodifflugia fulva type	0	0	0	0	0	0	0	0	0	0	0
Trigonopyxis arcula var. *minor*	0	0	0	0	0	0	0	0	0	0	0

Trigonopyxis arcula sensu *lato*	0	0	0	0	0	0	0	0	0	0	0
Trigonopyxis arcula var. *major*	0	0	0	0	0	0	0	0	0	0	0
Trinema lineara	0	0	0	0	0	0	0	0	0	0	0
Depth	**660**	**668**	**676**	**684**	**692**	**700**	**708**	**716**	**724**	**732**	**740**
Amphitrema flavum	39	7	7	0	10	0	12	0	3	7	0
Amphitrema stenostoma	0	0	0	0	0	0	0	0	0	0	0
Amphitrema wrightianum	0	0	0	0	0	0	0	0	0	0	0
Arcella catinus type	0	0	3	0	0	0	0	0	0	0	0
Arcella discoides type	0	0	0	0	0	0	0	0	0	0	0
Assulina muscorum	17	22	17	48	10	31	41	21	8	7	10
Assulina seminulum	0	0	0	0	10	8	0	3	0	0	10
Bullinularia indica	0	11	0	0	0	0	0	0	0	0	0
Centropyxis platystoma type	0	0	0	0	0	0	0	3	0	0	0
Cyclopyxis arcelloides type	22	30	17	19	30	15	12	18	3	18	5
Difflugia lucida type	0	0	0	0	0	0	0	0	0	0	0
Difflugia oblonga type	0	0	0	0	0	0	0	0	0	0	0
Difflugia pristis type	6	0	7	4	5	0	0	0	3	7	15
Difflugia pulex	11	30	47	4	20	46	35	33	72	46	60
Euglypha strigosa	0	0	0	0	0	0	0	0	0	0	0
Euglypha tuberculata type	0	0	0	4	0	0	0	0	0	0	0
Heleopera sphagni	0	0	0	0	0	0	0	0	0	0	0
Heleopera sylvatica	0	0	0	0	0	0	0	0	0	0	0
Hyalosphenia ovalis	0	0	0	7	0	0	0	0	0	0	0
Hyalosphenia papilio	0	0	0	0	0	0	0	0	0	0	0
Hyalosphenia subflava	0	0	0	0	0	0	0	0	0	0	0
Nebela collaris	0	0	0	7	0	0	0	0	3	0	0
Nebela militaris	0	0	3	0	10	0	0	0	8	7	0
Nebela tincta	0	0	0	0	0	0	0	0	0	0	0
Pseudodifflugia fulva type	0	0	0	0	0	0	0	0	0	0	0
Trigonopyxis arcula var. *minor*	0	0	0	0	0	0	0	18	0	0	0
Trigonopyxis arcula sensu *lato*	6	0	0	7	5	0	0	3	3	7	0
Trigonopyxis arcula var. *major*	0	0	0	0	0	0	0	0	0	0	0
Trinema lineara	0	0	0	0	0	0	0	0	0	0	0

Depth	**748**	**756**	**764**	**772**	**780**
Amphitrema flavum	3	18	26	11	66
Amphitrema stenostoma	0	0	0	0	0
Amphitrema wrightianum	0	0	0	0	0
Arcella catinus type	6	3	3	14	3
Arcella discoides type	0	0	0	0	0
Assulina muscorum	33	37	9	25	3
Assulina seminulum	0	7	14	0	2
Bullinularia indica	0	0	0	0	0
Centropyxis platystoma type	6	3	2	0	7
Cyclopyxis arcelloides type	6	5	3	4	3
Difflugia lucida type	0	0	0	4	0
Difflugia oblonga type	0	0	0	0	0
Difflugia pristis type	3	2	2	11	0
Difflugia pulex	33	17	14	14	5
Euglypha strigosa	0	0	0	0	0
Euglypha tuberculata type	0	0	0	0	0
Heleopera sphagni	6	0	0	0	2
Heleopera sylvatica	0	0	0	0	0
Hyalosphenia ovalis	0	0	0	0	0
Hyalosphenia papilio	3	0	10	18	7
Hyalosphenia subflava	0	0	0	0	0
Nebela collaris	0	0	0	0	2
Nebela militaris	0	8	17	0	0
Nebela tincta	3	0	0	0	0
Pseudodifflugia fulva type	0	0	0	0	0
Trigonopyxis arcula var. *minor*	0	0	0	0	0
Trigonopyxis arcula sensu *lato*	0	0	0	0	0
Trigonopyxis arcula var. *major*	0	0	0	0	0

Trinema lineara	0	0	0	0	0

4. Kortlandamossen

Plant macrofossils

Depth	346	350	354	358	362	366	370	374	378	382
Unidentified organic material	0	2	2	1	1	1	1	2	1	1
Ericacae rootlets	5	3	3	2	4	2	2	2	1	2
Ericacae bark	0	0	0	0	0	0	0	0	0	0
Ericacae wood	4	2	1	2	1	2	2	1	1	2
Monocotyledon (undiff)	4	3	2	2	4	2	5	2	1	2
Vaccinium oxycoccus leaf	2	0	0	0	1	0	0	1	0	0
Dicranum scoparium leaf	0	0	0	0	0	0	0	0	0	0
Polytrichum spp. leaf	0	0	0	0	0	0	0	0	0	0
Rhynchospora alba leaf	0	0	0	0	0	0	0	5	8	10
Trichophorum cespitosum leaf	0	0	0	0	0	0	0	0	0	0
Charcoal	2	0	0	0	0	0	0	0	0	0
Eriophorum spp. roots	0	1	2	3	5	7	1	18	9	14
Eriophorum vaginatum epidermis	3	1	0	0	0	5	0	1	1	5
Eriophorum angustifolium epidermis	0	0	0	0	0	0	0	4	9	6
Total *Sphagnum*	80	88	90	91	85	80	88	65	68	58
Sphagnum section *Acutifolia*	67	85	86	91	84	72	64	65	67	58
Sphagnum magellanicum	0	0	0	0	0	2	9	0	0	0
Sphagnum section *Cuspidata*	13	4	5	0	1	7	15	0	1	0
Brown mosses stems	0	0	0	0	0	0	0	0	0	0
Calluna vulgaris seeds	0	0	0	0	0	0	0	0	0	0
Erica tetralix seeds	0	0	0	0	0	0	0	0	0	0
Charcoal < 0.5 mm	114	72	12	9	42	30	0	0	0	0
Charcoal 0.5 mm - 1 mm	15	15	6	0	3	0	0	0	0	0
Charcoal 1 mm - 1.5 mm	12	3	0	0	0	0	0	0	0	0
Charcoal 1.5 mm - 2 mm	6	0	0	0	0	0	0	0	0	0
Charred remains	15	6	0	0	3	0	0	0	0	0
Acarid mites	0	3	0	0	3	3	3	0	0	0
Cennococcum spp.	0	0	0	0	0	0	0	0	0	0
Eriophorum spp. spindles	0	0	0	0	0	0	0	21	0	12

Depth	386	390	394	398	402	406	410	414	418	422
Unidentified organic material	1	2	3	2	2	1	1	2	1	1
Ericacae rootlets	0	5	12	10	6	2	1	3	0	2
Ericacae bark	0	2	2	1	1	1	0	1	0	2
Ericacae wood	0	3	2	4	2	1	0	0	1	1
Monocotyledon (undiff)	1	5	2	6	5	4	3	2	1	3
Vaccinium oxycoccus leaf	0	4	2	1	0	0	0	1	0	0
Dicranum scoparium leaf	1	0	0	0	0	0	0	0	0	0
Polytrichum spp. leaf	0	0	0	0	1	0	0	0	0	1
Rhynchospora alba leaf	0	0	0	0	0	0	0	0	0	0
Trichophorum cespitosum leaf	0	0	0	0	0	0	0	0	0	0
Charcoal	0	0	0	0	0	0	0	0	0	0
Eriophorum spp. roots	1	2	8	10	1	2	0	0	0	0
Eriophorum vaginatum epidermis	0	0	18	0	0	0	0	0	0	0
Eriophorum angustifolium epidermis	0	0	0	0	0	0	0	0	0	0
Total *Sphagnum*	95	78	51	65	81	90	94	91	96	91
Sphagnum section *Acutifolia*	94	75	46	61	80	88	93	89	95	89
Sphagnum magellanicum	1	0	2	1	0	1	1	0	1	1
Sphagnum section *Cuspidata*	0	3	4	3	1	1	0	2	0	1
Brown mosses stems	0	0	0	0	0	0	0	0	0	0
Calluna vulgaris seeds	0	0	0	3	3	0	0	0	0	0

Erica tetralix seeds	0	0	3	0	0	0	0	0	0	0
Charcoal < 0.5 mm	3	0	48	27	12	0	21	48	0	24
Charcoal 0.5 mm - 1 mm	0	3	0	0	0	0	3	0	0	3
Charcoal 1 mm - 1.5 mm	0	0	0	0	0	0	0	6	0	0
Charcoal 1.5 mm - 2 mm	0	0	6	0	0	0	0	0	0	0
Charred remains	0	0	6	0	0	0	0	3	0	0
Acarid mites	0	3	6	6	0	3	3	3	0	0
Cennococcum spp.	0	0	0	0	0	0	0	0	0	0
Eriophorum spp. spindles	0	0	3	0	0	0	0	0	0	0
Depth	**426**	**430**	**434**	**438**	**442**	**446**	**450**	**454**	**458**	**462**
Unidentified organic material	1	1	0	3	1	1	1	1	0	1
Ericacae rootlets	0	1	2	26	3	2	3	2	1	4
Ericacae bark	0	1	0	3	1	1	1	1	1	4
Ericacae wood	1	0	2	2	1	0	1	0	0	3
Monocotyledon (undiff)	1	2	2	4	4	3	1	2	1	4
Vaccinium oxycoccus leaf	1	0	0	0	1	0	1	0	0	1
Dicranum scoparium leaf	0	0	0	0	0	0	0	0	0	0
Polytrichum spp. leaf	0	0	0	0	0	0	0	0	0	0
Rhynchospora alba leaf	0	0	0	0	0	0	0	0	0	0
Trichophorum cespitosum leaf	0	0	0	0	0	0	0	0	0	0
Charcoal	0	0	0	0	0	0	0	0	0	0
Eriophorum spp. roots	0	0	1	0	3	0	6	2	0	4
Eriophorum vaginatum epidermis	0	0	0	0	0	0	11	0	0	1
Eriophorum angustifolium epidermis	0	0	0	0	0	0	0	0	0	0
Total *Sphagnum*	97	95	93	62	86	93	74	91	96	79
Sphagnum section *Acutifolia*	97	95	93	62	86	93	65	89	96	79
Sphagnum magellanicum	0	0	0	0	0	0	0	1	0	0
Sphagnum section *Cuspidata*	0	0	0	0	0	0	9	1	0	0
Brown mosses stems	0	0	0	0	0	0	0	0	0	0
Calluna vulgaris seeds	0	0	0	0	0	0	0	0	0	0
Erica tetralix seeds	0	0	0	0	0	0	0	0	0	0
Charcoal < 0.5 mm	0	9	0	69	3	6	0	6	6	6
Charcoal 0.5 mm - 1 mm	0	3	0	12	0	0	0	0	0	0
Charcoal 1 mm - 1.5 mm	0	0	0	0	0	0	0	0	0	0
Charcoal 1.5 mm - 2 mm	0	0	0	0	0	0	0	0	0	0
Charred remains	0	0	0	0	0	0	0	0	0	0
Acarid mites	0	3	0	3	0	0	3	0	0	0
Cennococcum spp.	0	0	0	0	0	0	0	0	0	0
Eriophorum spp. spindles	0	0	0	0	3	0	6	0	0	0
Depth	**466**	**470**	**474**	**478**	**482**	**486**	**490**	**494**	**498**	**502**
Unidentified organic material	1	1	0	1	1	1	1	0	1	2
Ericacae rootlets	3	3	1	1	3	2	5	1	6	2
Ericacae bark	1	1	0	1	3	1	0	1	2	3
Ericacae wood	4	1	1	1	1	1	4	0	3	1
Monocotyledon (undiff)	5	2	4	5	3	3	7	2	6	2
Vaccinium oxycoccus leaf	1	1	0	0	0	0	0	0	1	1
Dicranum scoparium leaf	0	0	0	0	0	0	0	0	0	0
Polytrichum spp. leaf	0	0	0	0	0	0	0	0	0	0
Rhynchospora alba leaf	0	0	0	0	0	0	0	0	0	0
Trichophorum cespitosum leaf	0	0	0	0	0	0	0	0	0	0
Charcoal	0	0	0	0	0	0	0	0	0	0
Eriophorum spp. roots	1	1	1	0	1	2	4	1	2	4
Eriophorum vaginatum epidermis	0	0	0	0	4	5	0	0	0	10
Eriophorum angustifolium epidermis	0	0	0	0	0	0	0	0	0	0
Total *Sphagnum*	83	91	92	91	84	85	79	95	79	73
Sphagnum section *Acutifolia*	83	91	92	91	84	84	78	95	76	73
Sphagnum magellanicum	0	0	0	0	0	0	1	0	0	0
Sphagnum section *Cuspidata*	0	0	0	0	0	2	0	0	2	0
Brown mosses stems	0	0	0	0	0	0	0	0	0	0
Calluna vulgaris seeds	0	0	0	0	0	0	0	0	0	0
Erica tetralix seeds	0	0	0	0	0	0	0	0	0	0
Charcoal < 0.5 mm	0	21	0	0	0	0	0	0	0	6
Charcoal 0.5 mm - 1 mm	0	12	0	0	0	0	0	0	0	0
Charcoal 1 mm - 1.5 mm	0	0	0	0	0	0	0	0	0	0

Charcoal 1.5 mm - 2 mm	0	0	0	0	0	0	0	0	0	0
Charred remains	0	0	0	0	0	0	0	0	0	0
Acarid mites	0	3	0	0	0	0	0	0	3	0
Cennococcum spp.	0	0	0	0	0	0	0	0	0	0
Eriophorum spp. spindles	0	0	0	0	0	0	0	0	0	0
Depth	**506**	**510**	**514**	**518**	**522**	**526**	**530**	**534**	**538**	**542**
Unidentified organic material	0	1	1	1	2	1	2	1	1	4
Ericacae rootlets	1	4	2	2	6	3	4	15	22	9
Ericacae bark	0	1	0	2	0	1	1	1	0	1
Ericacae wood	1	1	3	2	3	0	3	0	0	0
Monocotyledon (undiff)	2	3	5	3	22	10	3	8	18	11
Vaccinium oxycoccus leaf	0	1	0	0	0	0	0	0	0	0
Dicranum scoparium leaf	0	0	0	0	0	0	0	0	0	0
Polytrichum spp. leaf	0	0	0	3	4	5	2	0	0	0
Rhynchospora alba leaf	0	0	0	0	0	0	0	0	0	0
Trichophorum cespitosum leaf	0	0	0	0	0	0	0	0	0	0
Charcoal	0	0	0	0	0	0	0	0	0	0
Eriophorum spp. roots	1	4	0	3	3	0	2	3	1	1
Eriophorum vaginatum epidermis	0	2	0	0	0	4	36	9	42	69
Eriophorum angustifolium epidermis	0	0	0	0	0	0	0	0	0	0
Total *Sphagnum*	94	89	88	84	59	76	47	63	16	6
Sphagnum section *Acutifolia*	92	52	80	83	49	74	47	63	16	4
Sphagnum magellanicum	1	11	4	1	6	1	0	0	0	1
Sphagnum section *Cuspidata*	2	20	4	0	4	1	0	0	0	1
Brown mosses stems	0	0	1	0	0	0	0	0	0	0
Calluna vulgaris seeds	0	0	0	0	0	0	0	0	0	0
Erica tetralix seeds	0	0	0	0	0	0	0	0	0	0
Charcoal < 0.5 mm	0	0	0	15	0	3	9	6	0	3
Charcoal 0.5 mm - 1 mm	0	0	0	0	0	0	0	0	0	0
Charcoal 1 mm - 1.5 mm	0	0	0	3	0	0	0	0	0	0
Charcoal 1.5 mm - 2 mm	0	0	0	0	0	0	0	0	0	0
Charred remains	0	0	0	3	0	0	0	0	0	0
Acarid mites	0	0	0	0	0	0	0	0	0	0
Cennococcum spp.	0	0	0	3	0	0	0	0	0	0
Eriophorum spp. spindles	0	0	0	0	0	3	0	0	15	15

Depth	**546**	**550**	**554**	**558**	**562**	**566**	**570**	**574**
Unidentified organic material	1	3	1	14	23	14	24	65
Ericacae rootlets	9	7	10	13	5	1	4	1
Ericacae bark	0	0	0	1	1	3	12	4
Ericacae wood	1	2	0	2	2	3	3	1
Monocotyledon (undiff)	4	5	4	7	6	1	33	20
Vaccinium oxycoccus leaf	2	0	0	1	0	0	0	1
Dicranum scoparium leaf	0	0	0	0	0	0	0	0
Polytrichum spp. leaf	0	0	0	0	0	0	0	0
Rhynchospora alba leaf	0	0	0	0	0	0	0	0
Trichophorum cespitosum leaf	2	1	0	0	0	0	0	0
Charcoal	0	0	0	0	0	0	0	0
Eriophorum spp. roots	0	5	4	10	48	12	10	1
Eriophorum vaginatum epidermis	57	0	0	18	16	66	2	0
Eriophorum angustifolium epidermis	0	0	0	0	0	0	0	0
Total *Sphagnum*	24	78	81	34	1	0	13	7
Sphagnum section *Acutifolia*	24	36	75	10	1	0	5	6
Sphagnum magellanicum	0	39	6	0	0	0	8	0
Sphagnum section *Cuspidata*	0	3	0	24	0	0	0	1
Brown mosses stems	0	0	0	0	0	0	0	0
Calluna vulgaris seeds	0	0	0	0	0	0	0	0
Erica tetralix seeds	0	0	0	0	0	0	0	0
Charcoal < 0.5 mm	0	0	0	0	9	0	0	0
Charcoal 0.5 mm - 1 mm	0	0	0	0	0	0	0	0
Charcoal 1 mm - 1.5 mm	0	0	0	0	0	0	0	0
Charcoal 1.5 mm - 2 mm	0	0	0	0	0	0	0	0
Charred remains	0	0	0	0	0	0	0	0
Acarid mites	0	0	0	9	0	0	0	6
Cennococcum spp.	0	0	0	0	0	0	0	0

Eriophorum spp. spindles	0	0	0	0	6	60	0	0

Testate amoebae

Depth	346	350	354	358	362	366	370	374	378	382	386
Amphitrema flavum	78	86	91	82	62	60	82	83	74	81	34
Amphitrema wrightianum	3	1	0	0	1	1	2	0	0	0	0
Arcella catinus type	0	0	0	0	0	0	0	0	1	1	0
Arcella discoides type	0	0	0	0	0	0	0	1	0	0	0
Assulina muscorum	1	2	2	7	10	7	2	1	1	3	6
Assulina seminulum	3	2	1	5	2	2	3	2	1	1	10
Bullinularia indica	0	0	0	0	0	1	0	0	0	0	0
Centropyxis aculeata type	0	0	0	0	1	0	0	0	0	0	0
Cyclopyxis arcelloides type	1	1	0	0	2	1	2	1	0	1	2
Difflugia pristis type	3	1	1	1	4	1	3	1	2	1	2
Difflugia pulex	10	8	5	5	14	22	3	6	5	8	44
Difflugia rubescens	0	0	0	0	0	0	0	0	0	0	0
Heleopera petricola	0	0	0	0	0	0	0	0	3	0	1
Heleopera sphagni	0	0	0	0	0	1	0	1	4	5	0
Heleopera sylvatica	0	0	0	0	0	0	0	0	0	0	0
Hyalosphenia elegans	0	0	0	0	0	0	2	0	4	0	0
Hyalosphenia papilio	0	0	0	0	0	0	2	3	4	0	0
Hyalosphenia subflava	0	0	0	0	0	0	0	0	0	0	0
Nebela collaris	0	0	0	0	0	0	0	0	0	0	0
Nebela militaris	0	0	0	0	0	0	0	0	0	0	0
Pseudodifflugia fulva type	2	0	0	0	1	0	0	0	0	0	0
Trigonopyxis arcula var. *minor*	0	0	0	0	0	1	0	0	0	0	0
Trigonopyxis arcula sensu *lato*	0	0	0	1	3	1	0	0	0	0	0
Trigonopyxis arcula var. *major*	0	0	0	0	0	0	1	0	0	0	1

Depth	390	394	398	402	406	410	414	418	422	426	430
Amphitrema flavum	13	17	67	77	73	77	43	61	73	76	72
Amphitrema wrightianum	0	0	0	0	0	0	1	0	0	0	0
Arcella catinus type	0	0	0	0	0	0	0	0	0	2	0
Arcella discoides type	0	0	4	1	0	0	0	0	0	0	0
Assulina muscorum	14	1	6	3	5	3	11	2	5	0	3
Assulina seminulum	3	8	8	4	1	2	14	1	1	1	6
Bullinularia indica	1	0	0	0	0	0	0	0	0	0	0
Centropyxis aculeata type	0	0	0	0	0	0	0	0	0	0	0
Cyclopyxis arcelloides type	2	3	2	4	2	1	4	8	3	3	1
Difflugia pristis type	1	9	1	2	2	6	6	6	6	1	1
Difflugia pulex	62	59	11	7	12	10	21	19	8	12	9
Difflugia rubescens	0	0	0	0	0	0	0	0	0	0	0
Heleopera petricola	0	0	0	0	0	0	0	0	0	3	2
Heleopera sphagni	0	0	0	0	1	0	0	0	0	0	0
Heleopera sylvatica	0	0	0	0	0	0	0	1	1	0	0
Hyalosphenia elegans	0	0	0	0	0	1	0	0	0	0	0
Hyalosphenia papilio	0	0	0	0	2	0	0	1	0	3	4
Hyalosphenia subflava	0	0	0	0	0	0	0	0	0	0	0
Nebela collaris	0	0	0	0	0	0	0	0	0	0	0
Nebela militaris	0	0	0	0	1	0	0	0	0	0	0
Pseudodifflugia fulva type	3	3	0	0	0	0	0	0	1	0	0
Trigonopyxis arcula var. *minor*	0	0	0	0	0	0	0	0	0	0	0
Trigonopyxis arcula sensu *lato*	0	0	0	0	0	0	0	0	0	0	1
Trigonopyxis arcula var. *major*	0	0	1	2	0	0	0	0	1	0	1

Depth	434	438	442	446	450	454	458	462	466	470	474
Amphitrema flavum	41	9	59	57	72	72	33	47	18	27	21
Amphitrema wrightianum	0	0	0	0	0	0	0	0	0	0	0
Arcella catinus type	0	0	0	0	2	0	1	2	0	0	0
Arcella discoides type	0	0	0	0	0	0	0	0	0	0	0

Assulina muscorum	4	8	1	3	2	3	7	5	5	7	1
Assulina seminulum	2	9	0	5	2	3	9	2	7	18	4
Bullinularia indica	0	0	0	0	0	0	0	0	0	0	0
Centropyxis aculeata type	0	0	0	0	0	0	0	0	0	0	0
Cyclopyxis arcelloides type	2	0	1	0	2	1	3	4	1	3	2
Difflugia pristis type	2	3	1	2	2	3	6	2	1	4	3
Difflugia pulex	41	70	32	25	14	11	35	30	63	38	65
Difflugia rubescens	0	0	0	0	0	0	0	0	0	0	0
Heleopera petricola	2	0	2	3	2	2	0	0	0	0	0
Heleopera sphagni	0	0	0	0	0	0	0	0	0	0	0
Heleopera sylvatica	0	0	0	0	0	0	0	0	0	0	0
Hyalosphenia elegans	0	0	0	0	0	0	0	0	0	0	0
Hyalosphenia papilio	2	0	1	3	2	3	3	5	0	1	0
Hyalosphenia subflava	0	0	0	0	0	0	0	0	0	0	0
Nebela collaris	0	0	0	0	0	0	0	0	0	0	0
Nebela militaris	0	0	1	0	0	0	0	0	0	0	0
Pseudodifflugia fulva type	2	0	1	0	1	1	0	2	2	0	1
Trigonopyxis arcula var. *minor*	0	0	0	0	0	0	0	1	2	1	3
Trigonopyxis arcula sensu *lato*	0	2	1	0	0	1	3	1	1	1	0
Trigonopyxis arcula var. *major*	1	0	1	2	0	0	0	0	0	0	0
Depth	**478**	**482**	**486**	**490**	**494**	**498**	**502**	**506**	**510**	**514**	**518**
Amphitrema flavum	66	27	56	47	39	60	56	64	69	74	10
Amphitrema wrightianum	0	0	0	0	0	0	0	0	0	0	0
Arcella catinus type	0	0	0	0	4	1	1	1	0	0	0
Arcella discoides type	0	0	0	0	0	0	0	0	0	0	0
Assulina muscorum	1	4	3	2	4	2	6	4	8	1	4
Assulina seminulum	6	5	3	2	1	3	4	1	6	3	10
Bullinularia indica	0	1	1	2	0	0	0	0	0	0	0
Centropyxis aculeata type	0	0	0	0	0	0	0	0	0	0	0
Cyclopyxis arcelloides type	3	4	1	2	1	2	1	1	1	0	2
Difflugia pristis type	4	1	1	4	8	4	4	1	2	1	4
Difflugia pulex	19	50	34	40	28	25	20	27	14	20	66
Difflugia rubescens	0	0	0	0	0	0	0	0	0	0	0
Heleopera petricola	0	0	0	0	0	0	0	0	0	0	0
Heleopera sphagni	0	0	0	0	0	0	0	0	0	0	0
Heleopera sylvatica	0	0	0	0	0	0	0	0	0	0	0
Hyalosphenia elegans	0	0	0	0	0	0	0	0	0	1	0
Hyalosphenia papilio	0	1	0	0	1	0	0	0	1	0	0
Hyalosphenia subflava	0	0	0	0	0	0	0	0	0	0	0
Nebela collaris	0	0	0	0	0	0	0	1	0	0	0
Nebela militaris	0	0	0	0	0	0	0	0	0	0	0
Pseudodifflugia fulva type	2	0	1	0	1	0	0	0	0	0	0
Trigonopyxis arcula var. *minor*	0	4	0	0	7	1	3	0	0	0	2
Trigonopyxis arcula sensu *lato*	0	2	1	2	5	3	3	2	0	1	2
Trigonopyxis arcula var. *major*	0	0	0	0	0	0	0	0	0	0	0
Depth	**522**	**526**	**530**	**534**	**538**	**542**	**546**	**550**	**554**	**558**	**562**
Amphitrema flavum	6	12	2	0	0	0	3	2	8	12	46
Amphitrema wrightianum	0	0	0	0	0	0	0	0	0	0	0
Arcella catinus type	0	0	0	0	0	0	0	2	0	0	0
Arcella discoides type	0	0	0	0	0	0	0	0	0	0	0
Assulina muscorum	0	0	6	6	0	0	5	7	0	0	0
Assulina seminulum	0	0	23	11	0	0	13	13	2	0	0
Bullinularia indica	6	0	2	0	0	0	0	4	0	0	0
Centropyxis aculeata type	0	0	0	0	0	0	0	0	0	0	0
Cyclopyxis arcelloides type	2	4	9	11	16	21	10	2	4	4	5
Difflugia pristis type	6	2	13	11	8	3	3	2	0	8	0
Difflugia pulex	56	78	32	39	61	9	5	18	48	44	46
Difflugia rubescens	0	0	0	0	0	0	0	0	0	0	0
Heleopera petricola	0	0	0	0	0	0	0	0	0	0	0
Heleopera sphagni	0	0	0	0	0	0	0	0	0	4	0
Heleopera sylvatica	0	0	0	0	0	0	0	4	0	0	0
Hyalosphenia elegans	0	0	0	0	0	0	0	0	0	0	0
Hyalosphenia papilio	0	0	0	0	0	0	0	0	0	0	0
Hyalosphenia subflava	0	0	0	0	0	3	0	0	0	0	0

Nebela collaris	0	0	0	0	0	0	0	0	0	0	0
Nebela militaris	0	0	0	0	0	0	0	0	0	0	0
Pseudodifflugia fulva type	0	0	6	0	0	0	5	0	4	0	0
Trigonopyxis arcula var. *minor*	8	2	2	6	3	65	58	25	34	28	0
Trigonopyxis arcula sensu *lato*	16	2	6	11	13	0	0	22	0	0	3
Trigonopyxis arcula var. *major*	0	0	0	6	0	0	0	0	0	0	0

Depth	**566**	**570**	**574**
Amphitrema flavum	64	71	78
Amphitrema wrightianum	0	0	0
Arcella catinus type	0	2	0
Arcella discoides type	0	9	6
Assulina muscorum	4	7	0
Assulina seminulum	4	0	0
Bullinularia indica	0	0	0
Centropyxis aculeata type	0	0	0
Cyclopyxis arcelloides type	4	2	0
Difflugia pristis type	4	2	6
Difflugia pulex	16	5	8
Difflugia rubescens	0	0	3
Heleopera petricola	0	0	0
Heleopera sphagni	0	0	0
Heleopera sylvatica	0	0	0
Hyalosphenia elegans	0	0	0
Hyalosphenia papilio	0	0	0
Hyalosphenia subflava	0	0	0
Nebela collaris	0	0	0
Nebela militaris	0	0	0
Pseudodifflugia fulva type	0	0	0
Trigonopyxis arcula var. *minor*	2	0	0
Trigonopyxis arcula sensu *lato*	2	2	0
Trigonopyxis arcula var. *major*	0	0	0

5. Gällseredsmossen

Plant macrofossils

Depth	322	326	330	334	338	342	346	350	354	358
UOM	2	2	2	5	3	1	2	4	2	4
Total Ericaceae	43	9	14	70	23	17	9	21	13	35
Total Monocotyledon	3	2	6	15	9	3	2	4	3	4
Total Brown mosses	1	0	0	0	0	0	0	6	0	5
Total *Sphagnum* spp.	51	88	79	10	65	78	87	64	80	53
Charcoal	0	0	0	0	0	0	0	0	0	0
Charred remains	0	1	0	0	0	0	1	1	0	0
Ericaceae rootlets (undiff.)	34	8	11	57	20	15	6	17	13	30
Ericaceae bark (undiff.)	3	0	1	6	1	0	1	0	0	2
Ericaceae wood (undiff.)	2	1	2	6	1	2	2	1	0	2
Calluna vulgaris stem	2	0	0	0	1	0	0	0	0	1
Calluna vulgaris leaves	0	0	0	0	0	0	0	0	0	0
Calluna vulgaris seeds	0	0	0	0	0	0	0	0	0	0
Erica tetralix seeds	0	0	0	0	0	0	0	0	3	0
Vaccinium oxycoccus	2	0	0	1	0	0	0	3	0	0
Monocotyledon roots (undiff.)	3	1	0	3	2	1	1	1	2	2
Phragmites australis epidermis	0	0	0	0	0	0	0	0	0	0
Scheuchzeria palustris epidermis	0	0	0	0	0	0	0	0	0	0
Trichophorum cespitosum epidermis	0	0	0	3	0	0	0	0	0	0
Eriophorum vaginatum roots	0	0	6	8	4	2	1	3	1	2
Eriophorum vaginatum spindles	0	0	3	21	0	0	0	0	0	0
Eriophorum vaginatum epidermis	0	0	0	1	3	0	0	0	0	0
Eriophorum angustifolium epidermis	0	1	0	0	0	0	0	0	0	0
Brown mosses (undiff.) stems	0	0	0	0	0	0	0	0	0	5
Dicranum scoparium	1	0	0	0	0	0	0	0	0	0
Aulacomnium palustre	0	0	0	0	0	0	0	6	0	0
Calliergon cordifolium	0	0	0	0	0	0	0	0	0	0
Hypnum jutlandicum	0	0	0	0	0	0	0	0	0	0
Sphagnum austinii	19	41	23	5	56	42	57	27	10	6
Sphagnum magellanicum	0	0	0	0	0	1	0	0	0	0
Sphagnum papillosum	0	0	0	0	0	0	0	2	0	0
Sphagnum section *Acutifolia*	32	47	56	4	9	36	30	36	70	47
Sphagnum section *Cuspidata*	0	0	0	0	0	0	0	0	0	0
Acarid mites	3	0	0	0	0	6	0	0	0	6
Cennococcum spp.	6	15	21	0	6	0	0	18	18	12

Depth	362	366	370	374	378	382	386	390	394	398
UOM	3	6	4	2	2	4	2	2	2	2
Total Ericaceae	19	37	22	14	12	43	7	7	13	27
Total Monocotyledon	3	3	7	5	3	2	4	10	2	6
Total Brown mosses	0	2	0	0	0	13	1	1	0	1
Total *Sphagnum* spp.	74	52	66	80	83	39	85	79	82	64
Charcoal	0	0	0	0	0	0	0	0	0	0
Charred remains	0	2	1	0	0	0	0	0	1	0
Ericaceae rootlets (undiff.)	16	33	18	10	9	39	6	5	12	26
Ericaceae bark (undiff.)	0	2	1	1	1	2	0	1	0	1
Ericaceae wood (undiff.)	2	2	2	3	1	2	1	0	1	0
Calluna vulgaris stem	0	0	0	0	0	0	0	0	0	0
Calluna vulgaris leaves	0	0	0	0	0	0	0	0	0	0
Calluna vulgaris seeds	0	0	0	0	0	0	0	0	0	0

Erica tetralix seeds	0	0	0	0	6	6	3	0	6	0
Vaccinium oxycoccus	1	0	1	0	1	0	0	1	0	0
Monocotyledon roots (undiff.)	1	1	3	1	3	2	4	3	1	2
Phragmites australis epidermis	0	0	0	0	0	0	0	0	0	0
Scheuchzeria palustris epidermis	0	0	0	0	0	0	0	0	0	0
Trichophorum cespitosum epidermis	0	0	0	0	0	0	0	0	0	0
Eriophorum vaginatum roots	2	2	3	4	0	0	0	7	1	4
Eriophorum vaginatum spindles	0	0	0	0	0	0	0	3	0	0
Eriophorum vaginatum epidermis	0	0	1	0	0	0	0	0	0	0
Eriophorum angustifolium epidermis	0	0	0	0	0	0	0	0	0	0
Brown mosses (undiff.) stems	0	2	0	0	0	9	0	0	0	0
Dicranum scoparium	0	0	0	0	0	0	0	0	0	1
Aulacomnium palustre	0	0	0	0	0	4	0	0	0	0
Calliergon cordifolium	0	0	0	0	0	0	1	1	0	0
Hypnum jutlandicum	0	0	0	0	0	0	0	0	0	0
Sphagnum austinii	3	3	1	2	1	0	0	3	0	16
Sphagnum magellanicum	0	0	0	0	0	0	0	0	0	0
Sphagnum papillosum	0	0	0	0	0	0	0	0	0	0
Sphagnum section *Acutifolia*	71	50	65	78	82	39	85	75	82	48
Sphagnum section *Cuspidata*	0	0	0	0	0	0	0	0	0	0
Acarid mites	0	0	0	0	0	0	0	3	0	0
Cennococcum spp.	3	9	6	0	0	15	0	3	3	0
Depth	**402**	**406**	**410**	**414**	**418**	**422**	**426**	**430**	**434**	**438**
UOM	3	4	4	11	6	4	3	6	8	6
Total Ericaceae	19	15	15	21	20	14	12	25	22	31
Total Monocotyledon	5	6	4	57	6	9	3	4	10	19
Total Brown mosses	0	0	0	0	1	0	4	1	4	2
Total *Sphagnum* spp.	72	73	76	11	67	74	79	64	57	40
Charcoal	0	0	0	0	0	0	0	0	0	0
Charred remains	1	0	0	0	0	0	0	1	0	0
Ericaceae rootlets (undiff.)	19	14	13	12	17	13	10	23	20	27
Ericaceae bark (undiff.)	0	0	1	6	0	0	2	0	2	3
Ericaceae wood (undiff.)	0	1	1	2	1	1	0	1	0	0
Calluna vulgaris stem	0	0	0	0	0	0	0	0	0	0
Calluna vulgaris leaves	0	0	0	0	0	0	0	0	0	0
Calluna vulgaris seeds	0	0	0	0	0	0	6	0	0	0
Erica tetralix seeds	3	0	3	0	0	0	0	0	6	6
Vaccinium oxycoccus	0	0	0	1	2	0	0	1	0	1
Monocotyledon roots (undiff.)	2	4	3	2	3	5	3	2	10	6
Phragmites australis epidermis	0	0	0	0	0	0	0	0	0	0
Scheuchzeria palustris epidermis	0	0	0	0	0	0	0	0	0	0
Trichophorum cespitosum epidermis	0	0	0	0	0	0	0	0	0	4
Eriophorum vaginatum roots	3	1	0	9	3	3	0	2	0	2
Eriophorum vaginatum spindles	0	0	0	15	0	0	0	0	0	3
Eriophorum vaginatum epidermis	0	1	1	46	0	1	0	0	0	7
Eriophorum angustifolium epidermis	0	0	0	0	0	0	0	0	0	0
Brown mosses (undiff.) stems	0	0	0	0	1	0	0	0	0	0
Dicranum scoparium	0	0	0	0	0	0	0	0	0	0
Aulacomnium palustre	0	0	0	0	0	0	4	1	3	0
Calliergon cordifolium	0	0	0	0	0	0	0	0	0	0
Hypnum jutlandicum	0	0	0	0	0	0	0	0	1	2
Sphagnum austinii	3	59	23	6	4	1	0	0	0	3
Sphagnum magellanicum	0	0	1	0	0	0	0	0	0	0
Sphagnum papillosum	0	0	0	0	0	0	0	0	0	0
Sphagnum section *Acutifolia*	68	14	53	5	63	72	79	64	57	37
Sphagnum section *Cuspidata*	0	0	0	0	0	1	0	0	0	0
Acarid mites	0	0	0	0	0	0	0	3	0	0
Cennococcum spp.	0	6	3	0	0	3	0	9	0	0
Depth	**442**	**446**	**450**	**454**	**458**	**462**	**466**	**470**	**474**	**478**
UOM	8	7	30	14	25	14	4	3	9	8

Total Ericaceae	5	13	16	19	10	12	20	16	63	26
Total Monocotyledon	85	25	25	13	18	30	12	12	24	54
Total Brown mosses	0	0	0	0	0	0	0	0	0	0
Total *Sphagnum* spp.	2	53	29	54	47	45	60	69	3	13
Charcoal	0	0	0	0	0	0	3	0	0	0
Charred remains	0	0	0	1	2	1	12	1	5	4
Ericaceae rootlets (undiff.)	2	13	12	17	8	11	16	13	58	25
Ericaceae bark (undiff.)	1	0	1	1	0	0	0	1	2	0
Ericaceae wood (undiff.)	0	0	2	1	2	1	0	0	2	0
Calluna vulgaris stem	0	0	1	0	0	0	1	1	1	1
Calluna vulgaris leaves	0	0	0	0	0	0	2	0	0	0
Calluna vulgaris seeds	0	0	0	0	0	0	0	0	0	0
Erica tetralix seeds	0	0	0	0	0	9	3	0	0	3
Vaccinium oxycoccus	2	0	0	0	0	0	1	1	0	0
Monocotyledon roots (undiff.)	4	13	6	12	15	21	7	6	7	22
Phragmites australis epidermis	0	0	0	0	0	0	0	0	0	0
Scheuchzeria palustris epidermis	3	0	0	0	0	0	0	0	0	0
Trichophorum cespitosum epidermis	9	0	0	0	0	0	0	0	10	30
Eriophorum vaginatum roots	15	7	19	1	3	9	5	3	3	2
Eriophorum vaginatum spindles	6	0	0	0	0	0	0	0	0	0
Eriophorum vaginatum epidermis	53	5	0	0	0	0	0	3	4	0
Eriophorum angustifolium epidermis	1	0	0	0	0	0	0	0	0	0
Brown mosses (undiff.) stems	0	0	0	0	0	0	0	0	0	0
Dicranum scoparium	0	0	0	0	0	0	0	0	0	0
Aulacomnium palustre	0	0	0	0	0	0	0	0	0	0
Calliergon cordifolium	0	0	0	0	0	0	0	0	0	0
Hypnum jutlandicum	0	0	0	0	0	0	0	0	0	0
Sphagnum austinii	1	0	0	0	0	0	0	1	1	1
Sphagnum magellanicum	0	0	0	0	0	0	0	0	0	1
Sphagnum papillosum	0	0	0	0	0	0	0	0	0	0
Sphagnum section *Acutifolia*	1	53	29	54	47	44	41	19	2	11
Sphagnum section *Cuspidata*	0	0	0	0	0	1	18	49	0	0
Acarid mites	0	3	0	0	0	0	6	3	0	6
Cennococcum spp.	12	12	6	27	48	9	3	0	12	0
Depth	**482**	**486**	**490**	**494**	**498**	**502**	**506**	**510**	**514**	**518**
UOM	5	5	2	5	7	5	8	2	10	4
Total Ericaceae	44	20	6	6	14	42	7	3	7	6
Total Monocotyledon	50	67	12	16	76	29	8	5	21	18
Total Brown mosses	0	5	2	12	0	0	0	0	0	0
Total *Sphagnum* spp.	1	3	78	61	1	20	74	89	59	73
Charcoal	2	0	0	0	1	4	2	0	3	0
Charred remains	0	0	0	0	7	0	2	1	4	1
Ericaceae rootlets (undiff.)	43	18	4	6	9	28	7	2	5	3
Ericaceae bark (undiff.)	1	1	1	0	3	3	0	1	2	0
Ericaceae wood (undiff.)	0	0	1	0	1	11	0	0	0	3
Calluna vulgaris stem	0	0	0	0	0	0	0	0	0	0
Calluna vulgaris leaves	0	0	0	0	0	0	0	0	0	0
Calluna vulgaris seeds	0	0	0	0	0	0	0	0	0	0
Erica tetralix seeds	0	0	0	0	0	0	0	0	0	0
Vaccinium oxycoccus	0	1	0	0	1	0	0	0	0	0
Monocotyledon roots (undiff.)	10	5	10	10	4	4	6	5	17	16
Phragmites australis epidermis	0	0	0	0	0	0	0	0	0	0
Scheuchzeria palustris epidermis	0	0	0	0	0	0	0	0	0	0
Trichophorum cespitosum epidermis	1	0	0	0	0	0	0	0	0	0
Eriophorum vaginatum roots	9	29	2	0	4	0	2	0	2	2
Eriophorum vaginatum spindles	0	9	0	0	3	3	0	0	0	0
Eriophorum vaginatum epidermis	30	33	0	6	68	25	0	0	2	0
Eriophorum angustifolium epidermis	0	0	0	0	0	0	0	0	0	0
Brown mosses (undiff.) stems	0	5	2	6	0	0	0	0	0	0
Dicranum scoparium	0	0	0	0	0	0	0	0	0	0
Aulacomnium palustre	0	0	0	6	0	0	0	0	0	0
Calliergon cordifolium	0	0	0	0	0	0	0	0	0	0

Hypnum jutlandicum	0	0	0	0	0	0	0	0	0	0
Sphagnum austinii	0	1	0	0	0	0	0	0	0	0
Sphagnum magellanicum	0	0	0	0	0	0	0	0	0	0
Sphagnum papillosum	0	0	0	0	0	0	0	0	0	0
Sphagnum section *Acutifolia*	1	2	78	61	1	20	74	89	59	73
Sphagnum section *Cuspidata*	0	0	0	0	0	0	0	0	0	0
Acarid mites	3	0	0	0	0	0	0	0	3	0
Cennococcum spp.	9	6	0	24	36	78	12	0	12	9
Depth	**522**	**526**	**530**	**534**	**538**	**542**	**546**	**522**	**526**	**530**
UOM	5	13	9	52	15	29	33	5	13	9
Total Ericaceae	32	18	15	15	8	8	6	32	18	15
Total Monocotyledon	34	35	69	31	76	65	61	34	35	69
Total Brown mosses	0	1	0	0	0	0	0	0	1	0
Total *Sphagnum* spp.	29	33	7	1	0	0	0	29	33	7
Charcoal	0	0	0	0	0	0	0	0	0	0
Charred remains	2	0	1	0	0	1	0	2	0	1
Ericaceae rootlets (undiff.)	25	8	11	3	3	1	0	25	8	11
Ericaceae bark (undiff.)	0	3	0	3	0	4	2	0	3	0
Ericaceae wood (undiff.)	4	7	4	9	5	3	4	4	7	4
Calluna vulgaris stem	0	0	0	0	0	0	0	0	0	0
Calluna vulgaris leaves	0	0	0	0	0	0	0	0	0	0
Calluna vulgaris seeds	0	0	0	0	0	0	0	0	0	0
Erica tetralix seeds	0	0	0	0	0	0	0	0	0	0
Vaccinium oxycoccus	3	0	0	0	0	0	0	3	0	0
Monocotyledon roots (undiff.)	4	8	11	10	33	12	10	4	8	11
Phragmites australis epidermis	0	0	0	0	21	53	51	0	0	0
Scheuchzeria palustris epidermis	0	0	0	0	0	0	0	0	0	0
Trichophorum cespitosum epidermis	0	0	0	0	0	0	0	0	0	0
Eriophorum vaginatum roots	1	12	7	3	0	0	0	1	12	7
Eriophorum vaginatum spindles	0	6	0	0	0	0	0	0	6	0
Eriophorum vaginatum epidermis	29	15	51	18	22	0	0	29	15	51
Eriophorum angustifolium epidermis	0	0	0	0	0	0	0	0	0	0
Brown mosses (undiff.) stems	0	0	0	0	0	0	0	0	0	0
Dicranum scoparium	0	0	0	0	0	0	0	0	0	0
Aulacomnium palustre	0	1	0	0	0	0	0	0	1	0
Calliergon cordifolium	0	0	0	0	0	0	0	0	0	0
Hypnum jutlandicum	0	0	0	0	0	0	0	0	0	0
Sphagnum austinii	1	0	1	0	0	0	0	1	0	1
Sphagnum magellanicum	0	32	6	0	0	0	0	0	32	6
Sphagnum papillosum	0	0	0	0	0	0	0	0	0	0
Sphagnum section *Acutifolia*	25	0	0	0	0	0	0	25	0	0
Sphagnum section *Cuspidata*	3	0	0	0	0	0	0	3	0	0
Acarid mites	0	0	0	0	0	0	0	0	0	0
Cennococcum spp.	12	15	21	0	0	24	12	12	15	21

Testate amoebae

Depth	322	326	330	334	338	342	346	350	354	358	362
Amphitrema flavum	8	16	31	0	0	0	2	13	0	0	0
Amphitrema stenostoma	2	0	0	0	0	0	0	0	0	0	0
Amphitrema wrightianum	0	0	0	0	0	0	0	0	0	0	0
Arcella catinus type	0	0	0	0	0	0	0	0	0	0	0
Arcella discoides type	0	0	0	0	0	0	0	2	0	0	0
Assulina muscorum	31	5	5	3	7	8	14	6	6	8	8
Assulina seminulum	2	3	0	2	4	8	11	0	2	2	4
Bullinularia indica	0	2	0	2	0	0	0	0	0	0	6

Centropyxis cassis type	2	0	0	0	0	0	0	0	0	0	0
Corythion-Trinema type	0	0	0	0	0	0	0	0	0	0	0
Cyclopyxis arcelloides type	25	20	22	10	18	28	28	31	32	14	36
Cryptodifflugia oviformis	0	0	0	0	0	0	0	0	0	0	0
Difflugia bacillariarum	0	0	0	0	2	0	0	0	0	0	0
Difflugia globulosa	0	0	0	0	0	0	0	0	0	0	0
Difflugia lucida type	0	0	0	0	0	0	0	0	0	0	0
Difflugia oblonga type	0	0	0	0	2	0	0	0	0	0	0
Difflugia pristis type	16	9	5	13	2	0	4	8	8	2	6
Difflugia pulex	12	34	36	55	60	54	33	38	47	65	34
Difflugia rubescens	0	0	0	0	0	0	0	0	0	0	0
Euglypha rotunda type	0	0	0	0	0	0	0	0	0	0	0
Euglypha tuberculata type	0	0	0	0	0	0	0	0	0	0	0
Habrotrocha argusticolis	0	0	0	0	0	0	0	0	0	0	0
Heleopera petricola	0	0	0	0	0	0	0	0	0	0	0
Heleopera sphagni	0	0	0	0	0	0	0	0	0	0	0
Heleopera sylvatica	0	0	0	0	0	0	2	0	4	0	0
Hyalosphenia elegans	0	0	0	0	0	0	0	0	0	0	0
Hyalosphenia papilio	0	0	0	0	0	0	0	0	0	0	0
Hyalosphenia subflava	0	0	0	0	0	0	0	0	0	0	0
Nebela collaris	0	0	0	0	0	0	0	0	0	0	0
Nebela griseola type	0	0	0	0	0	0	0	0	0	0	0
Nebela militaris	2	5	0	0	0	0	0	0	0	0	0
Nebela minor	0	0	0	0	0	0	0	0	0	0	0
Nebela parvula	0	0	0	0	0	0	0	0	0	0	0
Nebela tincta	0	0	0	0	0	0	0	0	0	0	0
Pseudodifflugia fulva type	0	3	0	15	2	3	0	0	0	4	4
Sphenoderia lenta	0	0	0	0	0	0	0	0	0	0	0
Trigonopyxis arcula var. *minor*	0	0	0	0	0	0	0	0	0	2	0
Trigonopyxis arcula sensu *lato*	0	3	0	0	2	0	7	2	0	2	2
Trinema lineare	0	0	0	0	2	0	0	0	2	0	0
Depth	**366**	**370**	**374**	**378**	**382**	**386**	**390**	**394**	**398**	**402**	**406**
Amphitrema flavum	0	0	0	42	2	10	12	0	6	0	15
Amphitrema stenostoma	0	0	0	0	0	0	0	0	0	0	0
Amphitrema wrightianum	0	0	0	0	0	0	0	0	0	0	0
Arcella catinus type	0	0	2	0	0	0	0	0	0	2	0
Arcella discoides type	0	0	0	1	0	0	0	0	0	0	0
Assulina muscorum	2	6	2	5	2	6	15	0	14	14	11
Assulina seminulum	6	6	9	5	8	1	5	0	0	2	4
Bullinularia indica	0	2	0	0	2	0	0	2	0	0	0
Centropyxis cassis type	0	0	0	0	0	0	0	0	0	0	0
Corythion-Trinema type	0	0	0	0	0	0	0	0	0	0	0
Cyclopyxis arcelloides type	8	18	9	21	17	13	27	36	10	16	16
Cryptodifflugia oviformis	0	0	0	0	0	0	0	0	0	0	0
Difflugia bacillariarum	0	0	0	0	0	0	0	0	0	0	0
Difflugia globulosa	0	0	0	0	0	0	0	0	0	0	0
Difflugia lucida type	0	0	0	0	0	0	0	0	0	0	0
Difflugia oblonga type	0	0	0	0	0	0	0	0	0	0	0
Difflugia pristis type	4	8	10	7	13	4	2	2	2	8	4
Difflugia pulex	74	57	43	11	53	60	22	42	50	51	42
Difflugia rubescens	0	2	0	0	0	0	1	0	4	0	0
Euglypha rotunda type	0	0	0	0	0	0	0	0	0	0	0
Euglypha tuberculata type	0	0	0	1	0	0	0	0	0	0	0
Habrotrocha argusticolis	0	0	0	0	0	0	0	0	0	0	0
Heleopera petricola	0	0	0	0	0	0	1	0	0	0	0
Heleopera sphagni	0	0	0	0	0	0	0	0	0	0	0
Heleopera sylvatica	0	0	2	0	0	0	0	0	0	0	0
Hyalosphenia elegans	0	0	2	0	0	0	0	0	2	0	0
Hyalosphenia papilio	0	0	3	6	2	1	0	0	0	0	2
Hyalosphenia subflava	0	0	0	0	0	0	0	0	2	2	2
Nebela collaris	0	0	0	0	0	0	1	0	0	0	0
Nebela griseola type	0	0	0	0	0	0	0	0	0	0	0

Nebela militaris	0	2	16	1	0	4	5	8	2	0	4
Nebela minor	0	0	0	0	0	0	0	0	0	0	0
Nebela parvula	0	0	0	0	0	0	0	0	0	0	0
Nebela tincta	0	0	0	0	0	0	0	0	0	0	0
Pseudodifflugia fulva type	4	0	0	0	2	0	0	0	8	6	2
Sphenoderia lenta	0	0	0	0	0	0	5	0	0	0	0
Trigonopyxis arcula var. *minor*	0	0	0	0	0	0	2	0	0	0	0
Trigonopyxis arcula sensu *lato*	2	0	3	0	0	0	0	10	0	0	0
Trinema lineare	0	0	0	0	0	0	0	0	0	0	0
Depth	**410**	**414**	**418**	**422**	**426**	**430**	**434**	**438**	**442**	**446**	**450**
Amphitrema flavum	31	6	0	0	6	9	19	9	11	43	0
Amphitrema stenostoma	0	0	0	0	0	0	0	0	0	0	0
Amphitrema wrightianum	0	0	0	0	0	0	0	0	0	0	0
Arcella catinus type	0	0	0	0	0	0	0	0	0	0	0
Arcella discoides type	0	0	0	0	0	0	0	0	0	0	0
Assulina muscorum	4	12	9	45	5	3	2	26	2	2	7
Assulina seminulum	6	9	0	4	5	2	0	4	4	2	2
Bullinularia indica	0	0	0	0	0	0	0	0	0	0	2
Centropyxis cassis type	0	0	0	0	0	0	0	0	0	0	0
Corythion-Trinema type	0	0	0	0	0	0	0	0	0	0	0
Cyclopyxis arcelloides type	12	16	21	8	34	24	12	19	15	15	33
Cryptodifflugia oviformis	0	0	0	0	0	0	0	0	0	0	0
Difflugia bacillariarum	0	0	0	0	0	0	0	0	0	0	0
Difflugia globulosa	0	0	0	0	0	0	0	0	0	0	0
Difflugia lucida type	0	0	0	0	0	0	0	0	0	4	0
Difflugia oblonga type	0	0	0	0	0	0	0	0	0	0	0
Difflugia pristis type	8	3	9	0	6	2	10	4	13	0	15
Difflugia pulex	37	48	62	40	31	47	55	28	52	26	37
Difflugia rubescens	0	0	0	0	0	0	0	1	0	0	0
Euglypha rotunda type	0	0	0	0	0	0	0	0	0	0	0
Euglypha tuberculata type	0	0	0	0	0	0	0	0	0	0	0
Habrotrocha argusticolis	0	0	0	0	0	0	0	0	0	0	0
Heleopera petricola	0	0	0	0	0	0	0	0	0	0	0
Heleopera sphagni	0	0	0	0	2	2	0	0	0	0	0
Heleopera sylvatica	0	0	0	0	0	0	0	0	0	0	0
Hyalosphenia elegans	0	0	0	2	0	0	0	0	0	0	0
Hyalosphenia papilio	2	1	0	0	0	0	0	0	0	2	0
Hyalosphenia subflava	0	3	0	2	0	2	0	0	0	4	0
Nebela collaris	0	0	0	0	0	0	0	1	0	0	0
Nebela griseola type	0	0	0	0	0	0	0	0	0	0	0
Nebela militaris	0	1	0	0	6	5	2	1	2	2	5
Nebela minor	0	0	0	0	0	3	0	0	0	0	0
Nebela parvula	0	0	0	0	0	2	0	0	0	0	0
Nebela tincta	0	0	0	0	3	2	0	0	0	0	0
Pseudodifflugia fulva type	0	0	0	0	2	0	0	0	0	0	0
Sphenoderia lenta	0	0	0	0	0	0	0	0	0	0	0
Trigonopyxis arcula var. *minor*	0	0	0	0	0	0	0	0	0	0	0
Trigonopyxis arcula sensu *lato*	2	1	0	0	0	0	0	4	0	0	0
Trinema lineare	0	0	0	0	0	0	0	0	0	0	0
Depth	**454**	**458**	**462**	**466**	**470**	**474**	**478**	**482**	**486**	**490**	**494**
Amphitrema flavum	19	9	61	68	37	15	27	9	3	7	6
Amphitrema stenostoma	0	0	0	0	0	0	0	0	0	0	0
Amphitrema wrightianum	0	0	5	0	0	0	0	0	0	0	0
Arcella catinus type	0	0	0	1	0	0	0	0	0	7	0
Arcella discoides type	0	0	0	0	0	0	0	0	0	0	0
Assulina muscorum	29	2	3	14	19	2	27	23	25	33	48
Assulina seminulum	7	0	0	4	3	4	17	9	6	0	0
Bullinularia indica	0	0	0	0	0	2	0	0	0	0	0
Centropyxis cassis type	0	0	0	0	0	0	0	0	0	0	0
Corythion-Trinema type	0	0	0	0	0	0	0	0	0	0	0
Cyclopyxis arcelloides type	26	28	15	8	9	17	0	5	13	7	9

Cryptodifflugia oviformis	0	0	0	0	2	0	0	0	0	0	0
Difflugia bacillariarum	0	0	0	0	0	0	0	0	0	0	0
Difflugia globulosa	0	0	0	0	0	0	0	0	0	0	0
Difflugia lucida type	0	0	0	0	0	0	0	0	0	0	0
Difflugia oblonga type	0	0	0	0	0	0	0	0	0	0	0
Difflugia pristis type	1	6	8	1	2	21	2	0	0	7	0
Difflugia pulex	10	50	5	3	21	35	17	32	38	40	15
Difflugia rubescens	0	0	0	0	0	0	2	0	0	0	3
Euglypha rotunda type	0	0	0	0	0	0	2	0	0	0	0
Euglypha tuberculata type	0	0	0	0	0	0	0	0	0	0	0
Habrotrocha argusticolis	0	0	0	0	0	0	0	0	0	0	6
Heleopera petricola	0	0	0	0	0	0	0	0	0	0	0
Heleopera sphagni	0	0	0	0	0	0	0	0	0	0	0
Heleopera sylvatica	0	0	0	0	2	0	0	0	0	0	0
Hyalosphenia elegans	0	0	0	0	0	0	0	0	0	0	0
Hyalosphenia papilio	1	0	0	0	0	0	0	0	0	0	0
Hyalosphenia subflava	0	0	0	0	1	0	2	0	0	0	6
Nebela collaris	0	0	0	0	0	0	0	0	0	0	0
Nebela griseola type	0	0	5	0	0	0	0	0	0	0	0
Nebela militaris	4	5	0	0	1	0	2	0	0	0	3
Nebela minor	0	0	0	0	0	0	0	0	0	0	0
Nebela parvula	0	0	0	0	0	0	0	0	0	0	0
Nebela tincta	1	0	0	0	0	0	0	0	0	0	0
Pseudodifflugia fulva type	0	0	0	0	1	4	2	9	6	0	0
Sphenoderia lenta	0	0	0	0	0	0	0	0	0	0	0
Trigonopyxis arcula var. *minor*	0	0	0	0	0	0	0	0	0	0	0
Trigonopyxis arcula sensu *lato*	1	0	0	0	0	0	0	14	9	0	3
Trinema lineare	0	0	0	0	0	0	0	0	0	0	0
Depth	**498**	**502**	**506**	**510**	**514**	**518**	**522**	**526**	**530**	**534**	**538**
Amphitrema flavum	0	6	12	2	8	82	32	39	7	9	2
Amphitrema stenostoma	0	0	0	0	0	0	0	0	0	0	0
Amphitrema wrightianum	0	0	0	0	0	0	0	0	0	0	0
Arcella catinus type	0	0	4	4	0	0	0	0	0	0	0
Arcella discoides type	0	0	0	0	0	0	0	0	0	0	0
Assulina muscorum	33	19	10	41	12	10	8	35	5	2	4
Assulina seminulum	0	3	2	2	8	4	4	14	5	4	2
Bullinularia indica	0	0	2	0	0	0	0	1	0	0	0
Centropyxis cassis type	0	0	0	0	0	0	0	0	0	0	0
Corythion-Trinema type	0	0	0	0	0	0	0	3	0	6	2
Cyclopyxis arcelloides type	7	0	19	6	4	0	2	1	11	7	12
Cryptodifflugia oviformis	0	0	0	0	0	0	0	0	0	0	0
Difflugia bacillariarum	0	0	0	0	0	0	0	0	0	0	0
Difflugia globulosa	0	0	0	0	0	1	0	1	0	0	0
Difflugia lucida type	0	0	0	0	0	0	0	0	0	0	0
Difflugia oblonga type	0	0	0	0	0	0	0	0	0	0	0
Difflugia pristis type	13	3	6	2	6	1	2	0	9	6	2
Difflugia pulex	47	56	42	37	56	1	49	3	53	56	58
Difflugia rubescens	0	0	0	2	0	0	0	0	0	0	0
Euglypha rotunda type	0	0	0	0	0	0	0	0	0	0	0
Euglypha tuberculata type	0	0	0	0	0	0	0	0	0	0	0
Habrotrocha argusticolis	0	0	0	0	0	0	0	0	0	0	0
Heleopera petricola	0	0	0	0	0	0	0	1	0	0	0
Heleopera sphagni	0	0	0	0	0	0	0	0	0	0	0
Heleopera sylvatica	0	0	0	0	0	0	0	0	4	4	8
Hyalosphenia elegans	0	0	0	0	0	0	0	0	0	0	0
Hyalosphenia papilio	0	0	0	0	0	0	0	1	0	0	0
Hyalosphenia subflava	0	0	0	0	0	0	0	0	0	0	0
Nebela collaris	0	0	0	0	0	0	0	0	0	0	0
Nebela griseola type	0	0	0	0	0	0	0	0	0	0	0
Nebela militaris	0	6	0	2	0	0	0	0	2	4	2
Nebela minor	0	0	0	0	0	0	0	0	0	0	2
Nebela parvula	0	0	0	0	0	0	0	0	0	0	0

Nebela tincta	0	6	0	0	0	0	0	0	2	4	2
Pseudodifflugia fulva type	0	0	4	2	4	0	4	0	0	0	4
Sphenoderia lenta	0	0	0	0	0	0	0	0	0	0	0
Trigonopyxis arcula var. *minor*	0	0	0	0	2	0	0	0	0	0	0
Trigonopyxis arcula sensu *lato*	0	0	0	0	0	0	0	0	2	0	0
Trinema lineare	0	0	0	0	0	0	0	0	0	0	2
Depth	**542**	**546**	**542**	**546**	**542**	**546**	**542**	**546**	**542**	**546**	**542**
Amphitrema flavum	19	21	19	21	19	21	19	21	19	21	19
Amphitrema stenostoma	0	0	0	0	0	0	0	0	0	0	0
Amphitrema wrightianum	0	0	0	0	0	0	0	0	0	0	0
Arcella catinus type	0	0	0	0	0	0	0	0	0	0	0
Arcella discoides type	0	0	0	0	0	0	0	0	0	0	0
Assulina muscorum	6	2	6	2	6	2	6	2	6	2	6
Assulina seminulum	1	2	1	2	1	2	1	2	1	2	1
Bullinularia indica	0	0	0	0	0	0	0	0	0	0	0
Centropyxis cassis type	0	0	0	0	0	0	0	0	0	0	0
Corythion-Trinema type	3	2	3	2	3	2	3	2	3	2	3
Cyclopyxis arcelloides type	9	5	9	5	9	5	9	5	9	5	9
Cryptodifflugia oviformis	0	0	0	0	0	0	0	0	0	0	0
Difflugia bacillariarum	0	0	0	0	0	0	0	0	0	0	0
Difflugia globulosa	0	0	0	0	0	0	0	0	0	0	0
Difflugia lucida type	0	0	0	0	0	0	0	0	0	0	0
Difflugia oblonga type	0	0	0	0	0	0	0	0	0	0	0
Difflugia pristis type	1	3	1	3	1	3	1	3	1	3	1
Difflugia pulex	49	50	49	50	49	50	49	50	49	50	49
Difflugia rubescens	0	0	0	0	0	0	0	0	0	0	0
Euglypha rotunda type	0	0	0	0	0	0	0	0	0	0	0
Euglypha tuberculata type	0	0	0	0	0	0	0	0	0	0	0
Habrotrocha argusticolis	0	0	0	0	0	0	0	0	0	0	0
Heleopera petricola	0	0	0	0	0	0	0	0	0	0	0
Heleopera sphagni	0	0	0	0	0	0	0	0	0	0	0
Heleopera sylvatica	1	2	1	2	1	2	1	2	1	2	1
Hyalosphenia elegans	0	0	0	0	0	0	0	0	0	0	0
Hyalosphenia papilio	0	0	0	0	0	0	0	0	0	0	0
Hyalosphenia subflava	0	0	0	0	0	0	0	0	0	0	0
Nebela collaris	0	0	0	0	0	0	0	0	0	0	0
Nebela griseola type	0	0	0	0	0	0	0	0	0	0	0
Nebela militaris	7	3	7	3	7	3	7	3	7	3	7
Nebela minor	1	0	1	0	1	0	1	0	1	0	1
Nebela parvula	0	0	0	0	0	0	0	0	0	0	0
Nebela tincta	0	5	0	5	0	5	0	5	0	5	0
Pseudodifflugia fulva type	0	0	0	0	0	0	0	0	0	0	0
Sphenoderia lenta	0	0	0	0	0	0	0	0	0	0	0
Trigonopyxis arcula var. *minor*	0	0	0	0	0	0	0	0	0	0	0
Trigonopyxis arcula sensu *lato*	0	0	0	0	0	0	0	0	0	0	0
Trinema lineare	3	5	3	5	3	5	3	5	3	5	3

6. Swedish testate amoebae-based transfer function

7. Environmental variables

Site	Grid X	Grid Y	WTD (cm)	% Moisture	EC	pH
S7-1	6336058	1316830	10	93.14	45	4.09
S7-2	6336057	1316822	16	88.42	98	3.75
S7-3	6336053	1316818	45	94.34	52	3.52
S7-4	6336051	1316815	2	92.36	82	4.26
S7-5	6336055	1316809	36	81.58	107	3.53
S7-6	6336053	1316806	0	92.95	106	4.20
S7-7	6336055	1316800	17	94.35	108	3.42
S7-8	6336056	1316792	5	94.83	97	3.92
S7-9	6336056	1316789	25	94.62	82	3.91
S7-10	6336042	1316781	27	95.96	45	3.59
S7-11	6336037	1316790	10	85.00	54	3.79
S7-12	6336033	1316804	0	94.24	61	4.21
S7-13	6336035	1316807	12	91.12	48	4.17
S7-14	6336032	1316810	28	94.17	66	3.50
S7-15	6336033	1316814	0	95.76	116	3.80
S11-1	6342783	1312960	14	95.93	94	4.19
S11-2	6342784	1312956	0	96.60	62	4.02
S11-3	6342784	1312955	0	93.57	96	4.23
S11-4	6342778	1312948	18	89.88	102	3.42
S11-5	6342776	1312945	30	96.73	100	3.88
S11-6	6342772	1312942	0	95.36	120	3.52
S11-7	6342772	1312941	15	93.15	109	4.26
S11-8	6342763	1312941	23	93.50	108	3.49
S11-9	6342756	1312931	30	93.26	51	3.87
S11-10	6342753	1312931	10	90.10	76	3.79
S11-11	6342740	1312946	2	93.18	43	4.07
S11-12	6342748	1312949	30	93.24	100	3.79
S11-13	6342753	1312957	10	95.00	56	3.65
S11-14	6342754	1312958	0	88.81	43	4.26
S11-15	6342757	1312969	10	91.62	119	4.10
S3-1	6343275	1308250	35	94.83	114	3.42
S3-2	6343273	1308234	15	95.79	116	3.72
S3-3	6343261	1308222	15	96.41	56	3.81
S3-4	6343247	1308218	12	93.64	72	4.22
S3-5	6343244	1308216	0	95.23	61	4.16
S3-6	6343243	1308213	10	94.95	75	3.87
S3-7	6343247	1308207	25	94.19	56	3.89
S3-8	6343236	1308202	1	95.46	107	4.10
S3-9	6343231	1308199	30	94.31	49	3.77
S3-10	6343221	1308195	23	96.21	63	3.52
S3-11	6343210	1308199	10	95.82	96	3.99
S3-12	6343200	1308216	20	94.81	50	3.80
S3-13	6343207	1308226	0	94.58	51	3.75
S3-14	6343215	1308236	17	96.39	112	3.88
S3-15	6343229	1308237	10	95.24	43	4.16
GAL-1	6343408	1305989	0	94.08	57	3.53
GAL-2	6343401	1305988	9	97.10	121	4.02
GAL-3	6343390	1305999	20	95.98	102	3.51
GAL-4	6343382	1306005	3	89.25	44	4.07
GAL-5	6343381	1306006	0	96.95	91	3.68
GAL-6	6343382	1306011	0	96.54	120	3.77
GAL-7	6343376	1306016	1	95.87	83	3.73

GAL-8	6343373	1306020	22	95.13	108	4.22
GAL-9	6343369	1306025	19	97.25	42	3.77
GAL-10	6343366	1306026	2	95.58	111	3.75
GAL-11	6343365	1306026	0	96.62	95	3.70
GAL-12	6343361	1306029	60	95.64	94	3.72
GAL-13	6343354	1306032	25	96.36	100	3.78
GAL-14	6343353	1306025	5	95.16	117	4.05
GAL-15	6343359	1306013	70	95.17	67	3.78
N4-1	6643084	1305132	3	94.81	3.72	50
N4-2	6643104	1305120	33	92.05	3.78	90
N4-3	6643125	1305117	10	95.59	4.02	45
N4-4	6643128	1305117	1	95.65	4.06	54
N4-5	6643133	1305115	35	93.22	4.15	94
N4-6	6643158	1305104	35	95.32	3.34	56
N4-7	6643159	1305108	0	93.44	4.09	118
N4-8	6643163	1305108	2	95.51	3.75	102
N4-9	6643165	1305108	40	96.21	4.08	114
N4-10	6643169	1305107	5	94.23	3.87	73
N4-11	6643182	1305103	30	93.23	4.12	86
N4-12	6643182	1305103	2	94.10	4.04	119
N4-13	6643189	1305100	1	94.24	3.81	121
N4-14	6643198	1305097	22	92.86	3.61	63
N4-15	6643207	1305092	40	95.27	3.35	91
N2-1	6644731	1303999	0	91.59	3.67	116
N2-2	6644730	1304001	15	86.46	4.16	116
N2-3	6644721	1304006	20	94.94	3.95	114
N2-4	6644721	1304006	3	96.36	3.63	112
N2-5	6644721	1304006	25	97.57	3.79	70
N2-6	6644700	1304012	20	92.04	4.05	86
N2-7	6644700	1304012	3	93.73	4.09	73
N2-8	6644696	1304021	0	92.50	3.69	97
N2-9	6644693	1304026	25	95.71	4.18	90
N2-10	6644693	1304026	2	98.01	3.62	109
N2-11	6644709	1304026	3	95.91	3.97	53
N2-12	6644709	1304026	20	93.58	3.87	78
N2-13	6644709	1304051	0	86.51	3.83	119
N2-14	6644709	1304051	0	93.97	4.03	94
N2-15	6644709	1304051	25	95.73	3.51	86
N3-1	6644849	1303222	5	94.08	3.56	103
N3-2	6644843	1303225	10	96.33	3.92	87
N3-3	6644839	1303224	23	94.59	4.15	106
N3-4	6644835	1303220	9	94.61	3.86	105
N3-5	6644827	1303219	0	96.10	4.25	104
N3-6	6644813	1303216	2	93.97	3.50	91
N3-7	6644809	1303214	0	96.19	4.12	64
N3-8	6644808	1303211	2	92.70	4.13	52
N3-9	6644806	1303209	28	95.42	3.83	67
N3-10	6644798	1303211	30	95.75	3.93	94
N3-11	6644792	1303213	2	95.96	4.12	88
N3-12	6644784	1303218	40	94.35	3.62	86
N3-13	6644770	1303229	25	93.16	3.94	108
N3-14	6644767	1303227	0	96.05	4.05	75
N3-15	6644767	1303228	15	95.43	4.08	99
N1-1	6642356	1303937	20	96.26	3.50	85
N1-2	6642358	1303932	2	95.25	3.55	86
N1-3	6642358	1303929	26	96.40	3.95	113
N1-4	6642357	1303924	5	94.05	3.70	49
N1-5	6642356	1303916	30	92.38	3.75	109
N1-6	6642357	1303911	1	95.30	4.24	74
N1-7	6642355	1303907	40	95.28	3.66	104
N1-8	6642354	1303900	0	96.57	4.02	96
N1-9	6642352	1303891	4	90.92	4.25	68
N1-10	6642348	1303878	4	96.35	3.92	52
N1-11	6642344	1303868	40	90.04	3.85	90

N1-12	6642335	1303830	0	94.14	4.20	112
N1-13	6642329	1303826	0	90.30	3.77	104
N1-14	6642340	1303828	3	93.89	3.82	95
N1-15	6642349	1303824	0	91.73	3.79	74
N5-1	6650008	1302678	5	95.57	3.94	106
N5-2	6650012	1302675	5	93.04	3.81	50
N5-3	6650018	1302674	15	93.94	3.61	120
N5-4	6650024	1302672	25	95.60	3.70	60
N5-5	6650041	1302663	13	91.30	3.51	120
N5-6	6650060	1302664	30	93.46	4.08	121
N5-7	6650062	1302660	1	96.55	3.73	52
N5-8	6650080	1302655	0	92.63	3.97	75
N5-9	6650080	1302655	2	96.00	3.85	55
N5-10	6650092	1302651	15	92.22	4.07	62
N5-11	6650099	1302649	30	95.51	3.98	72
N5-12	6650103	1302643	1	94.89	4.14	78
N5-13	6650107	1302637	10	95.05	3.87	100
N5-14	6650109	1302634	17	95.16	3.86	107
N5-15	6650109	1302634	0	95.96	3.65	51
KOR-1	6641711	1302859	30	90.87	3.55	91
KOR-2	6641700	1302859	35	96.13	3.95	103
KOR-3	6641700	1302859	6	91.13	4.09	91
KOR-4	6641700	1302859	0	94.78	3.96	106
KOR-5	6641689	1302845	3	94.67	3.87	102
KOR-6	6641689	1302845	1	88.64	3.91	51
KOR-7	6641689	1302845	25	95.28	3.95	79
KOR-8	6641680	1302850	0	95.33	4.06	92
KOR-9	6641680	1302850	3	90.51	3.90	89
KOR-10	6641680	1302850	35	96.34	3.93	95
KOR-11	6641657	1302855	5	96.30	4.19	93
KOR-12	6641657	1302855	3	97.53	3.68	118
KOR-13	6641640	1302851	35	95.19	3.60	122
KOR-14	6641640	1302851	1	88.43	3.98	75
KOR-15	6641621	1302844	50	91.09	3.13	100

Testate amoebae counts

SampleId	GAL15	GAL14	GAL13	GAL12	GAL11	GAL10	GAL9	GAL8	GAL7
A#flavum	0	28	1	0	64	23	0	5	6
A#catin	0	0	0	0	0	1	0	0	1
A#cren	0	0	0	0	0	0	0	0	0
A#disc	0	5	1	0	2	4	0	0	24
A#gibb	0	0	0	0	0	0	0	0	0
A#hemis	0	0	0	0	0	0	0	0	0
A#musc	65	12	25	53	1	9	6	3	11
A#semi	0	2	4	3	0	2	27	0	0
B#indic	0	0	0	0	0	0	0	0	0
C#acul	0	0	0	0	0	0	0	0	0
C#cass	0	0	0	0	0	0	0	0	0
C#platy	0	0	0	0	0	0	0	0	0
C#ovifo	0	0	0	0	0	0	0	0	0
C#arcel	66	2	7	9	0	1	1	0	0
D#acumi	0	0	0	0	0	0	0	0	0
D#bacum	0	0	0	0	34	1	0	0	3
D#bacra	0	0	0	0	5	3	0	0	0
D#globu	0	19	0	0	10	4	0	0	3
D#lance	0	0	0	0	0	0	0	0	1
D#leidy	0	5	0	0	3	12	0	0	11

D#lucid	0	4	2	0	0	1	0	0	0
D#prist	0	0	0	0	1	0	0	0	0
D#pulex	0	0	0	0	0	0	0	0	2
D#rube	0	0	0	0	0	0	0	0	2
E#comp	0	0	0	0	0	2	0	0	1
E#cris	0	0	0	0	2	2	0	0	3
E#rotun	4	0	3	9	0	2	16	8	1
E#strig	3	2	2	0	0	8	1	1	14
E#tube	7	3	13	18	2	5	3	2	10
H#angu	0	0	2	2	0	5	2	0	2
H#petri	0	0	0	0	3	4	0	0	0
H#rosea	0	0	0	0	0	0	0	0	0
H#sphag	0	0	0	0	0	0	0	1	0
H#sylva	0	0	7	0	0	0	2	1	0
H#eleg	0	22	0	0	0	21	38	76	12
H#minu	0	0	0	0	0	0	0	1	1
H#papil	0	13	1	0	12	10	11	0	9
H#subf	0	0	1	0	0	0	0	0	0
N#bohe	0	0	0	0	0	0	0	0	0
N#cari	0	0	0	0	6	1	0	0	0
N#flab	0	0	0	0	0	0	0	0	0
N#gris	0	3	0	0	0	22	0	0	13
N#margi	0	0	0	0	2	0	0	0	0
N#milit	1	0	12	1	2	0	8	1	6
N#minor	1	1	14	0	0	0	8	1	4
N#parvu	0	1	25	3	2	0	6	0	5
N#tinc	1	1	26	18	0	0	16	51	6
N#vitre	0	0	0	0	0	2	1	0	1
N#waile	0	0	0	0	0	0	0	0	0
P#acrop	1	24	0	0	0	5	0	0	1
P#spino	0	0	0	0	0	0	0	0	0
P#fulv	0	0	0	0	0	0	0	0	0
S#lenta	0	0	0	0	0	0	0	0	0
T#denta	0	0	1	0	0	0	3	0	0
T#arcul	1	0	0	0	0	0	0	0	0
T#minu	0	0	0	1	0	0	0	0	0
T#line	1	1	1	1	0	0	1	0	0
T#cory	0	2	3	33	0	1	2	0	0
SampleId	**GAL5**	**GAL4**	**GAL3**	**GAL2**	**GAL1**	**S7-15**	**S7-14**	**S7-13**	**S7-12**
A#flavum	42	27	0	6	84	24	0	7	6
A#catin	0	0	0	0	0	0	0	0	0
A#cren	0	0	0	0	0	0	0	0	0
A#disc	1	10	0	0	0	10	16	0	9
A#gibb	0	0	0	0	0	1	0	0	0
A#hemis	0	0	0	0	0	0	1	0	0
A#musc	2	13	32	33	9	25	27	18	6
A#semi	1	1	0	0	8	4	1	3	3
B#indic	0	0	0	0	0	0	0	0	0
C#acul	0	0	0	0	0	0	0	0	0
C#cass	0	0	0	0	0	0	0	0	0
C#platy	0	0	0	0	0	1	0	0	0
C#ovifo	0	2	0	0	0	0	0	0	0
C#arcel	2	1	0	3	0	6	71	0	0
D#acumi	0	0	0	0	0	0	0	0	0
D#bacum	0	0	0	0	0	0	0	0	1
D#bacra	0	0	0	0	0	0	0	0	5
D#globu	38	2	0	0	2	5	1	0	7
D#lance	0	1	0	0	0	0	0	0	1
D#leidy	5	6	0	0	2	11	0	0	12
D#lucid	3	0	0	0	0	5	0	0	6
D#prist	0	1	0	0	0	8	0	0	0
D#pulex	0	0	2	0	0	0	0	0	0

D#rube	0	0	0	0	0	0	0	0	2
E#comp	0	0	6	0	1	4	0	0	5
E#cris	1	1	0	0	1	4	0	0	1
E#rotun	0	0	11	15	0	1	4	3	12
E#strig	1	2	17	0	4	0	0	0	11
E#tube	1	8	4	2	17	3	5	7	5
H#angu	0	6	21	9	3	1	1	1	0
H#petri	33	0	0	0	1	0	0	0	4
H#rosea	0	0	0	0	0	0	0	0	0
H#sphag	17	0	0	0	0	0	0	0	0
H#sylva	1	2	11	5	1	0	0	6	0
H#eleg	1	18	4	31	6	0	0	67	4
H#minu	0	2	2	1	0	0	0	1	0
H#papil	0	4	0	0	0	0	0	0	0
H#subf	1	0	4	0	0	0	0	0	0
N#bohe	0	3	0	1	1	1	0	0	1
N#cari	0	1	0	0	5	2	0	0	2
N#flab	0	2	0	0	0	0	0	0	1
N#gris	0	15	0	0	0	2	0	0	33
N#margi	0	0	0	0	2	2	0	0	0
N#milit	0	7	4	1	0	0	1	8	2
N#minor	0	1	0	0	2	0	6	4	0
N#parvu	1	5	13	30	1	1	4	6	3
N#tinc	0	2	6	11	0	11	3	14	7
N#vitre	0	0	0	0	0	0	0	0	0
N#waile	0	0	0	1	0	0	0	1	0
P#acrop	1	2	0	0	0	3	0	0	0
P#spino	0	0	0	0	0	0	0	0	0
P#fulv	0	0	0	0	0	0	0	0	0
S#lenta	0	0	0	0	0	0	0	0	0
T#denta	0	0	0	0	0	0	0	0	0
T#arcul	0	0	0	0	0	0	0	0	0
T#minu	0	0	0	0	0	0	0	0	0
T#line	0	0	0	0	0	2	0	2	0
T#cory	0	7	11	1	0	11	10	4	3
SampleId	**S7-11**	**S7-10**	**S7-9**	**S7-8**	**S7-7**	**S7-6**	**S7-5**	**S7-4**	**S7-3**
A#flavum	0	0	0	6	3	9	0	15	0
A#catin	0	0	0	0	0	0	0	0	16
A#cren	0	0	0	0	0	0	0	0	4
A#disc	0	0	0	0	0	29	0	0	0
A#gibb	0	0	0	0	0	0	0	0	0
A#hemis	0	0	0	0	0	0	0	0	0
A#musc	19	0	32	6	21	3	35	34	59
A#semi	3	55	13	7	4	4	2	21	2
B#indic	0	1	0	2	0	0	0	0	0
C#acul	0	0	0	0	0	0	0	0	0
C#cass	0	0	0	0	0	0	0	0	0
C#platy	0	0	0	0	0	0	0	0	0
C#ovifo	2	3	0	0	1	0	0	0	2
C#arcel	50	10	19	1	0	0	0	0	10
D#acumi	0	0	0	0	0	0	0	0	0
D#bacum	0	0	0	0	0	0	0	0	0
D#bacra	0	0	0	0	0	1	0	0	0
D#globu	0	0	0	0	0	4	0	0	0
D#lance	0	0	0	0	0	0	0	0	0
D#leidy	0	0	0	0	0	11	0	3	0
D#lucid	0	0	0	0	0	2	0	0	0
D#prist	0	0	3	0	0	0	0	0	0
D#pulex	0	0	5	0	0	0	0	0	0
D#rube	0	0	0	0	0	1	0	0	0
E#comp	0	0	0	0	0	48	0	3	0
E#cris	0	0	0	0	0	0	0	0	0

E#rotun	2	7	3	6	5	0	0	3	10
E#strig	2	0	0	0	0	1	0	0	0
E#tube	3	51	8	1	0	13	14	28	8
H#angu	9	0	0	4	10	0	0	0	0
H#petri	0	0	0	1	1	1	0	0	0
H#rosea	0	0	0	0	0	1	0	0	0
H#sphag	0	0	0	0	0	0	0	0	0
H#sylva	3	7	0	5	12	0	0	0	8
H#eleg	0	0	0	45	56	2	0	0	0
H#minu	0	3	32	5	4	0	0	0	4
H#papil	0	0	0	0	0	0	0	10	0
H#subf	2	0	11	0	4	0	2	0	4
N#bohe	0	0	0	1	0	5	0	7	0
N#cari	0	0	0	0	0	0	0	0	0
N#flab	1	0	0	6	0	3	0	0	0
N#gris	0	0	0	0	0	0	0	7	0
N#margi	0	0	0	0	0	0	0	0	0
N#milit	1	0	0	4	1	1	0	5	0
N#minor	0	1	3	2	1	1	0	4	2
N#parvu	12	0	0	25	5	4	2	0	0
N#tinc	13	0	8	21	7	3	28	0	2
N#vitre	0	0	0	0	0	0	0	0	0
N#waile	0	0	0	1	0	0	0	0	0
P#acrop	1	0	5	0	0	0	0	0	0
P#spino	0	0	0	0	0	0	0	0	0
P#fulv	0	0	0	0	0	0	0	0	0
S#lenta	0	0	0	0	0	0	0	0	0
T#denta	14	2	0	1	1	1	2	2	2
T#arcul	2	2	3	0	0	0	1	0	0
T#minu	0	0	3	0	0	0	0	0	0
T#line	1	1	3	0	2	1	14	4	6
T#cory	13	5	0	0	12	1	49	5	12
SampleId	**S7-2**	**S7-1**	**S11-15**	**S11-14**	**S11-13**	**S11-12**	**S11-11**	**S11-10**	**S11-9**
A#flavum	0	16	0	14	0	2	73	17	0
A#catin	0	0	0	0	0	0	0	0	0
A#cren	0	0	0	0	0	0	0	0	0
A#disc	0	1	0	1	0	0	5	3	0
A#gibb	0	0	0	1	0	0	0	0	0
A#hemis	0	0	0	0	0	0	0	0	0
A#musc	13	14	18	20	35	39	0	5	33
A#semi	3	5	1	2	7	8	5	1	0
B#indic	0	0	2	0	1	0	1	0	0
C#acul	0	0	0	0	0	0	0	0	0
C#cass	0	0	0	0	0	0	0	0	0
C#platy	0	0	0	0	0	0	0	0	0
C#ovifo	0	0	0	0	1	11	0	0	3
C#arcel	1	1	10	0	0	27	1	0	16
D#acumi	0	0	0	0	0	0	0	0	0
D#bacum	0	0	0	0	0	0	0	0	0
D#bacra	0	0	0	1	0	0	1	0	0
D#globu	0	1	0	41	0	0	0	0	0
D#lance	0	0	0	0	0	0	0	0	0
D#leidy	0	1	0	6	0	0	3	0	0
D#lucid	1	0	0	13	0	0	2	0	0
D#prist	0	0	0	1	0	0	0	0	0
D#pulex	0	0	0	1	1	0	0	0	0
D#rube	0	0	0	0	0	0	2	0	0
E#comp	0	0	0	0	0	0	1	0	0
E#cris	0	0	0	8	0	0	1	0	0
E#rotun	16	7	29	1	11	5	0	10	31
E#strig	8	1	1	2	0	0	2	1	0
E#tube	12	4	2	3	12	4	0	9	20

H#angu	1	4	7	0	3	0	0	4	0
H#petri	0	0	0	1	0	0	2	0	0
H#rosea	0	0	0	0	0	2	0	0	0
H#sphag	0	0	0	1	0	0	0	1	0
H#sylva	1	4	16	5	15	10	0	0	10
H#eleg	65	68	21	1	3	0	17	50	1
H#minu	6	2	0	0	1	1	1	0	9
H#papil	0	0	0	2	7	0	3	20	0
H#subf	0	1	0	0	0	0	0	0	0
N#bohe	0	0	1	0	0	0	1	1	0
N#cari	0	0	0	12	0	0	2	1	0
N#flab	0	4	3	2	0	0	0	2	0
N#gris	0	3	0	1	0	0	2	2	0
N#margi	0	0	0	4	0	0	0	0	0
N#milit	2	6	12	1	8	0	0	0	4
N#minor	1	4	6	4	7	0	0	1	3
N#parvu	6	0	10	2	4	2	2	12	2
N#tinc	15	4	9	0	9	1	0	10	5
N#vitre	0	0	0	0	0	0	0	0	0
N#waile	0	0	0	1	1	0	0	0	0
P#acrop	0	0	0	0	1	0	1	1	1
P#spino	0	0	0	0	0	0	0	0	0
P#fulv	0	0	0	0	3	0	0	0	0
S#lenta	0	0	0	0	0	0	26	0	0
T#denta	1	0	0	0	0	0	0	0	0
T#arcul	0	0	1	0	0	0	1	0	1
T#minu	0	0	0	0	0	0	0	0	0
T#line	0	0	0	0	0	0	0	0	0
T#cory	0	1	0	0	20	39	1	0	12
SampleId	**S11-8**	**S11-7**	**S11-6**	**S11-5**	**S11-4**	**S11-3**	**S11-2**	**S11-1**	
A#flavum	0	1	3	0	17	3	0	0	
A#catin	0	0	0	0	0	0	0	0	
A#cren	0	0	0	0	0	0	0	0	
A#disc	0	0	3	0	0	27	2	0	
A#gibb	0	0	1	0	0	0	0	0	
A#hemis	0	0	0	0	0	1	0	0	
A#musc	12	28	28	26	29	15	31	10	
A#semi	6	0	6	6	7	3	8	6	
B#indic	0	0	0	0	0	0	0	0	
C#acul	0	1	0	0	0	0	0	0	
C#cass	0	0	1	0	0	0	0	0	
C#platy	0	0	0	0	0	0	3	0	
C#ovifo	1	4	0	0	0	0	0	0	
C#arcel	30	0	5	74	0	2	7	38	
D#acumi	0	0	0	0	0	4	0	0	
D#bacum	0	0	0	0	0	2	0	0	
D#bacra	0	0	0	0	0	1	0	0	
D#globu	0	0	27	0	0	0	1	0	
D#lance	0	0	1	0	0	0	0	0	
D#leidy	0	0	3	0	0	1	2	0	
D#lucid	0	0	2	0	0	1	2	0	
D#prist	0	0	23	0	0	15	6	0	
D#pulex	0	0	0	0	0	0	0	0	
D#rube	0	0	0	0	0	0	0	0	
E#comp	0	0	0	0	0	4	5	0	
E#cris	0	0	1	0	0	4	0	0	

E#rotun	4	3	2	4	6	9	9	13	
E#strig	0	0	1	0	0	0	9	3	
E#tube	5	10	3	5	12	22	15	11	
H#angu	17	1	0	0	0	0	3	0	
H#petri	0	0	6	0	0	1	3	0	
H#rosea	0	0	0	0	0	0	0	0	
H#sphag	0	0	0	0	0	0	0	0	
H#sylva	28	7	2	0	5	0	3	9	
H#eleg	0	41	1	1	41	1	1	30	
H#minu	0	3	0	1	1	0	0	5	
H#papil	0	28	0	0	1	0	1	0	
H#subf	0	0	0	0	0	0	1	0	
N#bohe	0	0	1	0	0	3	1	1	
N#cari	0	0	2	0	0	1	4	0	
N#flab	0	0	2	1	0	0	5	0	
N#gris	0	0	0	0	0	3	7	0	
N#margi	0	0	9	0	0	0	0	0	
N#milit	3	4	0	2	1	0	0	3	
N#minor	1	3	0	5	0	1	4	4	
N#parvu	11	4	1	11	0	1	5	5	
N#tinc	22	4	7	12	24	4	6	2	
N#vitre	0	0	0	0	0	0	0	0	
N#waile	0	1	0	0	2	0	0	0	
P#acrop	4	0	1	0	0	5	0	0	
P#spino	0	0	0	0	0	1	1	0	
P#fulv	0	1	1	0	0	0	0	0	
S#lenta	0	0	0	0	0	0	0	0	
T#denta	0	0	0	0	0	0	0	0	
T#arcul	1	0	0	1	0	0	0	0	
T#minu	0	0	0	0	0	0	0	0	
T#line	1	4	2	1	1	6	1	1	
T#cory	6	4	1	2	4	9	8	10	
SampleId	KOR15	KOR14	KOR13	KOR12	KOR11	KOR10	**KOR9**	**KOR8**	**KOR7**
A#flavum	52	58	7	45	71	7	64	38	23
A#steno	0	0	0	0	0	0	0	0	0
A#wrigh	0	0	0	0	0	0	0	0	0
A#arto	0	0	0	1	0	0	0	0	0
A#catin	19	0	0	0	0	0	0	0	1
A#disc	0	0	0	3	1	0	1	1	0
A#gibb	0	0	0	0	0	0	0	0	0
A#hemis	0	0	0	0	0	0	0	0	0
A#vulg	0	0	0	0	0	0	0	0	0
A#musc	57	1	58	1	0	54	2	17	9
A#semi	3	1	31	7	0	25	2	7	6
B#indic	0	0	0	0	0	0	0	0	0
C#ovifo	1	0	0	0	0	0	0	0	0
C#sacc	0	0	0	0	0	0	0	0	0
C#arcel	0	0	3	1	0	0	0	0	0
D#bacum	0	0	0	0	0	0	0	0	0
D#bacra	0	0	0	0	0	0	1	1	0
D#globu	0	8	0	4	2	0	5	15	0
D#lance	0	0	0	0	0	0	0	2	0
D#leidy	0	0	0	2	2	0	5	14	0
D#lucid	0	0	0	1	1	0	0	7	0
D#oblon	0	0	0	0	0	0	0	0	0

D#prist	0	0	3	0	0	0	0	0	0
D#pulex	0	1	0	0	1	4	0	0	0
D#rube	0	0	0	0	0	0	0	8	0
E#comp	0	13	0	1	0	0	0	0	2
E#cris	0	1	0	0	0	2	1	0	0
E#rotun	5	0	0	0	0	0	0	0	0
E#strig	0	0	0	0	0	0	0	0	0
E#tube	1	4	0	1	1	9	1	1	2
H#angu	0	0	0	1	1	0	3	0	0
H#petri	0	11	0	8	7	0	9	0	0
H#sphag	0	0	0	3	0	0	1	4	0
H#sylva	4	0	0	1	0	9	0	0	2
H#eleg	0	17	31	27	34	20	11	1	68
H#minu	5	0	7	2	11	4	0	0	20
H#papil	0	29	0	42	12	4	37	20	0
H#subf	4	0	0	0	0	4	0	0	1
N#cari	0	1	0	1	0	0	4	1	0
N#coll	0	0	0	0	0	0	0	1	1
N#flab	0	0	0	0	0	0	0	0	0
N#gris	0	6	0	0	1	0	4	11	0
N#margi	0	0	0	0	0	0	0	0	0
N#milit	0	1	0	0	0	0	0	0	7
N#minor	0	0	0	0	0	0	0	0	3
N#parvu	0	0	0	0	1	0	0	0	1
N#tinc	0	0	0	0	0	0	0	0	5
N#vitre	0	0	0	0	0	0	0	0	0
N#waile	0	0	0	0	0	0	0	0	0
P#acrop	0	0	0	0	0	0	0	0	0
P#spino	0	0	0	0	0	0	1	3	0
P#fasc	0	0	3	0	0	0	0	0	0
P#fulv	0	0	0	0	4	4	0	0	0
S#lenta	0	0	0	0	0	0	0	0	0
T#arcul	0	0	7	0	0	2	0	0	0
T#minu	0	0	0	0	0	0	0	0	0
T#line	0	0	0	0	0	0	0	0	0
T#cory	0	0	0	0	0	0	0	0	0
SampleId	**KOR6**	**KOR5**	**KOR4**	**KOR3**	**KOR2**	**KOR1**	**N1-15**	**N1-14**	**N1-13**
A#flavum	62	64	67	70	11	31	71	43	84
A#steno	0	0	0	1	0	0	0	0	0
A#wrigh	0	0	0	0	0	0	0	0	0
A#arto	0	0	0	0	0	0	0	0	0
A#catin	0	0	0	0	16	1	0	0	0
A#disc	1	0	1	4	0	0	1	0	0
A#gibb	0	0	0	0	0	0	0	0	0
A#hemis	0	1	2	1	0	0	0	0	0
A#vulg	0	0	0	0	2	0	0	0	0
A#musc	1	1	3	4	85	9	2	2	1
A#semi	1	4	1	3	8	1	2	1	1
B#indic	0	0	0	0	1	0	0	0	0
C#ovifo	0	0	0	0	0	0	0	0	0
C#sacc	0	0	0	0	1	0	0	0	0
C#arcel	0	0	0	0	0	0	0	0	0
D#bacum	0	0	1	0	0	0	0	0	0
D#bacra	2	0	0	0	0	0	0	7	0
D#globu	5	8	14	11	0	0	2	7	7
D#lance	1	0	0	0	0	0	0	0	0
D#leidy	7	4	5	4	0	0	1	24	5
D#lucid	0	0	1	0	0	0	0	2	1
D#oblon	0	0	0	0	0	0	0	0	0
D#prist	0	0	0	0	0	0	0	0	0
D#pulex	0	0	0	0	1	0	0	1	0
D#rube	1	0	3	1	0	0	1	2	0

E#comp	0	5	0	1	0	1	2	0	0
E#cris	2	3	1	0	0	0	4	1	0
E#rotun	0	0	0	0	1	1	0	1	0
E#strig	4	0	2	0	1	8	11	2	0
E#tube	0	1	1	4	5	1	10	1	0
H#angu	1	0	3	1	0	0	1	1	3
H#petri	7	6	5	1	0	0	1	7	2
H#sphag	7	3	2	0	0	0	1	2	1
H#sylva	0	0	0	0	4	5	0	0	0
H#eleg	12	18	14	22	1	72	7	11	8
H#minu	0	0	4	1	1	5	0	0	0
H#papil	28	20	13	9	0	1	20	22	20
H#subf	0	0	0	0	1	0	0	0	0
N#cari	3	3	1	0	0	0	1	0	1
N#coll	0	0	0	0	0	0	0	0	1
N#flab	0	0	0	0	0	0	0	0	0
N#gris	1	2	6	4	0	0	1	8	9
N#margi	1	1	0	0	0	0	0	0	1
N#milit	1	0	0	1	1	0	1	0	0
N#minor	0	0	0	0	1	4	0	0	1
N#parvu	1	0	1	3	1	1	1	0	0
N#tinc	0	0	0	0	2	3	1	0	0
N#vitre	0	0	0	1	0	0	0	0	0
N#waile	1	0	0	0	0	1	0	0	0
P#acrop	1	6	1	3	0	0	7	4	3
P#spino	1	0	0	1	0	0	1	2	2
P#fasc	0	0	0	0	0	0	0	0	0
P#fulv	0	0	0	0	1	0	0	0	0
S#lenta	0	0	0	0	0	0	0	0	0
T#arcul	0	0	0	1	2	0	0	0	0
T#minu	0	0	0	0	0	0	0	0	0
T#line	0	0	0	1	0	0	0	0	0
T#cory	0	0	0	0	5	6	0	0	0
SampleId	**N1-12**	**N1-11**	**N1-10**	**N1-9**	**N1-8**	**N1-7**	**N1-6**	**N1-5**	**N1-4**
A#flavum	54	21	71	51	94	8	57	44	43
A#steno	0	0	0	0	0	0	0	0	0
A#wrigh	0	0	0	0	0	0	0	0	0
A#arto	0	0	0	0	0	0	0	0	0
A#catin	0	1	0	0	0	4	0	1	0
A#disc	20	0	3	3	0	0	1	0	2
A#gibb	0	0	0	0	0	0	0	0	0
A#hemis	3	0	0	11	0	0	1	0	2
A#vulg	0	0	0	0	0	0	0	0	0
A#musc	2	9	4	5	1	13	1	5	6
A#semi	1	1	1	3	3	1	1	2	3
B#indic	0	0	0	0	0	0	0	0	0
C#ovifo	0	0	0	0	0	0	0	0	0
C#sacc	0	0	0	0	0	0	0	0	0
C#arcel	0	0	0	1	0	0	0	0	0
D#bacum	0	0	0	0	1	0	0	0	0
D#bacra	0	0	0	0	4	0	0	0	1
D#globu	5	1	1	0	2	0	1	0	0
D#lance	0	0	0	0	0	0	0	0	1
D#leidy	3	0	8	5	6	0	4	0	2
D#lucid	0	0	0	0	0	0	0	0	0
D#oblon	0	0	0	0	1	0	0	0	0
D#prist	0	0	0	0	0	0	0	0	0
D#pulex	0	0	0	0	0	0	0	0	0
D#rube	0	0	0	1	0	0	0	0	0
E#comp	0	0	0	0	0	2	0	0	0
E#cris	0	0	4	1	2	0	0	0	1
E#rotun	8	0	1	1	0	0	0	1	0

E#strig	4	0	0	0	0	1	1	0	0
E#tube	2	12	0	4	1	3	3	0	3
H#angu	2	0	0	2	0	0	3	0	0
H#petri	3	0	0	3	2	1	4	7	4
H#sphag	1	1	2	1	0	0	1	2	3
H#sylva	0	3	0	0	0	0	0	1	2
H#eleg	20	42	19	35	9	74	50	60	55
H#minu	0	17	7	2	0	5	0	4	10
H#papil	11	4	18	7	14	29	16	20	5
H#subf	0	1	0	0	0	0	0	0	0
N#cari	4	0	2	2	1	0	0	0	0
N#coll	0	0	0	0	0	0	0	0	0
N#flab	0	0	0	0	0	0	0	0	0
N#gris	4	0	3	10	5	0	2	0	6
N#margi	0	0	0	0	0	0	0	0	0
N#milit	0	9	0	1	2	3	1	0	0
N#minor	0	1	0	0	0	0	0	0	0
N#parvu	0	1	2	0	1	0	0	0	1
N#tinc	0	20	0	0	0	0	0	0	1
N#vitre	0	0	0	0	0	0	0	0	0
N#waile	0	0	0	0	0	2	0	2	1
P#acrop	4	0	6	2	3	0	0	0	1
P#spino	0	0	0	0	0	0	0	0	0
P#fasc	0	0	0	0	0	0	0	0	0
P#fulv	0	0	0	0	0	0	0	0	0
S#lenta	0	0	0	0	0	0	0	0	0
T#arcul	0	1	0	0	0	0	0	3	0
T#minu	0	0	0	0	0	2	0	0	0
T#line	0	0	0	0	0	0	0	0	0
T#cory	0	3	0	0	0	3	0	0	0
SampleId	**N1-3**	**N1-2**	**N1-1**	**N3-15**	**N3-14**	**N3-13**	**N3-12**	**N3-11**	**N3-10**
A#flavum	12	39	37	49	31	2	51	67	1
A#steno	0	0	0	1	0	0	0	0	0
A#wrigh	0	0	0	0	0	0	0	0	0
A#arto	0	1	0	0	0	0	0	0	0
A#catin	8	0	0	0	0	0	0	0	0
A#disc	0	5	0	0	6	0	0	0	0
A#gibb	1	0	0	0	0	0	0	0	0
A#hemis	0	1	0	0	0	0	0	0	0
A#vulg	0	0	0	0	0	0	0	0	0
A#musc	16	1	3	9	2	6	6	1	34
A#semi	0	2	0	3	5	1	2	3	0
B#indic	0	0	0	0	0	0	0	0	0
C#ovifo	0	0	0	0	0	0	0	0	0
C#sacc	0	0	0	0	0	0	0	0	0
C#arcel	0	1	0	0	0	0	0	4	0
D#bacum	0	0	0	0	0	0	0	0	0
D#bacra	0	0	0	0	9	0	0	0	0
D#globu	0	0	0	0	23	0	0	1	0
D#lance	0	0	0	0	0	0	0	0	0
D#leidy	0	15	0	0	21	0	0	4	0
D#lucid	0	0	0	0	0	0	0	0	0
D#oblon	0	0	0	0	0	0	0	0	0
D#prist	0	0	0	0	0	0	0	0	0
D#pulex	0	2	0	0	0	0	0	0	3
D#rube	0	1	0	0	0	0	0	0	0
E#comp	0	0	0	0	0	0	0	0	2
E#cris	0	2	0	0	0	0	0	1	3
E#rotun	0	0	0	0	0	0	0	0	0
E#strig	0	5	0	4	0	0	1	3	9
E#tube	2	3	1	0	0	0	0	1	8
H#angu	0	2	0	0	0	0	0	0	0

H#petri	0	0	3	1	8	0	5	2	1
H#sphag	0	0	0	0	0	0	0	2	0
H#sylva	1	1	0	1	0	7	1	1	24
H#eleg	36	39	90	54	0	101	65	15	46
H#minu	3	0	6	9	0	3	7	0	13
H#papil	65	16	3	2	34	11	8	26	1
H#subf	0	0	0	0	0	0	0	0	0
N#cari	0	0	0	0	7	0	0	4	0
N#coll	0	0	0	0	0	0	0	0	0
N#flab	0	0	0	0	0	0	0	0	0
N#gris	0	9	0	0	0	0	0	0	0
N#margi	0	0	0	0	0	0	0	0	0
N#milit	0	3	4	16	0	15	0	0	2
N#minor	0	0	1	0	0	3	0	0	0
N#parvu	0	1	0	0	0	0	1	0	0
N#tinc	3	2	0	0	0	0	3	1	0
N#vitre	0	0	0	0	0	0	0	0	0
N#waile	2	1	0	1	0	1	1	0	1
P#acrop	0	0	4	0	2	0	0	3	0
P#spino	0	0	0	0	0	0	0	13	0
P#fasc	0	0	0	0	0	0	0	0	0
P#fulv	0	0	0	0	1	0	0	0	0
S#lenta	0	0	0	0	0	0	0	0	0
T#arcul	2	0	0	0	0	0	0	0	1
T#minu	0	0	0	0	0	0	0	0	0
T#line	0	0	0	0	0	0	0	0	0
T#cory	0	0	0	1	0	0	0	0	0
SampleId	**N3-9**	**N3-8**	**N3-7**	**N3-6**	**N3-5**	**N3-4**	**N3-3**	**N3-2**	**N3-1**
A#flavum	11	45	70	50	51	60	3	54	82
A#steno	0	1	4	0	0	0	0	0	0
A#wrigh	0	0	0	0	0	0	0	0	0
A#arto	0	0	2	0	0	0	0	0	0
A#catin	0	0	0	0	0	0	0	0	0
A#disc	0	4	5	10	1	0	0	5	1
A#gibb	0	0	0	0	0	0	0	0	0
A#hemis	0	2	4	3	0	0	0	1	0
A#vulg	0	1	0	0	0	0	0	0	0
A#musc	27	1	5	1	0	4	60	13	3
A#semi	2	1	2	1	1	5	7	5	5
B#indic	0	0	0	0	0	0	1	0	0
C#ovifo	0	0	0	0	0	0	0	0	0
C#sacc	0	0	0	0	0	0	0	0	0
C#arcel	0	0	0	0	0	0	0	1	0
D#bacum	0	0	0	0	1	0	0	0	0
D#bacra	0	4	0	0	3	0	0	0	0
D#globu	0	3	8	0	5	0	0	0	3
D#lance	0	0	0	0	0	0	0	0	0
D#leidy	0	16	2	9	16	1	0	0	1
D#lucid	0	3	1	0	0	0	0	0	0
D#oblon	0	0	0	0	0	0	0	0	0
D#prist	0	0	0	0	0	0	0	0	0
D#pulex	7	0	0	0	0	0	1	9	0
D#rube	0	1	0	2	0	0	0	1	0
E#comp	1	0	0	0	1	0	0	0	1
E#cris	3	2	0	1	0	0	1	0	0
E#rotun	0	0	0	0	0	0	0	0	0
E#strig	1	3	0	3	0	1	7	1	0
E#tube	3	0	1	1	1	2	20	4	0
H#angu	0	0	7	1	1	0	0	0	1
H#petri	0	8	2	2	7	0	0	0	1
H#sphag	0	2	4	4	5	0	0	0	1
H#sylva	7	0	0	0	0	4	16	0	2

H#eleg	48	13	10	21	1	33	23	26	29
H#minu	6	0	0	0	0	13	1	2	0
H#papil	9	32	13	30	43	8	0	7	11
H#subf	0	0	0	0	0	0	2	0	1
N#cari	0	0	1	0	0	0	0	0	0
N#coll	0	0	0	0	0	0	0	0	0
N#flab	0	0	0	0	0	0	0	0	0
N#gris	0	5	1	4	3	3	0	0	3
N#margi	0	0	0	0	0	0	0	0	0
N#milit	18	0	0	0	0	2	1	12	0
N#minor	0	0	0	0	0	0	0	0	0
N#parvu	0	0	0	1	0	1	0	4	1
N#tinc	1	0	0	1	0	3	0	2	4
N#vitre	0	0	0	0	0	0	0	0	0
N#waile	1	0	0	0	0	2	1	4	0
P#acrop	0	3	6	4	9	3	0	0	2
P#spino	0	0	0	0	0	6	0	0	0
P#fasc	0	0	0	0	0	0	0	0	0
P#fulv	0	0	0	0	0	0	0	0	0
S#lenta	0	0	0	0	0	0	0	0	0
T#arcul	0	0	0	0	0	0	2	0	0
T#minu	0	0	0	0	0	0	1	0	0
T#line	1	0	0	0	0	0	0	0	0
T#cory	1	0	2	0	0	0	4	0	0
SampleId	**N4-15**	**N4-14**	**N4-13**	**N4-12**	**N4-11**	**N4-10**	**N4-9**	**N4-8**	**N4-7**
A#flavum	5	8	116	40	4	79	8	77	91
A#steno	0	0	0	0	0	0	0	0	0
A#wrigh	0	0	0	0	0	0	0	0	0
A#arto	0	1	0	0	0	0	0	0	0
A#catin	0	0	0	0	0	0	0	0	0
A#disc	0	0	3	1	0	8	0	0	32
A#gibb	0	0	0	0	0	1	0	0	0
A#hemis	0	0	0	0	0	1	0	0	0
A#vulg	0	0	0	0	0	0	0	0	0
A#musc	0	24	1	4	26	2	68	2	1
A#semi	0	1	2	4	1	0	14	3	0
B#indic	0	0	0	0	0	0	1	0	0
C#ovifo	0	0	0	0	0	0	0	0	0
C#sacc	0	0	0	0	0	0	0	0	0
C#arcel	0	0	0	0	0	2	0	4	0
D#bacum	0	0	0	0	0	0	0	0	0
D#bacra	0	0	0	0	0	0	0	0	0
D#globu	0	0	1	0	0	0	0	0	0
D#lance	0	0	0	0	0	0	0	0	0
D#leidy	0	0	17	0	0	4	0	5	4
D#lucid	0	0	0	8	0	1	0	0	2
D#oblon	0	0	0	0	0	0	0	0	0
D#prist	1	0	0	1	0	0	0	0	0
D#pulex	0	0	0	11	2	2	0	0	0
D#rube	0	0	0	0	0	0	0	3	0
E#comp	0	0	0	0	0	0	0	0	0
E#cris	0	0	1	4	0	0	0	15	1
E#rotun	0	1	0	1	0	0	0	0	0
E#strig	0	4	2	7	3	1	2	7	4
E#tube	1	0	1	6	0	1	4	5	2
H#angu	0	0	0	0	0	2	0	0	0
H#petri	0	0	0	1	0	0	0	0	1
H#sphag	0	0	0	0	0	0	0	0	0
H#sylva	0	0	0	6	19	0	4	0	0
H#eleg	122	85	4	14	36	27	41	0	1
H#minu	0	2	0	0	4	1	1	0	0
H#papil	9	0	1	3	53	10	1	13	3

H#subf	0	0	0	0	0	0	0	1	0
N#cari	0	0	0	0	0	0	0	0	0
N#coll	0	1	0	0	0	0	0	0	0
N#flab	0	0	0	0	0	0	0	1	2
N#gris	0	0	0	4	0	2	0	0	0
N#margi	0	0	0	0	0	0	0	0	0
N#milit	5	12	0	11	0	1	0	0	0
N#minor	0	0	2	0	0	0	0	1	1
N#parvu	3	0	1	11	1	2	0	6	3
N#tinc	2	3	0	12	0	5	0	7	2
N#vitre	0	0	0	0	0	0	0	0	0
N#waile	0	0	0	0	0	0	4	0	0
P#acrop	1	0	0	1	0	0	0	0	0
P#spino	1	0	0	0	0	0	0	0	0
P#fasc	0	0	0	0	0	0	0	0	0
P#fulv	0	0	0	0	0	0	0	0	0
S#lenta	0	0	0	1	0	0	0	0	0
T#arcul	0	2	0	0	0	0	1	0	0
T#minu	0	0	0	0	0	0	1	0	0
T#line	0	0	0	1	0	0	0	0	0
T#cory	0	7	0	0	0	0	1	0	1
SampleId	**N4-6**	**N4-5**	**N4-4**	**N4-3**	**N4-2**	**N4-1**	**N5-15**	**N5-14**	**N5-13**
A#flavum	75	1	15	61	1	62	53	63	35
A#steno	0	0	0	0	0	0	3	0	3
A#wrigh	0	0	0	0	0	0	28	2	3
A#arto	0	0	0	0	0	0	0	0	0
A#catin	0	0	0	0	10	0	0	0	0
A#disc	0	0	39	5	0	8	8	0	1
A#gibb	0	0	0	0	0	2	0	0	0
A#hemis	0	0	4	0	0	0	0	0	0
A#vulg	0	0	0	0	21	0	0	0	0
A#musc	2	3	5	11	67	0	3	3	3
A#semi	0	39	4	1	10	3	2	1	6
B#indic	0	0	0	0	0	0	0	0	0
C#ovifo	0	0	0	0	0	0	0	0	0
C#sacc	0	0	0	0	0	0	0	0	0
C#arcel	0	2	0	4	0	0	0	3	0
D#bacum	0	0	0	0	0	0	0	0	0
D#bacra	0	0	0	0	0	0	0	0	0
D#globu	0	0	1	0	0	0	6	0	0
D#lance	0	0	0	0	0	0	0	0	0
D#leidy	0	0	14	0	0	2	3	0	0
D#lucid	0	0	0	0	0	1	0	0	0
D#oblon	0	0	0	0	0	0	0	0	0
D#prist	0	0	2	0	0	0	2	0	1
D#pulex	1	0	0	0	0	0	0	2	1
D#rube	0	0	1	0	0	0	3	0	2
E#comp	2	0	1	0	0	0	3	0	4
E#cris	0	0	4	0	0	0	4	0	2
E#rotun	0	1	1	0	0	0	0	0	0
E#strig	0	0	12	5	8	5	1	0	0
E#tube	0	0	11	3	0	0	1	1	1
H#angu	0	0	0	1	0	0	0	0	0
H#petri	0	0	0	1	0	0	4	3	0
H#sphag	0	0	0	0	0	0	0	0	0
H#sylva	1	1	1	0	6	0	1	2	0
H#eleg	45	93	3	41	7	35	8	37	36
H#minu	3	4	0	0	1	1	1	18	8
H#papil	19	0	1	7	0	13	6	9	1
H#subf	0	4	0	0	0	0	0	0	0
N#cari	0	0	6	0	0	0	1	0	0
N#coll	0	0	0	0	0	0	0	0	1

N#flab	0	0	3	0	0	1	0	0	0
N#gris	0	0	2	1	0	5	10	0	1
N#margi	0	0	0	0	0	2	0	0	0
N#milit	0	1	4	3	1	0	0	5	16
N#minor	0	0	0	1	1	2	0	0	3
N#parvu	0	0	16	0	0	3	0	0	0
N#tinc	0	0	0	3	6	5	0	1	14
N#vitre	0	0	0	0	0	0	0	0	0
N#waile	3	0	0	0	0	0	0	0	0
P#acrop	0	0	0	0	0	2	0	0	0
P#spino	0	0	1	1	0	0	0	0	0
P#fasc	0	0	0	0	0	0	0	0	0
P#fulv	0	0	0	0	0	0	0	0	0
S#lenta	0	0	0	0	0	0	0	0	0
T#arcul	0	2	0	0	6	0	0	0	0
T#minu	0	0	0	0	2	0	0	0	1
T#line	0	0	0	0	0	0	0	0	0
T#cory	0	0	1	1	0	0	0	0	6
SampleId	**N5-12**	**N5-11**	**N5-10**	**N5-9**	**N5-8**	**N5-7**	**N5-6**	**N5-5**	**N5-4**
A#flavum	85	40	39	64	9	49	37	1	64
A#steno	1	0	0	0	0	0	0	0	0
A#wrigh	0	0	2	0	0	0	0	1	0
A#arto	0	0	0	0	1	0	0	0	0
A#catin	0	0	4	0	0	0	0	0	0
A#disc	4	0	0	5	1	0	0	0	9
A#gibb	0	0	0	0	0	0	0	0	0
A#hemis	0	0	0	0	0	0	0	0	0
A#vulg	0	0	0	0	0	0	0	0	0
A#musc	2	5	9	0	4	2	10	35	7
A#semi	5	3	1	2	2	0	1	3	1
B#indic	0	0	0	0	0	0	0	0	0
C#ovifo	0	0	0	0	0	0	0	0	0
C#sacc	0	0	0	0	0	0	0	0	0
C#arcel	0	0	3	0	0	1	2	1	0
D#bacum	0	0	0	0	0	0	0	0	0
D#bacra	0	0	0	2	1	0	0	0	0
D#globu	3	0	0	0	58	6	0	0	0
D#lance	0	0	0	0	0	0	0	0	0
D#leidy	0	0	0	4	1	9	0	0	0
D#lucid	0	0	2	5	29	0	1	1	2
D#oblon	0	0	0	0	0	0	0	0	0
D#prist	0	0	1	5	20	1	1	0	3
D#pulex	0	3	1	0	0	1	0	1	0
D#rube	3	0	1	5	1	3	0	0	5
E#comp	1	1	0	0	0	0	1	0	1
E#cris	0	0	0	0	0	3	0	0	0
E#rotun	0	0	0	1	0	0	0	0	2
E#strig	0	1	0	2	0	1	0	10	1
E#tube	2	1	1	0	0	1	0	10	3
H#angu	0	0	0	2	1	1	0	0	4
H#petri	1	3	0	4	3	4	0	0	7
H#sphag	0	2	1	1	0	0	0	0	0
H#sylva	1	0	2	0	0	0	4	9	0
H#eleg	13	36	43	17	1	21	70	29	17
H#minu	8	24	18	1	0	2	5	15	1
H#papil	12	16	3	9	1	18	14	0	16
H#subf	0	0	0	0	0	0	0	0	0
N#cari	1	0	0	0	0	3	0	0	0
N#coll	0	0	0	0	0	0	0	0	0
N#flab	0	0	0	0	0	0	0	0	0
N#gris	8	0	0	9	0	19	0	0	6
N#margi	1	0	0	0	0	0	0	0	0

N#milit	0	5	8	0	0	1	1	21	0
N#minor	0	0	2	0	0	0	0	0	0
N#parvu	0	0	0	0	0	0	0	0	0
N#tinc	0	5	5	0	1	0	2	4	1
N#vitre	0	0	0	0	0	0	0	0	0
N#waile	0	0	0	0	0	0	1	0	0
P#acrop	0	5	5	9	17	8	0	0	2
P#spino	0	0	0	3	0	0	1	0	0
P#fasc	0	0	0	0	0	0	0	0	0
P#fulv	0	0	0	0	0	0	0	0	0
S#lenta	0	0	0	0	0	0	0	0	0
T#arcul	0	1	0	0	0	0	1	1	0
T#minu	0	0	0	0	0	0	0	1	0
T#line	0	0	0	0	0	0	0	0	0
T#cory	0	0	1	0	0	0	0	6	0
SampleId	**N5-3**	**N5-2**	**N5-1**	**N2-15**	**N2-14**	**N2-13**	**N2-12**	**N2-11**	**N2-10**
A#flavum	15	58	58	9	59	72	1	41	61
A#steno	0	0	0	0	2	1	0	0	0
A#wrigh	0	0	0	0	14	4	0	0	3
A#arto	0	2	0	0	0	0	0	0	0
A#catin	0	0	0	1	0	1	4	1	0
A#disc	0	5	6	0	2	0	0	1	9
A#gibb	0	0	0	0	0	0	0	0	0
A#hemis	0	0	0	0	0	0	0	0	1
A#vulg	0	0	0	0	0	0	0	0	0
A#musc	11	2	8	4	3	1	45	5	1
A#semi	3	2	2	0	5	1	9	2	1
B#indic	0	0	0	0	0	0	3	1	0
C#ovifo	0	0	0	0	0	0	0	0	0
C#sacc	0	0	0	0	0	0	0	0	0
C#arcel	0	0	0	1	1	0	2	0	0
D#bacum	0	0	0	0	0	0	0	0	0
D#bacra	0	0	0	0	2	1	0	0	1
D#globu	1	0	0	1	5	2	0	1	1
D#lance	0	0	0	0	0	0	0	0	0
D#leidy	0	3	2	0	10	21	0	6	6
D#lucid	1	0	0	2	0	0	0	0	0
D#oblon	0	0	0	0	0	0	0	0	0
D#prist	0	0	3	0	0	1	0	3	0
D#pulex	8	0	0	1	0	0	1	16	0
D#rube	0	0	0	0	2	0	0	1	0
E#comp	0	0	0	0	0	0	0	1	0
E#cris	1	0	1	0	2	1	5	13	3
E#rotun	8	0	0	1	0	0	2	0	0
E#strig	2	5	9	0	0	1	0	1	0
E#tube	2	1	3	0	4	1	5	1	3
H#angu	0	5	0	0	0	3	0	3	5
H#petri	0	5	0	7	1	4	0	5	2
H#sphag	0	0	0	2	0	0	0	5	1
H#sylva	4	2	0	0	0	0	32	1	0
H#eleg	30	23	23	62	16	2	0	14	31
H#minu	28	2	0	14	0	0	8	0	0
H#papil	0	22	12	40	4	11	1	20	9
H#subf	0	1	0	0	0	0	1	0	0
N#cari	0	2	0	0	1	3	0	0	0
N#coll	0	0	0	0	0	0	0	0	0
N#flab	0	0	2	0	0	0	1	0	0
N#gris	0	12	11	0	13	14	0	3	7
N#margi	0	0	0	0	0	0	0	0	0
N#milit	30	0	3	1	0	0	14	1	0
N#minor	0	0	2	0	0	0	3	1	0
N#parvu	0	0	0	0	0	0	0	0	0

N#tinc	6	0	6	4	2	0	6	1	0
N#vitre	0	0	0	0	0	0	0	0	1
N#waile	1	0	0	0	0	0	0	0	0
P#acrop	0	1	0	1	4	7	0	7	4
P#spino	0	1	0	0	0	0	1	0	1
P#fasc	0	0	0	0	0	0	0	0	0
P#fulv	0	0	0	0	0	0	0	0	0
S#lenta	0	0	0	0	0	0	0	0	0
T#arcul	0	0	0	0	0	0	3	0	0
T#minu	0	0	0	0	0	0	3	0	0
T#line	0	0	0	0	0	0	0	0	0
T#cory	1	0	0	0	0	0	1	0	0
SampleId	**N2-9**	**N2-8**	**N2-7**	**N2-6**	**N2-5**	**N2-4**	**N2-3**	**N2-2**	**N2-1**
A#flavum	3	64	41	9	9	64	49	58	58
A#steno	0	2	0	0	1	0	2	0	0
A#wrigh	0	14	0	0	0	8	12	0	11
A#arto	0	0	0	0	0	0	0	0	0
A#catin	0	0	0	0	2	1	0	0	0
A#disc	0	0	51	0	0	1	2	0	3
A#gibb	0	0	0	0	0	0	0	0	0
A#hemis	0	0	0	0	0	0	0	0	2
A#vulg	0	0	0	0	0	0	0	0	0
A#musc	52	2	1	3	30	4	3	6	0
A#semi	8	5	1	2	6	1	1	1	0
B#indic	0	1	0	0	2	0	0	0	0
C#ovifo	0	0	0	0	0	0	0	0	0
C#sacc	0	0	0	0	0	0	0	0	0
C#arcel	3	0	0	0	9	0	0	0	0
D#bacum	0	0	0	0	0	0	0	0	0
D#bacra	0	1	0	0	0	0	0	0	0
D#globu	0	11	3	1	0	4	4	0	2
D#lance	0	0	0	0	0	0	0	0	0
D#leidy	0	10	6	0	0	10	19	0	12
D#lucid	0	0	0	3	0	0	7	0	0
D#oblon	0	0	0	0	0	0	0	0	0
D#prist	0	1	1	0	0	0	0	0	0
D#pulex	0	0	0	2	0	0	0	4	0
D#rube	0	2	0	0	0	0	2	0	0
E#comp	0	0	0	0	0	0	0	0	1
E#cris	1	0	0	0	0	1	1	0	6
E#rotun	5	0	0	0	1	0	1	0	1
E#strig	5	2	0	0	3	4	7	0	1
E#tube	5	2	2	1	0	1	5	1	2
H#angu	0	7	4	0	0	3	1	0	0
H#petri	0	1	3	4	0	3	2	0	2
H#sphag	1	1	1	3	0	0	0	0	0
H#sylva	2	0	0	5	7	0	0	13	0
H#eleg	32	6	22	97	39	23	11	48	19
H#minu	16	0	0	5	14	0	0	2	8
H#papil	12	8	7	8	18	7	7	3	11
H#subf	2	0	0	0	1	0	0	0	0
N#cari	0	4	0	0	0	0	0	0	0
N#coll	0	0	0	0	0	0	0	0	0
N#flab	0	0	0	0	0	0	0	0	0
N#gris	0	0	1	0	0	4	12	0	6
N#margi	0	1	2	0	0	0	0	0	0
N#milit	1	1	0	4	0	0	0	8	0
N#minor	0	0	0	1	0	0	0	0	0
N#parvu	0	0	0	0	0	0	0	2	0
N#tinc	2	0	0	3	1	1	1	3	0
N#vitre	0	0	1	0	0	0	0	0	0
N#waile	0	0	0	0	0	0	0	2	0

P#acrop	0	6	2	2	1	7	3	0	3
P#spino	0	0	3	0	0	1	0	0	1
P#fasc	0	0	0	0	0	0	0	0	0
P#fulv	0	0	0	0	0	0	0	0	0
S#lenta	0	0	0	0	0	0	0	0	0
T#arcul	0	0	0	0	1	0	0	0	0
T#minu	0	1	0	0	0	0	0	0	0
T#line	0	0	0	0	0	0	0	0	0
T#cory	1	0	0	0	6	0	0	0	0

References

Aaby, B. (**1976**). Cyclic climatic variations in climate over the past 5500 years reflected in raised bogs. *Nature* **263,** 281-289.

Allen, J. R. M., Long, A. J., Ottley, C. J., Pearson, D. G., and Huntley, B. (**2007**). Holocene climate variability in northernmost Europe. *Quaternary Science Reviews* **26,** 1432-1453.

Alley, R. B., and Agustsdottir, A. M. (**2005**). The 8k event: cause and consequences of a major Holocene abrupt climate change. *Quaternary Science Reviews* **24,** 1123-1149.

Alley, R. B., Mayewski, P. A., Sowers, T., Stuiver, M., Taylor, K. C., and Clark, P. U. (**1997**). Holocene climatic instability: A prominent, widespread event 8200 yr ago. *Geology* **25,** 483-486.

Amesbury, M. J. (**2007**). "Fine-resolution peat-based palaeoclimate records of the late-Holocene." University of Southampton.

Amesbury, M. J., Barber, K. E., and Hughes, P. D. M. (**2011**). The methodological basis for fine-resolution, multi-proxy reconstructions of ombrotrophic peat bog surface wetness. *Boreas* **40,** 161-174.

Amesbury, M. J., Barber, K. E., and Hughes, P. D. M. (**2012a**). Can rapidly accumulating Holocene peat profiles provide sub-decadal resolution proxy climate data? *Journal of Quaternary Science***,** n/a-n/a.

Amesbury, M. J., Barber, K. E., and Hughes, P. D. M. (**2012b**). The relationship of fine-resolution, multi-proxy palaeoclimate records to meteorological data at Fågelmossen, Värmland, Sweden and the implications for the debate on

climate drivers of the peat-based record. *Quaternary International* **268,** 77-86.

Andersen, C., Koç, N., and Moros, M. (**2004**). A highly unstable Holocene climate in the subpolar North Atlantic: evidence from diatoms. *Quaternary Science Reviews* **23,** 2155-2166.

Andersson, S., and Schoning, K. (**2010**). Surface wetness and mire development during the late Holocene in central Sweden. *Boreas* **39,** 749-760.

Antonsson, K., and Seppa, H. (**2007**). Holocene temperatures in Bohuslan, southwest Sweden: a quantitative reconstruction from fossil pollen data. *Boreas* **36,** 400-410.

Arnell, N. W. (**2005**). Implications of climate change for freshwater inflows to the Arctic Ocean. *Journal of Geophysical Research* **110,** 0.

Arz, H. W., Lamy, F., and Patzold, J. (**2006**). A pronounced dry event recorded around 4.2 ka in brine sediments from the northern Red Sea. *Quaternary Research* **66,** 432-441.

Axford, Y., Miller, G. H., Geirsdottir, K., and Langdon, P. G. (**2007**). Holocene temperature history of northern Iceland inferred from subfossil midges. *Quaternary Science Reviews* **26,** 3344-3358.

Baker, P. A., Fritz, S. C., Garland, J., and Ekdahl, E. (**2005**). Holocene hydrologic variation at Lake Titicaca, Bolivia/Peru, and its relationship to North Atlantic climate variation. *Journal of Quaternary Science* **20,** 655-662.

Bakke, J., Dahl, S. O., Paasche, O., Lovlie, R., and Nesje, A. (**2005**). Glacier fluctuations, equilibrium-line altitudes and palaeoclimate in Lyngen, northern Norway, during the Lateglacial and Holocene. *Holocene* **15,** 518-540.

Bakke, J., Dahl, S. O., Paasche, O., Simonsen, J. R., Kvisvik, B., Bakke, K., and Nesje, A. (**2010**). A complete record of Holocene glacier variability at Austre Okstindbreen, northern Norway: an integrated approach. *Quaternary Science Reviews* **29,** 1246-1262.

Barber, D. C., Dyke, A., Hillaire-Marcel, C., Jennings, A. E., Andrews, J. T., Kerwin, M. W., Bilodeau, G., McNeely, R., Southon, J., Morehead, M. D., and Gagnon, J. M. (**1999**). Forcing of the cold event of 8,200 years ago by catastrophic drainage of Laurentide lakes. *Nature* **400,** 344-348.

Barber, K. E. (**1981**). "Peat stratigraphy and climate change: a palaeoecological test of the theory of cyclic peat bog regeneration." Balkema, Rotterdam.

Barber, K. E. (**1984**). A large-capacity Russian pattern sediment sampler. *Quaternary Newsletter* **44,** 28-31.

Barber, K. E. (**1994**). Deriving Holocene palaeoclimates from peat stratigraphy: some misconceptions regarding the sensitivity and coninuity of the record. *Quaternary Newsletter* **72,** 1-9.

Barber, K. E., Chambers, F. M., Dumayne-Peaty, L., Haslam, C. J., Maddy, D., and Stoneman, R. (**1994**). A sensitive high-resolution record of late-Holocene climate change from a raised bog in northern England. *The Holocene* **4,** 198-205.

Barber, K. E., Chambers, F. M., and Maddy, D. (**2003**). Holocene palaeoclimates from peat stratigraphy: macrofossil proxy climate records from three oceanic raised bogs in England and Ireland. *Quaternary Science Reviews* **22,** 521-539.

Barber, K. E., Chambers, F. M., and Maddy, D. (**2004**). Late Holocene climatic history of northern Germany and Denmark: peat macrofossil investigations at

Dosenmoor, Schleswig-Holstein, and Svanemose, Jutland. *Boreas* **33,** 132-144.

Barber, K. E., Dumayne-Peaty, L., Hughes, P. D. M., Mauquoy, D., and Scaife, R. (**1998**). Replicability and variability of the recent macrofossil and proxy-climate record from raised bogs: field stratigraphy and macrofossil data from Bolton Fell Moss and Walton Moss, Cumbria, England. *Journal of Quaternary Science* **13,** 515-528.

Barber, K. E., and Langdon, P. G. (**2007**). What drives the peat-based palaeoclimate record? A critical test using multi-proxy climate records from northern Britain. *Quaternary Science Reviews* **26,** 3318-3327.

Barber, K. E., Maddy, D., Rose, N., Stevenson, A. C., Stoneman, R., and Thompson, R. (**2000**). Replicated proxy-climate signals over the last 2000 yr from two distant UK peat bogs: new evidence for regional palaeoclimate teleconnections. *Quaternary Science Reviews* **19,** 481-487.

Bard, E., Hamelin, B., Arnold, M., Montaggioni, L., Cabioch, G., Faure, G., and Rougerie, F. (**1996**). Deglacial sea-level record from Tahiti corals and the timing of global meltwater discharge. *Nature* **382,** 241-244.

Barry, R. G., and Chorley, R. J. (**2010**). "Atmosphere, Weather and Climate." Routledge, Oxon.

Bartlein, P. J., Harrison, S. P., Brewer, S., Connor, S., Davis, B. A. S., Gajewski, K., Guiot, J., Harrison-Prentice, T. I., Henderson, A., Peyron, O., Prentice, I. C., Scholze, M., Seppa, H., Shuman, B., Sugita, S., Thompson, R. S., Viau, A. E., Williams, J., and Wu, H. (**2011**). Pollen-based continental climate reconstruction at 6 and 21 ka: a global synthesis. *Climate Dynamics* **37,** 775-802.

Behre, K. E. (**2007**). A new Holocene sea-level curve for the southern North Sea. *Boreas* **36,** 82-102.

Benson, L., Kashgarian, M., Rye, R., Lund, S., Paillet, F., Smoot, J., Kester, C., Mensing, S., Meko, D., and Lindstrom, S. (**2002**). Holocene multidecadal and multicentennial droughts affecting Northern California and Nevada. *Quaternary Science Reviews* **21,** 659-682.

Berger, A. (**1978**). Long Term Variations of Daily Insolation and Quaternary Climatic Changes. *Journal of Atmospheric Sciences* **35,** 2362-2367.

Berger, A., and Loutre, M. F. (**1991**). Insolation values for the cliamte of the last 10 million years. *Quaternary Science Reviews* **10,** 297-317.

Berger, W. H., and von Rad, U. (**2002**). Decadal to millennial cyclicity in varves and turbidites from the Arabian Sea: hypothesis of tidal origin. *Global and Planetary Change* **34,** 313-325.

Berner, K. S., Koç, N., Divine, D., Godtliebsen, F., and Moros, M. (**2008**). A decadal-scale Holocene sea surface temperature record from the subpolar North Atlantic constructed using diatoms and statistics and its relation to other climate parameters. *Paleoceanography* **23,** 1-15.

Bianchi, G. G., and McCave, I. N. (**1999**). Holocene Periodicity in North Atlantic Climate and Deep-Ocean Flow South of Iceland. *Nature***,** 515-517.

Bird, M. I., Austin, W. E. N., Wurster, C. M., Fifield, L. K., Mojtahid, M., and Sargeant, C. (**2010**). Punctuated eustatic sea-level rise in the early mid-Holocene. *Geology* **38,** 803-806.

Bird, M. I., Fifield, L. K., Teh, T. S., Chang, C. H., Shirlaw, N., and Lambeck, K. (**2007**). An inflection in the rate of early mid-Holocene eustatic sea-level rise:

A new sea-level curve from Singapore. *Estuarine Coastal and Shelf Science* **71,** 523-536.

Birks, H. J. B. (**1995**). Quantitative palaeoenvironmental reconstruction. *In* "Statistical Modelling of Quaternary Science Data." (D. Maddy, and J. S. Brew, Eds.). Quaternary Research Association, Cambridge.

Birks, H. J. B. (**1998**). Numerical tools in palaeolimnology - Progress, potentialities, and problems. *Journal of Paleolimnology* **20,** 307-332.

Birks, H. J. B., and Birks, H. H. (**2004**). "Quaternary Palaeoecology." Blackburn Press.

Birks, H. J. B., Line, J. M., Juggins, S., Stevenson, A. C., and ter Braak, C. J. F. (**1990**). Diatoms and pH reconstruction. *Philosophical Transactions of the Royal Society B* **327,** 263-278.

Birks, H. J. B., and Seppä, H. (**2004**). Pollen-based reconstructions of late-Quaternary climate in Europe - progress, problems and pitfalls. *Acta Palaeobotanica* **44,** 317-334.

Birks, H. J. B., and Seppä, H. (**2010**). Late-Quaternary palaeoclimatic research in Fennoscandia – A historical review. *Boreas* **39,** 655-673.

Bjune, A. E., Bakke, J., Nesje, A., and Birks, H. J. B. (**2005**). Holocene mean July temperature and winter precipitation in western Norway inferred from palynological and glaciological lake-sediment proxies. *Holocene* **15,** 177-189.

Blaauw, M. (**2010**). Methods and code for 'classical' age-modelling of radiocarbon sequences. *Quaternary Geochronology* **5,** 512-518.

Blackford, J. J., and Chambers, F. M. (**1991**). Proxy records of climate from blanket mires: evidence for a Dark Age (1400 BP) climatic deterioration in the British Isles. *The Holocene* **1,** 63-67.

Blackford, J. J., and Chambers, F. M. (**1993**). Determining the degree of peat decomposition for peat-based palaeoclimatic studies. *International Peat Journal* **5,** 7-24.

Blundell, A., and Barber, K. E. (**2005**). A 2800-year palaeoclimatic record from Tore Hill Moss, Strathspey, Scotland: the need for a multi-proxy approach to peat-based climate reconstructions. *Quaternary Science Reviews* **24,** 1261-1277.

Blundell, A., Charman, D. J., and Barber, K. (**2008**). Multiproxy late Holocene peat records from Ireland: towards a regional palaeoclimate curve. *Journal of Quaternary Science* **23,** 59-71.

Blytt, A. (**1876**). "Essay on the immigration of Norwegian flora during alternating rainy and dry periods." Cammermayer, Christiana.

Bobrov, A. A., Charman, D. J., and Warner, B. G. (**1999**). Ecology of testate amoebae (Protozoa : Rhizopoda) on peatlands in western Russia with special attention to niche separation in closely related taxa. *Protist* **150,** 125-136.

Bond, G. C., Kromer, B., Beer, J., Muscheler, R., Evans, M. N., Showers, W., Hoffmann, S., Lotti-Bond, R., Hajdas, I., and Bonani, G. (**2001**). Persistent solar influence on North Atlantic climate during the Holocene. *Science* **294,** 2130-6.

Bond, G. C., and Lotti, R. (**1995**). Iceberg Discharges into the North Atlantic on Millennial Time Scales During the Last Glaciation *Science* **267** 1005-1010.

Bond, G. C., Showers, W., Cheseby, M., Lotti, R., Almasi, P., deMenocal , P., Priore, P., Cullen, H., Hajdas, I., and Bonani, G. (**1997**). A Pervasive Millennial-Scale Cycle in North Atlantic Holocene and Glacial Climates. *Science* **278,** 1257-1266.

Booth, R. K. (**2002**). Testate amoebae as paleoindicators of surface-moisture changes on Michigan peatlands: modern ecology and hydrological calibration. *Journal of Paleolimnology* **28,** 329-348.

Booth, R. K. (**2008**). Testate amoebae as proxies for mean annual waiter-table depth in Sphagnum-dominated peatlands of North America. *Journal of Quaternary Science* **23,** 43-57.

Booth, R. K. (**2010**). Testing the climate sensitivity of peat-based paleoclimate reconstructions in mid-continental North America. *Quaternary Science Reviews* **29,** 720-731.

Booth, R. K., and Jackson, S. T. (**2003**). A high-resolution record of late-Holocene moisture variability from a Michigan raised bog, USA *The Holocene* **13** 863-876.

Booth, R. K., Jackson, S. T., Forman, S. L., Kutzbach, J. E., Bettis, E. A., Kreig, J., and Wright, D. K. (**2005**). A severe centennial-scale drought in mid-continental North America 4200 years ago and apparent global linkages. *Holocene* **15,** 321-328.

Booth, R. K., Lamentowicz, M., and Charman, D. J. (**2010**). Preparation and analysis of testate amoebae in peatland palaeoenvironmental studies. *Mires and Peat* **7,** Article 2.

Borgmark, A. (**2005**). Holocene climate variability and periodicities in south-central Sweden, as interpreted from peat humification analysis. *The Holocene* **15,** 387-395.

Borgmark, A., and Schoning, K. (**2006**). A comparative study of peat proxies from two eastern central Swedish bogs and their relation to meteorological data. *Journal of Quaternary Science* **21,** 109-114.

Borgmark, A., and Wastegård, S. (**2008**). Regional and local patterns of peat humification in three raised bogs in Värmland, south-central Sweden. *GFF2* **130,** 161-176.

Boygle, J. (**1998**). A little goes a long way : discovery of a new mid-Holocene tephra in Sweden. *Boreas* **27,** 195-199.

Boygle, J. (**2004**). Towards a Holocene tephrochronology for Sweden: geochemistry and correlation with the North Atlantic tephra stratigraphy. *Journal of Quaternary Science* **19,** 103-109.

Brader, A. V., van Winden, J. F., Bohncke, S. J. P., Beets, C. J., Reichart, G.-J., and de Leeuw, J. W. (**2010**). Fractionation of hydrogen, oxygen and carbon isotopes in n-alkanes and cellulose of three Sphagnum species. *Organic Geochemistry* **41,** 1277-1284.

Bradley, R. S., and Jones, P. D. (**1993**). 'Little Ice Age' summer temperature variations: their nature and relevance to recent global warming trends *The Holocene* **3,** 367-376.

Braun, H., Christl, M., Rahmstorf, S., Ganopolski, A., Mangini, A., Kubatzki, C., Roth, K., and Kromer, B. (**2005**). Possible solar origin of the 1,470-year glacial climate cycle demonstrated in a coupled model. *Nature* **438,** 208-211.

Broecker, W. S. (**2000**). Was a change in thermohaline circulation responsible for the Little Ice Age? *Proceedings of the National Academy of Sciences of the United States of America* **97,** 1339-1342.

Broecker, W. S. (**2003**). Does the trigger for abrupt climate change reside in the ocean or in the atmosphere? *Science* **300,** 1519-1522.

Bronk Ramsey, C. (**2009**). Bayesian analysis of radiocarbon dates. *Radiocarbon* **51,** 337-360.

Brooker, R. W., Maestre, F. T., Callaway, R. M., Lortie, C. L., Cavieres, L. A., Kunstler, G., Liancourt, P., Tielbörger, K., Travis, J. M. J., Anthelme, F., Armas, C., Coll, L., Corcket, E., Delzon, S., Forey, E., Kikvidze, Z., Olofsson, J., Pugnaire, F., Quiroz, C. L., Saccone, P., Schiffers, K., Seifan, M., Touzard, B., and Michalet, R. (**2008**). Facilitation in plant communities: the past, the present, and the future. *Journal of Ecology* **96,** 18-34.

Brown, K. J., Seppa, H., Schoups, G., Fausto, R. S., Rasmussen, P., and Birks, H. J. B. (**2012**). A spatio-temporal reconstruction of Holocene temperature change in southern Scandinavia. *Holocene* **22,** 165-177.

Bu, Z.-J., Rydin, H., and Chen, X. (**2011**). Direct and interaction-mediated effects of environmental changes on peatland bryophytes. *Oecologia* **166,** 555-563.

Cappers, R. T. J., Bekker, R. M., and Jans, J. E. A. (**2006**). "Digital Seed Atlas of the Netherlands. Archaeological Studies 4." Barkhuis, Groningen.

Carlson, A. E., LeGrande, A. N., Oppo, D. W., Came, R. E., Schmidt, G. A., Anslow, F. S., Licciardi, J. M., and Obbink, E. A. (**2008**). Rapid early Holocene deglaciation of the Laurentide ice sheet. *Nature Geoscience* **1,** 620-624.

Caseldine, C., and Gearey, B. (**2005**). A multiproxy approach to reconstructing surface wetness changes and prehistoric bog bursts in a raised mire system at Derryville Bog, Co. Tipperary, Ireland. *Holocene* **15,** 585-601.

Caseldine, C., Langdon, P., and Holmes, N. (**2006**). Early Holocene climate variability and the timing and extent of the Holocene thermal maximum (HTM) in northern Iceland. *Quaternary Science Reviews* **25,** 2314-2331.

Chambers, F. M., Barber, K. E., Maddy, D., and Brew, J. (**1997**). A 5500-year proxy-climate and vegetation record from blanket mire at Talla Moss, Borders, Scotland. *Holocene* **7,** 391-399.

Chambers, F. M., Beilman, D. W., and Yu, Z. (**2010**). Methods for determining peat humification and for quantifying peat bulk density, organic matter and carbon content for palaeostudies of climate and peatland carbon dynamics. *Mires and Peat* **7,** 1-10.

Chambers, F. M., and Blackford, J. J. (**2001**). Mid- and late-Holocene climatic changes: a test of periodicity and solar forcing in proxy-climate data from blanket peat bogs. *Journal of Quaternary Science* **16,** 329-338.

Chambers, F. M., Booth, R. K., De Vleeschouwer, F., Lamentowicz, M., Le Roux, G., Mauquoy, D., Nichols, J. E., and van Geel, B. (**2012**). Development and refinement of proxy-climate indicators form peats. *Quaternary International* **268,** 21-33.

Chambers, F. M., and Charman, D. J. (**2004**). Holocene environmental change: contributions from the peatland archive. *The Holocene* **14,** 1-6.

Chapman, M. R., and Shackleton, N. J. (**2000**). Evidence of 550-year and 1000-year cyclicities in North Atlantic circulation patterns during the Holocene. *The Holocene* **10,** 287-291.

Charman, D. J. (**1997**). Modelling hydrological relationships of testate amoebae (Protozoa: Rhizopoda) on New Zealand peatlands. *Journal of the Royal Society of New Zealand* **27,** 465-483.

Charman, D. J. (**2001**). Biostratigraphic and palaeoenvironmental applications of testate amoebae. *Quaternary Science Reviews* **20,** 1753-1764.

Charman, D. J. (**2007**). Summer water deficit variability controls on peatland water-table changes: implications for Holocene palaeoclimate reconstructions. *Holocene* **17,** 217-227.

Charman, D. J. (**2010**). Centennial climate variability in the British Isles during the mid-late Holocene. *Quaternary Science Reviews* **29,** 1539-1554.

Charman, D. J., Barber, K. E., Blaauw, M., Langdon, P. G., Mauquoy, D., Daley, T. J., Hughes, P. D. M., and Karofeld, E. (**2009**). Climate drivers for peatland palaeoclimate records. *Quaternary Science Reviews* **28,** 1811-1819.

Charman, D. J., Blundell, A., Chiverrell, R. C., Hendon, D., and Langdon, P. G. (**2006**). Compilation of non-annually resolved Holocene proxy climate records: stacked Holocene peatland palaeo-water table reconstructions from northern Britain. *Quaternary Science Reviews* **25,** 336-350.

Charman, D. J., Blundell, A., and MEMBERS, A. (**2007**). A new European testate amoebae transfer function for palaeohydrological reconstruction of ombrotrophic peatlands. *Journal of Quaternary Science* **22,** 209-221.

Charman, D. J., Brown, A. D., Hendon, D., and Karofeld, E. (**2004**). Testing the relationship between Holocene peatland palaeoclimate reconstructions and instrumental data at two European sites. *Quaternary Science Reviews* **23,** 137-143.

Charman, D. J., and Garnett, M. H. (**2005**). Chronologies for recent peat deposits using wiggle-matched radiocarbon ages: Problems with old carbon contamination. *Radiocarbon* **47,** 135-145.

Charman, D. J., and Hendon, D. (**2000**). Long-term changes in soil water tables over the past 4500 years: Relationships with climate and North Atlantic atmospheric circulation and sea surface temperature. *Climatic Change* **47,** 45-59.

Charman, D. J., Hendon, D., and Packman, S. (**1999**). Multiproxy surface wetness records from replicate cores on an ombrotrophic mire: implications for Holocene palaeoclimate records. *Journal of Quaternary Science* **14,** 451-463.

Charman, D. J., Hendon, D., and Woodland, W. A. (**2000**). "The identification of testate amoebae (Protozoa: Rhizipoda) in peats. QRA Technical Guide No. 9." Quaternary Research Association, London.

Charman, D. J., and Warner, B. G. (**1997**). The ecology of testate amoebae (Protozoa : Rhizopoda) in oceanic peatlands in Newfoundland, Canada: Modelling hydrological relationships for palaeoenvironmental reconstruction. *Ecoscience* **4,** 555-562.

Chen, J. L., Wilson, C. R., and Tapley, B. D. (**2006**). Satellite gravity measurements confirm accelerated melting of Greenland ice sheet. *Science* **313,** 1958-60.

Chiverrell, R. C. (**2001**). A proxy record of late Holocene climate change from May Moss, northeast England. *Journal of Quaternary Science* **16,** 9-29.

Clarke, G. K. C., Leverington, D. W., Teller, J. T., and Dyke, A. S. (**2004**). Paleohydraulics of the last outburst flood from glacial Lake Agassiz and the 8200 BP cold event. *Quaternary Science Reviews* **23,** 389-407.

COHMAP, M. (**1988**). Climatic Changes of the Last 18,000 Years: Observations and Model Simulations. *Science* **241,** 1043-1052.

Cullen, H. M., deMenocal, P. B., Hemming, S., Hemming, G., Brown, F. H., Guilderson, T., and Sirocko, F. (**2000**). Climate change and the collapse of the Akkadian empire: Evidence from the deep sea. *Geology* **28,** 379-382.

Daley, T. J., and Barber, K. E. (**2012**). Multi-proxy Holocene palaeoclimate records from Walton Moss, northern England and Dosenmoor, northern Germarny, assessed using three statistical approaches. *Quaternary International*.

Daley, T. J., Barber, K. E., Street-Perrott, F. A., Loader, N. J., Marshall, J. D., Crowley, S. F., and Fisher, E. H. (**2010**). Holocene climate variability revealed by oxygen isotope analysis of Sphagnum cellulose from Walton Moss, northern England. *Quaternary Science Reviews* **29,** 1590-1601.

Daley, T. J., Street-Perrott, F. A., Loader, N. J., Barber, K. E., Hughes, P. D. M., Fisher, E. H., and Marshall, J. D. (**2009**). Terrestrial climate signal of the "8200 yr B.P. cold event" in the Labrador Sea region. *Geology* **37,** 831-834.

Daley, T. J., Thomas, E. R., Holmes, J. A., Street-Perrott, F. A., Chapman, M. R., Tindall, J. C., Valdes, P. J., Loader, N. J., Marshall, J. D., Wolff, E. W., Hopley, P. J., Atkinson, T., Barber, K. E., Fisher, E. H., Robertson, I., Hughes, P. D. M., and Roberts, C. N. (**2011**). The 8200 yr BP cold event in stable isotope records from the North Atlantic region. *Global and Planetary Change* **79,** 288-302.

Daniels, R. E., and Eddy, A. (**1990**). "Handbook of European Sphagna." HMSO, London.

Dansgaard, W., Johnsen, S. J., Clausen, H. B., Dahl-Jensen, D., Gundestrup, N. S., Hammer, C. U., Hvidberg, C. S., Steffensen, J. P., Sveinbjornsdottir, A. E.,

Jouzel, J., and Bond, G. (**1993**). Evidence for general instability of past climate from a 250-kyr ice-core record. *Nature* **364,** 218-220.

Davis, B. A. S., and Brewer, S. (**2009**). Orbital forcing and role of the latitudinal insolation/temperature gradient. *Climate Dynamics* **32,** 143-165.

Davis, B. A. S., and Brewer, S. (**2011**). A unified approach to orbital, solar, and lunar forcing based on the Earth's latitudinal insolation/temperature gradient. *Quaternary Science Reviews* **30,** 1861-1874.

Davis, B. A. S., Brewer, S., Stevenson, A. C., and Guiot, J. (**2003**). The temperature of Europe during the Holocene reconstructed from pollen data. *Quaternary Science Reviews* **22,** 1701-1716.

De Vleeschouwer, F., Gérard, L., Goormaghtigh, C., Mattielli, N., Le Roux, G., and Fagel, N. (**2007**). Atmospheric lead and heavy metal pollution records from a Belgian peat bog spanning the last two millenia: human impact on a regional to global scale. *The Science of the Total Environment* **377,** 282-95.

De Vleeschouwer, F., Pazdur, A., Luthers, C., Streel, M., Mauquoy, D., Wastiaux, C., Le Roux, G., Moschen, R., Blaauw, M., Pawlyta, J., Sikorski, J., and Piotrowska, N. (**2012**). A millennial record of environmental change in peat deposits from the Misten bog (East Belgium). *Quaternary International*.

De Vleeschouwer, F. ß., Piotrowska, N., Sikorski, J. Ç., Pawlyta, J., Cheburkin, A., Le Roux, G. l., Lamentowicz, M., Fagel, N., and Mauquoy, D. (**2009**). Multiproxy evidence of `Little Ice Age' palaeoenvironmental changes in a peat bog from northern Poland. *The Holocene* **19,** 625-637.

Dearing, J. A. (**1997**). Sedimentary indicators of lake-level changes in the humid temperate zone: A critical review. *Journal of Paleolimnology* **18,** 1-14.

Debret, M., Bout-Roumazeilles, V., Grousset, F., Desmet, M., McManus, J. F., Massei, N., Sebag, D., Petit, J. R., Copard, Y., and Trentesaux, A. (**2007**). The origin of the 1500-year climate cycles in Holocene North-Atlantic records. *Climate of the Past* **3,** 679-692.

Debret, M., Sebag, D., Crosta, X., Massei, N., Petit, J. R., Chapron, J. R., and Bout-Roumazeilles, V. (**2009**). Evidence from wavelet analysis for a mid-Holocene transition in global climate forcing. *Quaternary Science Reviews* **28,** 2675-2688.

Deline, P., and Orombelli, G. (**2005**). Glacier fluctuations in the western Alps during the Neoglacial, as indicated by the Miage morainic amphitheatre (Mont Blanc massif, Italy). *Boreas* **34,** 456-467.

Delworth, T. L., and Mann, M. E. (**2000**). Observed and simulated multidecadal variability in the Northern Hemisphere. *Climate Dynamics* **16,** 661-676.

deMenocal, P., Ortiz, J., Guilderson, T., and Sarnthein, M. (**2000**). Coherent high- and low-latitude climate variability during the Holocene warm period. *Science* **288,** 2198-2202.

deMenocal, P. B. (**2001**). Cultural responses to climate change during the Late Holocene. *Science* **292,** 667-673.

Denton, G., and Broecker, W. (**2008**). Wobbly ocean conveyor circulation during the Holocene? *Quaternary Science Reviews* **27,** 1939-1950.

Denton, G. H., and Karlén, W. (**1973**). Holocene climatic variations - their pattern and possible cause. *Quaternary Research* **205,** 155-205.

Digerfeldt, G. (**1988**). Reconstruction and regional correlation of Holocene lake-level fluctuations in Lake Bysjon, South Sweden. *Boreas* **17,** 165-182.

Dima, M., and Lohmann, G. (**2009**). Conceptual model for millennial climate variability: a possible combined solar-thermohaline circulation origin for the ~1,500-year cycle. *Climate Dynamics* **32,** 301-311.

Ditlevsen, P. D., Andersen, K. K., and Svensson, A. (**2007**). The DO-climate events are probably noise induced: statistical investigation of the claimed 1470 years cycle. *Climate of the Past* **3,** 129-134.

Dodd, P. A., Heywood, K. J., Meredith, M. P., Naveira-Garabato, A. C., Marca, A. D., and Falkner, K. K. (**2009**). Sources and fate of freshwater exported in the East Greenland Current. *Geophysical Research Letters* **36,** 0.

Dumayne-Peaty, L., and Barber, K. E. (**1998**). Late Holocene vegetational history, human impact and pollen representativity variations in northern Cumbria, England. *Journal of Quaternary Science* **13,** 147-164.

Dupont, L. M. (**1986**). Temperature and rainfall variation in the Holocene based on comparative palaeoecology and isotope geology of a hummock and a hollow (Bourtangerveen, the Netherlands). *Review of Palaeobotany and Palynology* **48,** 71-159.

Dupont, L. M., and Benninkmeijer, C. A. M. (**1984**). Palaeobotanic and isotopic analysis of late Subboreal and early Subatlantic peat from Engbertsdijksveen-Vii, the Netherlands. *Review of Palaeobotany and Palynology* **41**.

Dyke, A. S., and Prest, V. K. (**1987**). Late Wisconsinan and Holocene History of the Laurentide Ice Sheet. *Géographie Physique et Quaternaire* **41,** 237-263.

Edvardsson, J., Leuschner, H. H., Linderson, H., Linderholm, H. W., and Hammarlund, D. (**2012**). South Swedish bog pines as indicators of Mid-Holocene climate variability. *Dendrochronologia* **30,** 93-103.

Einstein, A. (**1931**). "Cosmic Religion: With Other Opinions and Aphorisms." Covici-Friede, New York.

Fairbanks, R. G. (**1989**). A 17,000-YEAR GLACIO-EUSTATIC SEA-LEVEL RECORD - INFLUENCE OF GLACIAL MELTING RATES ON THE YOUNGER DRYAS EVENT AND DEEP-OCEAN CIRCULATION. *Nature* **342,** 637-642.

Fairbridge, R. W., and Hillairemarcel, C. (**1977**). 8,000-YR PALEOCLIMATIC RECORD OF DOUBLE-HALE 45-YR SOLAR-CYCLE. *Nature* **268,** 413-416.

Fleitmann, D., Burns, S. J., Mudelsee, M., Neff, U., Kramers, J., Mangini, A., and Matter, A. (**2003**). Holocene forcing of the Indian monsoon recorded in a stalagmite from Southern Oman. *Science* **300,** 1737-1739.

Fleming, K., Johnston, P., Zwartz, D., Yokoyama, Y., Lambeck, K., and Chappell, J. (**1998**). Refining the eustatic sea-level curve since the Last Glacial Maximum using far- and intermediate-field sites. *Earth and Planetary Science Letters* **163,** 327-342.

Franzén, L. G. (**2006**). Increased decomposition of subsurface peat in Swedish raised bogs: are temperate peatlands still net sinks of carbon? *Mires and Peat* **1,** Article 3.

Franzén, L. G., and Cropp, R. A. (**2007**). The Peatland/Ice Age hypothesis revised, adding a possible glacial pulse trigger. *Geografiska Annaler: Series A, Physical Geography* **89,** 301-330.

Giraudeau, J., Cremer, M., Manthe, S., Labeyrie, L., and Bond, G. (**2000**). Coccolith evidence for instabilities in surface circulation south of Iceland during Holocene times. *Earth and Planetary Science Letters* **179,** 257-268.

Godwin, H. (**1940**). Pollen analysis and forest history of England and Wales. *New Phytologist* **33,** 278-305.

Godwin, H. (**1975**). "History of the British Flora." Cambridge University Press, Cambridge.

Granath, G., Strengbom, J., and Rydin, H. (**2012**). Direct physiological effects of nitrogen on Sphagnum: a greenhouse experiment. *Functional Ecology* **26,** 353-364.

Grosjean, M., Suter, P. J., Trachsel, M., and Wanner, H. (**2007**). Ice-borne prehistoric finds in the Swiss Alps reflect Holocene glacier fluctuations. *Journal of Quaternary Science* **22,** 203-207.

Grosvernier, P., Matthey, Y., and Buttler, A. (**1997**). Growth Potential of Three Sphagnum Species in Relation to Water Table Level and Peat Properties with Implications for Their Restoration in Cut- Over Bogs. *Journal of Applied Ecology* **34,** 471-483.

Guiot, J., Harrison, S. P., and Prentice, I. C. (**1993**). RECONSTRUCTION OF HOLOCENE PRECIPITATION PATTERNS IN EUROPE USING POLLEN AND LAKE-LEVEL DATA. *Quaternary Research* **40,** 139-149.

Gunnarson, B. E., Borgmark, A., and Wastegard, S. (**2003**). Holocene humidity fluctuations in Sweden inferred from dendrochronology and peat stratigraphy. *Boreas* **32,** 347-360.

Gupta, A. K., Das, M., and Anderson, D. M. (**2005**). Solar influence on the Indian summer monsoon during the Holocene. *Geophysical Research Letters* **32**.

Haas, J. N., Richoz, I., Tinner, W., and Wick, L. (**1998**). Synchronous Holocene climatic oscillations recorded on the Swiss Plateau and at timberline in the Alps *The Holocene* **8** 301-309.

Harnisch, O. (**1927**). Einige Daten zur rezenten und fossil testacem Rhizopoden-Fauna der Sphagnen. *Archiv für Hydrobiologie* **18,** 246-360.

Harrison, S. P., Prentice, I. C., and Guiot, J. (**1993**). CLIMATIC CONTROLS ON HOLOCENE LAKE-LEVEL CHANGES IN EUROPE. *Climate Dynamics* **8,** 189-200.

Hays, J. D., Imbrie, J., and Shackleton, N. J. (**1976**). Variations in the Earth's Orbit: Pacemaker of the Ice Ages. *Science***,** 1121-1132.

Heal, O. W. (**1961**). The distribution of testate amoebae (Rhizopoda: testacea) in some fens and bogs in northern England. *Journal of the Linnean Society, Zoology* **44,** 369-382.

Heal, O. W. (**1963**). Morphological variation in certain testacea (Protozoa: Rhizopoda). *Archiv für Prostistenkunde* **106,** 351-368.

Heaton, T. J., Blackwell, P. G., and Buck, C. E. (**2009**). A bayesian approach to the estimation of radiocarbon calibration curves: The INTCAL09 methodology. *Radiocarbon* **51,** 1151-1164.

Heikkila, M., and Seppä, H. (**2003**). A 11,000 yr palaeotemperature reconstruction from the southern boreal zone in Finland. *Quaternary Science Reviews* **22,** 541-554.

Helama, S., Timonen, M., Holopainen, J., Ogurtsov, M. G., Mielikäinen, K., Eronen, M., Lindholm, M., and Meriläinen, J. (**2009**). Summer temperature variations in Lapland during the Medieval Warm Period and the Little Ice Age relative

to natural instability of thermohaline circulation on multi-decadal and multi-centennial scales. *Journal of Quaternary Science* **24,** 450-456.

Hendon, D., Charman, D. J., and Kent, M. (**2001**). Palaeohydrological records derived from testate amoebae analysis from peatlands in northern England: within-site variability, between-site comparability and palaeoclimatic implications. *The Holocene* **11,** 127-148.

Hill, M. O. (**1973**). Reciprocal averaging: an eigenvector method of ordination. *Journal of Ecology* **61,** 237-249.

Hill, M. O., and Gauch, H. G. (**1980**). Detrended Correspondence analysis: an improved ordination technique. *Vegetation* **42,** 47-58.

Hillaire-Marcel, C., de Vernal, A., Bilodeau, G., and Weaver, A. J. (**2001**). Absence of deep-water formation in the Labrador Sea during the last interglacial period. *Nature* **410,** 1073-1077.

Hoskins, B., James, I. N., and White, G. H. (**1983**). The shape, propagation and mean-flow interaction of large-sclae weather systems. *Journal of Atmospheric Sciences* **40,** 1595-1612.

Hu, F. S., Kaufman, D., Yoneji, S., Nelson, D., Shemesh, A., Huang, Y., Tian, J., Bond, G., Clegg, B., and Brown, T. (**2003**). Cyclic variation and solar forcing of Holocene climate in the Alaskan subarctic. *Science* **301,** 1890-1893.

Hughes, P. D. M. (**1997**). "The Palaeoecology of the Fen/Bog transition during the early- to mid-Holocene in Britain.", University of Southampton.

Hughes, P. D. M. (**2000**). A reappraisal of the mechanisms leading to ombrotrophy in British raised mires. *Ecology Letters* **3,** 7-9.

Hughes, P. D. M., and Barber, K. E. (**2003**). Mire development across the fen-bog transition on the Teifi floodplain at Tregaron Bog, Ceredigion, Wales, and a comparison with 13 other raised bogs. *Journal of Ecology* **91,** 253-264.

Hughes, P. D. M., and Barber, K. E. (**2004**). Contrasting pathways to ombrotrophy in three raised bogs from Ireland and Cumbria, England. *The Holocene* **14,** 65-77.

Hughes, P. D. M., Barber, K. E., Langdon, P. G., and Mauquoy, D. (**2000a**). Mire-development pathways and palaeoclimatic records from a full Holocene peat archive at Walton Moss, Cumbria, England. *The Holocene* **10,** 465-479.

Hughes, P. D. M., Blundell, A., Charman, D. J., Bartlett, S., Daniell, J. R. G., Wojatschke, A., and Chambers, F. M. (**2006**). An 8500cal. year multi-proxy climate record from a bog in eastern Newfoundland: contributions of meltwater discharge and solar forcing. *Quaternary Science Reviews* **25,** 1208-1227.

Hughes, P. D. M., Kenward, H. K., Hall, A. R., and Large, F. D. (**2000b**). A high-resolution record of mire development and climatic change spanning the Late-glacial-Holocene boundary at Church Moss, Davenham (Cheshire, England). *Journal of Quaternary Science* **15,** 697-724.

Hughes, P. D. M., Lomas-Clarke, S. H., Schulz, J., and Barber, K. E. (**2008**). Decline and localized extinction of a major raised bog species across the British Isles: evidence for associated land-use intensification *The Holocene* **18** 1033-1043.

Hughes, P. D. M., Lomas-Clarke, S. H., Schulz, J., and Jones, P. (**2007**). The declining quality of late-Holocene ombrotrophic communities and the loss of Sphagnum austinii (Sull. ex Aust.) on raised bogs in Wales. *The Holocene* **17,** 613-625.

Hughes, P. D. M., Mallon, G., Essex, H. J., Amesbury, M. J., Charman, D. J., Blundell, A., Chambers, F. M., Daley, T. J., and Mauquoy, D. (**2012**). The use of k-values to examine plant 'species signals' in a peat humification record from Newfoundland. *Quaternary International*.

Huntley, B. (**1991**). HOW PLANTS RESPOND TO CLIMATE CHANGE - MIGRATION RATES, INDIVIDUALISM AND THE CONSEQUENCES FOR PLANT-COMMUNITIES. *Annals of Botany* **67,** 15-22.

Huntley, B., Baillie, M., Grove, J. M., Hammer, C. U., Harrison, S. P., Jacomet, S., Jansen, E., Karlen, W., Koc, N., Luterbacher, J., Negendank, J., and Schibler, J. (**2002**). "Holocene palaeoenvironmental changes in north-west Europe: Climatic implications and the human dimension." Springer-Verlag Berlin, Berlin.

Hyvärinen, H. (**1973**). The deglaciation history of eastern Fennoscandia - recent data from Finland. *Boreas* **2,** 85-102.

Imbrie, J., Berger, A., Boyle, E. A., Clemens, S. C., Duffy, A., Howard, W. R., Kukla, G., Kutzbach, J., Martinson, D. G., McIntyre, A., Mix, A. C., Molfino, B., Morley, J. J., Peterson, L. C., Pisias, N. G., Prell, W. L., Raymo, M. E., Shackleton, N. J., and Toggweiler, J. R. (**1993**). ON THE STRUCTURE AND ORIGIN OF MAJOR GLACIATION CYCLES .2. THE 100,000-YEAR CYCLE. *Paleoceanography* **8,** 699-735.

Imbrie, J., and Imbrie, J. Z. (**1980**). MODELING THE CLIMATIC RESPONSE TO ORBITAL VARIATIONS. *Science* **207,** 943-953.

IPCC. (**2007**). "Fourth Assessment Report: Climate Change 2007: The AR4 Synthesis Report." Geneva: IPCC.

Iversen, K. (**1941**). Landnam i Danmarks stenalder. *Danmarks Geologiske Undersogelse II* **66**.

Ivy-Ochs, S., Kerschner, H., Maisch, M., Christl, M., Kubik, P. W., and Schluchter, C. (**2009**). Latest Pleistocene and Holocene glacier variations in the European Alps. *Quaternary Science Reviews* **28,** 2137-2149.

Jessen, K. (**1949**). Studies in Late-Quaternary deposits and flora-history of Ireland. *Proceedings of the Royal Irish Academy* **52B**.

Joerin, U. E., Nicolussi, K., Fischer, A., Stocker, T. F., and Schluchter, C. (**2008**). Holocene optimum events inferred from subglacial sediments at Tschierva Glacier, Eastern Swiss Alps. *Quaternary Science Reviews* **27,** 337-350.

Joerin, U. E., Stocker, T. F., and Schluchter, C. (**2006**). Multicentury glacier fluctuations in the Swiss Alps during the Holocene. *Holocene* **16,** 697-704.

Jones, R. T., Marshall, J. D., Fisher, E., Hatton, J., Patrick, C., Anderson, K., Lang, B., Bedford, A., and Oldfield, F. (**2011**). Controls on lake level in the early to mid Holocene, Hawes Water, Lancashire, UK. *Holocene* **21,** 1061-1072.

Jongman, R. H. G., ter Braak, C. J. F., and van Tongeren, O. F. R. (**1995**). "Data analysis in community and landscape ecology." Cambridge University Press, Cambridge.

Jouzel, J., Masson-Delmotte, V., Cattani, O., Dreyfus, G., Falourd, S., Hoffmann, G., Minster, B., Nouet, J., Barnola, J. M., Chappellaz, J., Fischer, H., Gallet, J. C., Johnsen, S., Leuenberger, M., Loulergue, L., Luethi, D., Oerter, H., Parrenin, F., Raisbeck, G., Raynaud, D., Schilt, A., Schwander, J., Selmo, E., Souchez, R., Spahni, R., Stauffer, B., Steffensen, J. P., Stenni, B., Stocker, T. F., Tison, J. L., Werner, M., and Wolff, E. W. (**2007**). Orbital and millennial

Antarctic climate variability over the past 800,000 years. *Science* **317,** 793-796.

Kaislahti Tillman, P., Holzkämper, S., Kuhry, P., Sannel, A. B. K., Loader, N. J., and Robertson, I. (**2010**). Stable carbon and oxygen isotopes in Sphagnum fuscum peat from subarctic Canada: Implications for palaeoclimate studies. *Chemical Geology* **270,** 216-226.

Kaplan, M. R., and Wolfe, A. P. (**2006**). Spatial and temporal variability of Holocene temperature in the North Atlantic region. *Quaternary Research* **65,** 223-231.

Karlén, W. (**1976**). Lacustrine sediments and tree-line variations as indicators of climatic fluctuations in Lappland, northern Sweden. *Geografiska Annaler: Series A, Physical Geography* **58,** 1-34.

Karlén, W. (**1988**). SCANDINAVIAN GLACIAL AND CLIMATIC FLUCTUATIONS DURING THE HOLOCENE. *Quaternary Science Reviews* **7,** 199-209.

Kaufman, D. S., Ager, T. A., Anderson, N. J., Anderson, P. M., Andrews, J. T., Bartlein, P. J., Brubaker, L. B., Coats, L. L., Cwynar, L. C., Duvall, M. L., Dyke, A. S., Edwards, M. E., Eisner, W. R., Gajewski, K., Geirsdottir, A., Hu, F. S., Jennings, A. E., Kaplan, M. R., Kerwin, M. N., Lozhkin, A. V., MacDonald, G. M., Miller, G. H., Mock, C. J., Oswald, W. W., Otto-Bliesner, B. L., Porinchu, D. F., Ruhland, K., Smol, J. P., Steig, E. J., and Wolfe, B. B. (**2004**). Holocene thermal maximum in the western Arctic (0-180 degrees W). *Quaternary Science Reviews* **23,** 529-560.

Keigwin, L. D. (**1996**). The Little Ice Age and Medieval warm period in the Sargasso Sea. *Science* **274,** 1504-1508.

Keigwin, L. D., Donnelly, J. P., Cook, M. S., Driscoll, N. W., and Brigham-Grette, J. (**2006**). Rapid sea-level rise and Holocene climate in the Chukchi Sea. *Geology* **34,** 861-864.

Kellner, E. (**2001**). Surface energy fluxes and control of evapotranspiration from a Swedish Sphagnum mire. *Agricultural and Forest Meteorology* **110,** 101-123.

Kerr, R. A. (**2000**). A North Atlantic Climate Pacemaker for the Centuries *Science* **288** 1984-1985.

Kleman, J., Hattestrand, C., Borgstrom, I., and Stroeven, A. (**1997**). Fennoscandian palaeoglaciology reconstructed using a glacial geological inversion model. *Journal of Glaciology* **43,** 283-299.

Knudsen, K. L., Sondergaard, M. K. B., Eiriksson, J., and Jiang, H. (**2008**). Holocene thermal maximum off North Iceland: Evidence from benthic and planktonic foraminifera in the 8600-5200 cal year BP time slice. *Marine Micropaleontology* **67,** 120-142.

Kovach, W. L. (**1995**). "Multivariate Data Analysis." Quaternary Research Association, London.

Kuder, T., and Kruge, M. A. (**1998**). Preservation of biomolecules in sub-fossil plants from raised peat bogs - a potential paleoenvironmental proxy. *Organic Geochemistry* **29,** 1355-1368.

Kuhlbrodt, T., Rahmstorf, S., Zickfeld, K., Vikebø, F., Sundby, S., Hofmann, N., Link, P., Bondeau, A., Cramer, W., and Jaeger, C. (**2009**). An Integrated Assessment of changes in the thermohaline circulation. *Climatic Change* **96,** 489-537.

Lamb, H. H. (**1982**). "Climate, History and the Modern World." Methuen, London.

Lambeck, K. (**1990**). LATE PLEISTOCENE, HOLOCENE AND PRESENT SEA-LEVELS - CONSTRAINTS ON FUTURE CHANGE. *Global and Planetary Change* **89,** 205-217.

Lamentowicz, L., Lamentowicz, M., and Gabka, M. (**2008**). Testate amoebae ecology and a local transfer function from a peatland in western Poland. *Wetlands* **28,** 164-175.

Lamentowicz, M., Lamentowicz, L., van der Knaap, W. O., Gabka, M., and Mitchell, E. A. D. (**2010**). Contrasting Species-Environment Relationships in Communities of Testate Amoebae, Bryophytes and Vascular Plants Along the Fen-Bog Gradient. *Microbial Ecology* **59,** 499-510.

Lamy, F., Arz, H. W., Bond, G. C., Bahr, A., and Patzold, J. (**2006**). Multicentennial-scale hydrological changes in the Black Sea and northern Red Sea during the Holocene and the Arctic/North Atlantic oscillation. *Paleoceanography* **21**.

Langdon, P. G., and Barber, K. E. (**2001**). New Holocene tephras and a proxy climate record from a blanket mire in northern Skye, Scotland. *Journal of Quaternary Science* **16,** 753-759.

Langdon, P. G., and Barber, K. E. (**2004**). Snapshots in time: precise correlations of peat-based proxy climate records in Scotland using mid-Holocene tephras. *Holocene* **14,** 21-33.

Langdon, P. G., and Barber, K. E. (**2005**). The climate of Scotland over the last 5000 years inferred from multiproxy peatland records: inter-site correlations and regional variability. *Journal of Quaternary Science* **20,** 549-566.

Langdon, P. G., Barber, K. E., and Hughes, P. D. M. (**2003**). A 7500-year peat-based palaeoclimatic reconstruction and evidence for an 1100-year cyclicity in bog surface wetness from Temple Hill Moss, Pentland Hills, southeast Scotland. *Quaternary Science Reviews* **22,** 259-274.

Langdon, P. G., Barber, K. E., and Lomas-Clarke, S. H. (**2004**). Reconstructing climate and environmental change in northern England through chironomid and pollen analyses: evidence from Talkin Tarn, Cumbria. *Journal of Paleolimnology* **32,** 197-213.

Lie, O., Dahl, S. O., Nesje, A., Matthews, J. A., and Sandvold, S. (**2004**). Holocene fluctuations of a polythermal glacier in high-alpine eastern Jotunheimen, central-southern Norway. *Quaternary Science Reviews* **23,** 1925-1945.

Litt, T., Scholzel, C., Kuhl, N., and Brauer, A. (**2009**). Vegetation and climate history in the Westeifel Volcanic Field (Germany) during the past 11 000 years based on annually laminated lacustrine maar sediments. *Boreas* **38,** 679-690.

Loisel, J., and Garneau, M. (**2010**). Late Holocene paleoecohydrology and carbon accumulation estimates from two boreal peat bogs in eastern Canada: Potential and limits of multi-proxy archives. *Palaeogeography Palaeoclimatology Palaeoecology* **291,** 493-533.

Lousier, J. D., and Parkinson, D. (**1981**). The disappearance of the empty tests of litter- and soil-testate amoebae (Testacea, Rhizopoda, Protozoa). *Archiv fuer Prostistenkunde* **124,** 312-336.

Lundqvist, J. (**1957**). "C14-datering av rekurrensytor i Värmland." Sveriges Geologiska Undersökning C554.

Lundqvist, J. (**1958**). "Beskrivning till jordartskarta över Värmlands län." Sveriges Geologiska Undersökning Ca 38.

Magny, M. (**1993**). Holocene fluctuations of lake levels in the French Jura and sub-Alpine ranges, and their implications for past general circulation patterns *The Holocene* **3** 306-313.

Magny, M. (**2004**). Holocene climate variability as reflected by mid-European lake-level fluctuations and its probable impact on prehistoric human settlements. *Quaternary International* **113,** 65-79.

Magny, M., Begeot, C., Guiot, J., Marguet, A., and Billaud, Y. (**2003a**). Reconstruction and palaeoclimatic interpretation of mid-Holocene vegetation and lake-level changes at Saint-Jorioz, Lake Annecy, French Pre-Alps. *Holocene* **13,** 265-275.

Magny, M., Bégeot, C. G. J., and Peyron, O. (**2003b**). Contrasting patterns of hydrological changes in Europe in response to Holocene climate cooling phases. *Quaternary Science Reviews* **22,** 1589-1596.

Magny, M., Bossuet, G., Ruffaldi, P., Leroux, A., and Mouthon, J. (**2011**). Orbital imprint on Holocene palaeohydrological variations in west-central Europe as reflected by lakelevel changes at Cerin (Jura Mountains, eastern France). *Journal of Quaternary Science* **26,** 171-177.

Magny, M., and Haas, J. N. (**2004**). A major widespread climatic change around 5300 cal. yr BP at the time of the Alpine Iceman. *Journal of Quaternary Science* **19,** 423-430.

Magny, M., Leuzinger, U., Bortenschlager, S., and Haas, J. (**2006**). Tripartite climate reversal in Central Europe 5600-5300 years ago. *Quaternary Research* **65,** 3-19.

Magyari, E., Sumegi, P., Braun, M., Jakab, G., and Molnar, M. (**2001**). Retarded wetland succession: anthropogenic and climatic signals in a Holocene peat bog profile from north-east Hungary. *Journal of Ecology* **89,** 1019-1032.

Mann, D. H., and Hamilton, T. D. (**1995**). Late Pleistocene and Holocene paleoenvironments of the North Pacific coast. *Quaternary Science Reviews* **14,** 449-471.

Marchal, O., Cacho, I., Stocker, T. F., Grimalt, J. O., Calvo, E., Martrat, B., Shackleton, N., Vautravers, M., Cortijo, E., van Kreveld, S., Andersson, C., Koc, N., Chapman, M., Sbaffi, L., Duplessy, J. C., Sarnthein, M., Turon, J. L., Duprat, J., and Jansen, E. (**2002**). Apparent long-term cooling of the sea surface in the northeast Atlantic and Mediterranean during the Holocene. *Quaternary Science Reviews* **21,** 455-483.

Matthews, J. A. (**2007**). Neoglaciation in Europe. *In* "Encyclopedia of Quaternary Science." (S. Elias, Ed.). Elsevier, Amsterdam.

Matthews, J. A., Berrisford, M. S., Dresser, P. Q., Nesje, A., Dahl, S. O., Bjune, A. E., Bakke, J., John, H., Birks, B., Lie, O., Dumayne-Peaty, L., and Barnett, C. (**2005**). Holocene glacier history of Bjornbreen and climatic reconstruction in central Jotunheimen, Norway, based on proximal glaciofluvial stream-bank mires. *Quaternary Science Reviews* **24,** 67-90.

Matthews, J. A., and Briffa, K. R. (**2005**). The 'Little Ice Age': Re-Evaluation of an evolving concept. *Geografiska Annaler: Series A, Physical Geography* **87,** 17-36.

Matthews, J. A., Dahl, S. O., Nesje, A., Berrisford, M. S., and Andersson, C. (**2000**). Holocene glacier variations in central Jotunheimen, southern Norway based on distal glaciolacustrine sediment cores. *Quaternary Science Reviews* **19,** 1625-1647.

Mauquoy, D. (**1997**). "Testing the Sensitivity of the Palaeoclimatic signal from ombrotrophic peat stratigraphy." University of Southampton.

Mauquoy, D., and Barber, K. E. (**1999**). A replicated 3000 yr proxy−climate record from Coom Rigg Moss and Felecia Moss, the Border Mires, northern England. *Journal of Quaternary Science* **14,** 263-275.

Mauquoy, D., and Barber, K. E. (**2002**). Testing the sensitivity of the palaeoclimatic signal from ombrotrophic peat bogs in northern England and the Scottish Borders. *Review of Palaeobotany and Palynology* **119,** 219-240.

Mauquoy, D., Hughes, P. D. M., and Van Geel, B. (**2010**). A protocol for plant macrofossil analysis of peat deposits. *Mires and Peat* **7,** Article 6.

Mauquoy, D., Yeloff, D., van Geel, B., and Blundell, A. (**2008**). Two decadally resolved records from north-west European peat bogs show rapid climate changes associated with solar variability during the mid-late Holocene. *Journal of Quaternary Science* **23,** 745-763.

McClymont, E. L., Mauquoy, D., Yeloff, D., Broekens, P., van Geel, B., Charman, D. J., Pancost, R. D., Chambers, F. M., and Evershed, R. P. (**2008**). The disappearance of Sphagnum imbricatum from Butterburn Flow, UK. *Holocene* **18,** 991-1002.

McDermott, F., Mattey, D. P., and Hawkesworth, C. (**2001**). Centennial-scale holocene climate variability revealed by a high-resolution speleothem delta O-18 record from SW Ireland. *Science* **294,** 1328-1331.

McMullen, J. A. (**2000**). "Palaeoecology and Conservation Management of Lowland Raised Bogs." University of Southampton.

Menounos, B., Clague, J. J., Osborn, G., Luckman, B. H., Lakeman, T. R., and Minkus, R. (**2008**). Western Canadian glaciers advance in concert with climate change circa 4.2 ka. *Geophysical Research Letters* **35**.

Milankovitch, M. (**1941**). "Kanon der Erdbestahlung und seine Anwendung auf das Eiszeitproblem." K\"onigliche Serbische Akademie.

Mitchell, E. A. D., Buttler, A. J., Warner, B. G., and Gobat, J. M. (**1999**). Ecology of testate amoebae (Protozoa : Rhizopoda) in Sphagnum peatlands in the Jura mountains, Switzerland and France. *Ecoscience* **6,** 565-576.

Mitchell, E. A. D., Payne, R. J., and Lamentowicz, M. (**2008**). Potential implications of differential preservation of testate amoeba shells for paleoenvironmental reconstruction in peatlands. *Journal of Paleolimnology* **40,** 603-618.

Moros, M., Andrews, J. T., Eberl, D. D., and Jansen, E. (**2006**). Holocene history of drift ice in the northern North Atlantic: Evidence for different spatial and temporal modes. *Paleoceanography* **21**.

Moros, M., Emeis, K., Risebrobakken, B., Snowball, I., Kuijpers, A., McManus, J., and Jansen, E. (**2004**). Sea surface temperatures and ice rafting in the Holocene North Atlantic: climate influences on Northern Europe and Greenland. *Quaternary Science Reviews* **23,** 2113-2126.

Moschen, R., Kuhl, N., Peters, S., Vos, H., and Lucke, A. (**2011**). Temperature variability at Durres Maar, Germany during the Migration Period and at High Medieval Times, inferred from stable carbon isotopes of Sphagnum cellulose. *Climate of the Past* **7,** 1011-1026.

Moschen, R., Kuhl, N., Rehberger, I., and Lucke, A. (**2009**). Stable carbon and oxygen isotopes in sub-fossil Sphagnum: Assessment of their applicability for palaeoclimatology. *Chemical Geology* **259,** 262-272.

Nesje, A. (**2009**). Latest Pleistocene and Holocene alpine glacier fluctuations in Scandinavia. *Quaternary Science Reviews* **28,** 2119-2136.

Nesje, A., Bakke, J., Dahl, S. O., Lie, O., and Matthews, J. A. (**2008**). Norwegian mountain glaciers in the past, present and future. *Global and Planetary Change* **60,** 10-27.

Nesje, A., Bjune, A. E., Bakke, J., Dahl, S. O., Lie, O., and Birks, H. J. B. (**2006**). Holocene palaeoclimate reconstructions at Vanndalsvatnet, western Norway, with particular reference to the 8200 cal. yr BP event. *Holocene* **16,** 717-729.

Nesje, A., and Dahl, S. O. (**1993**). LATEGLACIAL AND HOLOCENE GLACIER FLUCTUATIONS AND CLIMATE VARIATIONS IN WESTERN NORWAY - A REVIEW. *Quaternary Science Reviews* **12,** 255-261.

Nesje, A., and Dahl, S. O. (**2001**). The Greenland 8200 cal. yr BP event detected in loss-on-ignition profiles in Norwegian lacustrine sediment sequences. *Journal of Quaternary Science* **16,** 155-166.

Nesje, A., and Dahl, S. O. (**2003**). The 'Little Ice Age' - only temperature? *Holocene* **13,** 139-145.

New, M., Lister, D., Hulme, M., and Makin, I. (**2002**). A high-resolution data set of surface climate over global land areas. *Climate Research* **21,** 1-25.

Niggemann, S., Mangini, A., Mudelsee, M., Richter, D. K., and Wurth, G. (**2003**). Sub-Milankovitch climatic cycles in Holocene stalagmites from Sauerland, Germany. *Earth and Planetary Science Letters* **216,** 539-547.

O'Brien, S. R., Mayewski, P. A., Meeker, L. D., Meese, D. A., Twickler, M. S., and Whitlow, S. I. (**1995**). COMPLEXITY OF HOLOCENE CLIMATE AS

RECONSTRUCTED FROM A GREENLAND ICE CORE. *Science* **270,** 1962-1964.

O'Hare, G., Sweeney, J., and Wilby, R. (**2005**). "Weather, Climate and Climate Change." Pearson Education Limited, Harlow.

Oerlemans, J. (**2001**). "Glaciers and Climate Change." A.A. Balkema, Lisse.

Oppo, D. W., McManus, J. F., and Cullen, J. L. (**2003**). Palaeo-oceanography: Deepwater variability in the Holocene epoch. *Nature* **422,** 277-278.

Osvald, H. (**1923**). "Die Vegetation des Hochmoores Komosse." Svenska Vaxscociologisk Sallskapets Handlinger 1.

Overbeck, F. (**1947**). Studien zur Hochmoorentwicklung in Niedersachsen und die Bestimmung der Humifizierung bei stratigraphisch-pollenanalytischen Mooruntersuchungen. *Planta* **35,** 1-56.

Overbeck, F. (**1975**). "Botanisch-geologische Moorkunde." Karl Wachholz Verlag, Neumuenster.

Palastanga, V., van der Schrier, G., Weber, S. L., Kleinen, T., Briffa, K. R., and Osborn, T. J. (**2011**). Atmosphere and ocean dynamics: contributors to the European Little Ice Age? *Climate Dynamics* **36,** 973-987.

Parviainen, M., and Luoto, M. (**2007**). Climate envelopes of mire comples types in Fennoscandia. *Geografiska Annaler: Series A, Physical Geography* **89,** 137-151.

Paul, A., and Schulz, M. (**2002**). "Holocene climate variability on centennial-to-millennial time scales: 2. Internal and forced oscillations as possible causes." Springer-Verlag Berlin, Berlin.

Payne, R. J., Charman, D. J., Matthews, S., and Eastwood, W. J. (**2008**). Testate amoebae as palaeohydrological proxies in Surmene Agacbasi Yaylasi peatland (Northeast Turkey). *Wetlands* **28,** 311-323.

Payne, R. J., Kishaba, K., Blackford, J. J., and Mitchell, E. A. D. (**2006**). Ecology of testate amoebae (Protista) in south-central Alaska peatlands: building transfer-function models for palaeoenvironmental studies. *Holocene* **16,** 403-414.

Peltier, W. R. (**2002**). On eustatic sea level history: Last Glacial Maximum to Holocene. *Quaternary Science Reviews* **21,** 377-396.

Peltier, W. R., and Fairbanks, R. G. (**2006**). Global glacial ice volume and Last Glacial Maximum duration from an extended Barbados sea level record. *Quaternary Science Reviews* **25,** 3322-3337.

Penman, H. L. (**1948**). Natural Evaporation from Open Water, Bare Soil and Grass *Proceedings of the Royal Society of London. Series A. Mathematical and Physical Sciences* **193** 120-145.

Persch, F. (**1950**). Zur postgrazialen Wald- und Moorentwicklung im Hohen Venn. *Decheniana* **104,** 81-93.

Persson, C. (**1966**). Försök till tefrokronologisk datering av några svenska torvmossar. *Geologiska Föreningens i Stockholm Förhandlingar* **88,** 361-394.

Peyron, O., Guiot, J., Cheddadi, R., Tarasov, P., Reille, M., de Beaulieu, J. L., Bottema, S., and Andrieu, V. (**1998**). Climatic reconstruction in Europe for 18,000 yr B.P. from pollen data. *Quaternary Research* **49,** 183-196.

Prentice, I. C., Guiot, J., Huntley, B., Jolly, D., and Cheddadi, R. (**1996**). Reconstructing biomes from palaeoecological data: A general method and its application to European pollen data at 0 and 6 ka. *Climate Dynamics* **12,** 185-194.

Proust, M. (**1913-1927**). "A la recherche du temps perdu." Grasset & Gallimard.

Pyne-O'Donnell, S. (**2011**). The taphonomy of Last Glacial–Interglacial Transition (LGIT) distal volcanic ash in small Scottish lakes. *Boreas* **40,** 131-145.

Pyne-O'Donnell, S., Hughes, P. D. M., Froese, D. G., Jensen, B. J. L., Kuehn, S. C., Mallon, G., Amesbury, M. J., Charman, D. J., Daley, T. J., Loader, N. J., Mauquoy, D., Street-Perrott, F. A., and Woodman-Ralph, J. (**2012**). High-precision ultra-distal Holocene tephrochronology in North America. *Quaternary Science Reviews* **56,** 6-11.

Reimer, P. J., Baillie, M. G. L., Bard, E., Bayliss, A., Beck, J. W., Blackwell, P. G., Bronk Ramsey, C., Buck, C. E., Burr, G. S., Edwards, R. L., Friedrich, M., Grootes, P. M., Guilderson, T. P., Hajdas, I., Heaton, T. J., Hogg, A. G., Hughen, K. A., Kaiser, K. F., Kromer, B., McCormac, F. G., Manning, S. W., Reimer, R. W., Richards, D. A., Southon, J. R., Talamo, S., Turney, C. S. M., Van Der Plicht, J., and Weyhenmeyer, C. E. (**2009**). IntCal09 and Marine09 Radiocarbon Age Calibration Curves, 0-50,000 Years Cal BP. *Radiocarbon* **51,** 1111-1150.

Renson, V., Fagel, N., Mattielli, N., Nekrassoff, S., Streel, M., and De Vleeschouwer, F. (**2008**). Roman road pollution assessed by elemental and lead isotope geochemistry in East Belgium. *Applied Geochemistry* **23,** 3253-3266.

Renssen, H., Goosse, H., and Fichefet, T. (**2002**). Modeling the effect of freshwater pulses on the early Holocene climate: The influence of high-frequency climate variability. *Paleoceanography* **17**.

Renssen, H., Goosse, H., Fichefet, T., and Campin, J. (**2001**). The 8.2 kyr BP event simulated by a Global Atmosphere-Sea-Ice-Ocean Model. *Geophys. Res. Lett.* **28,** 1567-1570.

Renssen, H., Seppa, H., Heiri, O., Roche, D. M., Goosse, H., and Fichefet, T. (**2009**). The spatial and temporal complexity of the Holocene thermal maximum. *Nature Geoscience* **2,** 410-413.

Rinterknecht, V. R., Clark, P. U., Raisbeck, G. M., Yiou, F., Bitinas, A., Brook, E. J., Marks, L., Zelcs, V., Lunkka, J. P., Pavlovskaya, I. E., Piotrowski, J. A., and Raukas, A. (**2006**). The last deglaciation of the southeastern sector of the Scandinavian Ice Sheet. *Science* **311,** 1449-1452.

Rodwell, J. S. (**1991**). "British Plant Communities - Mires and heath." Cambridge University Press, Cambridge.

Rohling, E. J., and Palike, H. (**2005**). Centennial-scale climate cooling with a sudden cold event around 8,200 years ago. *Nature* **434,** 975-979.

Rosqvist, G., Jonsson, C., Yam, R., Karlen, W., and Shemesh, A. (**2004**). Diatom oxygen isotopes in pro-glacial lake sediments from northern Sweden: a 5000 year record of atmospheric circulation. *Quaternary Science Reviews* **23,** 851-859.

Russell, J. M., and Johnson, T. C. (**2005**). Late Holocene climate change in the North Atlantic and equatorial Africa: Millennial-scale ITCZ migration. *Geophysical Research Letters* **32**.

Rydin, H., and Jeglum, J. K. (**2006**). "The Biology of Peatlands." Oxford University Press, Oxford.

S.N.H. (**2009**). Raeburn Flow - Site management statement, Dumfries.

Salonen, J. S., Seppä, H., Valiranta, M., Jones, V. J., Self, A., Heikkila, M., Kultti, S., and Yang, H. D. (**2011**). The Holocene thermal maximum and late-Holocene cooling in the tundra of NE European Russia. *Quaternary Research* **75,** 501-511.

Sarnthein, M., Van Kreveld, S., Erlenkeuser, H., Grootes, P. M., Kucera, M., Pflaumann, U., and Schulz, M. (**2003**). Centennial-to-millennial-scale periodicities of Holocene climate and sediment injections off the western Barents shelf, 75 degrees N. *Boreas* **32,** 447-461.

Schmidt, R., Koinig, K. A., Thompson, R., and Kamenik, C. (**2002**). A multi proxy core study of the last 7000 years of climate and alpine land-use impacts on an Austrian mountain lake (Unterer Landschitzsee, Niedere Tauern). *Palaeogeography Palaeoclimatology Palaeoecology* **187,** 101-120.

Schulz, M., and Paul, A. (**2002a**). Holocene Climate Variability on Centennial to Millennial Time Scales: Climate Records from the North-Atlantic Realm. *In* "Climate Development and History of the North Atlantic Realm." pp. 41-54. Springer-Verlag, Berlin, Heidelberg.

Schulz, M., and Paul, A. (**2002b**). "Holocene climate variability on centennial-to-millennial time scales: 1. Climate records from the North-Atlantic realm." Springer-Verlag Berlin, Berlin.

Schulz, M., Prange, M., and Klocker, A. (**2007**). Low-frequency oscillations of the Atlantic Ocean meridional overturning circulation in a coupled climate model. *Climate of the Past* **3,** 97-107.

Seppä, H. (**2002**). Mires of Finland: Regional and local controls of vegetation, landforms and long-term dynamics. *Fennia* **180,** 43-60.

Seppä, H., and Birks, H. J. B. (**2001**). July mean temperature and annual precipitation trends during the Holocene in the Fennoscandian tree-line area: pollen-based climate reconstructions. *Holocene* **11,** 527-539.

Seppä, H., Bjune, A. E., Telford, R. J., Birks, H. J. B., and Veski, S. (**2009**). Last nine-thousand years of temperature variability in Northern Europe. *Climate of the Past Discussions* **5,** 1521-1552.

Seppä, H., Hammarlund, D., and Antonsson, K. (**2005**). Low-frequency and high-frequency changes in temperature and effective humidity during the Holocene in south-central Sweden: implications for atmospheric and oceanic forcings of climate. *Climate Dynamics* **25,** 285-297.

Sernander, R. (**1894**). "Studier ofver den gotlandska vegetationens utvecklingshistoria." Upsala University.

Sernander, R. (**1908**). On the evidence of postglacial changes of climate furnished by the peat-mosses of northern Europe. *Geologiska Föreningens i Stockholm* **30,** 456-478.

Shennan, I., Lambeck, K., Horton, B., Innes, J., Lloyd, J., McArthur, J., Purcell, T., and Rutherford, M. (**2000**). Late Devensian and Holocene records of relative sea-level changes in northwest Scotland and their implications for glacio-hydro-isostatic modelling. *Quaternary Science Reviews* **19,** 1103-1135.

Shennan, I., Peltier, W. R., Drummond, R., and Horton, B. (**2002**). Global to local scale parameters determining relative sea-level changes and the post-glacial isostatic adjustment of Great Britain. *Quaternary Science Reviews* **21,** 397-408.

Shuman, B., and Plank, C. (**2011**). Orbital, ice sheet, and possible solar controls on Holocene moisture trends in the North Atlantic drainage basin. *Geology* **39,** 151-154.

Sillasoo, Ü., Mauquoy, D., Blundell, A., Charman, D. J., Blaauw, M., Daniell, J. R. G., Toms, P., Newberry, J., Chambers, F. M., and Karofeld, E. (**2007**). Peat multi-proxy data from Männikjärve bog as indicators of late Holocene climate changes in Estonia. *Boreas* **36,** 20-37.

Smith, A. J. E. (**2004**). "The Moss Flora of Britain and Ireland." Cambridge University Press, Cambridge.

Smith, D. E., Harrison, S., Firth, C. R., and Jordan, J. T. (**2011**). The early Holocene sea level rise. *Quaternary Science Reviews* **30,** 1846-1860.

Snowball, I., and Sandgren, P. (**1996**). Lake sediment studies of Holocene glacial activity in the Karsa valley, northern Sweden: Contrasts in interpretation. *Holocene* **6,** 367-372.

Springer, G. S., Rowe, H. D., Hardt, B., Edwards, R. L., and Cheng, H. (**2008**). Solar forcing of Holocene droughts in a stalagmite record from West Virginia in east-central North America. *Geophysical Research Letters* **35**.

Stace, C. (**1991**). "New Flora of the British Isles." Cambridge University Press, Cambridge.

Staubwasser, M., Sirocko, F., Grootes, P. M., and Segl, M. (**2003**). Climate change at the 4.2 ka BP termination of the Indus valley civilization and Holocene south Asian monsoon variability. *Geophysical Research Letters* **30**.

Steig, E. J. (**1999**). Mid-Holocene Climate Change. *Science* **266,** 1485-1487.

Steinecke, F. (**1927**). Leitformen und Leitfossilien des Zehlaubruches: die Bedeutung der fossilen Mikro-organismen fuer Erkenntniss der Nekrozonosen eines Moores. *Botanisches Archive: Zeitschrift fuer die gesamte Botanik* **19,** 327-344.

Stoneman, R. (**1993**). "Holocene palaeoclimates from peat stratigraphy: extending and refining the model." University of Southampton.

Stoneman, R., Barber, K. E., and Maddy, D. (**1993**). Present and past ecology of Sphagnum imbricatum and its significance in raised-peat-climate modelling. *Quaternary Newsletter* **70,** 14-22.

Stuiver, M., and Braziunas, T. F. (**1993**). Sun, ocean, climate and atmospheric 14CO2 : an evaluation of causal and spectral relationships. *The Holocene* **3,** 289-305.

Stuiver, M., Grootes, P. M., and Braziunas, T. F. (**1995**). The GISP2 delta O-18 climate record of the past 16,500 years and the role of the sun, ocean, and volcanoes. *Quaternary Research* **44,** 341-354.

Sutton, R. T., and Hodson, D. L. R. (**2003**). Influence of the Ocean on North Atlantic Climate Variability 1871-1999. *Journal of Climate* **16,** 3296.

Sutton, R. T., and Hodson, D. L. R. (**2005**). Atlantic Ocean forcing of North American and European summer climate. *Science* **309,** 115-8.

Swindles, G. T., Blundell, A., Roe, H. M., and Hall, V. A. (**2010**). A 4500-year proxy climate record from peatlands in the North of Ireland: the identification of widespread summer 'drought phases'? *Quaternary Science Reviews* **29,** 1577-1589.

Swindles, G. T., Charman, D. J., Roe, H. M., and Sansum, P. A. (**2009**). Environmental controls on peatland testate amoebae (Protozoa: Rhizopoda) in the North of Ireland: Implications for Holocene palaeoclimate studies. *Journal of Paleolimnology* **42,** 123-140.

Swindles, G. T., Morris, P. J., Baird, A. J., Blaauw, M., and Plunkett, G. (**2012a**). Ecohydrological feedbacks confound peat-based climate reconstructions. *Geophys. Res. Lett.* **39,** L11401.

Swindles, G. T., Patterson, R. T., Roe, H. M., and Galloway, J. M. (**2012b**). Evaluating periodicities in peat-based climate proxy records. *Quaternary Science Reviews* **41,** 94-103.

Swindles, G. T., Plunkett, G., and Roe, H. M. (**2007**). A multiproxy climate record from a raised bog in County Fermanagh, Northern Ireland: a critical examination of the link between bog surface wetness and solar variability. *Journal of Quaternary Science* **22,** 667-679.

Swindles, G. T., and Roe, H. M. (**2007**). Examining the dissolution characteristics of testate amoebae (Protozoa : Rhizopoda) in low pH conditions: Implications for peatland palaeoclimate studies. *Palaeogeography Palaeoclimatology Palaeoecology* **252,** 486-496.

Swingedouw, D., Mignot, J., Braconnot, P., Mosquet, E., Kageyama, M., and Alkama, R. (**2009**). Impact of Freshwater Release in the North Atlantic under Different Climate Conditions in an OAGCM. *Journal of climate* **22,** 6377-6403.

Telford, R. J., and Birks, H. J. B. (**2005**). The secret assumption of transfer functions: problems with spatial autocorrelation in evaluating model performance. *Quaternary Science Reviews* **24**.

Telford, R. J., and Birks, H. J. B. (**2009**). Evaluation of transfer functions in spatially structured environments. *Quaternary Science Reviews* **28,** 1309-1316.

Telford, R. J., and Birks, H. J. B. (**2011**). A novel method for assessing the statistical significance of quantitative reconstructions inferred from biotic assemblages. *Quaternary Science Reviews* **30,** 1272-1278.

ter Braak, C. J. F., and Juggins, S. (**1993**). Weighted averaging partial least squares regression (WA-PLS): an improved method for reconstructing environmental variable from species assemblages. *Hydrobiologica* **269,** 485-502.

ter Braak, C. J. F., and van Dam, H. (**1989**). Inferring pH from diatoms: a comparison of old and new calibration methods. *Hydrobiologica* **178,** 209-223.

Thompson, D. W. J., Lee, S., and Baldwin, M. P. (**2002a**). Atmospheric processes governing the Northern Hemisphere annual mode/North Atlantic Oscillation. *In* "The North Atlantic Oscillation: climatic significance and environmental impact." (J. W. Hurrell, Y. Kushnir, G. Ottersen, and M. Visbeck, Eds.). American Geophysical Union, Washington DC.

Thompson, L. G., Mosley-Thompson, E., Davis, M. E., Henderson, K. A., Brecher, H. H., Zagorodnov, V. S., Mashiotta, T. A., Lin, P. N., Mikhalenko, V. N., Hardy, D. R., and Beer, J. (**2002b**). Kilimanjaro ice core records: Evidence of Holocene climate change in tropical Africa. *Science* **298,** 589-593.

Thompson, L. G., Mosley-Thompson, E., Davis, M. E., Lin, P. N., Henderson, K., and Mashiotta, T. A. (**2003**). Tropical glacier and ice core evidence of climate change on annual to millennial time scales. *Climatic Change* **59,** 137-155.

Thompson, L. G., Mosley-Thompson, E., and Henderson, K. A. (**2000**). Ice-core palaeoclimate records in tropical South America since the Last Glacial Maximum. *Journal of Quaternary Science* **15,** 377-394.

Thornalley, D. J. R., Elderfield, H., and McCave, I. N. (**2009**). Holocene oscillations in temperature and salinity of the surface subpolar North Atlantic. *Nature* **457,** 711-4.

Thornalley, D. J. R., McCave, I. N., and Elderfield, H. (**2010**). Freshwater input and abrupt deglacial climate change in the North Atlantic. *Paleoceanography* **25,** 0.

Tipping, R. (**1995a**). Holocene evolution of a lowland Scottish landscape: Kirkpatrick Fleming. Part I, peat- and pollen-stratigraphic evidence for raised moss development and climatic change *The Holocene* **5** 69-81.

Tipping, R. (**1995b**). Holocene evolution of a lowland Scottish landscape: Kirkpatrick Fleming. Part II, regional vegetation and land-use change *The Holocene* **5** 83-96.

Tipping, R. (**1995c**). Holocene evolution of a lowland Scottish landscape: Kirkpatrick Fleming. Part III, fluvial history *The Holocene* **5** 184-195.

Tolonen, K. (**1986**). Rhizopod analysis. *In* "Handbook of Holocene palaeoecology and palaeohydrology." (B. E. Berglund, Ed.), pp. 645-666. John Wiley, Chichester.

Tolonen, K., Warner, B. G., and Vasander, H. (**1985**). Regeneration of two coastal raised bogs in eastern North America. *Annales Academiae Scientiarum Fennicae* **Series A139,** 5-51.

Tolonen, K., Warner, B. G., and Vasander, H. (**1994**). Ecology of testaceans (Protozoa, Rhizopoda) in mires in southern Finland: II, Multivariate analysis. *Archiv fuer Protistenkunde* **144,** 97-112.

Tröels-Smith, J. (**1955**). "Karakterisering af löse jordarter. Characterization of unconsolidated sediments." C.A.Reitzels forlag, Kobenhavn.

Turney, C., Baillie, M., Clemens, S., Brown, D., Palmer, J., Pilcher, J., Reimer, P., and Leuschner, H. H. (**2005**). Testing solar forcing of pervasive Holocene climate cycles. *Journal of Quaternary Science* **20,** 511-518.

Valiantzas, J. (**2006**). Simplified versions for the Penman evaporation equation using routine weather data. *Journal of Hydrology* **331,** 690-702.

Vallis, G. K., and Gerber, E. (**2008**). Local and hemispheric dynamics of the North Atlantic Oscillation, annular patterns and the zonal index. *Dynamics of Atmospheres and Oceans* **44,** 184-212.

van Bellen, S., Garneau, M., and Booth, R. K. (**2011**). Holocene carbon accumulation rates from three ombrotrophic peatlands in boreal Quebec, Canada: Impact of climate-driven ecohydrological change. *Holocene* **21,** 1217-1231.

Van Geel, B., Buurman, J., and Waterbolk, H. T. (**1996**). Archaeological and palaeoecological indications of an abrupt climate change in The Netherlands, and evidence for climatological teleconnections around 2650 BP. *Journal of Quaternary Science* **11,** 451-460.

van Kreveld, S., Sarnthein, M., Erlenkeuser, H., Grootes, P., Jung, S., Nadeau, M. J., Pflaumann, U., and Voelker, A. (**2000**). Potential Links Between Surging Ice Sheets, Circulation Changes, and the Dansgaard-Oeschger Cycles in the Irminger Sea, 60-18 Kyr. *Paleoceanography* **15,** 425-442.

Verschuren, D., and Charman, D. J. (**2008**). Latitudinal linkages in late Holocene moisture-balance variation. *In* "Natural Climate Variability and Global Warming." pp. 189-231. Blackwell Publishing Ltd., Chichester.

Viau, A. E., Gajewski, K., Fines, P., Atkinson, D. E., Sawada, M. C., and Viau, E. (**2002**). Widespread evidence of 1500 yr climate variability in North America during the past 14 000 yr. *Geology* **30,** 455-458.

Viau, A. E., Gajewski, K., Sawada, M. C., and Fines, P. (**2006**). Millennial-scale temperature variations in North America during the Holocene. *Journal of Geophysical Research-Atmospheres* **111**.

von Post, L. (**1916**). Einige suedschwedische Quellmoore. *Bulletin of the Geological Institute, University of Upsala* **15,** 219-278.

Walker, D., and Walker, P. M. (**1961**). Stratigraphic evidence of regeneration in some Irish bogs. *Journal of Ecology* **49,** 169-185.

Wallach, D., and Goffinet, B. (**1989**). Mean squared error of predicition as a criterion for evaluating and comparing system models. *Ecological Modelling* **44,** 299-306.

Waller, M. P., and Long, A. J. (**2003**). Holocene coastal evolution and sea-level change on the southern coast of England: a review. *Journal of Quaternary Science* **18,** 351-359.

Wanner, H., Beer, J., Butikofer, J., Crowley, T. J., Cubasch, U., Fluckiger, J., Goosse, H., Grosjean, M., Joos, F., Kaplan, J. O., Kuttel, M., Muller, S. A., Prentice, I. C., Solomina, O., Stocker, T. F., Tarasov, P., Wagner, M., and Widmann, M. (**2008**). Mid- to Late Holocene climate change: an overview. *Quaternary Science Reviews* **27,** 1791-1828.

Wanner, H., and Bütikofer, J. (**2008**). Holocene Bond Cycles: Real or Imaginary? *Geografie-Sbornik CGS* **113,** 338-350.

Wastegård, S. (**2005**). Late Quaternary tephrochronology of Sweden: a review. *Quaternary International* **130,** 49-62.

Wastegård, S., Rundgren, M., Schoning, K., Andersson, S., Bjorck, S., Borgmark, A., and Possnert, G. (**2008**). Age, geochemistry and distribution of the mid-Holocene Hekla-S/Kebister tephra. *The Holocene* **18,** 539-549.

Wastiaux, C., and Schumacker, R. (**2003**). "Topographie de surface et de subsurface des zones tourbeuses des réserves naturelles domaniales des Hautes-Fagnes." University of Liege, Liege.

Weber, C. A. (**1900**). Über die Moore, mit besonderer Berücksichtigung der zwischen Unterweser und Unterelbe liegenden. *Jahresbericht der Manner von Morgenstern* **3,** 3-23.

Weber, C. A. (**1908**). Aufbau und Vegetationen der Moore Norddeutschlands Englers. *Botanischer Jahresbericht* **40,** 29-34.

Weber, C. A. (**1926**). Grenzhorizont und Klimaschwankungen. *Abhandlungen des Naturwissenschaftlichen Vereins Bremen* **26,** 98-106.

Weckström, J. A. N., Seppä, H., and Korhola, A. (**2010**). Climatic influence on peatland formation and lateral expansion in sub-arctic Fennoscandia. *Boreas* **39,** 761-769.

Wein, R. W. (**1973**). Eriophorum Vaginatum L. *Journal of Ecology* **61,** 601-615.

Wendt, C. (**1996**). "Das Hohe Venn - Wandern mit offenen Augen." Meyer & Meyer, Aachen.

Whittaker, R. H. (**1967**). Gradient analysis of vegetation. *Biological Reviews* **42,** 207-264.

Wiersma, A. P., and Renssen, H. (**2006**). Model-data comparison for the 8.2 ka BP event: confirmation of a forcing mechanism by catastrophic drainage of Laurentide Lakes. *Quaternary Science Reviews* **25,** 63-88.

Wilmshurst, J. M., Wiser, S. K., and Charman, D. J. (**2003**). Reconstructing Holocene water tables in New Zealand using testate amoebae: differential preservation of tests and implications for the use of transfer functions. *Holocene* **13,** 61-72.

Wirtz, K. W., Lohmann, G., Bernhardt, K., and Lemmen, C. (**2010**). Mid-Holocene regional reorganization of climate variability: Analyses of proxy data in the frequency domain. *Palaeogeography, Palaeoclimatology, Palaeoecology* **298,** 189-200.

Woodland, W. A., Charman, D. J., and Sims, P. C. (**1998**). Quantitative estimates of water tables and soil moisture in Hoocene peatlands from testate amoebae. *The Holocene* **8,** 261-273.

Yeloff, D., and Mauquoy, D. (**2006**). The influence of vegetation composition on peat humification: implications for palaeoclimatic studies. *Boreas* **35,** 662-673.

Yu, Y. T., Yang, T. B., Li, J. J., Liu, J. F., An, C. R., Liu, X. Y., Fan, Z., Lu, Z. Y., Li, Y. P., and Su, X. (**2006**). Millennial-scale Holocene climate variability in the NW China drylands and links to the tropical Pacific and the North Atlantic. *Palaeogeography Palaeoclimatology Palaeoecology* **233,** 149-162.

Yu, Z. C., Beilman, D. W., and Jones, M. C. (**2009**). Sensitivity of Northern Peatland Carbon Dynamics to Holocene Climate Change. *In* "Carbon Cycling in

Northern Peatlands." (A. J. Baird, L. R. Belyea, X. Comas, A. S. Reeve, and L. D. Slater, Eds.), pp. 55-69. Geophysical Monograph Series. Amer Geophysical Union, Washington.

Yu, Z. C., Campbell, I. D., Campbell, C., Vitt, D. H., Bond, G. C., and Apps, M. J. (**2003**). Carbon sequestration in western Canadian peat highly sensitive to Holocene wet-dry climate cycles at millennial timescales. *Holocene* **13,** 801-808.